Mixed layer nitrogen cycling in the Southern Ocean: seasonality, kinetics, and biogeochemical implications

Mhlangabezi Mdutyana

A thesis presented for the degree of

Doctor of Philosophy

Department of Oceanography

Faculty of Science

UNIVERSITY OF CAPE TOWN

June 2021

I wish to dedicate this thesis to my mother, Mrs Nomtandazo Mdutyana, Sisters; Nosicelo and Ntombozuko Mdutyana. In memory of my brother Unathi Mdutyana, sister Veliswa Mdutyana and grandmother Nonzwakazi Botomani. Ndiyabulela ngenkuthazo ne nkxaso yenu!

Philippians 4:8 "Finally, brethren, whatever things are true, whatever things are noble, whatever things are just, whatever things are pure, whatever things are lovely, whatever things are of good report, if there is any virtue and if there is anything praiseworthy—meditate on these things".

This work has been supervised by:

Supervisor 1

Dr Sarah E. Fawcett
Department of Oceanography
University of Cape Town
Cape Town, South Africa

Supervisor 2

Dr Sandy J. Thomalla
Southern Ocean Carbon and Climate Observatory (SOCCO)
Council for Scientific and Industrial Research, Rosebank
Cape Town, South Africa

I confirm that I have been granted permission by the University of Cape Town's Doctoral Degrees Board to include the following publications in my PhD thesis, and where co-authorship is involved, my co-authors have agreed that I may include the publications:

Mdutyana M., Thomalla S.J, Philibert R., Ward B.B. and Fawcett S.E. (2020). The seasonal cycle of nitrogen uptake and nitrification in the Atlantic sector of the Southern Ocean. *Global Biogeochemical Cycles* 34, e2019GB006363. https://doi.org/ 10.1029/2019GB006363

Mdutyana, M., Sun, X., Burger, J.M., Flynn, R.F., Smith, S., van Horsten, N.R., Roychoudhury, A.N., Planquette, H., Bucciarelli, E., Thomalla, S.J., Ward, B.B., and Fawcett, S.E. The kinetics of ammonium uptake and oxidation across the African sector of the Southern Ocean. *Limnology and Oceanography*. *Under review*

Plagiarism declaration

I know the meaning of plagiarism and hereby declare that this is my own work. I have done all analyses of the data, creating of the figures, and writing the discussions of the results. The contents of this dissertation have not been submitted in whole or in part for consideration for any other degree or qualification in this, or any other University. This dissertation does not include any work as a result of collaboration unless specified in the text.

Signed by candidate

Signature: Date: June 2021

Acknowledgements

I would like to thank my supervisors, Dr Sarah Fawcett and Dr Sandy Thomalla, for their valued advice, guidance and invaluable support. I thank Dr Sandy Thomalla for inviting me to take part in the 2015 winter cruise to the Southern Ocean (my first Southern Ocean expedition), which is when the journey for this PhD began. I thank Dr Sarah Fawcett for her supervision, mentorship, student specific tailored training, and for the opportunities she afforded me throughout the PhD, starting from the MSc period.

I would like to thank the captains and crew of the R/V *S.A. Agulhas II* for their professional support throughout the Southern Ocean expeditions.

I would like to thank the Marine Biogeochemistry Lab team at the University of Cape Town (UCT) for their assistance, especially Tanya Marshall for her valuable help during the modifications of kinetic parameter curves in chapter 4.

I would like to thank Dr R. Roman for the onboard and ashore analysis of nutrients during the 2015 winter and summer cruises and for helping with anything related to computer problems. I would like to thank Mrs C. Karriem for extensive administrative support, I would like to thank Mr Ian Newton from the Stable Light Isotope Laboratory at UCT for PM analyses.

I would like to thank Prof Bess Ward for allowing me to learn everything Mass Spec related, during my visits to Princeton University, Department of Geosciences to analyse my nitrification samples. I also thank the Ward Lab group, namely X. Sun, J. Qixing, J. Lueders-Dumont and S. Oleynik, for their expert assistance during my visits under Princeton's Visiting Student Research Collaborator program.

I would like to acknowledge all the funding sources that made this Ph.D. possible: First, the South African National Research Foundation (NRF) that awarded me an NRF/CSIR (SOCCO) M.Sc. bursary and an Innovation Doctoral Scholarship and the Harry Crossley Foundation for a Research Fellowship. Second, I would like to acknowledge the travel funding I received from UCT (Postgraduate Travel Grant) and the NRF (Equipment-related Travel and Training Grant) that supported my research visits to Princeton University. Third, data collection and analysis for this Ph.D. was made possible by the NRF's South African National Antarctic Programme,

the Department of Science and Innovation’s Biogeochemistry Research Infrastructure Platform (BIOGRIP), UCT’s University Research Council and Vice-Chancellor Future Leaders 2030 programme, the CSIR's Parliamentary Grant. UCT; through a Vice Chancellor Future Leaders Award, a Research committee equipment grant and a Royal Society, and the US National Science Foundation.

My friends and fellow nerds (Kolisa, Ramontsheng, Sbongile, Precious, Raquel, and Mishka) thank you for moral support.

I would like to thank Tumi (my Muntu) for everything you have done for me during the last push of the Ph.D., lock-downing with you was one of the best decisions of 2020.

Ayinophela lencwadi ndingabulelanga uMakhumalo, umama ondizalayo, isineke othe wabonakalisa sona malunga nokuqhubekeka kwale ndlela yokufunda siyancomeka. Ndibamaba ngazo zozibini. Khumalo, Mtungwa!!!

Lastly, I thank Aviwe and Chuma the people who received me in Cape Town when I moved here in late 2015. Ndiyabulela ngobuhlobo esithe sabukhulisa iminyaka le, saxhasana kwi meko esiye safumaneka sikuzo. Nilusapho lwam nithanda ningathandi. Ndithi kuni mazenethole makwande nalapho nithatha khona, ndiyambulela uSomandla, uSmaki ngani!!!

List of Tables

List of Figures

Table of Contents

Thesis abstract

The alternation between summertime nitrate drawdown and wintertime nitrate recharge is central to the role of the Southern Ocean in setting atmospheric CO_2. However, active cycling of nitrogen (N) in the seasonally-varying mixed layer – including the production of ammonium and its subsequent removal via phytoplankton uptake and nitrification (i.e., the oxidation of ammonium to nitrite and then nitrate) – remains poorly understood. Following the "new production paradigm", phytoplankton production fueled by ammonium ("regenerated production") results in no net drawdown of CO_2 to the deep ocean, while growth supported by nitrate ("new production") can be equated to CO_2 removal provided that mixed-layer nitrification is negligible. While non-zero mixed-layer nitrification has been measured in many ocean regions, very few data exist for the Southern Ocean. This thesis presents new N cycle data collected across the Southern Ocean south of Africa in winter and summer that emphasize the integral role of mixed-layer N transformations in Southern Ocean productivity and biological CO_2 drawdown.

To evaluate the new production paradigm as a framework for quantifying Southern Ocean carbon export potential, rates of net primary production (NPP), N uptake (as ammonium and nitrate) and nitrification (ammonium and nitrite oxidation) were measured across the Atlantic sector in winter and summer. Winter mixed-layer NPP and total N (i.e., ammonium + nitrate) uptake were strongly decoupled, likely due to elevated heterotrophic bacterial consumption of ammonium. In summer, NPP and total N were generally well-coupled, although dissolved organic N apparently supported more than a third of NPP at some stations. Nitrification accounted for >100% of the nitrate consumed by phytoplankton in winter, rendering the new production paradigm ill-suited for quantifying carbon export in this season. By contrast, of the >50% of summertime NPP fueled by nitrate, <4% on average derived from mixed-layer nitrification. While the near-zero mixed-layer nitrification rates measured in summer could be taken as confirmation that nitrate uptake is a good proxy for Southern Ocean carbon export potential, a portion of the nitrate consumed in the summertime euphotic zone was produced in the winter mixed layer and will thus not support net carbon dioxide removal on an annual basis.

Despite the high rates of ammonium uptake and oxidation measured in winter Southern Ocean surface waters, mixed-layer ammonium concentrations remain fairly high, indicating an imbalance between ammonium production and consumption. Kinetics experiments conducted across the Indian sector (37-62ºS) reveal a seasonal switch from a phytoplankton community with a high affinity for ammonium in summer to one with a lower affinity in winter, even though phytoplankton at similar latitudes achieved a comparable maximum specific ammonium uptake

rate in summer and winter. Rates of ammonium oxidation showed a Michaelis-Menten response to substrate availability only when the ambient ammonium concentration was ≤90 nM. This, coupled with half-saturation constants (K_m values) of 28-137 nM (i.e., indicating a very high affinity for ammonium) suggest a dominant role for ammonia oxidizing archaea in mixed-layer nitrification. The maximum rate of ammonium oxidation was near-constant across the transect (37-62ºS), despite a significant gradient in sea surface temperature, light availability and ammonium concentration, perhaps due to iron limitation of ammonium oxidation, which has been hypothesized from culture experiments but not yet shown in the environment. It is possible that iron depletion in the surface Southern Ocean may limit the role of winter mixed-layer nitrification in offsetting phytoplankton CO_2 drawdown annually.

To better understand the controls on nitrifier ecology in the surface Southern Ocean, a series of nitrite oxidation kinetics experiments were conducted across the Indian sector (37- 62ºS) in winter. All experiments yielded a Michaelis-Menten relationship with substrate concentration, yet the nitrite oxidation rates only increased significantly at nitrite concentrations >115-245 nM, suggesting that nitrite oxidizers require a minimum (i.e., "threshold") nitrite concentration to produce nitrate. Low derived K_m values (134-403 nM) that increased with increasing ambient nitrite indicate a high affinity of nitrite oxidizers for substrate, in contrast to results from culture experiments. Throughout the Southern Ocean mixed layer, ambient nitrite concentrations are rarely less than 150 nM, regardless of season. Coincident measurements of ammonium and nitrite oxidation in the mixed layer suggest that nitrite oxidation is the rate-limiting step for nitrification in the winter Southern Ocean. This, combined with a possible nitrite concentration threshold for nitrite oxidation, may explain the perennial non-zero mixed-layer nitrite. A possible explanation for the apparent threshold nitrite requirement of nitrite oxidizers is undersaturation of the heme-rich nitrite oxidoreductase enzyme, perhaps driven by the limited availability of iron in Southern Ocean surface waters.

The findings described in this thesis yield new insights into the active cycling of N within the Southern Ocean's mixed layer, and particularly emphasize the need for seasonally-resolved parallel N- and iron cycle investigations to fully understand the role of nitrification in biological CO_2 removal and N supply. Climate change-driven warming and acidification of Southern Ocean surface waters is already driving changes in microbial community composition, nutrient supply, and primary productivity. If we are to better predict the Southern Ocean's future role in CO_2 sequestration and global ocean fertility, an improved understanding of the controls on mixed layer N cycling, particularly nitrification, is essential.

Chapter 1: General introduction and thesis overview

1.1 Marine productivity and the biological carbon pump

The ocean is the largest active reservoir of carbon on Earth (Emerson and Hedges 2008), and absorbs and stores large amounts of anthropogenic carbon dioxide (CO_2) (Takahashi et al. 2002). The biological removal of carbon from the surface waters is made possible by the ocean's biological carbon pump (Volk and Hoffert 1985). This mechanism involves the fixation of atmospheric CO_2 during photosynthesis by phytoplankton, the microscopic plants that inhabit the sunlit upper layer of the ocean (the "euphotic zone") and are responsible for ~50% of global primary productivity (Field et al. 1998). Photosynthesis by phytoplankton, supported by nutrients such as nitrogen (N), phosphorus (P; mainly as phosphate, PO_4^{3-}) and iron, results in the production of particulate organic matter (POM; including particulate organic carbon and N) that supports higher trophic levels. A small percentage of the POM escapes recycling in the euphotic zone to sink into the deep ocean, where it remains for decades to centuries, with a tiny fraction eventually buried in the sediments (Volk and Hoffert 1985). The biological pump links the carbon cycle with other biogeochemical processes such the uptake of inorganic N (and P) by phytoplankton (which decreases CO_2) and the remineralization of organic N (and P) back to its inorganic forms (which increases CO_2).

The "new production paradigm" is a useful framework for examining the potential for phytoplankton-produced carbon to be exported from the euphotic zone. First proposed by Dugdale and Goering (1967), the new production paradigm defines the growth of phytoplankton on nitrate (NO_3^-) originating below the euphotic zone, augmented by N_2 fixation, as "new production", while growth on ammonium (NH_4^+) and other recycled N forms is termed "regenerated production". Over sufficient time and space scales, new production must be balanced by the flux of POM out of the euphotic zone (i.e., "export production"), which maintains the sequestration of CO_2 in the ocean interior (Dugdale and Goering 1967; Eppley and Peterson 1979). NO_3^- assimilation by phytoplankton is thus a key determinant of the ocean's biological carbon sink, and exclusively so in high-latitude regions where N_2 fixation is not favoured (González et al. 2014; Raes et al. 2020; Hörstmann et al. 2021).

The f-ratio (shorthand for "flux ratio") is a metric commonly employed to evaluate the contribution of new production to total production (i.e., new + regenerated production), and thus the fraction of primary production exported from the euphotic zone (Eppley and Peterson

1979). Oceanic regions that are dominated by regenerated production contribute little to the export of carbon from surface waters and hence, are characterized by low f-ratios, while the opposite is true for regions where new production dominates. The application of the new production paradigm as first defined, where new production is equated to NO_3^- uptake and regenerated production to NH_4^+ uptake, relies on certain assumptions, such as negligible N_2 fixation and atmospheric N deposition (both new N sources), no uptake of dissolved organic nitrogen (DON; a complex mixture of regenerated N forms), and negligible euphotic zone nitrification (which results in the production of regenerated NO_3^-) (Dugdale and Goering 1967). When euphotic zone nitrification and/or DON uptake overlap with NO_3^- and NH_4^+ assimilation, the application of the new production paradigm as a framework for estimating export production becomes complicated (e.g., Bronk et al. 1994; Yool et al. 2007). For example, failing to account for regenerated NO_3^- produced by euphotic zone nitrification has been shown to cause an overestimation of new (and thus export) production by >50% (Yool et al. 2007), while not measuring DON uptake may result in regenerated production being underestimated by up to 70% (Bronk et al. 1994).

1.2 Research location: The Southern Ocean

1.2.1 Southern Ocean hydrography

The regional focus of this thesis is the open Southern Ocean, defined here as the waters south of the Subtropical Front and north of the Continental Zone, where seasonal variations in light and temperature coincide with large oscillations in primary productivity (Arrigo et al. 2008). The large-scale circulation of the Southern Ocean is dominated by the eastward-flowing Antarctic Circumpolar Current (ACC), which fully encircles Antarctica. The ACC divides the Southern Ocean into frontal zones (the Subantarctic Zone (SAZ), Polar Frontal Zone (PFZ) and Antarctic Zone (AZ)) via its associated hydrographic fronts (the Subantarctic Front (SAF), Polar Front (PF) and Southern ACC Front (SACCF)) (Figure 1.1; Whitworth and Nowlin 1987; Orsi et al. 1995). The northern boundary of the SAZ is demarcated by the Subtropical Front (STF), while south of the SACCF is the Southern Boundary (SB), which is defined as the southernmost extent of Upper Circumpolar Deep Water (UCDW), although it is not a dynamical front (Talley et al. 2011).

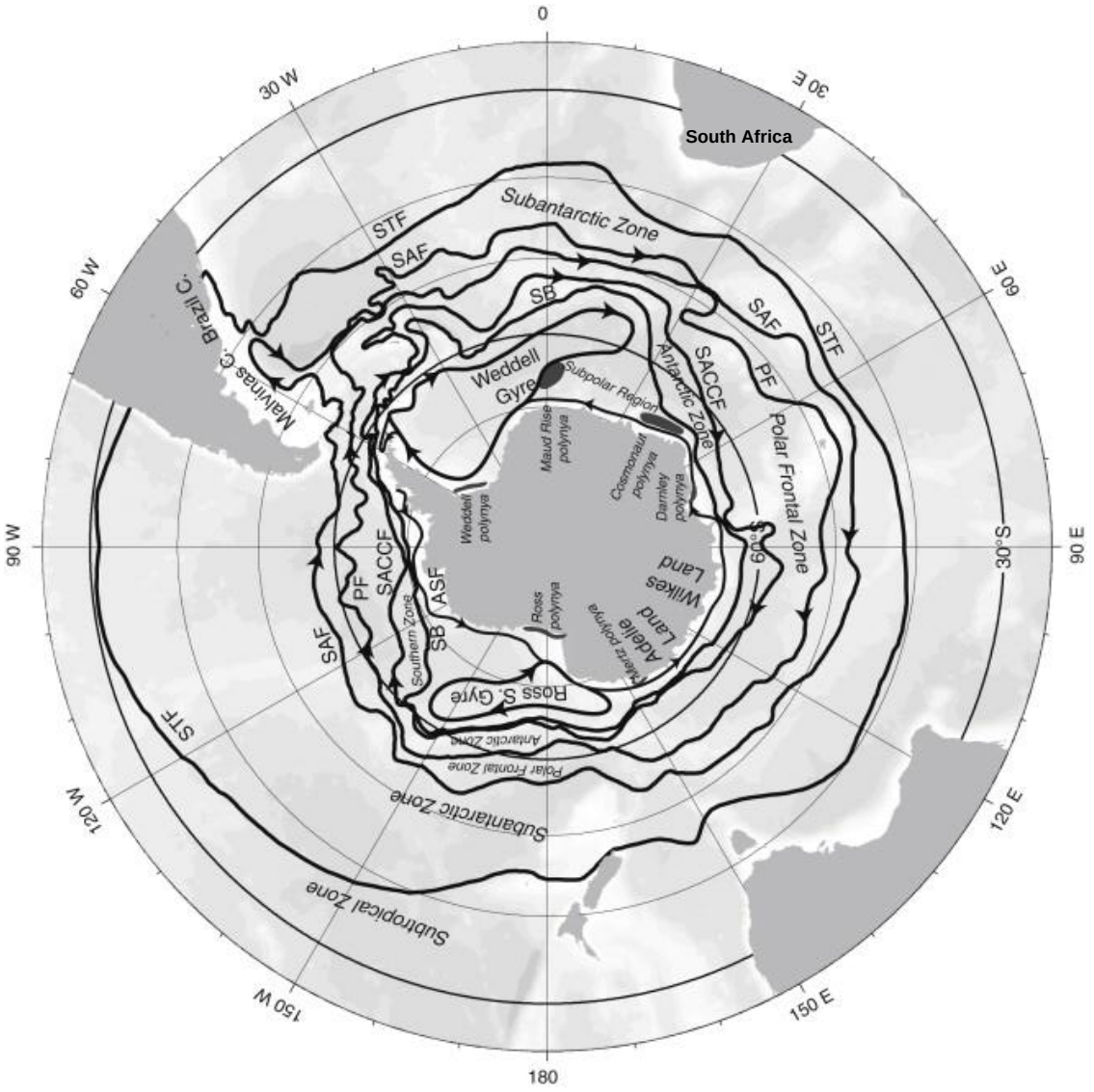

Figure 1. 1: Schematic showing the climatological positions of the Southern Ocean fronts; STF, SAF, PF, SACCF ASF (Antarctic Slope Front) and SB (Southern Boundary), and their respective frontal zones (Orsi et al. 1995a). The focus of this thesis are the waters south of South Africa between 36ºS and 62ºS and 8.7ºE and 30ºE. Figure taken from Talley et al. (2011).

The STF divides the STZ and SAZ and is considered the northern boundary of the SAF (Deacon 1982; Orsi et al. 1995a). The currents associated with the STF can be thought of as extensions of the western boundary currents in each basin (Graham and De Boer 2013); in the case of the African sector, the STF is associated with the Agulhas Return Current (Lutjeharms and Ansorge 2001). The STF is a region of high temperatures and salinity, which contribute equally to the formation of the mixed layer (Pollard et al. 2002). This region has low surface nutrient (i.e., NO_3^-) concentrations, with nutrients supplied to the STF via northward-flowing Subantarctic Surface Water (SASW), which is underlaid by Subantarctic Mode Water (SAMW) that can be penetrated by the thick wintertime mixed layers of the STZ (Talley et al.

2011). Nutrient-poor Subtropical Surface Water (STSW) is also entrained into the STF from the north (Smythe-Wright et al. 1998).

The SAF forms the southern boundary of the SAZ, which is considered the largest frontal zone of the ACC (Orsi et al. 1995a; Pollard et al. 2002). The upper SAZ water masses include Subantarctic Surface Water (SASW), which can extend as deep as 500 m, and Subantarctic Mode Water (SAMW), which forms near the SAF due to wintertime cooling and mixing of SASW and STSW (Hanawa and Talley 2001). SAMW appears as a thick layer of near-uniform properties (Talley et al. 2011) that subducts in the SAZ and flows northwards to become part of the permanent pycnocline, ultimately enriching the surface waters of the subtropical gyres with nutrients(Toggweiler et al. 1991; Sarmiento et al. 2004; Marinov et al. 2006; Downes et al. 2011; Talley et al. 2011) Beneath SASW and SAMW flows Antarctic Intermediate Water (AAIW), which is thought to form from the sinking of Antarctic Surface Water (AASW) across the SAF. AAIW is an unusually low-salinity water mass that can still be observed as far as 10-20ºN in the Atlantic and ~5ºS in the Indian Ocean (Talley et al. 2011). AAIW is underlaid by Upper and Lower Circumpolar Deep Water (UCDW and LCDW, respectively) and Antarctic Bottom Water (AABW), the latter formed in the Weddell and Ross Seas (Orsi et al. 1999). In the SAZ, temperature plays a dominant role in the formation of the mixed layer compared to salinity (Pollard et al. 2002), and nutrients are supplied through vertical mixing with the underlying thermocline and large-scale Ekman transport of surface waters (AASW) originating in the AZ (McCartney 1975; Gordon et al. 1977; Sigman et al. 1999; Sarmiento et al. 2004; Swart et al. 2015).

The PF forms the boundary between the PFZ and the AZ and is located centrally within the ACC. The PFZ between the PF and the SAF is a highly dynamic region characterized by a sharp transition from near-isothermal SASW to the warmer, saltier waters of the SAF (Gordon et al. 1977; Talley et al. 2011). The PFZ hosts numerous strong eddies formed from meanders of the PF and SAF (Savchenko et al. 1978) that contribute to heat exchange between the north and the south (Talley et al. 2011). The water masses of the PFZ include AASW, UCDW, LCDW and AABW. Surface nutrients are advected northwards from the AZ and into the PFZ through Ekman transport of AASW (Sigman et al. 1999; Sarmiento et al. 2004). Additionally, the PF is characterized by Ekman upwelling that brings nutrients to the surface (Hense et al. 2003; Meskhidze et al. 2007). This upwelling of nutrients is due to strong winds that drive the upwelling of UCDW (Whitworth and Nowlin 1987).

The AZ is located south of the PF and is divided by the SACCF into a northern and southern domain, the Open AZ and Polar AZ, respectively (Talley et al. 2011). The OAZ is permanently ice-free while the PAZ is characterized by seasonal ice cover (Whitworth 1980; Orsi et al. 1995a). The AZ has similar water masses to the PFZ, although the SACCF denotes the southern extent of UCDW (Talley et al. 2011) such that while UCDW underlies the OAZ surface, this water mass is largely absent from the PAZ, the surface layer of which is underlain by LCDW (Whitworth and Nowlin 1987; Sigman et al. 1999; Difiore et al. 2010). LCDW is higher in salinity and oxygen and lower in NO_3^- than UCDW because it incorporates some North Atlantic Deep Water (Whitworth and Nowlin 1987). The formation of a temperature minimum (T_{min}) layer in the summertime AZ is a common phenomenon whereby the wintertime low-temperature surface layer becomes the subsurface water mass beneath the summer mixed layer (Gordon et al. 1977; Toole 1981). The T_{min} is sometimes described as a summertime record of winter conditions, reflecting the initial state from which the surface AZ evolves over the course of the summer (Altabet and Francois 2001; Difiore et al. 2010). Nutrients are supplied to the AZ surface from depth through UCDW upwelling driven by Ekman divergence, as well as winter cooling and sea-ice formation (the latter in the PAZ) that cause the mixed layer to deepen (Orsi et al. 1995a; Pollard et al. 2002; Talley et al. 2011). Seasonal mixing-driven trace metal dynamics are enhanced in the AZ, with increased iron concentrations observed during spring/summer due to the melting of sea ice and migrating icebergs (Cefarelli et al. 2011; Lin et al. 2011; Vernet et al. 2011; Lannuzel et al. 2016).

The marginal ice zone (MIZ), which includes the PAZ (Orsi et al. 1995a), is a biologically-active zone of unconsolidated sea-ice cover (e.g. Squire, 1998). The MIZ is a hydrodynamically and biogeochemically complex region in the Southern Ocean and is extremely variable throughout the seasons, showing seasonal waning and waxing in terms of area of hundreds of thousands of square kilometres (Parkinson 2014). The MIZ extent reaches minimum values in summer (~1.8 million km^2) (Turner et al. 2017; Meehl et al. 2019), while in late winter, sea-ice extent reaches a maximum (~12 million km^2) (Parkinson 2014; Massonnet et al. 2015; Turner et al. 2017). The melting of sea ice in spring and summer has been reported to be accompanied by phytoplankton blooms due to freshening that stratifies the upper layer and an enhanced supply of iron (Lancelot et al. 1993; Lannuzel et al. 2016; Tedesco et al. 2019).

1.2.2. Southern Ocean carbon and nutrient cycling

The absorption and storage of CO_2 in the ocean is facilitated by two processes: 1) the solubility pump and 2) the biological pump (Volk and Hoffert 1985). The solubility pump is the physico-chemical mechanism that transports dissolved inorganic carbon (DIC) into the deep ocean from the surface, helping to maintain the ocean's vertical gradient of DIC and facilitating the storage of CO_2 at depth (Volk and Hoffert 1985). The solubility pump is driven by the solubility of CO_2 in seawater, with more CO_2 dissolving at colder temperatures, combined with the ocean's thermohaline circulation, which involves deep-water formation at high latitudes and the subsequent transfer of surface CO_2 to depth in these waters. In the open ocean, about 35% of the surface DIC transport to depth occurs by the solubility pump (Toggweiler et al. 2003), with the remainder due to the biological pump.

In the Southern Ocean, the contribution of the solubility pump to CO_2 uptake differs with season and region (Metzl 2009; Lenton et al. 2013). The solubility pump in the SAZ is dominated by winter CO_2 uptake driven by low sea-surface temperatures, while summer is characterized by slight outgassing of CO_2 due to increased temperature (Mongwe et al. 2016; 2018). By contrast, south of the PF, most of the year is dominated by the outgassing of CO_2 because of the upwelling of deep waters rich in CO_2 (Metzl et al. 2006; Mongwe et al. 2016; 2018). The action of the solubility pump is overprinted by that of the biological pump, however, and it is the combination of the two that yields the seasonal cycle in air-sea CO_2 exchange. The biological pump is most effective in the Southern Ocean during the spring and summer seasons as compared to winter. During the growing season (spring/summer), both the SAZ and AZ are strong net sinks for CO_2, with the biological pump dominating over the solubility pump (Gruber et al. 2009; Takahashi et al. 2009; Majkut et al. 2014; Mongwe et al. 2016; 2018). In winter, the SAZ remains a CO_2 sink because of the dominant influence of the solubility pump (i.e., the cold surface temperatures), while the AZ becomes a CO_2 source due to the combination of a weak biological pump and the upwelling of CO_2-rich deep waters (Gruber et al. 2009; Takahashi et al. 2009; Mongwe et al. 2018). Over an annual cycle, both the SAZ and AZ appear to be CO_2 sinks (of ~0.64 Pg C yr^{-1} and <0.1 Pg C yr^{-1}, respectively), although the SAZ is a much stronger sink than the AZ (Gruber et al. 2009; Takahashi et al. 2009; Landschützer et al. 2015; Mongwe et al. 2018).

In the Southern Ocean, constituting ~20% of the ocean's surface area, is one of the most important carbon sinks globally (Schlitzer 2002; Takahashi et al. 2002), and plays a

disproportionate role in regulating the global ocean's biological pump and Earth's climate (Knox and McElroy 1984; Sarmiento and Toggweiler 1984; Siegenthaler and Wenk 1984; Sigman and Boyle 2000; Sigman et al. 2010). Annually, the global ocean takes up ~30% of anthropogenic CO_2 emissions, of which about 40% is absorbed by Southern Ocean waters south of the STF (Takahashi et al. 2009; Devries 2014; Siegel et al. 2014; Frölicher et al. 2015; Gruber et al. 2019b). It has been estimated that without the Southern Ocean's biological pump, atmospheric CO_2 concentrations could be 50% higher than present levels (Cox et al. 2000; Siegel et al. 2014). However, despite the significant role of the Southern Ocean's in CO_2 drawdown, this region actually constitutes a "leak" in the global ocean's biological pump because the macronutrients (i.e., NO_3^- and PO_4^{3-}) supplied from depth are never fully consumed in the mixed layer (Broecker 1982; Weber and El-sayed 1987; Priddle et al. 1998; Sigman and Boyle 2000).

Southern Ocean nutrient cycling shows a strong seasonal cycle (Henley et al. 2020 and references therein) that is both physically and biologically mediated. Winter is characterized by deep mixed layers that entrain nutrients from depth into surface waters. The lack of available light in this season, driven by both the deep mixed layers and low solar radiation (Sallée et al. 2010; du Plessis et al. 2017a), means that the nutrients are not immediately consumed. Physical nutrient recharge in winter is accompanied by high rates of *in situ* biological NO_3^- production (Smart et al. 2015; Mdutyana et al. 2020) and high NH_4^+ concentrations (Mdutyana et al. 2020; Henley et al. 2020), the latter presumably deriving from elevated remineralisation in late summer through winter. In other words, the winter season is dominated by mixing and by biological processes that produce recycled nutrients (i.e., remineralisation and nitrification) and not by photoautotrophic nutrient consumption, causing the biological pump to be weak (e.g., Philibert et al. 2015; Smart et al. 2015; Mongwe et al. 2018; Mdutyana et al. 2020). By contrast, shallow mixed layers in summer driven by increased temperatures, combined with high incident solar radiation and in the most southern waters, by an input of freshwater due to sea-ice melt, provide sufficient light for photosynthesis. The shallow summer mixed-layer depths coincide with high rates of net primary production, which, at least in early summer, is predominantly supported by NO_3^- uptake (Joubert et al. 2011; Peng et al. 2018; Mdutyana et al. 2020)(e.g., Joubert et al. 2011; Johnson et al. 2017; Mdutyana et al. 2020). Additionally, rates of euphotic zone nitrification are negligible in summer (Trull et al. 2008; DiFiore et al. 2009; Kemeny et al. 2016; Fripiat et al. 2019; Mdutyana et al. 2020), such that the potential for carbon export is high.

The Southern Ocean is well-known for the incomplete removal of euphotic zone nutrients during the growing season and is thus referred to as a high-nutrient, low-chlorophyl (HNLC) region. The inability of phytoplankton to completely consume surface nutrients is broadly thought to be due to a combination of iron and light limitation (Martin 1990; Nelson and Smith 1991; Sunda and Huntsman 1997), although other drivers of phytoplankton productivity have been considered and are discussed below. Winter mixing is the dominant mechanism of nutrient supply to Southern Ocean surface waters, yet it supplies unequal quantities of macronutrients and iron, resulting in iron-limited conditions (Croot et al. 2007; Ellwood et al. 2008; Bowie et al. 2009; Janssen et al. 2020). This is because the depth of ferricline (i.e., the maximum derivative of iron concentration with depth) is typically considerably deeper than the winter mixed layer and the nutricline (Tagliabue et al. 2014; Janssen et al. 2020). Iron is thus limiting to productivity across the open Southern Ocean year-round, and dominantly responsible for its HNLC status (Banse 1996; Boyd et al. 2001, 2007; Hiscock et al. 2008; Moore et al. 2013; Janssen et al. 2020). While there are other mechanisms of iron supply to the Southern Ocean, including aeolian deposition, resuspension of shelf sediments, ice melt, and possibly also a contribution from hydrothermal vent systems, these inputs are typically small and/or localized, particularly at the scale of the open Southern Ocean (Blain et al. 2007; Cassar et al. 2007; Salter et al. 2007; Pollard et al. 2009; Boyd and Ellwood 2010; Tagliabue et al. 2010; Ardyna et al. 2019).

1.3 Drivers of phytoplankton productivity in the Southern Ocean

Phytoplankton productivity in the Southern Ocean is regulated by several environmental factors characterized as either bottom-up (light availability, temperature, resource availability – i.e., macro- and micronutrients) or top-down controls (grazing by zooplankton, viral infection) (e.g., Martin et al. 1990; Nelson and Smith 1991; Banse 1996; Sunda and Huntsman 1997; Smith and Lancelot 2004; Cochlan 2008; Boyd et al. 2012). The relative importance of these factors varies with Southern Ocean sector (i.e., longitude), zone (i.e., latitude), and season, resulting in spatial and seasonal variations in phytoplankton biomass, productivity, community composition, and nutrient uptake regime (i.e., new versus recycled nutrient dependence) (Arrigo and McClain 1994; Mengesha et al. 1998; Thomalla et al. 2011b; Shadwick et al. 2015; Mdutyana et al. 2020). Productivity in the Southern Ocean is often discussed in the context of the “Antarctic Paradox” (Priddle et al. 1992; Tréguer and Jacques

1992), which refers to the fact that mixed-layer macronutrients are never fully consumed by phytoplankton, rendering productivity (i.e., biomass accumulation and export) lower than the available macronutrients suggest it should be. In the subsections below, the potential influence of various biogeochemical and environmental factors on phytoplankton productivity in the Southern Ocean is discussed, with a view to better understanding the role of phytoplankton in carbon production and export.

1.3.1 Macronutrients

In general, phytoplankton productivity in the open Southern Ocean is not limited by the macronutrients NO_3^- and PO_4^{3-}, the concentrations of which remain elevated in the mixed layer throughout the growing season (Sarmiento and Toggweiler 1984; Priddle et al. 1995; Sarmiento et al. 2004; Mdutyana et al. 2020), as is characteristic of an HNLC ecosystem (Minas et al. 1986; Moore and Abbott 2000). However, the macronutrient silicate ($Si(OH)_4$) is limiting to some phytoplankton between the STF (perennially) and the northern PF (seasonally) (Boyd 2002; Pollard et al. 2002; Brzezinski et al. 2003b; Sarmiento et al. 2004) where its concentration averages <5 μM (Henley et al. 2020; Weir et al. 2020). By contrast, $Si(OH)_4$ limitation does not occur south of the PF where mixed-layer ambient $Si(OH)_4$ concentrations of 24-78 μM are typically observed (Franck et al. 2000; Tagliabue et al. 2012; Le Moigne et al. 2013; Henley et al. 2020; Weir et al. 2020). These high $Si(OH)_4$ concentrations are supplied in CDW that upwells in the vicinity of the ACC. $Si(OH)_4$ limitation particularly affects the growth of diatoms (Boyd 2002), an ecologically-significant group of phytoplankton that require dissolved $Si(OH)_4$ to biomineralize their opal (i.e., amorphous biogenic silica) frustules. Because the opal shells of diatoms are relatively dense, they effectively facilitate carbon export from surface waters, rendering diatoms an important direct driver of the biological pump (in the Southern Ocean and globally; Buesseler 1998; Ducklow et al. 2001a). One caveat to this is that large, heavily-silicified diatoms in the iron-limited Southern Ocean have been observed to decouple carbon and $Si(OH)_4$ drawdown, removing $Si(OH)_4$ more effectively than carbon, while smaller diatom species are more effective carbon exporters (Assmy et al. 2013). Diatoms are also considered NO_3^- specialists (Litchman et al. 2006; Fawcett and Ward 2011; Glibert et al. 2016), such that in the framework of the new production paradigm, this phytoplankton group contributes significantly to export production (Tréguer and Pondaven 2000).

The Subantarctic region of the Southern Ocean (i.e., the combined SAZ and PFZ between the STF and PF) experiences $Si(OH)_4$ limitation because diatoms preferentially utilise $Si(OH)_4$ over NO_3^- in AASW (i.e., in a ratio >1:1, which is the ratio expected for optimally-growing diatoms; Hutchins and Bruland 1998; Takeda 1998; Ragueneau et al. 2000; Mosseri et al. 2008). This preferential $Si(OH)_4$ uptake happens under iron-limited conditions (Franck et al. 2000; Pondaven et al. 2000; Smith et al. 2000; Brzezinski et al. 2003), largely in the AZ. As a result, northward-flowing AASW is high in NO_3^- and PO_4^{3-} but very low in $Si(OH)_4$ (Sarmiento et al. 2004; Henley et al. 2020), which favours the growth of non-diatom phytoplankton such as dinoflagellates, prymnesiophytes, and cryptophytes (Balch et al. 2011; Quéguiner 2013; Deppeler and Davidson 2017 and references therein). The dominance of non-siliceous phytoplankton north of the AZ has implications for the biological pump since these species tend to sink more slowly than opal-ballasted diatoms (Buesseler 1998a; Ducklow et al. 2001a; Armstrong et al. 2009). Therefore, $Si(OH)_4$ limitation of diatoms in the Southern Ocean may represent a missed opportunity for carbon drawdown (Armstrong et al. 2001; Brzezinski et al. 2003). Additionally, the preferentially removal of $Si(OH)_4$ relative to NO_3^- and PO_4^{3-} south of the PF results in northward-flowing SAMW and AAIW that are $Si(OH)_4$-deplete (Sarmiento et al. 2004; Freeman et al. 2018). These waters (SAMW in particular) supply the thermocline of the low-latitude ocean with nutrients (Toggweiler et al. 1991) in a ratio that is set when they subduct at their formation regions (Sarmiento et al. 2004). Iron-limited diatoms in the polar Southern Ocean thus play a major role in determining phytoplankton community composition in the low latitudes and North Atlantic, as well as influencing the potential for N_2 fixation (Weber and Deutsch 2010). That is, when SAMW upwells in the subtropical ocean, the fact that it is $Si(OH)_4$-deplete means that it cannot support the growth of high abundances of diatoms. The subsequent consumption of NO_3^- and PO_4^{3-} by non-diatom phytoplankton, which apparently tends towards a ratio of 20:1, suggests that low-latitude phytoplankton may be more strongly N limited than previously recognized (Karl et al. 1997; Weber and Deutsch 2010), thus expanding the requirement (i.e., the environmental selection pressure) for N_2 fixation.

Another macronutrient that is of nutritional value to phytoplankton is NH_4^+, the most reduced form of N that is far less energetically-expensive than NO_3^- to assimilate (Dortch 1990). One might thus expect NH_4^+ to be the preferred N nutrient for phytoplankton growth (Thompson et al. 1989), and in most regions, mixed-layer NH_4^+ is consumed as rapidly as it is produced (Glibert et al. 1982; La Roche 1983), yielding ambient concentrations <200 nM (Brzezinski 1988; Paulot et al. 2015; Henley et al. 2020). In the Southern Ocean, NH_4^+ displays a seasonal

gradient, with summer mixed layers characterized by NH_4^+ concentrations below detection while winter mixed-layer NH_4^+ concentrations appear to be elevated, particularly in the PFZ and AZ (Sambrotto and Mace 2000; Daly et al. 2001; Savoye et al. 2004; Philibert et al. 2015; Henley et al. 2020; Mdutyana et al. 2020). It is not surprising to observe low NH_4^+ concentrations in the summer given how rapidly this nutrient is consumed by phytoplankton (Glibert et al. 1982; La Roche 1983), but the high concentrations observed in winter are perhaps unexpected given that NH_4^+ removal processes are expected to dominate the mixed-layer N cycle in this season (Koike et al. 1986; Serebrennikova and Fanning 2004; Philibert et al. 2015; Smart et al. 2015; Mdutyana et al. 2020; Raes et al. 2020) given that the environmental factors (e.g., deep mixed layers and low light availability; Dortch 1990; du Plessis et al. 2017) should favour NH_4^+ uptake (over NO_3^-) and NH_4^+ oxidation (Koike et al. 1986; Mdutyana et al. 2020). The seasonal dynamics of the mixed-layer NH_4^+ cycle have not been investigated in the Southern Ocean to-date, despite the implications for the export of carbon (Yool et al. 2007; Mdutyana et al. 2020; Raes et al. 2020). For instance, the shift to a winter phytoplankton community dominated by smaller cells that have a preference for NH_4^+ (Mulholland and Lomas 2008) will not lead to export production in both a direct (i.e., smaller cells are less likely to sink and will instead enter the microbial loop; Fenchel 2008) and indirect (i.e., new production paradigm; Dugdale and Goering 1967; Eppley and Peterson 1979) sense.

Elevated concentrations of NH_4^+ can have an inhibitory effect on the uptake of NO_3^- by phytoplankton, although this effect appears to be highly variable (e.g., McCarthy 1981; Dortch 1990; Wheeler and Kokkinakis 1990; Varela and Harrison 1999). Indeed, the available culture and field studies report NO_3^- uptake inhibition by NH_4^+ ranging from near-zero to 100%, depending on a variety of factors such as light, nutrient history (including the ambient NH_4^+ concentration) and species composition (e.g., Kokkinakis and Wheeler 1987; Booth 1988; Dortch 1990 and references therein; Wheeler and Kokkinakis 1990; Bagwell 2009). In certain regions, NH_4^+ inhibition of NO_3^- uptake has been observed at NH_4^+ concentrations as low as ~100-200 nM (Varela and Harrison 1999; Cochlan and Bronk 2011), while elsewhere, NH_4^+ concentrations >1 μM were not fully inhibitory (McCarthy 1981; Dortch 1990). NH_4^+ inhibition of NO_3^- uptake complicates application of the new production paradigm (Jacques 1991a) and amounts to an inefficiency in the biological pump because allochthonous NO_3^- left unconsumed in surface waters represents a missed opportunity for carbon drawdown (Flynn et al. 2018).

In the Southern Ocean, the role of NH_4^+ inhibition of NO_3^- uptake has not been widely studied, but the available observations suggest an inhibitory effect at NH_4^+ concentrations >1 µM (occasionally between 0.5 µM and 1 µM; Cochlan 1986; Kristiansen and Fabrot 1991; Reay et al. 2001; Cochlan et al. 2002). General consensus thus seems to be that NH_4^+ inhibition of NO_3^- uptake is minor in the open Southern Ocean mixed layer, but may occur near fronts and/or in coastal waters where NH_4^+ accumulates to concentrations >>1 µM (Koike et al. 1986; Goeyens et al. 1995; Krell et al. 2005; Henley et al. 2017). It is important to note that in coastal waters, impediment of the biological pump by NH_4^+ inhibition is only relevant if the NH_4^+ derives from *in situ* regeneration rather than being supplied from land as in the latter case, the NH_4^+ constitutes a new- rather than a regenerated N source to phytoplankton. That said, it has been suggested based on observations from the open Southern Ocean that the late-summer increase in NH_4^+ concentrations and coincident decline in NO_3^- uptake rates could indicate NH_4^+ inhibition of NO_3^- drawdown (Mengesha et al. 1998). However, such a decline in NO_3^- consumption and increase in reliance on regenerated N forms more likely reflects iron-limitation of phytoplankton growth (see below; Morel et al. 1991; Price et al. 1994; Timmermans et al. 1998; Lourey et al. 2003). In total, very little work has focused on NH_4^+ cycling in the Southern Ocean, such that our knowledge of the potential for NH_4^+ inhibition of NO_3^- uptake and the implications thereof remains limited.

1.3.2 Iron and other micronutrients

Phytoplankton require the micronutrient iron for various enzymatic functions and electron transport systems including photosynthesis and N acquisition (Geider and La Roche 1994; Raven et al. 1999; Morel and Price 2003). Iron is also the main component of ferredoxin, which facilitates the intracellular storage of photosynthetically-incorporated energy, and is found in both the NO_3^- and nitrite (NO_2^-) reductase enzymes (Verstreate et al. 1980; de Baar et al. 1990). These enzymes reduce NO_3^- through NO_2^- to NH_4^+, which is readily incorporated by phytoplankton and used for the production of amino acids and proteins (Raven 1988; 1990). Phytoplankton that use NO_3^- as their primary N source have a higher iron requirement than those that depend mainly on regenerated N (Morel et al. 1991; Price et al. 1994), and under iron-deplete conditions, phytoplankton have been observed to down-regulate iron-containing enzymes involved in NO_3^- assimilation (Timmermans et al. 1994) and turn to enhanced reliance on NH_4^+ (Timmermans et al. 1998).

The Southern Ocean presents two broadly different environments in terms of mixed-layer iron conditions: 1) the open Southern Ocean, where mixed-layer iron concentrations are perennially low (i.e., < 0.2 nM; Tagliabue et al. 2012 and references therein) and 2) naturally iron-fertilized regions, predominantly encountered near the Subantarctic islands (e.g., Kerguelen, Crozet, South Georgia; Korb et al. 2005; Blain et al. 2007; Seeyave et al. 2007; Cavagna et al. 2015). Here, shoaling bathymetry drives regular upwelling of deeper waters (e.g., Schallenberg et al. 2018), the iron reservoir of which is often augmented by interaction with iron-rich basaltic sediments (e.g., Zhang et al. 2008), and retention zones are created overlying shallow plateaus, also yielding an enhanced supply of recycled iron (e.g., Planquette et al. 2007). These regions are commonly known for persistent, large phytoplankton blooms, a phenomenon that is referred to as the Island Mass Effect (IME). The IME tends to be associated with elevated rates of net primary production (NPP), NO_3^- uptake and carbon export (e.g., Korb et al. 2005; Blain et al. 2007; Seeyave et al. 2007; Lourantou and Metzl 2011; Jones et al. 2012; 2015; Cavagna et al. 2015; Planchon et al. 2015). By contrast, iron is supplied to surface waters in the open Southern Ocean by ice melting, upwelling, diapycnal diffusion and mixed layer entrainment (Grotti et al. 2001; Moore et al. 2002; Law et al. 2003; Alderkamp et al. 2012; Tagliabue et al. 2014).

Iron concentrations in open Southern Ocean surface waters are low (<0.2 nM), and a north to south gradient has been suggested, with the highest concentrations occurring further south (Tagliabue et al. 2014; Mtshali et al. 2019; Viljoen et al. 2019); this trend is not always observed, however (Tagliabue et al. 2012). Within the open Southern Ocean are regions of slightly higher iron concentrations, such as at frontal features, melting sea ice and icebergs, and near active hydrothermal vents (Aguilar-Islas et al. 2008; Herraiz-Borrenguero et al. 2016; Ardyna et al. 2019). Additionally, iron concentrations are generally higher in the winter season due to the deep mixed layers that entrain subsurface iron into the shallows (Tagliabue et al. 2014; Mtshali et al. 2019). Surface iron replenishment is quite difficult, however (Tagliabue et al. 2014; Janssen et al. 2020), because the depth at which iron concentrations begin to rise (ferricline depth) is much greater than the nutricline depth (Croot et al. 2007). The existence of this deep ferricline has been suggested to be due to the disproportionately high demand for iron by phytoplankton (particularly diatoms), which results in extremely low concentrations of iron in shallow waters (Christian et al. 2001), as well as the fact that iron adsorbs onto particles sinking out of the euphotic zone (Boyd et al. 2012a).

The role of iron in phytoplankton utilisation of N has been recognized since the early 1900s (Gran 1931; Hart 1934). Gran (1931) surmised based on experiments with temperate phytoplankton that diatoms in the Southern Ocean may be iron-limited since NO_3^- and PO_4^{3-} were always high, while Hart (1934) proposed that iron was one of the factors limiting primary production in the Weddell Sea, Bransfield Strait and Bellingshausen Sea. However, shipboard iron-enrichment experiments conducted under trace metal-clean conditions and displaying enhanced phytoplankton growth in response to iron additions were not performed until the late 1980s and early 1990s (de Baar et al. 1990; Martin et al. 1990; 1991; Buma et al. 1991). Indeed, in perhaps the most famous study of iron and phytoplankton in HNLC regions, including the Southern Ocean, Martin et al. (1991) showed that phytoplankton grown in bottles with added iron quickly bloomed, increasing their growth rates to near-optimum values, and strongly removing NO_3^-. Since then, the importance of iron for phytoplankton growth in the Southern Ocean has been repeatedly demonstrated, both through small- and large-scale iron-enrichment experiments and in naturally iron-fertilized environments such as Kerguelen Island and the Crozet Plateau (e.g., Nelson and Smith 1991; Sunda and Huntsman 1997; Boyd et al. 1999, 2007; Korb et al. 2005; Blain et al. 2007; Seeyave et al. 2007; Cavagna et al. 2015). Iron has a potential to change phytoplankton community structure, with a shift from smaller phytoplankton cells to dominance by diatoms often observed when phytoplankton are incubated in seawater spiked with iron (Boyd et al. 2000). Such a shift is good for export production as diatoms generally sink faster than other phytoplankton groups (Buesseler 1998a; Ducklow et al. 2001b; Armstrong et al. 2009). On the other hand, increased iron concentrations do not always stimulate diatom growth. Indeed, a shift from a diatom-dominated phytoplankton community to one dominated by smaller *Phaeocystis spp* was observed in response to iron enrichment in the Ross Sea and interpreted as indicating that *Phaeocystis spp* may need more iron to bloom than diatoms (Coale et al. 2003). While a phytoplankton community dominated by smaller cells could imply a negative effect on carbon export, *Phaeocystis spp* fixes far more carbon per PO_4^{3-} consumed than diatoms (Arrigo et al. 1999, 2000), making them important contributors to carbon export.

Other trace metals such as copper, zinc, and manganese are also essential to phytoplankton growth and nutrient uptake (Bruland 1980; Rueter and Morel 1981; De La Rocha et al. 2000; Twining and Baines 2013;Cloete et al. 2019) and so have the potential to limit productivity. For example, zinc is required in carbonic anhydrase, responsible for CO_2 hydration during photosynthesis (Twining and Baines 2013), and during the uptake of $Si(OH)_4$ by diatoms

(Rueter and Morel 1981; De La Rocha et al. 2000), manganese is necessary for water oxidation during photosynthesis, and copper is required for photosynthetic electron transport (da Silva and Williams 2001). Recently, phytoplankton activity was shown to be co-limited by manganese and iron in the central Drake Passage (Browning et al. 2021) and *Phaeocystis antarctica* in culture and the Ross Sea were found to experience co-limitation of manganese and iron (Wu et al. 2019).

1.3.3 Light availability

Light is necessary for phytoplankton primary production because during photosynthesis, it is absorbed as photons and converted to chemical energy in the form of ATP (adenosine triphosphate) (Behrenfeld and Milligan 2013). This chemical energy is then used to reduce water and CO_2 to produce three-carbon sugars. The dependence of phytoplankton uptake of N (NO_3^-, NH_4^+ and urea) on light availability often follows a rectangular hyperbolic relationship that can be mathematically fit by a Michaelis-Menten-type equation (e.g., MacIsaac and Dugdale 1972; Slawyk 1979; Paasche et al. 1984; Cochlan et al. 1991; Priscu et al. 1991; Muggli and Smith 1993; Kudela et al. 1997; Hu and Smith 1998; Kudela and Cochlan 2000; Lim et al. 2006). That said, growth on NO_3^- requires far more energy than NH_4^+ and urea (Dortch 1990; Lomas 2004), leading to the expectation that NO_3^- uptake rates should decrease with depth in the euphotic zone while reduced N uptake rates remain fairly constant or even increase (e.g., Peng et al. 2018; Kim et al. 2020; Mdutyana et al. 2020). In the Southern Ocean, the reliance of N uptake on irradiance has not received much attention and the research that exists reports unclear and/or contradictory observations (Glibert et al. 1982; Collos and Slawyk 1986). There is, however, agreement in that NH_4^+ requires less irradiance while NO_3^- requires more (Slawyk 1979; Nelson and Smith 1986; Hu and Smith 1998). Photoinhibition of N uptake has also been observed (e.g., MacIsaac and Dugdale 1972; Hu and Smith 1998; Planas et al. 1999), but it appears to be unusual. Overall, the relationship of NO_3^- uptake to light availability is unclear in the Southern Ocean during summer when maximum rates have been observed throughout the euphotic zone in some cases (Joubert et al. 2011; Thomalla et al. 2011b; Philibert et al. 2015), while in others, maximum rates were measured only at the surface (Mdutyana et al. 2020). One explanation for this contrasting response is that the studies cited above occurred at different times during the summer growing season, as well as in different years. The phytoplankton assemblage changes over the course of a growing season, which is

near-certain to affect the community-level response (in terms of N uptake and productivity) to light availability (Hu and Smith 1998).

In the Southern Ocean, phytoplankton are exposed to light conditions that are controlled by three factors: 1) the time of year, 2) the degree of ice cover, and 3) the depth of vertical mixing, (Smith and Sakshaug 1990; Cochlan 2008). In general, it appears that Southern Ocean phytoplankton are well-adapted to their *in situ* light conditions, altering their maximum photosynthetic rates and efficiencies as the ambient light field changes (Harrison and Platt 1986). The amount of photosynthetically active radiation (PAR) available at the surface is dependent on the latitude and seasonal and diurnal effects, while at-depth irradiance depends on the light attenuation coefficient of a particular column of seawater. Light penetration decreases exponentially with depth, and light attenuation is strongly controlled by the abundance of phytoplankton and their detrital products (particulate and dissolved), which alter light absorption and scattering (Morel 1988). Light is considered insufficient for phytoplankton growth at the depth by which it has attenuated to between 1 and 0.1% of its surface value (i.e., the euphotic zone depth; Kirk 1984). However, more important than whether phytoplankton are at times located below the euphotic zone is the relationship between the euphotic zone and mixed layer depths, as this determines whether phytoplankton receive sufficient light energy for total photosynthesis to exceed total respiration. The "critical depth", first articulated by Sverdrup (1953) for the North Atlantic, refers to the mixed layer depth required for water column-integrated phytoplankton production to exceed respiration, resulting in the initiation of a bloom. While a number of other hypotheses have since been put forward to explain bloom development (e.g., the changes in mixing intensity rather than mixing depth ("critical turbulence hypothesis"; Huisman et al. 1999); the balance between phytoplankton growth and grazing ("dilution-recoupling hypothesis"; Behrenfeld 2010), the seasonality of the mixed layer depth and its positioning relative to the critical depth remains key to bloom initiation in the Southern Ocean (e.g., Swart et al. 2015).

Mixed layer depths in the Southern Ocean display strong seasonality and zonal gradients, with winter characterized by deeper mixed layer depths than spring and summer (Dong et al. 2008; Sallée et al. 2010; Du Plessis et al. 2019). The different sectors of the Southern Ocean also vary in their maximum winter mixed layer depths with the Indian and Pacific sectors characterized by deeper mixed layers (160-400 m) than the Atlantic sector (100-180 m; Dong et al. 2008), and the AZ experiencing shallower winter mixed layers (80-250 m) than the SAZ (160-320 m;

Dong et al. 2008; Sallée et al. 2010; Du Plessis et al. 2019). The timing of phytoplankton bloom formation in the Southern Ocean can be affected by transient events of mixed-layer deepening and re-stratification, which can both delay the start of the bloom and sustain productivity throughout the summer (Thomalla et al. 2011a; Carranza and Gille 2015; Swart et al. 2015). Phytoplankton growing in a shoaled mixed layer depth are exposed to light for longer periods, which results in production exceeding respiration (Sverdrup 1953), leading to the formation of a phytoplankton bloom provided that growth is not nutrient (i.e., iron) limited. In other words, phytoplankton growth is strongly affected by the shoaling and deepening of the mixed layer (Nelson and Smith 1991), which affects not only light availability but also nutrient supply.

1.3.4 Temperature

Temperature is expected to play a role in controlling phytoplankton growth rates, photosynthesis, uptake of N, and community composition and succession (e.g., Eppley 1972; Neori and Holm-Hansen 1982; Tilzer et al. 1986; Raven and Geider 1988; Davidson 1991; Lomas and Glibert 1999a; b; Berges et al. 2002) given the effect of this variable on enzyme function (Tilzer and Dubinsky 1987). Across the Southern Ocean, the mixed-layer temperature gradient is large, with sea surface temperatures ranging from -1.8°C near Antarctica to ~17°C at the STF. Seasonally, the change in temperature is far smaller, on the order of 1°C to 2°C. While considerable work has been done investigating the influence of temperature on photosynthesis and N uptake (e.g., Davidson 1991 and references therein; Thompson et al. 1992a; b), most of the available data are for experiments conducted at temperatures far higher than those applicable to the polar Southern Ocean. An additional complication is that the natural gradient in temperature with latitude in the Southern Ocean coincides with a gradient in light and nutrient availability, such that disentangling the effect of temperature from other drivers is complex (e.g., Slawyk 1979; Chapter 3 of this thesis).

Phytoplankton consumption rates of NO_3^- and NH_4^+ appear to display different responses to temperature changes, although in the field, it is difficult to separate the temperature effect from that of phytoplankton assemblage changes and nutrient availability (Slawyk 1979; Olson 1980; Kanda et al. 1985; Harrison et al. 1996). There is also some evidence that the negative effect of temperature on phytoplankton growth is enhanced under high-nutrient and low-light conditions (Baird et al. 2001). Additionally, polar Southern Ocean phytoplankton appear to be psychrotolerant rather than psychrophilic, which means that their optimal temperatures for

growth and photosynthesis are higher than the *in situ* temperatures that they experience (Tilzer et al. 1986; Smith and Harrison 1991; Reay et al. 2001). Nonetheless, Southern Ocean species achieve their maximum growth rates at temperatures that are considerably lower than the optimal growth temperatures of temperate and tropical species (2-9°C versus >>10°C), with a sharp decline in Southern Ocean phytoplankton growth observed for temperatures outside this range (Fiala and Oriol 1990; Boyd et al. 2013; Coello-Camba and Agustí 2017). Temperature has been shown to exert a control on NH_4^+ uptake, especially in winter (Olson 1980; Glibert et al. 1982; Reay et al. 2001), although to a lesser extent than on NO_3^- uptake (Reay et al., 2001). On the other hand, in Antarctic sea-ice when phytoplankton were examined for their specific uptake (i.e., N uptake normalised by biomass; a proxy for growth rate) capabilities in relation to temperature, specific NO_3^- uptake increased with increasing temperature while specific NH_4^+ uptake did not show any temperature dependence (Priscu et al. 1989). In the Arctic Ocean, by contrast, NH_4^+ uptake has been observed to be affected by changes in temperature (Baer et al. 2014).

While the fairly small, seasonal temperature changes may present unique challenges to phytoplankton growth in the Southern Ocean, temperature might be more important in one season while in another season, phytoplankton growth and ecology might be dominantly controlled by other environmental factors such as light and/or macronutrient- and iron availability (Boyd 2002; Smith and Lancelot 2004; Viljoen et al. 2019).

1.3.5 Grazing

Prior to the recognition of iron limitation in Southern Ocean surface waters, many researchers believed that the summertime bloom was terminated by increased grazing pressure (Hart 1942; Chisholm and Morel 1991), which both reduced the capacity for rapid phytoplankton growth and provided a competing N source to phytoplankton in the form of regenerated NH_4^+ (e.g., El-Sayed 1984). It remains possible that this dynamic is important, and it may be strongly related to the onset of iron limitation (Tagliabue et al. 2014). The relationship between phytoplankton and zooplankton strongly controls the quantity of exportable carbon in Southern Ocean (Banse 1996; Smetacek et al. 2004). Larger phytoplankton are predominantly grazed upon by meso- and microzooplankton, which contribute to carbon sinking out of the euphotic zone through faecal pellet production (Banse 1996; Irigoien et al. 2005). By contrast, when the ambient conditions promote the growth of small phytoplankton, they are grazed upon by

microzooplankton that channel carbon into the microbial loop within the euphotic zone, resulting in enhanced carbon and nutrient recycling and minimal carbon removal (Banse 1996; Froneman and Perissinotto 1996; Fielding et al. 2007).

While it is broadly recognized that iron availability exerts the dominant control on phytoplankton growth rates in the open Southern Ocean (e.g., Martin 1990; Nelson and Smith 1991; Sunda and Huntsman 1997), grazing nonetheless plays an important role in biogeochemical cycling and the structure and function of phytoplankton communities. Indeed, grazing represents a mechanism by which iron is recycled in surface waters (Rafter et al. 2017; Ratnarajah et al. 2018; Richon et al. 2020). For example, under iron replete conditions, *Phaeocystis* and small and/or weakly-silicified diatoms grow fast and develop into blooms that fuel upper trophic levels and export carbon below the euphotic zone, while under iron-limitation, grazing pressure exerted by copepods on microzooplankton can result in bloom formation of large and heavily-silicified diatoms because their predators are feeding elsewhere (Smetacek et al. 2004). Viral lysis – the breakdown of plankton cell membranes following viral infection – has been shown to be important in structuring phytoplankton communities in other oceanic regions (e.g., Evans et al. 2003; Baudoux et al. 2006; Lara et al. 2017; Mateus 2017; Zhang et al. 2020a), while in the Southern Ocean, some studies have found to be less important, with grazing playing the dominant role (Brussaard et al. 2008; Evans and Brussaard 2012). However, recent work from the Southern Ocean and Antarctic coastal waters indicate that viral lysis might be more important than previously thought, especially in controlling phytoplankton community composition in different seasons (Biggs et al. 2021; Evans et al. 2021).

The bottom-up and top-down controls on phytoplankton growth described above do not operate in isolation. Instead, it is the interaction of these controls, along with the composition of the phytoplankton community, that determines the extent of phytoplankton growth and N uptake in the Southern Ocean. For example, mixed layer depth (light availability) in combination with iron availability should have different effects on the activity of different phytoplankton groups. Diatoms under replete iron conditions perform better when the mixed layer is shallow, meaning that in summer when iron concentrations are relatively high, diatoms become most important in the uptake of NO_3^- (Viljoen et al. 2018). In winter, even with the elevated iron concentrations (Tagliabue et al. 2014), diatom growth becomes hampered by the deep mixed layers (Viljoen et al. 2018). As a further example, high iron and low light conditions (such as in early spring) favour the growth of smaller phytoplankton like *Phaeocystis spp* (Tozzi and Smith 2017;

Wojtasiewicz et al. 2019). Additionally, both light and temperature may influence the extent to which NH_4^+ inhibits NO_3^- uptake, with diatoms and dinoflagellates in temperate waters experiencing a decrease in the extent of NH_4^+ inhibition with a decline in temperature (Lomas and Glibert 1999a; b), while cultures of the diatom, *Thalassiosira pseudonana*, experienced no inhibition under low light, whereas at moderate and high light, NO_3^- uptake was inhibited by 60-70% (Yin et al. 1998).

1.4 Nitrification and its environmental controls

Nitrification is a two-step biological process facilitated by distinct groups of microorganisms (bacteria and archaea) that results in the oxidation of NH_4^+ (actually, ammonia (NH_3), which exists in equilibrium with NH_4^+) via NO_2^- to NO_3^-. NH_4^+ oxidation is performed by two separate groups of microorganisms: ammonia oxidizing archaea (AOA) (Francis et al. 2005; Könneke et al. 2005; Hallam et al. 2006b; Wuchter et al. 2006) and ammonia oxidizing bacteria (AOB) (Rotthauwe et al. 1997; Purkhold et al. 2000), with AOA being relatively more abundant shallower in the water column (Newell et al. 2013; Peng et al. 2016; Shiozaki et al. 2016). NH_4^+ oxidation was previously thought to occur in two steps, the oxidation of NH_4^+ to hydroxylamine (NH_2OH) and the subsequent oxidation of NH_2OH to NO_2^-, while NO_2^- oxidation is a single-step process. Recently, however, NH_4^+ oxidation was found to be a three-step process, whereby the NH_2OH resulting from the NH_4^+ oxidation is first converted to nitric oxide (NO) and then to NO_2^- (Kozlowski et al. 2016a; Caranto and Lancaster 2017). For decades it was also believed that no microorganism could catalyse both steps of the nitrification pathway until a complete nitrifying organism (i.e., capable of concomitant NH_4^+ and NO_2^- oxidation) belonging to the nitrite oxidizing bacteria (NOB) *Nitrospira* genus and referred to as "comammox" was discovered in a biofilm and cultivated in the laboratory (Daims et al. 2015; van Kessel et al. 2015). To date, however, comammox has not been found in the ocean.

Nitrification is an important pathway in N cycle, linking its most oxidized and reduced components, contributing to their distribution in the ocean, and exerting a control on carbon export potential. It is therefore necessary to understand the constraints imposed on nitrification by environmental factors, which are additionally important for parameterizing nitrification in biogeochemical models. In the open ocean, nitrification may be controlled to a greater- or lesser extent by several environmental factors (light, temperature, salinity, and oxygen) and micro- and macronutrient availabilities (copper, iron, NH_4^+ and NO_2^-), each discussed below.

1.4.1 Substrate availability

NO_2^- and NH_4^+ concentrations in the mixed layer of most of the open ocean are near-zero (Lomas and Lipschultz 2006; Paulot et al. 2015; Zakem et al. 2018); therefore, assuming nitrification is not limited by some other factor (e.g., light; see below), there is an expectation that increased substrate availability should result in higher rates of substrate oxidation. NO_2^- oxidation rates at the base of the mixed layer have been shown to increase as ambient NO_2^- concentrations rise (Olson 1981a; Peng et al. 2018; Mdutyana et al. 2020), yet it has historically proven difficult to experimentally show the dependence of NH_4^+ oxidation on substrate availability by natural assemblages in the open ocean (Olson 1981a; Ward and Kilpatrick 1990). The lack of a successful demonstration of substrate dependence by NH_4^+ oxidizers has been interpreted as indicative of a very high affinity for NH_4^+ (Olson 1981a; Ward and Kilpatrick 1990); this was later confirmed by Martens-Habbena et al. (2009) who found a high affinity (low K_m = 134 nM) for NH_4^+ in the AOA, *Nitrosomopumilus maritimus* SCM1, in a culture study. Later studies conducted *in situ* using natural assemblages confirmed the high affinity of AOA for NH_4^+, reporting an even lower K_m (of between 27 and 98 nM) than was derived in culture (Horak et al. 2013; Newell et al. 2013; Peng et al. 2016). *In situ* kinetics associated with NO_2^- oxidation are limited compared to those derived from culture studies, with NO_2^- affinity by NOB in culture proving extremely low, with very high K_m values (from 9-544 µM; Nowka et al. 2015; Ushiki et al. 2017). By contrast, the affinity of NOB for NO_2^- from the limited *in situ* marine studies is orders of magnitude higher, evinced by the low K_m values (ranging from 0.07-0.51 µM; Olson 1981; Sun et al. 2017; Zhang et al. 2020).

It is generally easier to demonstrate substrate dependence of a biogeochemical pathway when the ambient nutrient of interest occurs at low concentrations, except in special cases where the organisms are adapted to high concentrations (e.g., NOB in high-NO_2^- (1.8 ± 0.2 µM) waters of oxygen deficient zones have been reported to have a K_m of 8.0 ± 2.4 µM; Sun et al. 2021). The Southern Ocean has seasons of replete mixed-layer NH_4^+ concentrations (e.g., Henley et al. 2020; Mdutyana et al. 2020) and NO_2^- concentrations are perennially elevated within the mixed layer compared to the lower latitudes (200-400 nM; Cavagna et al. 2015; Zakem et al. 2018; Fripiat et al. 2019; Mdutyana et al. 2020). It is thus possible that these higher substrate concentrations will stimulate elevated rates of nitrification. Indeed, a few studies have observed increasing rates of oxidation coincident with higher NH_4^+ and NO_2^- concentrations in the mixed layer (Olson 1981; Bianchi et al. 1997; Mdutyana et al. 2020). However, prior to the work

presented in this thesis, no substrate-addition experiments had been conducted for NH_4^+ or NO_2^- oxidation in the open Southern Ocean.

1.4.2 Light availability

Light availability is thought to regulate nitrification in two ways: First, via direct light inhibition of nitrifying organisms (Schön and Engel, 1962; Hooper and Terry, 1974; Horrigan et al. 1981; Vanzella et al. 1989; Olson 1981) and second, by phytoplankton outcompeting nitrifiers for N substrate in the euphotic zone because of the replete light conditions (Ward 1985, 2005a; Smith et al. 2014; Zakem et al. 2018). The net effect is that nitrifiers are generally more active around the base of the mixed layer than at the surface (e.g., Ward et al. 1989; Yool et al. 2007; Beman et al. 2012; Peng et al. 2015; 2018; Shiozaki et al. 2019), although a number of studies have observed rates of nitrification throughout the euphotic zone that are high relative to the upward supply and consumption of subsurface NO_3^- (e.g., Dore and Karl 1996; Wankel et al. 2007; Yool et al. 2007; Cavagna et al. 2015; Mdutyana et al. 2020). That nitrification is generally higher at-depth in the euphotic zone/mixed layer (i.e., under conditions of low light availability) might be taken as an indication that direct light inhibition of nitrifiers exerts a dominant control on the distribution of nitrification. However, several studies have demonstrated that phytoplankton growth on NH_4^+ in the euphotic zone most strongly controls the activity of nitrifiers by rapidly depleting the NH_4^+ substrate (Ward 2005b; Smith et al. 2014; Zakem et al. 2018). In other words, once phytoplankton NH_4^+ consumption becomes light-limited, nitrifiers can maximise their uptake of the available substrate, resulting in a peak in the nitrification rates around the base of the mixed layer/euphotic zone.

Different nitrifying organisms also seem to experience light inhibition differently, with NOB apparently more sensitive to light than AOB in both culture and various marine environments (Bock 1965; Olson 1981b; Vanzella et al. 1989; Guerrero and Jones 1996). Additionally, AOA appear to be less light-inhibited than NOB, but have been reported to be more photosensitive than AOB, particularly at lower light intensities (Merbt et al. 2012a; Qin et al. 2014). In the case of AOA, this sensitivity has been shown to vary with strain, with SCM1 observed to be significantly less photosensitive than two other isolates (HCA1 and SP0) at both low and high light (Qin et al. 2014). Additionally, there appear to be two broad ecotypes of AOA that occupy two different parts of the water column (Francis et al. 2005; Hallam et al. 2006a; Mincer et al. 2007; Beman et al. 2008; Santoro et al. 2010; Sintes et al. 2013; Luo et al. 2014). The shallow-

ecotype may have adaptive mechanisms to reduce light induced-damage (Sintes et al. 2013; Luo et al. 2014; Santoro et al. 2017), although other variables such as substrate (Sintes et al. 2013; Smith et al. 2016) and micronutrient availability (Amin et al. 2013) have also been hypothesized to drive the depth-preference of AOA ecotypes. The putative light tolerance of the shallow AOA ecotype may help to explain elevated rates of nitrification within the euphotic zone in some ocean regions, although this is unlikely the only reason.

1.4.3 Temperature

Temperature is broadly important for bacterial activities (Delille 2004), yet nitrifying organisms are not known to be strongly affected by temperature (Bianchi et al. 1997; Horak et al. 2013; Baer et al. 2014). Instead nitrifiers appear to be well-adapted to the environmental conditions in which they are found (Ward 2008 and references therein). This notion is supported by the observation that nitrifying organisms occur in environments characterized by a broad range of temperatures (-5 to 97°C; Jones et al. 1988; Thamdrup and Fleischer 1998; Erguder et al. 2009; Ngugi et al. 2016; Rani et al. 2017), with nitrifiers adapted to warm environments achieving comparable rates of nitrification at elevated temperatures as cold-temperature-adapted nitrifiers living in cold environments. For example, Arctic sediment nitrifiers show a range of optimal temperatures of 14 to 40°C (Thamdrup and Fleischer 1998), while deep-sea brine nitrifiers can function at temperatures as high as 65°C (Ngugi et al. 2015; 2016). Additionally, a broad range of temperatures is thought to be important for regulating the distribution of ammonia oxidizing organisms in various environments including the water column (Mosier and Francis 2008; Dang et al. 2010; Cardoso et al. 2013; He et al. 2018). In sum, while temperature is important for all biological rates, the regulatory effect of this parameter on nitrification seems to be weaker than that of a number of other variables (Ward 2008 and references therein).

1.4.4 Salinity

Salinity exerts an important (potentially dominant) control on nitrification in rivers (Pakulski et al. 1995, 2000) and estuaries (Somville 1984; De Bie et al. 2001; Bernhard et al. 2010; Santos et al. 2020) where this parameter can be highly variable. The activity, abundance, and diversity

of ammonia oxidizers have been shown to be highly impacted by changes in salinity in estuaries (Francis et al. 2003; Li et al. 2015; Zhang et al. 2015; Santos et al. 2018). For instance, although some ammonia oxidizers are halotolerant (Bernhard et al. 2007; Wang and Gu 2014), high salinity appears to decrease estuarine AOB populations (Bernhard et al. 2005; 2010). Additionally, short-term fluctuations in salinity (daily fluctuations) in estuarine sediments have recently been shown to negatively affect both AOA and AOB, decreasing nitrification rates compared to conditions of constant salinity (Santos et al. 2020). NOB communities are also affected by high salinity, declining in abundance relative to AOA (Monteiro et al. 2017). While there is evidence of the role of salinity in estuaries, salinity does not fluctuate much in the open ocean and is thus not expected to affect the rates of nitrification in the Southern Ocean. However, while ice melt should cause a change in salinity, whether it impacts the rates of nitrification is currently unknown.

1.4.5 Oxygen

Nitrifiers are traditionally considered obligate aerobes, requiring molecular oxygen for respiration and for N oxidation reactions (Ward 2011). However, nitrifiers have also been found under microaerophilic conditions (Bristow et al. 2016; Penn et al. 2016), leading to suggestions that they thrive at fairly low-oxygen concentrations and in interface environments (e.g., sediment-water interface, across sharp oxygen gradients; Ward 2008 and references therein). While the majority of the open ocean is oxygenated, there are a few oceanic regions with low- to zero-oxygen concentrations in the water column, known as oxygen deficient zones (ODZs). Curiously, these zones appear to support high rates of NO_2^- oxidation, including under anoxic conditions (Lam et al. 2009; Zehr 2009; Füssel et al. 2012; Sun et al. 2021), although there is always the danger that oxygen may have been introduced into experiments during sampling and/or incubation processing.

Nonetheless, the fact that nitrification is possible in the ODZs suggests the existence of a group(s) of nitrifiers with a high affinity for low concentrations of oxygen (Füssel et al. 2012; Bristow et al. 2016; Sun et al. 2017). Sun et al. (2017) observed the inhibition of NOB in the Eastern Tropical North Pacific (ETNP) ODZ by the addition of incremental quantities of oxygen, resulting in a decrease in NO_2^- oxidation rates with increasing oxygen. By contrast, Bristow et al. (2016) observed a rise in both NH_4^+ and NO_2^- oxidation rates in the ODZ off Chile in response to oxygen additions, although both processes were still detectable under

conditions of virtually zero oxygen. In the case of NO_2^- oxidation, there appeared to be two main groups of NOB – one adapted to extremely low oxygen conditions (i.e., with a K_m of <5 nM O_2 when the experimental NO_2^- oxidation rates were plotted against oxygen concentration) and the other adapted to higher oxygen (K_m of ~2 μM O_2), while NH_4^+ oxidation was best described by a single-component Michaelis-Menten model, yielding a K_m of ~330 nM O_2 (Bristow et al. 2016). The implication of these findings, strongly supported by molecular analyses (i.e., DNA sequencing, metagenomics and metatranscriptomics; Sun et al. 2019, 2021), is that some NOB are especially adapted for lower oxygen environments, with marine NOB more broadly having different oxygen sensitivities and affinities (Watson and Waterbury 1971; Bristow et al. 2016; Ngugi et al. 2016; Füssel et al. 2017; Sun et al. 2017). Indeed, Sun et al. (2021) recently showed niche differentiation of NOB along an oxygen gradient in the ETNP ODZ, with novel clades of NOB present in high abundances in zero-oxygen waters. It is worth saying however, that oxygen may not be important for nitrification in the Southern Ocean as the entire region is well oxygenated.

1.4.6 Trace metal availability

In the Southern Ocean, iron is the major micronutrient that limits primary production and N uptake by phytoplankton (e.g., de Baar et al. 1990; Moore et al. 2013). In nitrifying organisms, the enzymes that facilitate the oxidation of NH_4^+ to NO_3^- via NO_2^- require trace metals (iron and copper) as cofactors and as part of their electron transport chain complexes (Morel and Price 2003; Walker et al. 2010). Iron is an important cofactor in the enzymes that are responsible for NH_4^+ and NO_2^- oxidation by nitrifying bacteria (Sundermeyer-Klinger et al. 1984; Meincke et al. 1992; Arp et al. 2002; Wei et al. 2006; Lücker et al. 2010; Walker et al. 2010). AOB possess iron-rich *cytochrome c* proteins that they use for the oxidation of hydroxylamine to NO, catalysed by the iron-rich hydroxylamine oxidoreductase (HAO) complex (Arp et al. 2002; Walker et al. 2010). NOB also contain iron-rich enzymes, such as nitrite oxidoreductase, which is responsible for the conversion of NO_2^- to NO_3^- (Meincke et al. 1992; Spieck et al. 1998). While no genes have yet been discovered in the open ocean that encode an iron-containing HAO in AOA analogous to that of AOB (e.g., Hallam et al. 2006a; Wei et al. 2006; Walker et al. 2010; Blainey et al. 2011; Mosier et al. 2012; Amin et al. 2013), some AOA species (*N. maritimus* SCM1 and *Candidatus* Nitrosopelagicus brevis) possess iron-sulphur ferredoxin (Santoro et al. 2015; Carini et al. 2018; Qin et al. 2018), hypothesized

to be important for AOA electron transport (Shafiee et al. 2019). Recently, a culture study examining NH_4^+ oxidation by the globally-abundant AOA, *N. maritimus* SCM1, indicated that iron is necessary for AOA NH_4^+ oxidation and that these nitrifiers may have both a high iron requirement and a low affinity for iron (Shafiee et al. 2019). To-date, however, no open ocean study has directly tested the dependence of N oxidation on iron availability. Anecdotal evidence of the role played by iron during nitrification in the Southern Ocean is that naturally iron-fertilized regions (e.g., Kerguelen Island, South Georgia Island and others) have been observed to support high rates of nitrification compared to nearby HNLC waters (Cavagna et al. 2015; Dehairs et al. 2015; Fripiat et al. 2015; Mdutyana et al. 2020).

Copper is not thought to dominantly limit primary production across most of the Southern Ocean because its concentrations are fairly high (Monteiro and Orren 1985; Ellwood 2008; Heller and Croot 2015; Cloete et al. 2019). This element plays an important role in the oxidation of NH_4^+ to NO_2^- by both AOA and AOB as the cofactor of the enzyme, ammonia monooxygenase (AMO) (Lieberman and Rosenzweig 2005), and is thought to be involved in electron transport in AOA (Hallam et al. 2006a; Wei et al. 2006; Walker et al. 2010; Blainey et al. 2011; Amin et al. 2013; Santoro et al. 2015). The requirement of AOA for copper has been tested in culture, and it was found that NH_4^+ oxidation can be limited by copper (Amin et al. 2013). A wastewater study evaluating the role of copper in NH_4^+ oxidation observed stimulated NH_4^+ oxidation rates when copper was added, although AOB appeared unaffected by the addition of copper, meaning that the enhancement was due to AOA (Gwak et al. 2020). As with iron, the influence of copper availability on nitrification has not been investigated in the Southern Ocean – it is possible that copper may be limiting in the northern regions of the Southern Ocean where ambient copper concentrations are much lower than to the south (0.5 versus 2.0 nM; Ellwood et al. 2008; Heller and Croot 2015; Cloete et al. 2019).

1.5 Distribution and composition of nitrifier communities in the open ocean

Nitrification is conducted by distinctly different groups of microorganisms, with AOA and AOB facilitating NH_4^+ oxidation and NOB catalysing NO_2^- oxidation. AOA were discovered in the early 2000s when genes encoding for AMO were detected from a 1.2 Gb fosmid library of a sandy soil ecosystem (Treusch et al. 2005), which eventually led to the isolation of the first ammonia-oxidizing MG-1 archaeon, *Nitrosopumilus maritimus*, from a seawater aquarium (Könneke et al. 2005). The composition and distribution of nitrifier communities, which varies

with depth in the water column and spatially across most of the open ocean, will influence the cycling of N and its implications for carbon (e.g., Beman et al. 2008; Newell et al. 2011; Füssel et al. 2012; Pachiadaki et al. 2017; Pajares and Ramos 2019; Sun et al. 2021). However, in the Southern Ocean there is little data on nitrifier community composition, with only a single study to-date from the Pacific sector (Raes et al. 2020).

Overall, AOA outnumber AOB in the global ocean (e.g., Beman et al. 2008; Newell et al. 2011; Pajares et al. 2019) and while the mesopelagic water column can be dominated by either NH_4^+ oxidizing group (Church et al. 2010; Newell et al. 2013; Shiozaki et al. 2016), AOA appear to dominate the upper layer, including the euphotic zone (Beman et al. 2012; Newell et al. 2013; Shiozaki et al. 2016). It has been hypothesized that the dominance of AOA is due to the fact that 1) they have an extremely high affinity for NH_4^+ (Martens-Habbena et al. 2009; Horak et al. 2013; Newell et al. 2013; Peng et al. 2016; Zhang et al. 2020b); 2) at depth where NH_4^+ concentrations are depleted, AOA can get their nutrition by oxidizing other N forms such as urea (Sintes et al. 2013; Santoro et al. 2017; Laperriere et al. 2021); and 3) there are two broad AOA ecotypes that occupy different depth ranges in the water column (Francis et al. 2005; Hallam et al. 2006; Mincer et al. 2007; Beman et al. 2008; Santoro et al. 2010; Sintes et al. 2013; Luo et al. 2014), including a shallow-ecotype that appears to be photo-tolerant (Sintes et al. 2013; Luo et al. 2014; Santoro et al. 2017).

NOB have historically received less attention than ammonia oxidizers, likely because of 1) the difficulty in growing them in the laboratory (Lebedeva et al. 2008; Vekeman et al. 2013; Nowka et al. 2015), although it is worth noting that AOA are also extremely challenging to cultivate ((Könneke et al. 2005; Martens-Habbena et al. 2009; Santoro and Casciotti 2011; Santoro et al. 2011); 2) the discovery of AOA (Könneke et al. 2005) that re-energized research into NH_4^+ oxidation (Daims et al. 2016); 3) the fact that NH_4^+ oxidation has long been considered the rate-limiting step in the nitrification pathway (Kendall 1998; Kowalchuk and Stephen 2001 and references therein); and 4) the idea that NOB possess little in the way of physiological flexibility (Daims et al. 2016). However, NOB play a critical role in the marine N cycle, counteracting N loss by producing NO_3^- from NO_2^- and removing a potentially toxic form of N from the environment (Castellani and Niven 1955; Lewis and Morris 1986). Additionally, NOB are quite diverse and belong to seven genera that occupy different environments (Daims et al. 2016). The majority of marine NOB belong to the *Nitrospina* and *Nitrospira* genera (Füssel et al. 2012; Jorgensen et al. 2013; Beman et al. 2013; Levipan et al. 2014; Nunoura et al. 2015; Ngugi et al. 2016; Sun et al. 2019; 2021), the latter being the most

diverse and ubiquitous (Daims et al. 2001; Lebedeva et al. 2008; 2011). Nitrite oxidoreductase (NXR), the enzyme possessed by NOB that is responsible for oxidizing NO_2^- to NO_3^-, belongs to the group of molybdopterin-binding enzymes and has three substrate-binding subunits, NxrA, NxrB and NxrC (Lücker et al. 2010; 2013). The positioning of subunit NxrA within the cell is different in the different genera of NOB, which may have implications for energy allocation during NO_2^- oxidation (Lücker et al. 2010; Daims et al. 2016). Some NOB (*Nitrospira* and *Nitrospina*) have a periplasmic subunit NxrA, and the protons produced in the periplasm during NO_2^- oxidation contribute to the energy budget of the cell (Lücker et al. 2010, 2013; Koch et al. 2015). By contrast, the NxrA subunit is located in the cytoplasm of *Nitrococcus* and *Nitrobacter* (Spieck et al. 1996; Starkenburg et al. 2006), which means that these NOB have to transport NO_2^- and NO_3^- across the cytoplasmic membrane and that the protons generated during NO_2^- oxidation do not contribute to their cellular energy budget. This difference has been hypothesized to influence the economy of NO_2^- oxidation in the environment (Daims et al. 2016).

Until recently, it was believed that no single nitrifying organism could perform complete NH_4^+ oxidation to NO_3^-, despite the fact that complete nitrification (i.e., "comammox") theoretically yields more energy than either of the two steps (Costa et al. 2006). Comammox was discovered via enrichment from an aquaculture system and biofilm, and was found to belong to the *Nitrospira* genus (Daims et al. 2015; van Kessel et al. 2015). Comammox *Nitrospira* has since been hypothesized to be widespread in freshwater and terrestrial systems (Daims et al. 2015; van Kessel et al. 2015; Pinto et al. 2015; Palomo et al. 2016; Xia et al. 2018), as well as present in coastal waters (Xia et al. 2018). While there are no currently known open ocean comammox (Daims et al. 2015; Xia et al. 2018), this organism appears to be adapted to an oligotrophic lifestyle (Kits et al. 2017), such that it may yet be discovered in the open ocean. That said, this organism is unlikely to exist in the Southern Ocean given observations of a decoupling between the two steps of the nitrification pathway (Bianchi et al. 1997; Mdutyana et al. 2020).

1.6 Methodological approaches for investigating the upper ocean nitrogen cycle

Direct measurements of N cycle rates are most commonly made via the addition of a stable N isotope tracer (i.e., ^{15}N), an approach that has greatly advanced our understanding of N transport, uptake, assimilation, and regeneration in the ocean (see Lipschultz 2008 for a review; Mulholland and Lomas 2008; Ward 2008). The basic principle is that ^{15}N added to a source N

pool is transferred to the product N pool at the same rate as the naturally occurring ^{14}N and ^{15}N source; measurement of the extent of ^{15}N enrichment in the product pool over time allows for the rate of N transformation to be determined. This approach was initially focused on tracing ^{15}N from the dissolved nutrient pool (e.g., NO_3^-) to the particle pool (i.e., phytoplankton biomass, or particulate organic N; PON), largely because of the relative ease with which PON can be filtered from seawater (Dugdale and Wilkerson 1986; Knap et al. 1996; Lipschultz 2008 and references therein). Since then, an increasing awareness of the complexity of the N cycle, coupled with improvements in the analytical instrumentation and methods used for ^{15}N analysis and measurement of low concentrations of inorganic and organic N species, means that virtually all N cycle processes are amenable to investigation using the ^{15}N tracer approach.

One of the widest applications of the ^{15}N tracer method is in experiments designed to quantify phytoplankton N uptake rates in the ocean. Here, ^{15}N-labelled substrate (most often, $^{15}NH_4^+$ or $^{15}NO_3^-$) is added to natural seawater samples (ideally at $\leq$10% of the ambient concentration) that are then incubated for a period (hours) under simulated *in situ* temperature and light conditions. The added ^{15}N tracer that is incorporated into the biomass (PON) is then analysed using an elemental analyser (EA) coupled to an isotope ratio mass spectrometer (IRMS) that measures the atom percent (at%) enrichment of ^{15}N in the filtered PON. A similar approach can be used to measure net primary production (NPP; the fixation of inorganic carbon into particulate organic carbon (POC) biomass) via the addition of $H^{13}CO_3^-$ and the subsequent measurement of ^{13}C enrichment in the filtered POC (Cullen 2001). In order to precisely calculate the export production from NO_3^- and NH_4^+ uptake, measuring simultaneous N uptake and NPP is necessary (see Chapter 2 of this thesis; Peng et al. 2018; Mdutyana et al. 2020).

Nitrification rate measurements have come a long way from the days of monitoring changes in the concentrations of NH_4^+, NO_2^- or NO_3^- over the course of lengthy incubations (Rakestraw 1936; Von Brand et al. 1937), although this approach can still be useful for demonstrating net nitrification or modelling the combined net rate of nitrate production and consumption (Ward 2011). The most effective way of measuring nitrification is via the addition of ^{15}N isotope tracers and the subsequent tracking of either the enrichment or dilution of the unlabelled or labelled N pool, respectively (e.g., Olson 1981a; Ward et al. 1984; Ward 2011). The development of methods allowing for the conversion of NO_2^- and NO_3^- to N_2O gas (via the addition of azide in the case of NO_2^- (McIlvin and Altabet 2005) and using denitrifying bacteria that under anaerobic conditions convert NO_3^- to N_2O (Sigman et al. 2001), and the subsequent analysis of the ^{15}N-enriched N_2O via IRMS (Sigman et al. 2001; McIlvin and Casciotti 2011;

Weigand et al. 2016) has vastly improved our ability to accurately, precisely, and easily measure the rates of both NH_4^+ and NO_2^- oxidation in seawater (e.g., Santoro et al. 2010, 2020; Newell et al. 2011; 2013; Buchwald et al. 2015; Peng et al. 2015; 2018; Sun et al. 2017; 2019; 2021; Mdutyana et al. 2020; Raes et al. 2020).

N transformation kinetics experiments that focus on deriving kinetic parameters are incredibly rare as they are difficult and time-consuming to conduct and analyse. For example, in the Southern Ocean, only one study has investigated N uptake kinetics (Cochlan and Bronk 2001b), with none of the experiments conducted in the open ocean. Additionally, prior to the work detailed in this thesis, no nitrification kinetics experiments had been undertaken in the Southern Ocean. The basic idea behind a kinetic experiment is that the dependence of a biogeochemical process (e.g., N uptake or oxidation) on the availability of a particular substrate can be examined via the incremental addition of that substrate (labelled with ^{15}N) and the subsequent analysis of the rate of its transfer to or from the product pool, as outlined above. These experiments should yield a hyperbolic Michaelis-Menten relationship of N transformation rate to N substrate concentration provided that the rate of the transformation is limited by the substrate under investigation (e.g., MacIsaac and Dugdale, 1969; Ward and Kilpatrick, 1990; Harrison et al. 1996; Cochlan & Bronk, 2001; Horak et al. 2013; Newell et al., 2013; Peng et al. 2016). This means, for example, that it is not possible to conduct NO_3^- uptake kinetics experiments across most of the Southern Ocean given that NO_3^- is not limiting to phytoplankton. The kinetic parameters derived from the resultant Michaelis-Menten function – the maximum rate of substrate transformation (V_{max}) and the half-saturation constant (K_m), which is the substrate concentration at which the reaction rate (V) = $V_{max}/2$ – reveal important information about the physiological capabilities of, and constraints upon, the organisms consuming the substrate. The advent of the denitrifier method and the capacity to analyse N_2O via IRMS (Sigman et al. 2001; McIlvin and Casciotti 2011; Weigand et al. 2016) has greatly enhanced our ability to precisely measure very low additions of ^{15}N tracer, a requirement for accurate determination of the lower N transformation rates, necessary for the derivation of K_m in particular.

The ^{15}N methods have some negative, sometimes unavoidable, shortcomings. When phytoplankton communities growing under low N concentrations *in situ* are exposed to ^{15}N tracer additions that are high compared to the ambient concentrations, uptake rates become stimulated (Lipschultz 2008 and references therein). In this case, the rates should be considered potential rates. Also, nitrification can be influenced by isotope dilution resulting from the

production of newly-remineralized $^{14}NH_4^+$ that can then also be nitrified to NO_3^-. The stimulation of rates by ^{15}N tracer added to phytoplankton uptake experiments can lead to overestimation of the transport rates, while isotopic dilution during nitrification experiments by $^{14}NH_4^+$ can result in underestimation of the rates.

Throughout my thesis, I have employed ^{15}N isotope approaches to measure both N (NH_4^+ and NO_3^-) uptake and nitrification (NH_4^+ and NO_2^- oxidation), as well as quantifying NPP via ^{13}C-labeled carbon uptake. N uptake and NPP are seldom measured concurrently even though phytoplankton are responsible for both. The work described in chapter 2 exemplifies how considering these two elemental cycles together provides more information than can be gleaned from examining either one alone, and as a result, the work places additional important constraints on the functioning of the upper-ocean ecosystem. Nitrification measurements made using the ^{15}N isotope approach are discussed at length throughout the thesis; in all chapters, care has been taken to consider the implications of, and correct for, isotope dilution and/or stimulation of the N transformation rates due to ^{15}N-tracer addition.

1.7 Thesis Outline

This thesis is focused on characterizing N uptake and nitrification in the mixed layer of the Southern Ocean, and investigating the environmental factors influencing these processes. The work described herein was conducted across all the major frontal zones of two sectors of the Southern Ocean, the east Atlantic and west Indian sectors, referred to collectively in Chapter 3 as the "African sector". Broadly, the research presented here has enhanced the community's understanding of the complex relationship between upper-ocean N cycling and the biological pump in the vastly understudied Southern Ocean.

In the literature review above (*Chapter 1: General introduction and thesis overview*), I have introduced key concepts important for the entirety of the thesis, including the links between N and carbon cycling, and the known drivers of phytoplankton N uptake and nitrification by NH_4^+ and NO_2^- oxidizing organisms. I have also described the relevant analytical methods used for N cycle measurements. Below, I briefly summarize the contents of the remaining chapters.

Chapter 2: The seasonal cycle of nitrogen uptake and nitrification in the Atlantic sector of the Southern Ocean

N uptake by phytoplankton in the Southern Ocean has been widely studied, but with measurements concentrated in the summer season. In particular, wintertime rates of N uptake are limited, with no simultaneous measurements of NPP and N uptake in this season. Additionally, prior to the work described in this chapter, there existed no measurements of nitrification in the open Southern Ocean in summer or winter. Rates of NPP, N uptake (in the form of NH_4^+ and NO_3^-), and nitrification (both NH_4^+ and NO_2^- oxidation) were measured throughout the upper 200 m during two cruises, in winter (July 2015) and summer (Dec 2015-Feb 2016). The results demonstrate the importance of measuring N uptake concurrently with NPP, from which phytoplankton reliance on N sources other than NH_4^+ and NO_3^- can be inferred, and of simultaneously measuring nitrification and NO_3^- uptake, particularly in winter. Broadly, the data suggest that export production can be equated to NO_3^- uptake in summer (i.e., in the framework of the new production paradigm; Dugdale and Goering 1967), with a few exceptions where organic N uptake appeared to support significant (unmeasured) rates of regenerated production. Summer was characterized by a low- to undetectable contribution of nitrification to NO_3^- uptake by phytoplankton in the mixed layer, while in winter, regenerated NO_3^- constituted >100% of that assimilated by phytoplankton. Despite the negligible nitrification rates measured in summer, on an annual basis, the Southern Ocean does not suit the application of the new production paradigm as a framework for quantifying export production. This is because the NO_3^- utilised by phytoplankton in summer is partly regenerated in the deep winter mixed layer that has become the T_{min} layer that lies just below, and constantly exchanges with, the summer mixed layer.

Chapter 3: The kinetics of ammonium uptake and oxidation across the African sector of the Southern Ocean

In the winter season, the open Southern Ocean hosts elevated NH_4^+ concentrations (0.5-1.5 μM) throughout the mixed layer, particularly south of the Subantarctic Front. As reported in Chapter 2 of this thesis, high rates of NH_4^+ uptake and oxidation have been measured in the winter mixed layer across the Southern Ocean, yet mixed-layer NH_4^+ concentrations remain high (Mdutyana et al. 2020). The goal of the present chapter was thus to better understand the controls on the persistently elevated winter mixed-layer NH_4^+ concentrations by examining the

physiological capacity of phytoplankton in winter and summer and ammonia oxidizers in winter for NH_4^+ consumption. The kinetic parameters reported here are the first such data for the open Southern Ocean. The V_{max} associated with NH_4^+ uptake by phytoplankton was dominantly controlled by light in winter and temperature in summer, while the K_m increased with increasing ambient NH_4^+ concentrations and was three-fold higher in winter (150-405 nM) than in summer (41-115 nM). Wintertime NH_4^+ oxidation rates adhered to a Michaelis-Menten relationship with NH_4^+ substrate only at stations where the ambient NH_4^+ concentration was <100 nM. This, coupled with K_m estimates of <130 nM, indicates a dominant role for AOA (over AOB) in facilitating NH_4^+ oxidation in the Southern Ocean mixed layer. Curiously, V_{max} was nearly invariant across the transect despite large gradients in temperature, light, and NH_4^+ concentration. It is thus possible that NH_4^+ oxidation was iron-limited, which is consistent with 1) an observed positive correlation between vertical profiles of NH_4^+ oxidation rates and iron concentrations measured on the same cruise and 2) recent findings from a culture study of the ubiquitous AOA, *N. maritimus* SCM1 (Shafiee et al. 2019). If verified, iron limitation of AOA *in situ* may explain the lack of complete consumption of NH_4^+ in the Southern Ocean mixed layer in winter. An important implication of this notion is that iron depletion may limit the role of mixed-layer nitrification, which is significant relative to NO_3^- uptake in winter (Mdutyana et al. 2020), in offsetting biological CO_2 drawdown annually. The results described in this chapter thus raise important new questions about parallel N and iron cycling in the Southern Ocean that warrant future research.

Chapter 4: Controls on nitrite oxidation in the upper Southern Ocean: insights from winter kinetics experiments across the Indian sector

NO_2^- oxidation measurements are limited in the open ocean, especially the Southern Ocean, and no kinetics experiments have to-date been conducted in Southern Ocean waters. While most of the oxygenated ocean is characterized by near-negligible NO_2^- concentrations throughout the mixed layer, it is noteworthy that the Southern Ocean hosts perennially elevated mixed-layer NO_2^- (>100 nM; Mdutyana et al. 2020; Smart et al. 2020). The goal of the work presented in this chapter was to determine the physiological constraints imposed on NOB (and thus on NO_3^- production) across the upper layer of the Southern Ocean through measurements of NO_2^- oxidation kinetics in winter, with implications for understanding the cause(s) of the elevated NO_2^- concentrations in the mixed layer. The derived values of V_{max} increased with decreasing light and increasing ambient NO_2^-, indicating a role for photoinhibition and

substrate availability in controlling the distribution of NO_2^- oxidation in the winter mixed layer across the Southern Ocean. The derived K_m values were very strongly correlated with the ambient NO_2^- concentrations, a trend that holds for other oceanic regions too. Interestingly, while the affinity of Southern Ocean NOB for NO_2^- was high (K_m < 403 ± 24 nM), at least compared to values derived from culture studies, there seemed to be an ambient NO_2^- concentration threshold (of >100 nM) that was required before NO_2^- oxidation rates increased substantially. Possible explanations for this threshold requirement are explored in this chapter, including iron limitation of NOB and undersaturation of the nitrite oxidoreductase enzyme (NXR) associated with the dominant genera of NOB. The findings reported herein have implications for the production of NO_3^- and its role in moderating new production in the Southern Ocean.

Chapter 5: Knowledge gaps and future directions

All three data chapters of this thesis (Chapters 2 through 4) include extensive and detailed concluding sections. Therefore, in this final chapter, I have chosen not to repeat those conclusion and implications, but to instead outline some of the knowledge gaps that my work has highlighted, suggest some future research directions, and consider the implications of climate change for Southern Ocean mixed-layer N cycling given the results of my investigations.

Chapter 2: The seasonal cycle of nitrogen uptake and nitrification in the Atlantic sector of the Southern Ocean

This chapter has been published as:
Mdutyana M., Thomalla S.J, Philibert R., Ward B.B. and Fawcett S.E. (2020). The seasonal cycle of nitrogen uptake and nitrification in the Atlantic sector of the Southern Ocean. *Global Biogeochemical Cycles* 34, e2019GB006363. https://doi.org/ 10.1029/2019GB006363

Abstract

Net primary production (NPP) fuelled by nitrate is often equated with carbon export, providing a metric for CO_2 removal to the deep ocean. This "new production paradigm" assumes that nitrification, the oxidation of regenerated ammonium to nitrate, is negligible in the sunlit upper ocean. While surface layer nitrification has been measured in other oceanic regions, very few data exist for the Southern Ocean. Rates of NPP, nitrogen (N) uptake, and nitrification were measured in the upper 200 m across the Atlantic Southern Ocean in winter and summer. Rates of winter mixed-layer nitrate uptake were low, while ammonium uptake was surprisingly high. NPP was also low, such that NPP and total N (nitrate+ammonium) uptake were decoupled; we attribute this to ammonium consumption by heterotrophic bacteria. By contrast, NPP and total N uptake were strongly coupled in summer except at two stations where an additional regenerated N source, likely dissolved organic N, apparently supported 30-45% of NPP. Summertime nitrate uptake rates were fairly high and nitrate fuelled >50% of NPP, indicating the potential for significant carbon export. Nitrification supplied <10% of the nitrate consumed in summertime surface waters, while in winter, mixed-layer nitrification was on average 16-times higher than nitrate uptake. Despite the near-zero nitrification rates measured in the summer mixed layer, the classically-defined f-ratio does not well-represent Southern Ocean carbon export potential annually. This is because some fraction of the nitrate regenerated in the winter mixed layer is likely supplied to phytoplankton in summer; its consumption cannot, therefore, be equated with export.

2.1 Introduction

Biological carbon production in oceanic surface waters followed by organic carbon export to the deep ocean (i.e., via the "biological pump") is a major contributor to the Southern Ocean's carbon dioxide (CO_2) sink, removing an estimated 3 Pg of carbon from surface waters south of 30°S annually (~33% of the global ocean's organic carbon flux) (Schlitzer, 2002; Takahashi et al. 2002). This mechanism, combined with physico-chemical processes, makes the Southern Ocean the most important oceanic region for natural and anthropogenic CO_2 removal (Caldeira and Duffy, 2000; Sabine et al. 2004; DeVries, 2014; Frölicher et al. 2015; DeVries et al. 2017; Gruber et al. 2019). Much uncertainty remains in our ability to quantify the Southern Ocean CO_2 sink, however (e.g., Takahashi et al. 2009; Landschützer et al. 2015; Gray et al. 2018), in part due to a poor understanding of the role of primary production. Phytoplankton never fully consume the macronutrients (nitrate and phosphate) available in Southern Ocean surface waters due to a combination of light and iron (and at times, silicate) limitation (Martin 1990; Nelson and Smith 1991; Sunda and Huntaman 1997; Brzezinski et al. 2003). This amounts to a "leak" in the global ocean's biological pump, since more complete consumption of Southern Ocean surface nutrients could theoretically lower atmospheric CO_2 (Sarmiento and Toggweiler, 1984; Sigman and Boyle, 2000).

In the open ocean, carbon export can be estimated by quantifying key processes in the nitrogen (N) cycle. The "new production paradigm" defines nitrate (NO_3^-) as a "new" nutrient source to phytoplankton because it is mainly transported into the euphotic zone from depth through physical processes such as upward vertical mixing (Dugdale and Goering, 1967). Ammonium (NH_4^+), by contrast, is considered a "regenerated" nutrient as it is produced in the euphotic zone through recycling (e.g., as a by-product of heterotrophic metabolism or a consequence of grazing). At an ecosystem level, the relative importance of new versus regenerated N uptake can be quantified by the f-ratio, a measure of the proportion of phytoplankton growth supported by deep NO_3^- relative to that fuelled by NO_3^- + NH_4^+ (Eppley and Peterson, 1979). Over appropriate timescales (i.e., annually), the upward flux of N into surface waters must be balanced by an equivalent N loss, such that the consumption of NO_3^- by phytoplankton can be used to estimate the downward flux of organic carbon ("export production"), assuming that carbon and N are incorporated into biomass in a known ratio (Dugdale and Goering, 1967; Eppley and Peterson, 1979).

Using the new production paradigm as originally defined to infer export production relies on the following assumptions: 1) the oceanic system is in steady state, meaning that any N loss from the euphotic zone through grazing and/or organic matter sinking is balanced by the input of new N; 2) there is no long-term storage of N in the euphotic zone; 3) there is little to no contribution of N_2 fixation, atmospheric N deposition or dissolved organic N (DON) to N uptake; and 4) the rate of nitrification (the oxidation of NH_4^+ to nitrite (NO_2^-) and then NO_3^-; see below) is low compared to NO_3^- uptake in the euphotic zone. Violation of one or more of these assumptions can render the new production paradigm an inadequate framework for understanding and/or quantifying biological carbon export (Dugdale and Goering, 1967; Eppley and Peterson, 1979; Bronk et al. 1994; Fernández and Raimbault, 2007; Yool et al. 2007).

Nitrification is the chemoautotrophic process by which heterotrophically-regenerated NH_4^+ is oxidized to NO_2^- and NO_3^-. NH_4^+ oxidation is performed by ammonia-oxidizing archaea and bacteria (AOA and AOB) while NO_2^- oxidation is conducted by nitrite-oxidizing bacteria (NOB). Nitrification was long considered insignificant in euphotic zone waters due to nitrifier light inhibition (Schön and Engel, 1962; Hooper and Terry, 1974; Horrigan et al. 1981; Olson, 1981b) and competition with phytoplankton for NH_4^+ (Ward, 1985; 2005; Smith et al. 2014; Zakem et al. 2018). However, numerous studies have demonstrated that significant rates of nitrification can occur in the euphotic zone, particularly near its base (e.g., Ward et al. 1989; Dore and Karl, 1996; Yool et al. 2007; Beman et al. 2012; Peng et al. 2015). In these cases, some fraction of the NO_3^- consumed by phytoplankton constitutes a regenerated rather than a new N source and should thus be subtracted from estimates of new production to avoid overestimating carbon export potential.

Direct measurements of euphotic zone nitrification are extremely limited in the Southern Ocean (Olson, 1981a; Bianchi et al. 1997; Cavagna et al. 2015; Raes et al. 2020). The only two studies that have directly measured nitrification in the open Southern Ocean were conducted in early spring (Olson 1981a) and autumn (Bianchi et al. 1997), with no data available for the winter or summer. In the winter, a role for surface water nitrification in replenishing nutrients has been hypothesized (Sanders et al. 2007) given the low light levels and deep mixed layers (Sverdrup 1953; Mitchell and Holm-Hansen, 1991; Nardelli et al. 2017). NO_3^- isotope measurements from the polar Southern Ocean support this hypothesis, suggesting significant rates of mixed-layer nitrification in winter (Smart et al. 2015). In addition, most Southern Ocean N uptake studies

were conducted during spring and summer (e.g., Waldron et al. 1995; Mengesha et al. 1998; Sambrotto and Mace 2000; Savoye et al. 2004; Lucas et al. 2007; Joubert et al. 2011; Thomalla et al. 2011; Cavagna et al. 2015; Tripathy et al. 2017) with very few in winter (Cota et al. 1992; Philibert et al. 2015). Since it is the proportion of nitrification relative to autotrophic NO_3^- uptake that matters for estimates of carbon export potential, this paucity of data prevents us from fully understanding the seasonality of the upper Southern Ocean N cycle and its implications for atmospheric CO_2 drawdown.

Multiple physical processes supply NO_3^- to the Southern Ocean euphotic zone, including vertical mixing, Ekman upwelling, lateral advection, and enhanced advection and mixing associated with small-scale dynamics (Hense et al. 2003; Moore et al. 2004; Meskhidze et al. 2007; Carranza and Gille, 2015; Swart et al. 2015). In the Antarctic Zone (AZ) south of the Polar Front (PF), surface cooling and brine rejection during sea ice formation in winter deepen the mixed layer, importing subsurface NO_3^- into surface waters. This is augmented by perennial Ekman upwelling of NO_3^--rich deep waters driven by the circumpolar westerly winds (Gordon et al. 1977). During spring and summer, sea ice melt and surface warming shoal the mixed layer, and phytoplankton encounter sufficient light to begin consuming the available NO_3^-. The water underlying this spring/summer mixed layer, which was part of the preceding winter mixed layer, retains the low temperatures (<1.2°C) of the winter AZ surface, forming the summer subsurface temperature minimum layer (T_{min} layer) (Gordon et al. 1977; Toole, 1981). The T_{min} layer, taken to represent the initial state from which the surface ocean evolves in spring/summer (Altabet and Francois, 2001), exchanges water with both the overlying summer mixed layer and the high-NO_3^- Circumpolar Deep Water (CDW) below (Whitworth and Nowlin, 1987; DiFiore et al. 2010). In the more northerly Polar Frontal and Subantarctic Zones (PFZ and SAZ, respectively), winter heat loss and summer heat gain drive seasonal changes in mixed layer depth that drive upward vertical mixing of thermocline NO_3^- into surface waters (McCartney, 1975). In addition, large-scale Ekman circulation drives net equatorward surface flow into the PFZ and SAZ, transporting AZ NO_3^- northwards (Gordon et al. 1977). Seasonal N cycling in the upper AZ may thus be important for the chemistry of surface waters north of the PF.

To evaluate the new production paradigm as a framework for quantifying the cycling of N and carbon in the Southern Ocean during winter and summer, I directly measured carbon fixation,

N uptake, and nitrification across the Atlantic sector in both seasons. Rates of net primary production (NPP), NH_4^+ and NO_3^- uptake, and NH_4^+ and NO_2^- oxidation were quantified along the GoodHope repeat hydrographic line between South Africa and Antarctica, which traverses all the major zones of the Southern Ocean (Ansorge et al. 2005). With the resultant data, I attempt to address the following questions: 1) How do the rates of NPP, N uptake, and nitrification differ between seasons? 2) Are NPP and N uptake coupled, and if not, why not? 3) How important is mixed-layer NO_3^- regeneration (i.e., nitrification) relative to autotrophic NO_3^- assimilation in both seasons and annually? 4) What are the implications of the above for estimates of Southern Ocean carbon export?

2.2 Materials and Methods

2.2.1 Sampling location

Sampling was conducted aboard the R/V *SA Agulhas II* along the GoodHope line, with four stations (stations 1-4) sampled on a winter cruise (W15; July-August 2015) between Cape Town and 56°S (the northern extent of the winter sea ice) and six stations (stations 1-4, a station near South Georgia island (SG), and an Ice Shelf station (IS)) sampled during a summer cruise (SANAE55; December 2015-February 2016) between Cape Town and Antarctica (Figure 2.1). On both cruises, stations 1-4 were sampled within a two-week period, in July 2015 and January 2016, respectively, while SG was sampled at the end of December 2015 and IS was sampled at the end of January 2016.

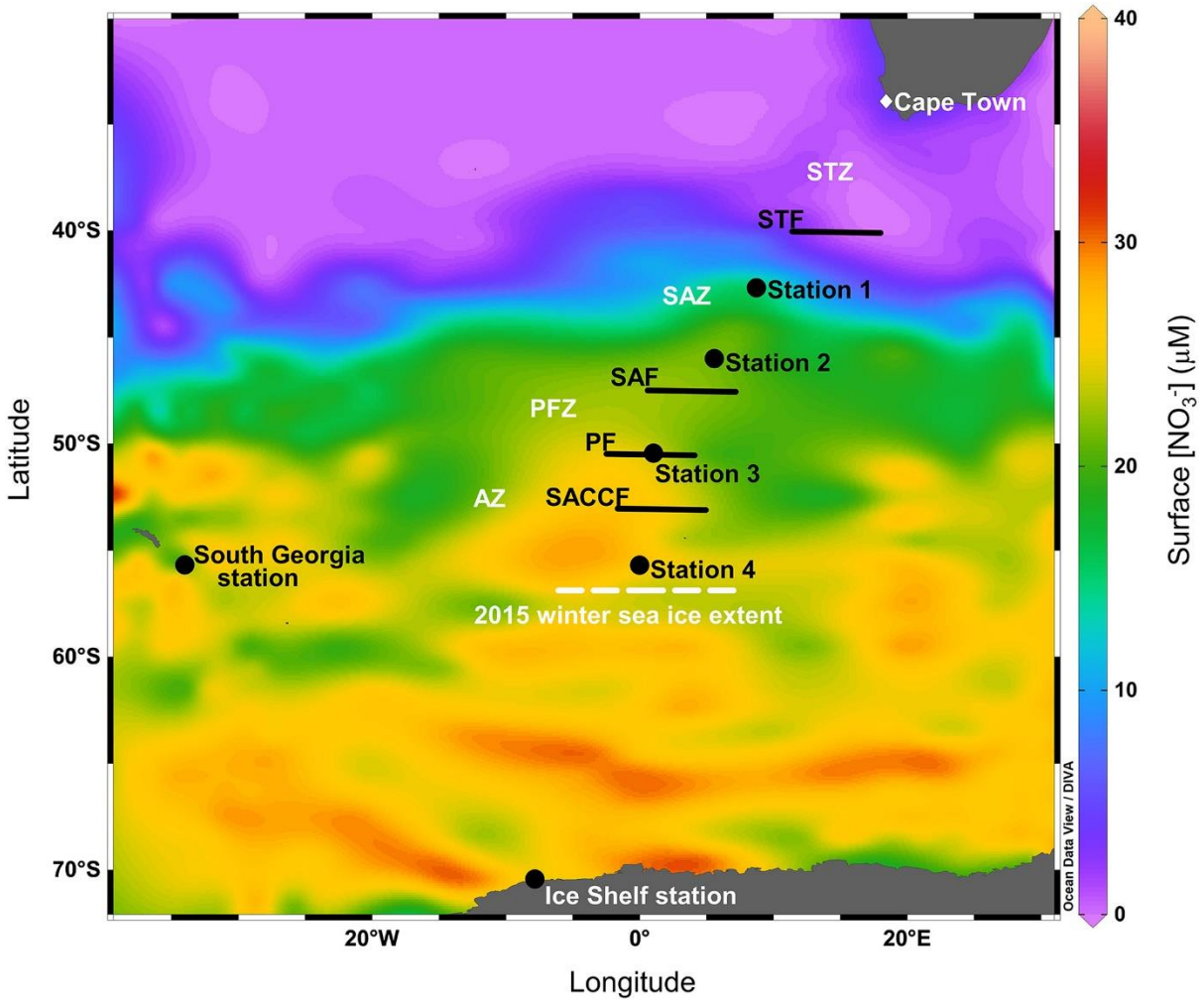

Figure 2.1: Map showing the location of the stations sampled between Cape Town and Antarctica along the GoodHope line overlain on summertime surface nitrate concentration ([NO3−]) climatology (WOA18). Stations 1–4 were sampled in winter and summer while the South Georgia (SG) and Ice Shelf (IS) stations were sampled only in summer. The mean positions of the major fronts, identified according to Orsi et al. (1995), are indicated by the horizontal black lines (STF, Subtropical Front; SAF, Subantarctic Front; PF, Polar Front; SACCF, Southern Antarctic Circumpolar Current Front) and the major Southern Ocean zones relevant to this study are labeled (SAZ, Subantarctic Zone; PFZ, Polar Frontal Zone; AZ, Antarctic Zone). The dashed white line indicates the northern extent of the sea ice encountered during the winter cruise. Figure made using Ocean Data View (Schlitzer 2015).

2.2.2 Shipboard incubation experiments

Seawater was collected using a CTD-rosette equipped with 24 x 12 L Niskin bottles and transferred into acid-washed polycarbonate Nalgene bottles following 200 µm pre-filtration to remove large grazers. Samples were collected from depths representing 55%, 30%, 10%, and 1% of the available photosynthetically active radiation (PAR), as well as from 200 m (hereafter, "dark"). In winter, samples were also collected at the mixed layer depth (MLD), approximated from the CTD temperature profiles measured on the down-casts as the shallowest depth at which temperature changed by 0.2°C relative to a reference depth of 10 m (de Boyer Montégut et al. 2004). MLDs calculated from potential density after the cruise yielded similar values to

those estimated during sampling. Hereafter, the temperature-derived MLDs are used because these are the depths from which samples were collected in winter. The winter temperature-derived MLDs were always deeper than 1% PAR but shallower than 200 m (Figure 2.2; Table 2.1). A separate MLD sample was not collected in summer because the mixed layer was either shallower than the base of the euphotic zone (stations 1, 4, SG and IS) or fairly similar to it (stations 2 and 3). The dark and MLD incubation bottles were covered with opaque black plastic prior to filling to prevent light penetration.

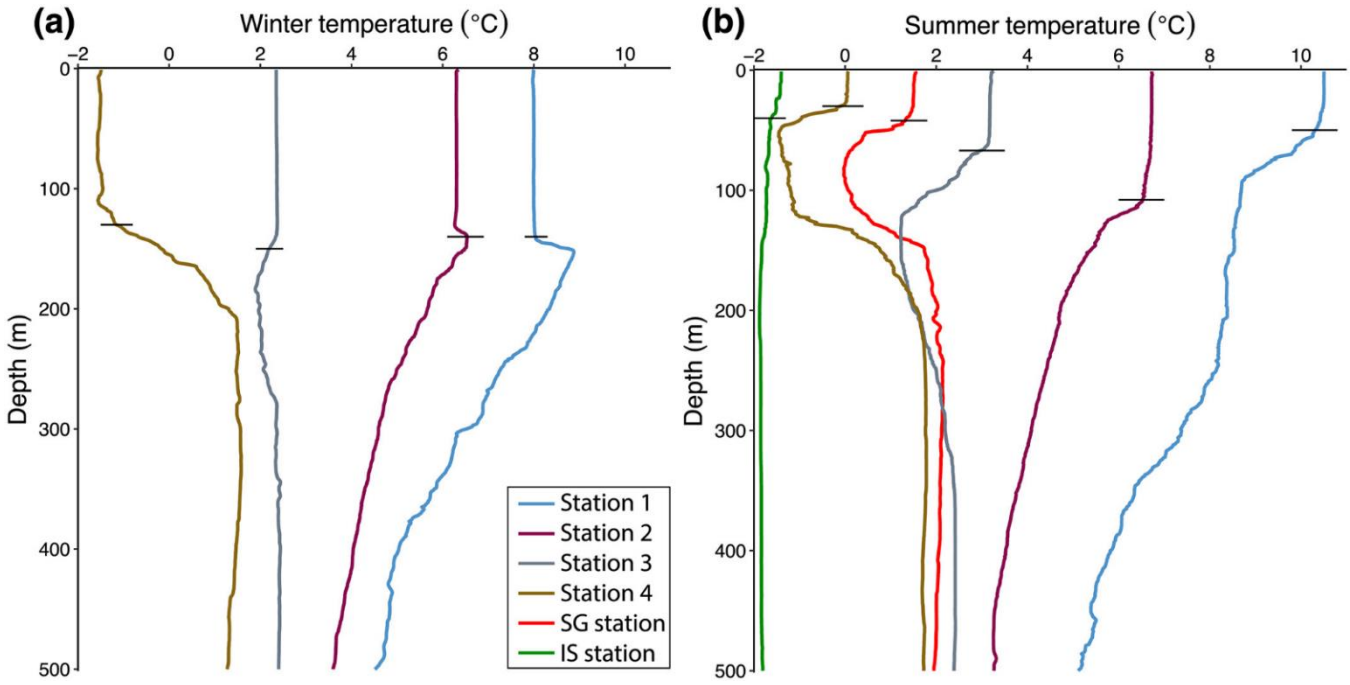

Figure 2.2: CTD-derived temperature profiles for all stations sampled in (a) winter and (b) summer. The horizontal black lines represent the temperature-derived MLDs.

From each depth, duplicate bottles were amended with $^{15}NO_3^-$ to measure NO_3^- uptake (final tracer concentration of 2.05 μM). An additional set of duplicate bottles was amended with $^{15}NH_4^+$ to measure NH_4^+ uptake and oxidation (final tracer concentration of 0.2 μM). The NH_4^+ bottles from the 1% light depth, MLD and 200 m were also amended with $^{14}NO_2^-$ (0.2 μM) to act as an "isotope trap" for the NH_4^+ oxidation experiments given the low ambient NO_2^- concentrations. Duplicate bottles from four light depths (55%, 10%, 1% and dark) were amended with $^{15}NO_2^-$ in order to measure NO_2^- oxidation. From all NH_4^+ and NO_2^- incubation bottles, initial (T_0) subsamples (50 mL) were collected immediately after the addition of $^{15}NH_4^+$+$^{14}NO_2^-$ and $^{15}NO_2^-$, and final (T_f) subsamples were taken upon incubation termination.

Subsamples were stored frozen at -20°C until analysis. All incubation bottles were also amended with $H^{13}CO_3^-$ (final tracer concentration of 100 µM) so that NPP could be measured concurrently with N uptake.

Sample bottles were incubated in custom-built on-deck incubators equipped with neutral density screens and supplied with running surface seawater to simulate *in situ* light and temperature conditions. Incubations lasted 24 hours to ensure sufficient transfer of the isotope tracer to the product pool that was ultimately measured; this is particularly relevant for the NH_4^+ and NO_2^- oxidation experiments and possibly for N uptake in winter, which are expected to be slow. However, the long incubation period means that our N uptake rates may be underestimated due to the potential loss of ^{15}N through its release by phytoplankton into the dissolved organic N (DON) pool (Bronk et al. 1994) and/or the dilution of the $^{15}NH_4^+$ pool by the ammonification of unlabelled particulate organic N (Glibert et al. 1982) (see section 3.3 and *Appendix A2.1* for a discussion of NH_4^+ isotope dilution). The uptake experiments were terminated by filtering the incubated water through pre-combusted 0.7 µm Whatman glass fibre (GF/F) filters to collect the particulate organic biomass. The GF/Fs were oven-dried shipboard at 45°C for 24 hours, fumed with hydrochloric acid for 24 hours inside a desiccator to remove inorganic carbon, further oven-dried for 3 hours, then pelletized into tin cups and stored in a desiccator for less than a month until analysis.

Table 2. 1: Winter and Summer Surface Layer-Integrated Rates Measured at All Stations Station

	Station 1	Station 2	Station 3	Station 4	South Georgia (SG) station	Ice Shelf (IS) station
Winter						
Sampling date	28/07/2015	29/07/2015	01/08/2015	03/08/2015		
Latitude	42ºS	45ºS	50ºS	55ºS	55ºS	70ºS
Longitude	8.7ºS	6.6ºS	1.1ºS	0.0ºS	-34ºS	-7.8ºS
MLD (m)	**140**	**140**	**150**	**130**		
1% PAR (m)	83	83	115	115		
NPP (mmol C m^{-2} d^{-1})	7.08	5.93	6.49	4.38		
ρNO_3^- (mmol N m^{-2} d^{-1})	0.39	0.54	0.21	0.13		
ρNH_4^+ (mmol N m^{-2} d^{-1})	4.34	6.46	9.47	3.50		
f-ratio	0.10	0.11	0.03	0.04		
$NH_4^+{}_{ox}$ (mmol N m^{-2} d^{-1})	1.96	3.20	9.87	1.61		
$NO_2^-{}_{ox}$ (mmol N m^{-2} d^{-1})	*	5.56	6.90	6.53		
$NH_4^+{}_{ox}/\rho NO_3^-$	5.07	5.98	46.6	12.7		
$NO_2^-{}_{ox}/\rho NO_3^-$	25.2	2.80	12.6	15.8		
f-ratio$_{(corrected)}$ ($NH_4^+{}_{ox}$)	-0.33	-0.38	-1.00	-0.41		
f-ratio$_{(corrected)}$ ($NO_2^-{}_{ox}$)	*	-0.72	-0.69	-1.77		
$NH_4^+{}_{ox}/\rho NH_4^+$	0.45	0.50	1.04	0.46		
Summer						
Sampling date	05/01/2016	07/01/2016	08/01/2016	09/01/2016	29/12/2015	26/01/2016
Latitude	42ºS	45ºS	50ºS	55ºS	55ºS	70ºS
Longitude	8.7ºS	6.6ºS	2.0ºS	0.0ºS	-34ºS	-7.8ºS
MLD (m)	50	**108**	**67**	30	42	40
1% PAR (m)	**83**	80	48	**55**	**55**	**70**
NPP (mmol C m^{-2} d^{-1})	31.4	44.8	57.3	40.8	48.0	20.7
ρNO_3^- (mmol N m^{-2} d^{-1})	1.70	2.30	3.46	3.89	6.95	2.85
ρNH_4^+ (mmol N m^{-2} d^{-1})	1.57	5.60	1.34	1.15	1.07	0.81
f-ratio	0.52	0.29	0.72	0.77	0.87	0.78
$NH_4^+{}_{ox}$ (mmol N m^{-2} d^{-1})	0.08	0.12	0.03	0.04	0.16	0.08
$NO_2^-{}_{ox}$ (mmol N m^{-2} d^{-1})	0.16	0.18	0.05	0.03	0.50	0.03
$NH_4^+{}_{ox}/\rho NO_3^-$	0.05	0.05	0.01	0.01	0.02	0.03
$NO_2^-{}_{ox}/\rho NO_3^-$	0.10	0.08	0.01	0.01	0.07	0.01
f-ratio$_{(corrected)}$ (DON)	0.52	0.29	**0.40**	**0.55**	0.87	0.78
f-ratio$_{(corrected)}$ ($NH_4^+{}_{ox}$)	0.50	0.28	0.72	0.76	0.85	**0.76**
f-ratio$_{(corrected)}$ ($NO_2^-{}_{ox}$)	**0.47**	**0.27**	0.71	0.77	**0.80**	0.77
$NH_4^+{}_{ox}/\rho NH_4^+$	0.05	0.02	0.02	0.04	0.15	0.10

Note. *In winter, rates were integrated to the MLD, while in summer, rates were integrated to the base of the euphotic zone (1% PAR) at Stations 1, 4, SG, and IS and to the MLD at Stations 2 and 3 (see section 2.7 for details). For the "MLD" and "1% PAR" rows, the bold text indicates the surface layer over which the rates were integrated. The asterisk (*) symbol indicates that no data are available. In summer, the value of the "f ratio(corrected)" shown in bold text indicates the most conservative estimate of the seasonal f ratio after urea assimilation and nitrification (using the higher of the NH_4^+ ox versus NO_2^- ox rate) have been accounted for. We note that ρNH_4^+ does not take into account possible isotope dilution due to NH_4^+ regeneration. Experiments were not conducted at the SG or IS stations in winter.*

2.2.3 Nutrient concentrations

Seawater samples were collected at regular intervals through the upper 200 m for analysis of nutrient concentrations. In winter, nutrient samples were analysed shipboard for NO_3^-+NO_2^- and NO_2^- concentrations, while samples for NH_4^+ concentrations and all summer nutrient samples were immediately frozen at -20°C until analysis on shore directly after the cruises. The concentration of NO_3^-+NO_2^- was determined using a Lachat QuickChem® flow-injection autoanalyzer in a configuration optimized for high concentrations (detection limit of 1.3 µM and precision of ±0.26 µM). Ambient NO_2^- concentrations were measured manually using the colorimetric method of Grasshoff et al. (1983) (detection limit of 0.004 µM and precision of ±0.002 µM). NH_4^+ concentrations were analysed using the fluorometric method of Holmes et al. (1999) (detection limit of 0.05 µM and precision of ±0.02 µM).

2.2.4 Carbon and N biomass concentrations and NPP and N uptake rates

The concentration and isotopic composition of particulate organic carbon (POC) and N (PON) on the GF/F filters was analyzed using a Delta V Plus isotope ratio mass spectrometer (IRMS) coupled to a Flash 2000 elemental analyser, with a detection limit of 2 µg C and 1 µg N and precision of ±0.005 At% for both C and N. The rates of carbon fixation (i.e., NPP) and NO_3^- and NH_4^+ uptake were calculated according to the equations of Dugdale & Wilkerson (1986) as follows:

$$\rho M = \frac{([PM] \times At\%_{final})}{(At\%_{initial} - At\%_{natural\ abundance}) \times T} \quad (2.1a)$$

where

$$At\%_{final} = (At\%_{measured} - At\%_{natural\ abundance}) \quad (2.1b)$$

and

$$At\%_{initial} = \frac{([M]_{ambient} \times (At\%_{natural\ abundance}) + [M]_{tracer} \times 99\%)}{([M]_{initial})} \quad (2.1c)$$

Here, M refers to the species of interest: C, NO_3^- or NH_4^+; ρM is the transport rate of that species (µM d^{-1}); [PM] is the concentration of POC or PON (µM) collected at the end of each incubation; $At\%_{natural\ abundance}$ is 1.07% for ^{13}C and 0.365% for ^{15}N; $[M]_{ambient}$ is the water column concentration of dissolved inorganic carbon (DIC), NO_3^- or NH_4^+ (µM) at the time of

sampling, measured at the surface for DIC (Bakker et al. 2016) and at all experiment depths for NO_3^- and NH_4^+ (Figure 2.3a-d); $At\%_{measured}$ refers to the % ^{13}C or ^{15}N measured in the PM by IRMS while $At\%_{final}$ corrects this value for the % ^{13}C or ^{15}N initially present (taken to be $At\%_{natural\ abundance}$); $At\%_{initial}$ refers to the % ^{13}C or ^{15}N in the incubation seawater directly following tracer addition; $[M]_{tracer}$ is the concentration of ^{13}C or ^{15}N tracer added; $[M]_{initial} = [M]_{ambient} + [M]_{tracer}$; and T refers to incubation length (days).

Specific uptake rates (V_M) were calculated by normalizing ρM to the ambient [PM] (i.e., $V_M = \rho M/PM$) and used to calculate the f-ratio according to Eppley and Peterson (1979) as:

$$\text{f ratio} = \frac{V_{NO3}}{V_{NO3} + V_{NH4}} \tag{2.2}$$

2.2.5 Ammonium oxidation

Using the azide method of McIlvin and Altabet (2005) as amended by Peng et al. (2015), NO_2^- produced from NH_4^+ oxidation was converted to N_2O gas that was then measured by IRMS. In brief, a 1:1 fresh mixture of 2 M sodium azide and 20% acetic acid buffer was prepared daily and purged with helium gas (He) for 20 minutes to remove any N_2O produced from NO_2^- in the reagents. Samples were aliquoted into gas-tight vials that were purged with He for 10 minutes, after which 0.4 mL of sodium azide/acetic acid buffer was added to each vial. Vials were incubated for 1 hour at room temperature, and sample pH was then adjusted to >12 via the addition of 0.3 mL of 10 M sodium hydroxide (NaOH).

The concentration of N_2O and ratio of $^{45}N_2O/^{44}N_2O$ (where $^{45}N_2O$ derives from $^{15}NO_2^-$, the latter produced from the oxidation of $^{15}NH_4^+$) were measured using a Delta V Plus IRMS with a custom-built purge-and-trap front end (McIlvin and Casciotti, 2011). This configuration yields a detection limit of 0.2 nmol of N with a precision in $\delta^{15}N$ of 0.1‰ ($\delta^{15}N$, in ‰ vs. air, = $(^{15}N/^{14}N_{sample}/^{15}N/^{14}N_{air} - 1) \times 1000$). The $\delta^{15}N$ of NO_2^- was calculated from $^{45}N_2O/^{44}N_2O$ according to Peng et al. (2015).

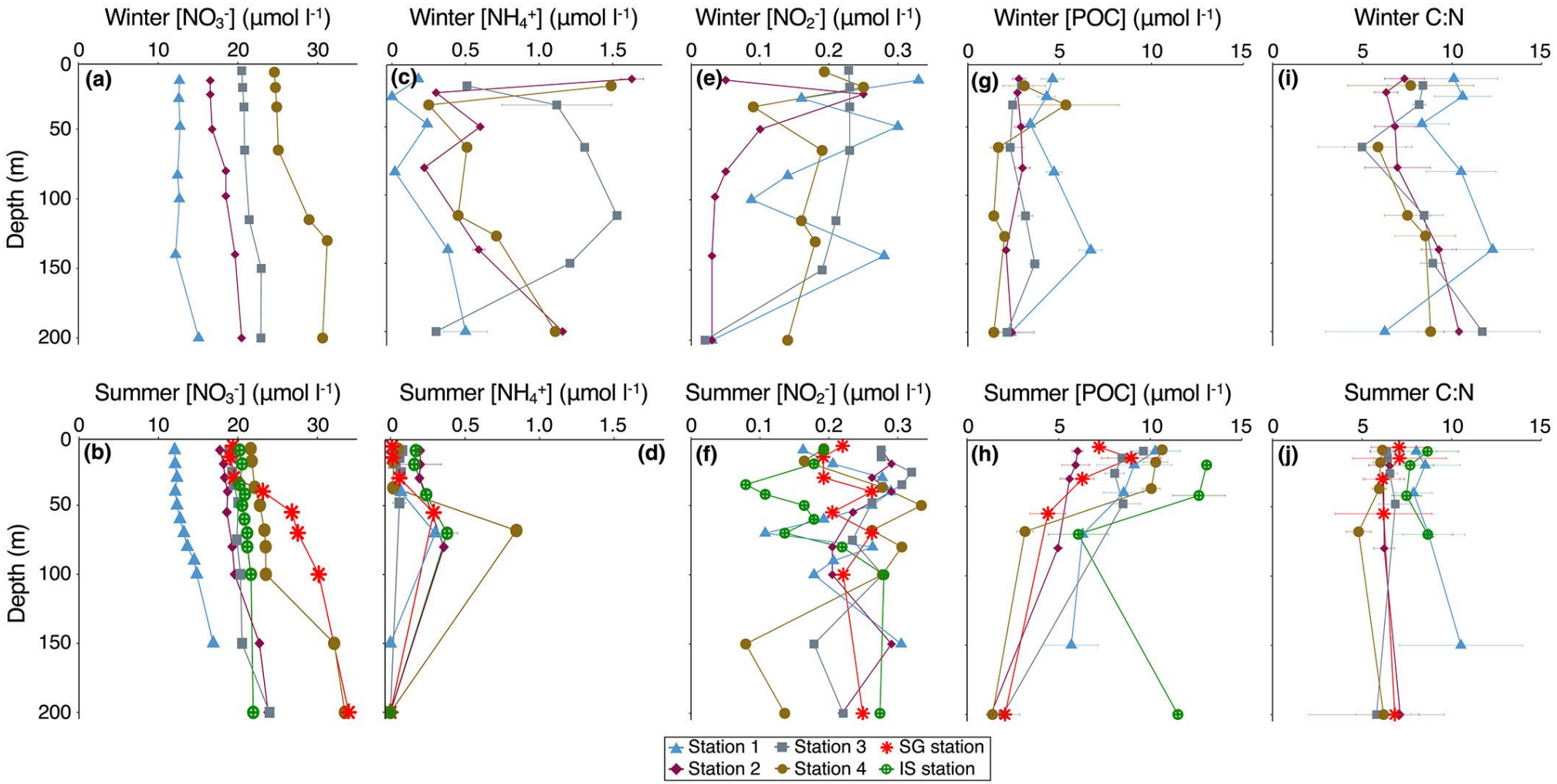

Figure 2.3: Upper water column (0–200 m) concentrations in winter and summer of (a and b) NO_3^-, (c and d) NH_4^+, (e and f) NO_2^-, and (g and h) POC, as well as biomass C:N ratios (i and j).

The rate of NH_4^+ oxidation ($NH_4^+{}_{ox}$; nM d^{-1}) was calculated following Peng et al. (2015) as:

$$NH_4^+{}_{ox} = \frac{\Delta[^{15}NO_2^-]}{f_{NH_4^+}^{15} \times T} \quad (2.3)$$

Where $\Delta[^{15}NO_2^-]$ is the change in the concentration of $^{15}NO_2^-$ (nM) between the start and end of the incubation due to $^{15}NH_4^+$ oxidation, calculated as the difference in the measured $\delta^{15}N$ of NO_2^- between the T_f and T_0 samples, $f_{NH_4}^{15}$ is the fraction of the NH_4^+ substrate labelled with ^{15}N at the start of the incubation, and T is the incubation length (days). All $^{15}NO_2^-$ produced during the incubations was assumed to derive from $^{15}NH_4^+$ oxidation. The detection limits for winter and summer $NH_4^+{}_{ox}$ rates ranged from 0.02 to 1.87 nM d^{-1} and 0.02 to 4.61 nM d^{-1}, respectively. While not discussed here, specific NH_4^+ oxidation rates ($\lambda_{NH4\_ox} = NH_4^+{}_{ox}/[NH_4^+]$) are included in the data product associated with this study.

2.2.6 Nitrite oxidation

The denitrifier-IRMS method (Sigman et al. 2001; McIlvin and Casciotti, 2011) was used to measure the $\delta^{15}N$ of NO_3^- produced from $^{15}NO_2^-$ oxidation. Prior to isotope analysis, samples were treated with sulfamic acid (15 mM) for 1 hour to remove any NO_2^- remaining at the end of the experiments, after which sample pH was adjusted to ~7-8 via the addition of 2 M NaOH. To account for inefficiencies in NO_2^- removal, both T_f and T_0 samples were treated with sulfamic acid and analysed for $\delta^{15}N\text{-}NO_3^-$ (more accurately, $\delta^{15}N\text{-}NO_3^-+NO_2^-$), with the difference between them taken as the $^{15}NO_3^-$ enrichment due to NO_2^- oxidation (Peng et al. 2015). International reference materials (IAEA-N3, USGS 34, USGS 32) were used for calibration of the measured $\delta^{15}N\text{-}NO_3^-$.

The rate of NO_2^- oxidation ($NO_2^-{}_{ox}$; nM d^{-1}) was calculated following Peng et al. (2015) as:

$$NO_2^-{}_{ox} = \frac{\Delta[^{15}NO_3^-]}{f_{NO_2^-}^{15} \times T} \quad (2.4)$$

Where $\Delta[^{15}NO_3^-]$ is the change in the concentration of $^{15}NO_3^-$ (nM) between the start and end of the incubation due to NO_2^- oxidation, calculated as the difference in the measured $\delta^{15}N$ of NO_3^- between the T_f and T_0 samples, $f_{NO_2}^{15}$ is the fraction of the NO_2^- substrate labelled with ^{15}N at the start of the incubation, and T is the incubation length (days). Detection limits for $NO_2^-{}_{ox}$ rates ranged from 0.1 to 2.17 nM d^{-1} and 0.24 to 2.68 nM d^{-1} for winter and summer, respectively. While not discussed here, specific NO_2^- oxidation rates ($\lambda_{NO2\_ox} = NO_2^-/[NO_2^-]$) are included in the data product associated with this study.

2.2.7 Choice of upper layer integration depth

Summertime rates (NPP, ρNO_3^-, ρNH_4^+, $NH_4^+{}_{ox}$ and $NO_2^-{}_{ox}$) were typically trapezoidally-integrated to the base of the euphotic zone, assuming that phytoplankton would have been active wherever the light levels were ≥1% PAR. Exceptions to this were stations 2 and 3, at which the mixed layer was deeper than the base of the euphotic zone (Table 2.1). Here, phytoplankton would have been regularly mixed out of the euphotic zone, such that a more appropriate integration depth is the base of the mixed layer. Incubation experiments were not conducted at the MLD at stations 2 and 3, however, so MLD rates were approximated by linearly interpolating between the rates measured at 1% PAR and 200 m (Peng et al., 2018). The wintertime rates were integrated to the MLD, which was always deeper than the euphotic zone (Table 2.1). Hereafter, "surface layer-integrated" is used to refer to either euphotic zone- or MLD-integrated rates, depending on which surface-layer boundary was deeper.

2.3 Results

2.3.1 Hydrography and nutrient concentrations

Temperatures over the upper 200 m were generally lower in winter than summer, with deeper mixed layers computed for the winter (average of 140 m) than the summer (average of 56 m) and deeper MLDs in the SAZ than the AZ in both seasons (Figure 2.2). The winter MLDs were similar to the maximum values expected for the Atlantic sector (typically ≤200 m in the SAZ and ≤150 m in the PFZ and AZ; Sallée et al. 2010; Du Plessis et al. 2017). Below the mixed layer, the T_{min} was evident at the PFZ/AZ stations (3, 4 and SG) in summer and a T_{max} layer was apparent at the SAZ stations (1 and 2) in winter. Underlying the T_{min}/T_{max}, the temperatures (and nutrient concentrations; see below) were characteristic of Circumpolar Deep Water (CDW) in the AZ, Antarctic Intermediate Water (AAIW) in the PFZ, and Subantarctic Mode Water (SAMW) in the SAZ (Orsi et al. 1995).

The winter stations were characterized by mixed layers that were deeper than the base of the euphotic zone (average depth of 99 m; Table 2.1), yielding an almost homogenous vertical distribution of NO_3^- in euphotic zone waters (Figure 2.3a). In summer, most stations were characterized by MLDs shallower than 1% PAR (average depth of 65 m) and NO_3^- showed a more nutrient-like profile (Figure 2.3b). There was almost no winter-to-summer difference in

the average mixed-layer NO_3^- concentration at each station, possibly because the winter sampling occurred before the period of maximum NO_3^- recharge and/or the summer sampling before the period of maximum NO_3^- drawdown (Johnson et al. 2017). Surface layer NO_3^- concentrations increased with increasing latitude, with the exception of the southernmost IS station in summer where the intermediate NO_3^- concentration of Lower CDW (LCDW) was observed (Figure 2.3b). In winter, NH_4^+ concentrations in the upper 200 m ranged from below detection to 1.63 µM (Figure 2.3c), showed no robust trend with depth, and were significantly higher at station 3 (average of 1.00 ± 0.40 µM) than at the other stations (average of 0.57 ± 0.25 µM). Summertime NH_4^+ concentrations were lower than in winter (average of 0.13 ± 0.03 µM; range from below detection to 0.84 µM) and generally reached a maximum near the base of the euphotic zone (Figure 2.3d). NO_2^- was present throughout the upper 200 m at similar concentrations in both seasons, averaging 0.16 ± 0.02 µM in winter and 0.23 ± 0.01 µM in summer (Figure 2.3e and f).

2.3.2 Particulate organic carbon concentrations and rates of NPP

In winter, all the stations were characterized by a low and roughly homogenous vertical distribution of POC in the mixed layer (ranging from 1.41 to 6.69 µM; average of 3.06 ± 0.24 µM) (Figure 2.3g), and no robust relationship was observed between latitude and POC. The wintertime biomass C:N ratios varied from 1.4 to 6.6 over the upper 200 m (seasonal average of 8.4 ± 0.6) (Figure 2.3i). Summertime surface layer POC concentrations at stations 1-4 were on average higher than in winter, ranging from 3.16 to 10.65 µM (seasonal average of 7.85 ± 0.58 µM) (Figure 2.3h). The vertical POC distribution appeared to follow the light curve, with higher concentrations in surface waters that decreased with depth to a minimum below the euphotic zone. Stations 1-4 and SG were characterized by similar levels of biomass accumulation (surface layer averages ranging from 5.70 ± 0.40 µM to 8.57 ± 1.45 µM), while maximum concentrations were observed at the IS station (euphotic zone average of 11.96 ± 1.82 µM). The summertime C:N ratios were fairly constant throughout the surface layer at each station (range of 4.8 to 8.8; seasonal average of 6.9 ± 0.2), with slightly higher C:N ratios at station 1 and IS (average of 8.3 ± 0.3 and 8.1 ± 0.6, respectively) (Figure 2.3j).

Rates of NPP measured during winter were extremely low and roughly invariant throughout the mixed layer at all stations, with a seasonal average of 44 ± 1.6 nM d^{-1} (mixed-layer averages of 40 ± 2.2 to 47 ± 3.5 nM d^{-1}). Summertime rates were much higher, with a seasonal average

of 674 ± 260 nM d^{-1} (surface layer averages of 320 ± 20 to 1064 ± 187 nM d^{-1}), and generally decreased with depth as light levels declined. NPP in summer was higher to the south (stations 3, 4, and SG), with the highest rates observed at station 3 (surface layer average of 1044 ± 205 nMd^{-1}) (Figures 2.4a, 2.4f, 2.5a, 2.6a, 2.7a and 2.7d).

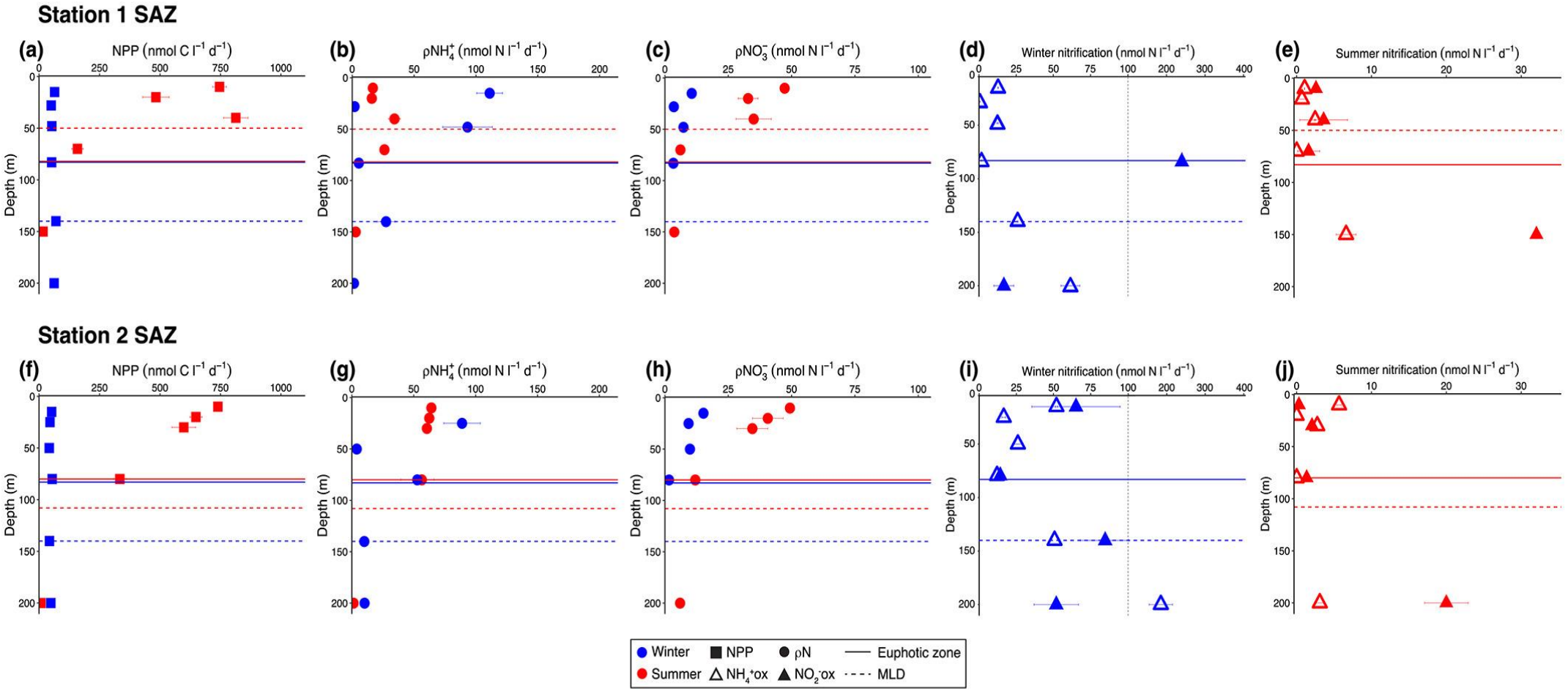

Figure 2.4: Upper water column (0–200 m) rate measurements at Stations 1 (SAZ; 42°S) and 2 (SAZ; 45°S) in winter and summer. Station 1: (a) NPP, (b) ρNH_4^+ (c) ρNO_3^-, (d) nitrification (NH_4^+ ox and NO_2^- ox) in winter and (e) nitrification (NH_4^+ ox and NO_2^- ox) in summer. Station 2: (f) NPP, (g) ρNH_4^+, (h) ρNO_3^-, (i) nitrification (NH_4^- ox and NO_2^- ox) in winter, and (j) nitrification (NH_4^+ ox and NO_2^- ox) in summer. For panels (d) and (i), the x axis to the left of the dashed gray vertical line has been expanded to better show the rates lower than 100 nM d^{-1}. Blue and red symbols represent winter and summer, respectively. On all panels, the MLD is shown by the dotted horizontal line and the euphotic zone depth by the solid horizontal line, in blue for winter and red for summer. Error bars indicate the standard error of replicate experiments, each measured at least twice. Where error bars are not visible, they are smaller than the data markers. Note that ρNH_4^+ does not take into account possible isotope dilution due to NH_4^+ regeneration.

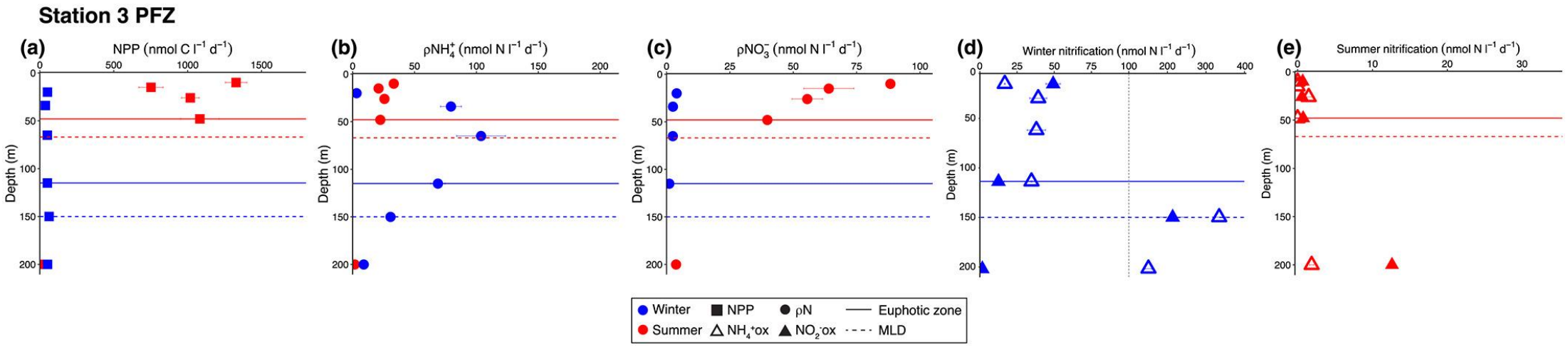

Figure 2.5: Upper water column (0–200 m) rate measurements at Station 3 (PFZ; 50°S) in winter and summer. Panels and symbols are the same as in Figure 2.4.

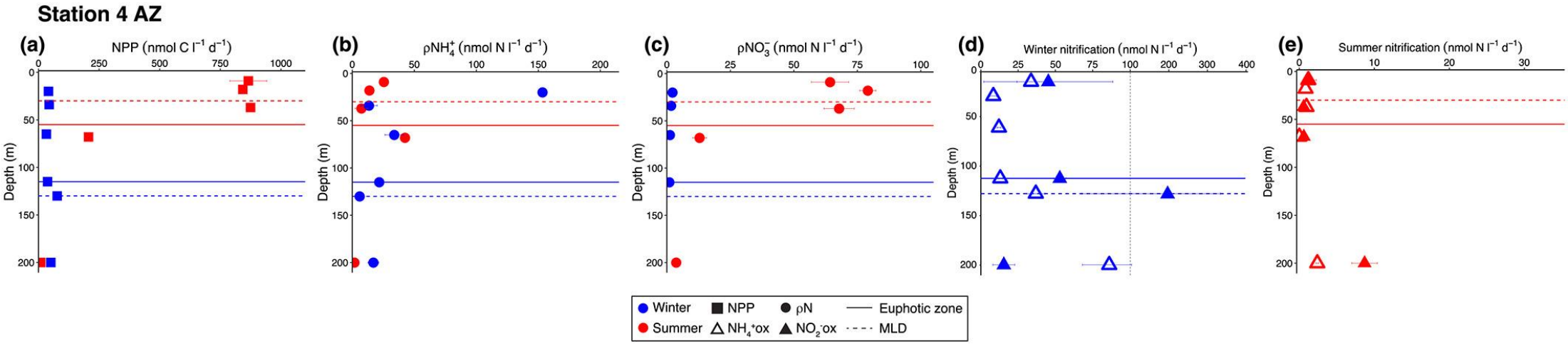

Figure 2.6: Upper water column (0–200 m) rate measurements at Station 4 (AZ; 55°S) in winter and summer. Panels and symbols are the same as in Figure 2.4.

2.3.3 Nitrogen uptake rates

The winter stations were characterized by low euphotic zone NO_3^- uptake rates (ρNO_3^-) averaging 1.52 ± 0.24 to 9.02 ± 2.42 nM d^{-1} (seasonal average of 4.81 ± 1.49 nM d^{-1}) (Figures 2.4c, 2.4h, 2.5c, 2.6c). The rates tended to decrease slightly with depth and were two- to three-fold higher in the SAZ than the PFZ and AZ. No relationship was observed between ρNO_3^- and NO_3^- concentration (Figure 2.8a). The NH_4^+ uptake rates (ρNH_4^+) were about 10-fold higher than ρNO_3^-, with mixed-layer averages of 45.7 ± 24.4 to 115.8 ± 70.1 nM d^{-1} (seasonal average of 66.6 ± 14.4 nM d^{-1}) (Figures 2.4b, 2.4g, 2.5b, 2.6b). These elevated ρNH_4^+ rates were generally higher in the surface than at depth and appeared to co-vary with the ambient NH_4^+ concentration (Figure 2.8b). No relationship was apparent with latitude.

In summer, surface layer-averaged ρNO_3^- at stations 1-4 was an order of magnitude higher than in winter, ranging from 30.3 ± 7.5 to 61.9 ± 8.8 nM d^{-1} (seasonal average of 45.6 ± 6.8 nM d^{-1}) (Figures 2.4c, 2.4h, 2.5c, 2.6c). The rates decreased with depth along with the decline in light availability. Integrated ρNO_3^- increased from north to south, as did the contribution of ρNO_3^- to total N uptake (Table 2.1). The IS station was characterized by similar ρNO_3^- to stations 1-4 (Figure 2.7e) while ρNO_3^- at the SG station was significantly higher (surface layer average of 81.3 ± 30.7 nM d^{-1} and euphotic zone-integrated rate of 7.0 mmol m^{-2} d^{-1}; Figure 2.7b). In general, all the summer stations were characterized by lower ρNH_4^+ than ρNO_3^-, except station 2 where ρNH_4^+ was twice ρNO_3^-. The maximum surface layer-integrated ρNH_4^+ was observed at this station (5.6 mmol N m^{-2} d^{-1}; Table 2.1).

Note that the estimates of ρNH_4^+ were not corrected for possible NH_4^+ regeneration in the incubation bottles, which can dilute the ^{15}N-NH_4^+ substrate pool during tracer experiments, potentially yielding underestimates of ρNH_4^+ if not accounted for (Glibert et al. 1982) (see *Appendix A2.1*). However, the ambient euphotic zone NH_4^+ concentrations were relatively high (Figure 2.3c and d), which buffers ρNH_4^+ against isotope dilution to some extent. In addition, using the only available estimate of NH_4^+ regeneration for the open Southern Ocean (50 nM d^{-1}; Goeyens et al. 1991), I calculate that ρNH_4^+ may have been underestimated by a factor of 1.09 to 1.24 (1.19 on average). Such underestimation, while not insignificant, does not change the general observed trends. For example, the ratio of ρNO_3^- to ρNH_4^+ remains >1 (i.e., ρNO_3^- dominates) in all cases where it was >1 when NH_4^+ regeneration was assumed to be zero.

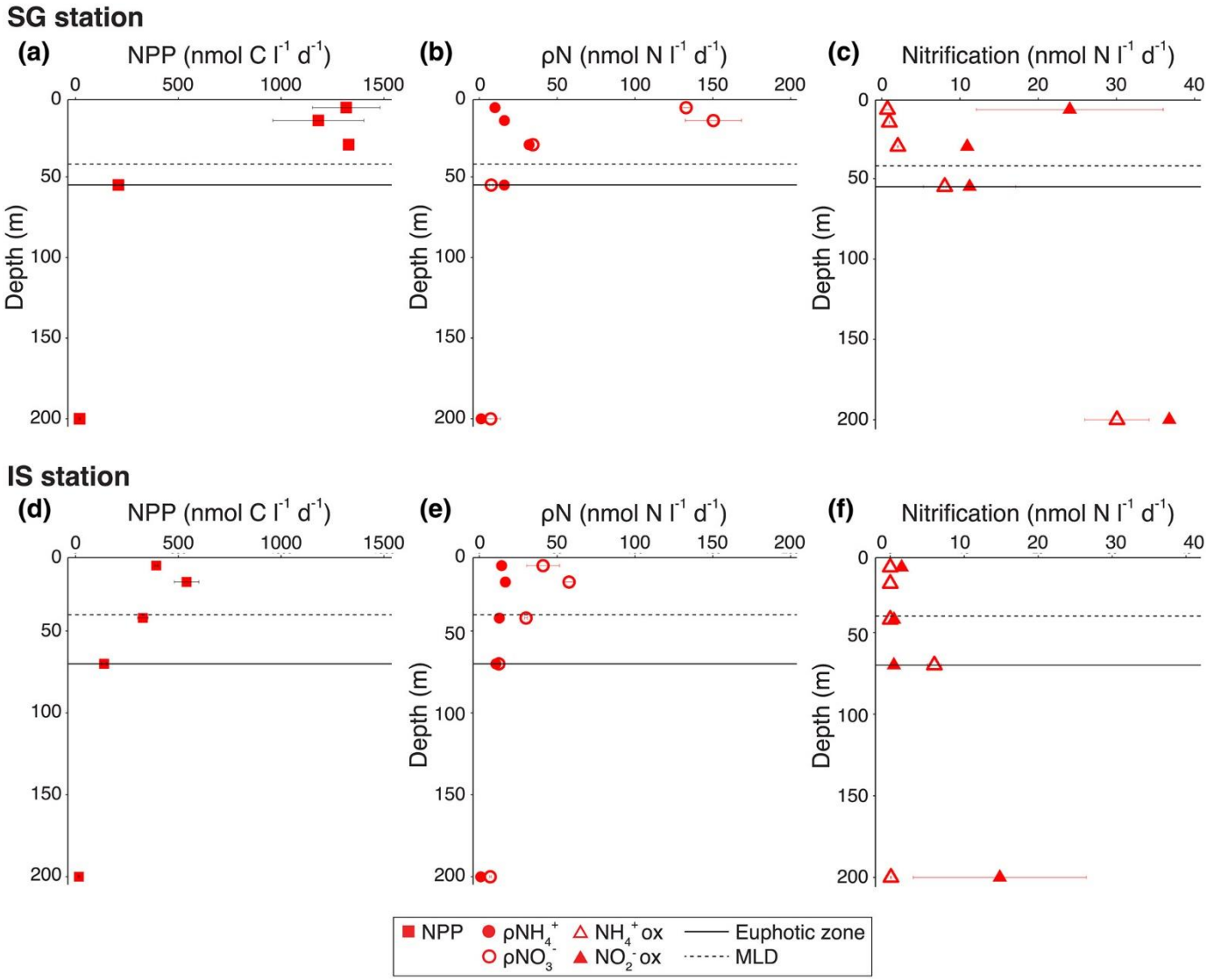

Figure 2.7: Summertime upper water column (0–200 m) rates measured at the SG station (55°S) of (a) NPP, (b) ρN (i.e., ρNO_3^- and ρNH_4^+), and (c) nitrification ($NH_4^+{}_{ox}$ and $NO_2^-{}_{ox}$), and at the IS station (70°S) of (d) NPP, (e) ρN, and (f) nitrification. The MLD is shown by the dotted horizontal line and the euphotic zone depth by the solid horizontal line. Error bars indicate the standard error of replicate experiments, each measured at least twice. Where error bars are not visible, they are smaller than the data markers. Note that ρNH_4^+ does not take into account possible isotope dilution due to NH_4^+ regeneration.

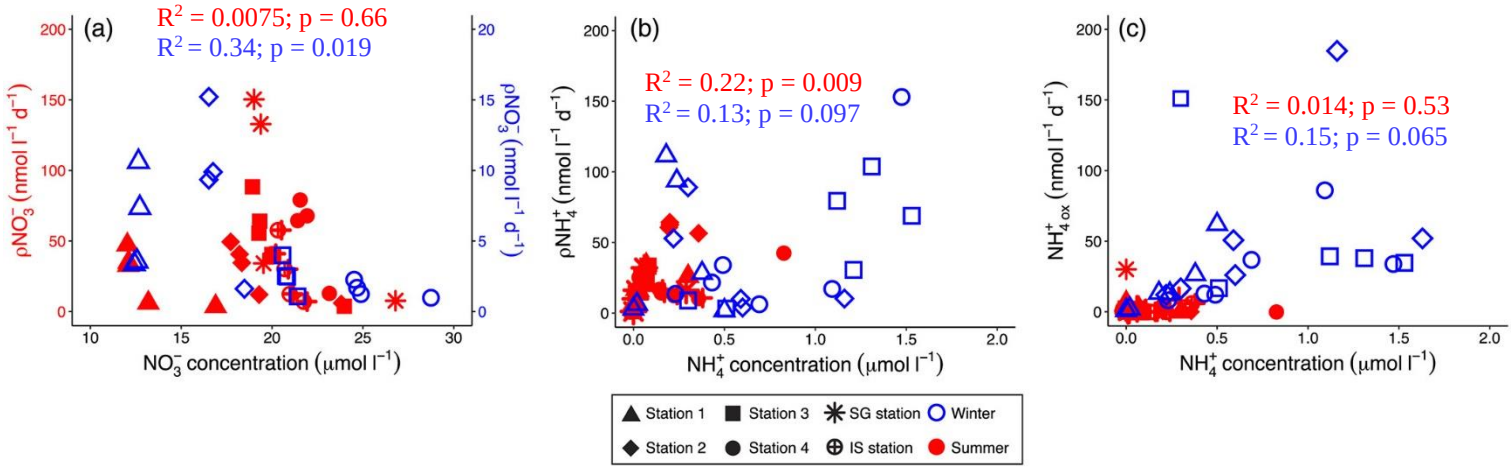

Figure 2.8: Relationship between the measured rates of (a) NO_3^- uptake and the ambient NO_3^- concentration, (b) NH_4^+ uptake and the ambient NH_4^+ concentration, and (c) NH_4^+ oxidation and the ambient NH_4^+ concentration. Blue symbols represent winter and red symbols represent summer. In panel (a), the left-hand *y* axis (red) applies to the summer data and the right-hand *y* axis (blue) to the winter data.

Finally, the ^{13}C-enrichment of the DIC pool will not be altered by regeneration rates on the order of 50 nM d^{-1} (~330 nM d^{-1} equivalent assuming Redfield stoichiometry) because of the high ambient DIC concentrations (≥2000 µM). Thus, if ρNH_4^+ were greatly underestimated, V_C should be higher than $V_{NH4}+V_{NO3}$ (where $V_M = \rho M/PM$; see section 2.4). In other words, if the specific rates of carbon fixation and N uptake are balanced, $V_C:(V_{NH4}+V_{NO3}) = 1:1$, so if V_{NH4} were underestimated, $V_C:(V_{NH4}+V_{NO3}) > 1:1$. This is the case only at station 3 and possibly station 4, where other factors could explain the carbon and N decoupling (see section 2.4.1.3). I conclude that ignoring NH_4^+ regeneration had a fairly minor effect in this case; however, the estimates of ρNH_4^+ should nonetheless be considered potential rates.

2.3.4 Nitrification rates

2.3.4.1 Ammonium oxidation

In winter, the average mixed-layer NH_4^+ oxidation rates ($NH_4^+{}_{ox}$) at stations 1-4 ranged from 10.7 ± 4.0 to 92.6 ± 54.0 nM d^{-1} (seasonal average of 38.9 ± 15.9 nM d^{-1}) and $NH_4^+{}_{ox}$ was measurable in euphotic zone waters at all stations (Figures 2.4d, 2.4i, 2.5d, 2.6d). The rates roughly co-varied with ambient NH_4^+ concentrations ≤0.7 µM, above which there appeared to be no relationship of NH_4^+ox with NH_4^+ concentration (Figure 2.8c).

In summer, stations 1-4 were characterized by $NH_4^+{}_{ox}$ rates that were ten- to one hundred-fold lower than those measured in winter. $NH_4^+{}_{ox}$ was low or below detection in the surface layer

(seasonal average of 1.1 ± 0.3 nM d^{-1}), increasing slightly at 200 m (Figure 2.4e, 2.4j, 2.5e, 2.6e). Similar $NH_4^+{}_{ox}$ rates were observed at the IS station (range of below detection to 6.0 nM d^{-1}), with the highest rate at the base of the euphotic zone (Figure 2.7f). The SG station was characterized by the highest summertime rates, three- to twelve-fold higher than those measured at the other stations (range of 0.7 to 30.1 nM d^{-1}; Figure 2.7c). The SG station also showed a clear increase in $NH_4^+{}_{ox}$ with depth, with the maximum rate observed at 200 m.

2.3.4.2 Nitrite oxidation

Wintertime mixed-layer NO_2^- oxidation rates ($NO_2^-{}_{ox}$) at stations 1-4 averaged 54.8 ± 17.0 to 98.4 ± 69.8 nM d^{-1} (seasonal average of 81.7 ± 19.2 nM d^{-1}) and were highest near the base of the mixed layer (Figures 2.4d, 2.4i, 2.5d, 2.6d). In summer, the $NO_2^-{}_{ox}$ rates at stations 1-4 were low in the surface layer (station average of 0.7 ± 0.1 to 2.6 ± 0.8; seasonal average of 1.3 ± 0.4 nM d^{-1}) and reached a maximum at 200 m (range of 8.7 to 32.0 nM d^{-1}; seasonal average of 18.3 ± 4.4 nM d^{-1}) (Figures 2.4e, 2.4j, 5e, 6e). While the IS station showed similar $NO_2^-{}_{ox}$ rates to stations 1-4 (Figure 2.7f), the SG station was characterized by relatively high rates, both within the euphotic zone (range of 10.9 to 24.0 nM d^{-1}) and at 200 m (36.8 nM d^{-1}) (Figure 2.7c); these were the highest $NO_2^-{}_{ox}$ rates measured for the summer.

2.3.5 f-ratio estimates

The surface layer depth-weighted average f-ratios, calculated using equation 2.2, were very low in winter (range of 0.03 to 0.11; seasonal average of 0.07) and generally decreased from north to south (Table 2.1). In summer, the f-ratios were much higher (range of 0.29 to 0.87; seasonal average of 0.66) and increased southwards, with the highest f-ratio computed for the SG station.

2.4 Discussion

2.4.1 Seasonal trends in NPP and N uptake across the Atlantic Southern Ocean

2.4.1.1 Rates of carbon production in the context of earlier measurements

The summertime surface-integrated rates of NPP, ranging from 31 to 58 mmol C m^{-2} d^{-1}, are similar to rates measured previously in the PFZ near South Georgia Island (34 to 45 mmol C m^{-2} d^{-1}) (Gilpin et al. 2002) where productivity is expected to be high due to an enhanced input of iron (Korb et al. 2005) and possibly silicate (Whitehouse et al. 2000). In a late summer study conducted along the GoodHope line, Joubert et al. (2011) did not measure NPP directly, but the total carbon production implied by their N uptake rates is consistent with our measurements (approximately 44 ± 19 mmol C m^{-2} d^{-1} assuming an NPP:N uptake ratio of 106:16; Redfield 1934). Our rates are double those measured in the open Atlantic Southern Ocean during spring (17-25 mmol C m^{-2} d^{-1}; Jochem et al. 1995) and late summer (4-22 mmol C m^{-2} d^{-1}; Froneman et al. 2001), possibly because our sampling occurred after the mixed layer had shoaled sufficiently to relieve phytoplankton from light limitation (as might have been experienced in spring) but before the onset of extreme iron deficiency (as likely occurred in late summer). No clear latitudinal gradient is observed in summertime NPP, with the maximum rate occurring in the PFZ (station 3). This, too, is consistent with earlier work from the Atlantic sector showing similar rates of NPP across the SAZ and AZ and elevated production in the PFZ (Froneman et al. 1995; 2001). Station 3 was located very close to the PF where surface divergence drives the upward supply of nutrient-rich (including iron and silicate) waters to the euphotic zone (Hense et al. 2000; Tremblay et al. 2002), which likely explains the higher productivity of this station.

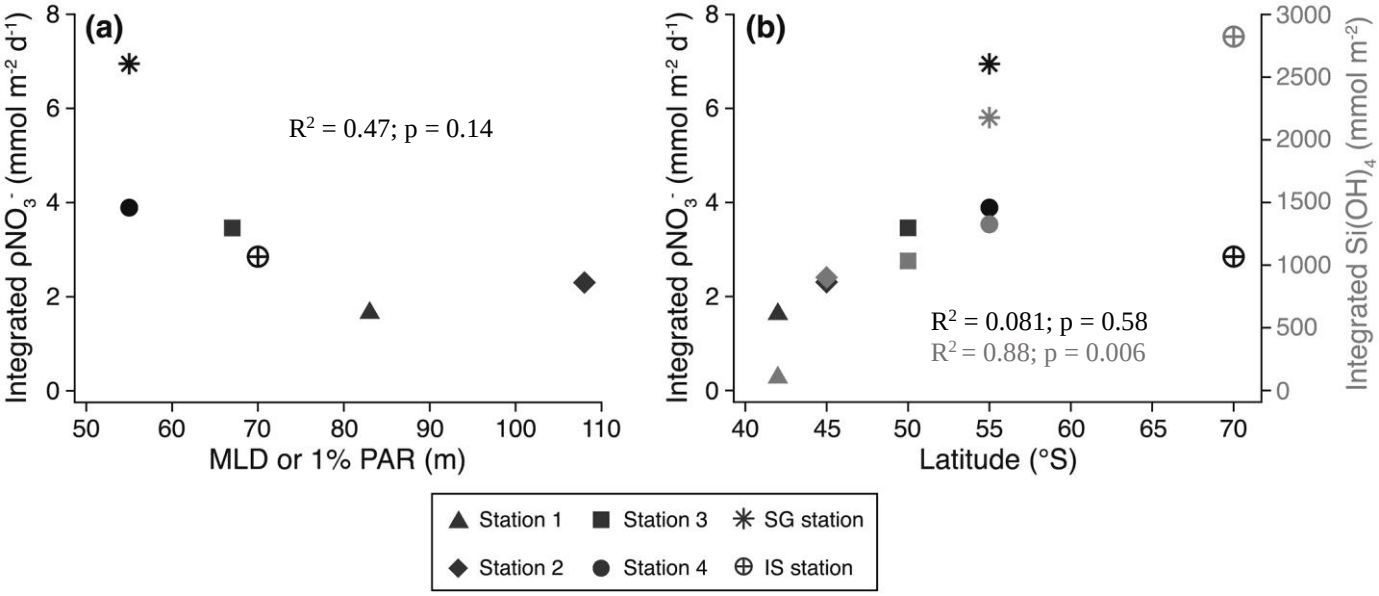

Figure 2.9: Summertime surface layer-integrated rates of nitrate uptake (ρNO_3^-; black symbols) as a function of (a) mixed layer or euphotic zone depth (1% PAR) and (b) latitude. In panel (b), the measured surface layer-integrated silicate ($Si(OH)_4$) concentration is also shown (gray symbols). "Surface layer" is the euphotic zone at Stations 1, 4, SG, and IS and the mixed layer at Stations 2 and 3 (Table 2.1; see section 2.2.7 for details).

MLD-integrated NPP (4 to 7 mmol C m^{-2} d^{-1}) is significantly lower in the winter and similar to the lone existing measurement from the wintertime Southern Ocean south of Africa (~11 mmol C m^{-2} d^{-1} in the SAZ; Froneman et al. 1999), as well as to winter data from the AZ off the West Antarctic Peninsula (1 ± 0.4 mmol C m^{-2} d^{-1}; Kottmeier and Sullivan, 1987). Our NPP data are thus consistent with previous characterizations of the Southern Ocean as productive in summer and largely biologically-dormant in winter (Heywood and Whitaker 1984; Smith and Nelson 1986). This is supported by the higher biomass C:N ratios observed in winter (8.4 ± 1.2) versus summer (6.7 ± 0.6), which suggest a role for heterotrophic degradation in autumn/early winter, driving the preferential remineralization of organic N over C (Schneider et al. 2003), and the dominance of balanced phytoplankton growth in summer that yields biomass with a C:N ratio similar to the Redfield ratio of 6.63:1 (Redfield 1934; Martiny et al. 2013). However, it is worth mentioning that the C:N ratio depends on a number of biological parameters like phytoplankton community composition, growth rates and environmental conditions; the assumption of Redfield C:N is made in the context of this understanding.

2.4.1.2 Potential drivers of nitrate versus ammonium uptake

On average across the transect, summer is characterized by higher depth-integrated ρNO_3^- than ρNH_4^+ (except at station 2), yielding f-ratios >0.5 (Table 2.1). I note that while ρNH_4^+ may be underestimated due to NH_4^+ isotope dilution (Glibert et al. 1982) leading to overestimates of the f-ratio, accounting for a realistic rate of NH_4^+ regeneration (~50 nM d^{-1}; Goeyens et al. 1991) does not change this general trend (see section 2.3.3. and *Appendix A2.1*). The apparent preference of phytoplankton for NO_3^- over NH_4^+ may be due to the >10-fold higher concentration of NO_3^- than NH_4^+, as well as the higher light availability characteristic of the summer. While surface NO_3^- concentrations are perennially high across the summertime Southern Ocean, phytoplankton need a great deal of energy to reduce NO_3^- during assimilation (Syrett 1956, 1981; reviewed by Glibert et al. 2016); thus, ρNO_3^- will decrease under low light conditions regardless of NO_3^- availability (Dorch, 1990) (Figure 2.8a). By contrast, NH_4^+ is less energetically expensive to assimilate but is present in summertime surface waters at relatively low concentrations, such that NH_4^+ availability likely constrains ρNH_4^+ (Figure 2.8b). Plotting surface layer-integrated ρNO_3^- as a function of MLD/euphotic zone depth shows that ρNO_3^- increases as the surface layer shoals (Figure 2.9a), confirming an important role for light in driving phytoplankton reliance on NO_3^-. A light-related control on NO_3^- versus NH_4^+ uptake is further supported by the observation that at all summer stations, ρNO_3^- decreases with depth while ρNH_4^+ is often constant or even higher towards the base of the euphotic zone/mixed layer.

While light availability seems to exert a dominant control on the seasonal cycle of NO_3^- assimilation in the Southern Ocean (Olson 1980; Hu and Smith 1998; Sambrotto and Mace 2000), it is unlikely to be the only explanation for the summertime variability in ρNO_3^-, with iron and silicate availability, as well as phytoplankton community composition, also playing a role (Hutchins et al. 2001; Tagliabue et al. 2012; Ganghi et al. 2012). Intracellular NO_3^- reduction has a high iron requirement (Sunda 1989) such that ρNO_3^- is reduced under low iron conditions. In a compilation of thousands of dissolved iron measurements from the Southern Ocean, Tagliabue et al. (2012) found that surface waters in the Atlantic SAZ/PFZ and AZ in summer are characterized by similar iron concentrations (averages of 0.30 ± 0.55 nM and 0.47 ± 0.69 nM, respectively), which suggests that latitudinal differences in iron availability do not explain the tendency for higher NO_3^- drawdown to the south (Figure 2.9b). That said, whether the iron concentrations varied across the different zones at the time of sampling is unknown.

In the PFZ and AZ, high surface silicate concentrations favour the growth of diatoms (Franck et al. 2000; Le Moigne et al. 2013), a group of phytoplankton considered NO_3^- specialists (Litchman et al. 2006; Fawcett and Ward 2011); the generally higher silicate availability in the AZ may thus favour higher ρNO_3^- (Figure 2.9b). Given the relationship of upper Southern Ocean silicate concentrations to latitude, however (Read et al. 2002; Sarmiento et al. 2004; Demuynck et al. 2019), which also affects light (and perhaps iron) availability, it is impossible to disentangle a potential silicate control on ρNO_3^-.

Table 2. 2: A selection of previously measured N uptake rates (ρNO_3^-, ρNH_4^+, and ρUrea) and f ratios for the Indian, Atlantic, and Pacific sectors of the open Southern Ocean

Region and Season	ρNO_3^-	ρNH_4^+	ρUrea	ρN	f-ratio	Incubation (hrs)	Reference
[a]Atlantic Sector (winter, July 2015 GoodHope line)						24	This study
SAZ (42-45°S)	0.47	5.40		5.87	0.11		
PFZ (50°S)	0.21	9.47		9.68	0.03		
AZ (55°S)	0.13	3.50		3.63	0.04		
[a]Atlantic Sector (winter, July 2012 GoodHope line)						24	Philibert et al.
SAZ (42-45°S)	1.02	32.9		33.92	0.03		(2015)
PFZ (50°S)	1.92	10.02		11.94	0.16		
AZ (55°S)	5.08	12.46		17.54	0.29		
Atlantic Sector (summer, January 2016 GoodHope line)						24	This study
[b]SAZ (42-45°S)	2.00	3.59		5.59	0.41		
[c]PFZ (50°S)	3.46	1.34		4.80	0.72		
[a]AZ (55°S)	3.89	1.15		5.04	0.77		
[a]South Georgia (PFZ; 50°S; 33°W)	6.95	1.07		8.02	0.87		
[a]Ice shelf (70°S; 07°E)	2.85	0.81		3.66	0.78		
Atlantic Sector (summer, March 2012 GoodHope line)						24	Joubert et al.
SAZ (42-44°S)	5.11	0.92	4.31	10.34	0.49		(2011)
PFZ (45-50°S)	1.97	1.16	2.13	5.26	0.41		
AZ (51-57°S)	3.39	1.27	2.86	7.51	0.45		
[c]Atlantic Sector (summer, March 2013 GoodHope line)						12	Philibert et al.
SAZ (43°S)	0.27	6.02		6.29	0.04		(2015)
[c]Indian Sector (late summer, April/May 1999)						10-24	Thomalla et al.
SAZ (41-46°S)	0.94	5.26	6.48	12.67	0.09		(2011)
[c]Indian Sector (late summer, February-March 2006)						4-6	Prakash et al.
SP4_SAZ (43°S)	1.58	0.99	0.48	3.05	0.52		(2015)
SP3_PFZ (58°S)	0.92	0.58	0.22	1.72	0.53		
[c]Indian Sector (summer, February-April 2009)						4	Gandhi et al.
Transect A (35-66°S)	0.6-2.4 (1.3[d])	0.8-1.6 (1.1[d])	0.9-1.8 (1.3[d])		0.2-0.5		(2012)
Transect B (35-65°S)	0.3-4.1 (1.7[d])	0.8-1.5 (1.1[d])	0.9-2.2 (1.3[d])		0.1-0.7		
[e]Indian Sector (spring, October-December 2001)						12	Savoye et al.
SAZ/STF (49-51°S)				4.40	0.53		(2004)
PFZ (54-57°S)				5.60	0.56		
AZ				9.60	0.61		
[c]Pacific sector (summer, December/February 1997)						3-24	Sambrotto and
PFZ (57-61°S)	2-5 (2.3[d])				0.05-0.48		Mace (2000)

[a] Integrated over the MLD. [b] Average of two stations, 42°S integrated to MLD, 45°S integrated to euphotic zone depth (see text for details). [c] Integrated over the euphotic zone. [d] Averages of ranges. [e] Integrated over upper 70 m of the water column.

The general preference for NO_3^- over NH_4^+ across the summertime Southern Ocean is attributed to the alleviation of light and iron limitation of phytoplankton since sampling took place late enough in the season for stratification to have set in but prior to the exhaustion of iron. This should favour the proliferation of larger NO_3^--consuming phytoplankton including diatoms in regions with adequate surface silicate. In addition, the north-south increase in both ρNO_3^- and the f-ratio can be explained by the combined influence of light, iron, and silicate, and possibly also phytoplankton community composition. Finally, I note that surface layer-integrated ρNH_4^+ is both proportionally and absolutely higher at the SAZ stations, particularly at station 2, even though the ambient NH_4^+ concentration is low. This may indicate enhanced recycling and a phytoplankton community dominated by smaller cells in the SAZ (Froneman et al. 2001) where mixed layers are deeper (i.e., potentially driving some degree of light limitation; Sallée et al. 2010; du Plessis et al. 2017) and silicate concentrations are lower (Sarmiento et al. 2004). Our summertime rates of NO_3^- and NH_4^+ uptake are broadly consistent with previous work in all sectors of the Southern Ocean (Table 2.2; Savoye et al. 2004; Joubert et al. 2011; Gandhi et al. 2012; Prakash et al. 2015), although higher rates of NH_4^+ than NO_3^- uptake have also been observed. For example, Philibert et al. (2015) measured rates of NH_4^+ uptake >10-times higher than coincident ρNO_3^- in the SAZ along the GoodHope line. However, they sampled in late summer (late February/early March) when iron and silicate limitation are expected to be highest (Hutchins et al. 2001; smith and bue et al. 2012), N recycling should be enhanced (Timmermans et al. 1998; Hutchings et al. 2001), and the phytoplankton community is more likely to be dominated by smaller cells (Gandhi et al. 2012).

2.4.1.3 Additional sources of N to phytoplankton

Above and in the f-ratio calculations (equation 2.2), ρNH_4^+ is equated with regenerated production, which may underestimate this flux because it does not consider the possibility of DON uptake by phytoplankton (i.e., compounds such as urea and cyanate; Bronk 2002; Widner et al. 2016). Urea is a highly labile form of DON with a turnover time of minutes to days (Bronk et al. 1998) that has been shown to contribute significantly to regenerated production in the Southern Ocean in late summer (Joubert et al. 2011; Gandhi et al. 2012; Prakash et al. 2015) and early autumn (Thomalla et al. 2011). Additionally, while measurements of cyanate uptake are scarce, this N species has been estimated to support as much as 10% of total N uptake in the oligotrophic North Atlantic (Widner et al. 2016), with lower contributions measured in coastal waters (Widner and Mulholland 2017) and the eastern tropical north Pacific (Widner et

al. 2018). To our knowledge, there are no measurements of cyanate uptake from the Southern Ocean, although a gene encoding cyanate acquisition (the transporter *cynA*), typically associated with surface cyanobacteria, has been found in the Amundsen and Bellinghausen Seas (Kamennaya and Post 2013). Ignoring phytoplankton consumption of urea and possibly cyanate (or indeed, any form of labile DON) during mid-summer may thus lead to an overestimation of carbon export potential (Bronk et al. 1994; Fernández and Raimbault 2007; Peng et al. 2018). To address this the specific rates of N uptake versus C fixation (i.e., V_{N_total} (= V_{NO3}+V_{NH4}) vs. V_C) are plotted (Figure 2.10a). In theory, if all surface layer productivity is supported only by NO_3^- and NH_4^+, then V_{N_total} and V_C, averaged over the MLD/euphotic zone, should fall along a 1:1 line. This proves to be the case for stations 1, 2, SG, and IS. The implication is that, at least at the time of our sampling, summertime NPP was supported near-exclusively by NO_3^- and NH_4^+ at these stations, while at stations 3 and 4, 45 ± 28% and 30 ± 16% of carbon production was fuelled by an alternative N source (i.e., V_C is 45 ± 28% and 30 ± 16% higher than V_{N_total}, indicating a decoupling between these two variables).

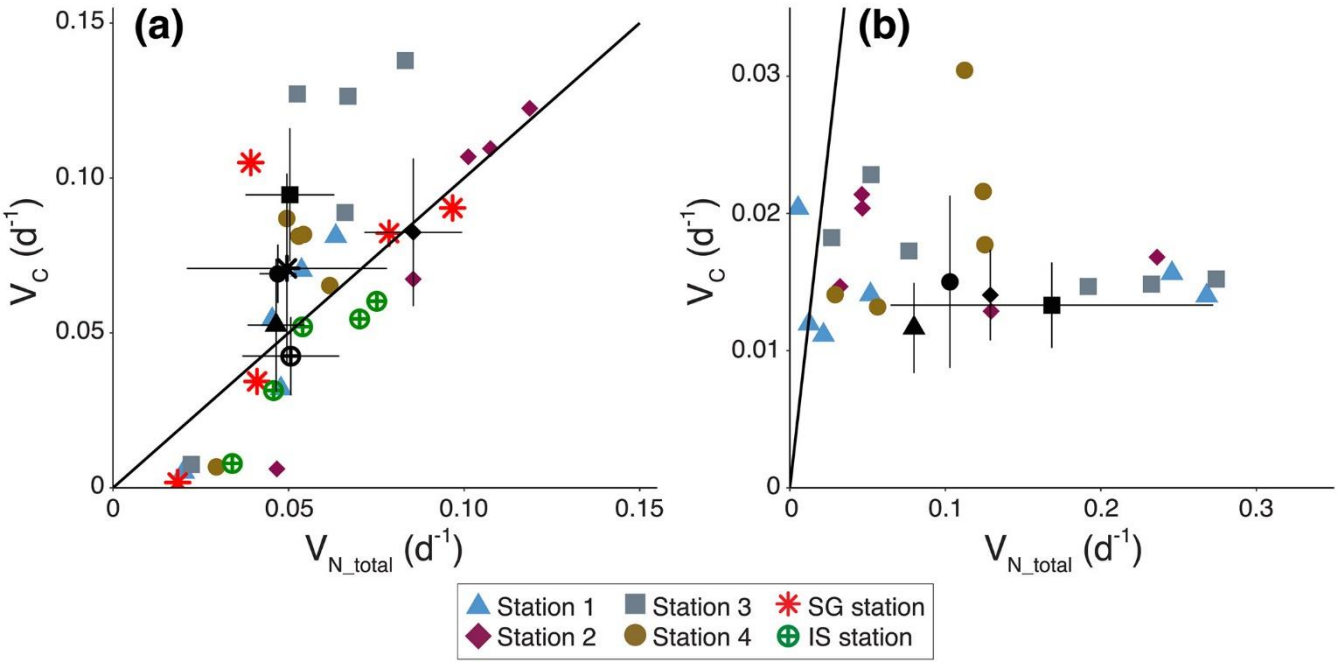

Figure 2.10: Specific uptake rates of carbon (V_C = NPP/POC) versus nitrogen (V_{N_total} = V_{NO3} + V_{NH4}) for (a) summer and (b) winter. Coloured symbols show the rates at the individual incubation depths, and the corresponding black symbols represent the 0–200 m-weighted average rates at each station. Integrating to the base of the mixed layer or euphotic zone rather than 200 m makes little difference to the averages because the specific rates at 200 m are very low. The solid black line represents V_C:V_{N_total} = 1:1, which is expected for balanced phytoplankton growth assuming that the only N forms being assimilated are NO_3^- and NH_4^+.

The most obvious candidate for this "missing" N is some form of regenerated DON, which, if it fueled all the NPP not accounted for by ρNO_3^- and ρNH_4^+, would significantly decrease carbon export potential at stations 3 and 4. Alternatively, the "missing" N source could have been new rather than regenerated, which would increase carbon export potential. The only available N_2 fixation data from the open Southern Ocean (measured southwest of the Kerguelen Plateau) suggest an average mixed-layer rate of <0.005 d^{-1} (González et al. 2014), which is an order of magnitude too low to account for the "missing" N consumption implied by Figure 2.10a (0.044 ± 0.012 d^{-1} and 0.022 ± 0.004 d^{-1} at stations 3 and 4, respectively). Moreover, given the evidence that low temperature (Staal et al. 2003; Moore et al. 2004), low iron (Paerl et al. 1994; Berman-Frank et al. 2001; Kustka et al. 2003), and/or high NO_3^- (Holl and Montoya 2005; Knapp et al. 2012) are unfavourable for N_2 fixation, this process is unlikely to ever be significant in Southern Ocean surface waters. In addition, modeling studies suggest virtually no atmospheric N deposition to the Atlantic Southern Ocean, particularly south of 50°S where stations 3 and 4 are located (Kanakidou et al. 2012; Jickells et al. 2017). Thus, it is most likely that the "missing" N source was regenerated, implying that regenerated production may have been underestimated and the f-ratio overestimated at these two stations.

2.4.1.4 Evidence for heterotrophic bacterial ammonium uptake in winter

Winter is characterized by a MLD-integrated ρNH_4^+ that is 10- to 70-fold higher than ρNO_3^-. This trend has been observed previously in the winter Southern Ocean, with similar findings reported for the Weddell/Scotia Sea (Cota et al. 1992) and GoodHope line (Philibert et al. 2015). One possibility is that the low light available to phytoplankton during winter driven by the deep MLDs and low insolation favor NH_4^+ over NO_3^- consumption (Syrett, 1981; Dortch, 1990). Indeed, previous observations of the apparent preference of Southern Ocean phytoplankton for NH_4^+ in winter have been explained thus (Cota et al. 1992; Philibert et al. 2015). However, our concurrent measurements of NPP and N uptake show that a significant fraction of the NH_4^+ consumption occurs without the rate of carbon fixation expected if the NH_4^+ were consumed by phytoplankton. Instead, a comparison of V_{N_total} and V_C reveals that NPP and N uptake are strongly decoupled during winter (Figure 2.10b), with as much as ten times more N consumed (mainly in the form of NH_4^+; Table 2.1) than carbon fixed. I note that ρNH_4^+ can be overestimated from isotope tracer experiments when ambient NH_4^+ concentrations are so low that the addition of ^{15}N-NH_4^+ stimulates uptake (Lipschultz 2008). However, in part due to the relatively high winter mixed-layer NH_4^+ concentrations, our ^{15}N-

NH_4^+ additions were always ≤10% of the ambient pool. The high measured ρNH_4^+ is thus attributed to high rates of NH_4^+ assimilation by heterotrophic bacteria, which would yield no carbon fixation.

There are very few direct measurements of heterotrophic bacterial N uptake in the Southern Ocean, with no studies conducted in winter. For summer, the only available data are from coastal waters near the Antarctic Peninsula where the bacterial NH_4^+ demand was ~17% of the total community NH_4^+ uptake rate (Tupas and Koike 1990; 1991). Cochlan and Bronk (2001) report similar potential ρNH_4^+ by heterotrophic bacteria in the summertime Ross Sea. The paucity of Southern Ocean data notwithstanding, marine heterotrophic bacterial uptake of inorganic N is well documented, with bacteria showing a strong preference for NH_4^+ over urea and NO_3^- (Kirchman et al. 1991; 1994; Allen et al. 2002; Bradley et al. 2010). For example, a study conducted in the Arctic during autumn measured rates of NH_4^+ uptake by heterotrophic bacteria that were 43-80% higher than those attributed to phytoplankton (Fouilland et al. 2007). The low light availability that characterizes the wintertime Southern Ocean makes it difficult for phytoplankton to thrive (Smith and Sakshaug, 1990). This, coupled with the relatively high ambient NH_4^+ concentrations that appear to typify the winter mixed layer, may favour bacterial NH_4^+ consumption. For the AZ south of Africa, Smart et al. (2015) hypothesize that autumn/early winter surface waters are characterized by intense N recycling. Heterotrophic bacteria must play a central role in such recycling, possibly in both the production and consumption of NH_4^+.

One implication of heterotrophic bacterial NH_4^+ consumption is that previous winter (and possibly even summer) studies of N uptake that did not include synchronous measurements of NPP may have overestimated autotrophic productivity. For example, if the high winter mixed layer-integrated ρNH_4^+ reported by Philibert et al. (2015) were solely due to phytoplankton, NPP would need to be higher than is typically measured in summer (i.e., ≥60 mmol C m^{-2} d^{-1}, assuming a C:N uptake ratio of 106:16). For the Atlantic Southern Ocean during late summer/early autumn, Probyn and Painting (1985) attributed 75% of the measured NH_4^+ assimilation to "picoplankton". Some portion of that NH_4^+ may have been consumed by heterotrophic bacteria given that they overlap in size with picophytoplankton (<1 µm). Without co-occurring measurements of NPP and ρNH_4^+, the heterotrophic contribution to NH_4^+ uptake cannot be quantified.

2.4.1.5 Carbon and nitrogen cycling in potentially naturally iron-fertilized regions

Southern Ocean NPP is not limited by N but by a combination of iron (Martin, 1990; Smetacek et al. 2012) and light availability (Nelson and Smith, 1991), with $Si(OH)_4$ playing a role in SAZ waters (Hutchins et al. 2001; Pollard et al. 2002). However, there are naturally iron-fertilised regions of the Southern Ocean (Ardyna et al. 2019 and references therein) that have been shown to support high rates of NPP and NO_3^- uptake (yielding high estimates of carbon export potential), such as the waters near Subantarctic islands (Korb et al. 2005; Seeyave et al. 2007; Blain et al. 2007; Cavagna et al. 2015) and associated with melting sea ice and ice shelves (Wang et al. 2014; St Laurent et al., 2019; Twelves et al., 2020) (see *Appendix A2.2*). Iron concentrations were not measured in this study so iron limitation of phytoplankton (or the extent of its alleviation) cannot be directly evaluated. However, two of the summer stations are located in regions that may experience less iron-limited conditions – near the island of South Georgia (55˚S; 33˚W) and at the Fimbul Ice Shelf (70˚S; 07˚E) (SG and IS; Figure 2.1).

The SG station is characterized by a higher ρNO_3^- and f-ratio than all the other stations, and a higher rate of NPP than all but station 3 (Table 2.1). In addition, the NO_3^- concentration gradient between the T_{min} and the surface is steeper at SG (8.6 µM) than at the other stations at a similar latitude (1.5 µM at station 4; 1.1 µM at station 3), indicating a higher degree of seasonal NO_3^- drawdown at SG. Likewise, the T_{min}-to-surface gradient in silicate concentration is 17.9 µM at SG and only 4.2 µM at station 4 (not shown). Thus, silicate also suggests higher seasonal productivity at SG, and further implies that NPP is driven largely by diatoms, a group considered disproportionately important for carbon export (Buesseler 1998b). Our observations can be explained by the alleviation of phytoplankton iron limitation, which enhances NO_3^- reductase activity (Timmermans et al. 1994) and may increase the affinity of diatoms for silicate (Brzezinski et al. 2005; Mosseri et al. 2008). Indeed, elevated dissolved iron concentrations have been measured in the upper 200 m around South Georgia in summer (as high as 7.70 nM, versus <0.4 nM in the open Atlantic sector; Nielsdóttir et al. 2012; Tagliabue et al. 2012; Schlosser et al. 2018) and large, long-lasting phytoplankton blooms are regularly observed downstream of the plateau (Atkinson et al. 2001; Korb et al. 2004; Borrione and Schlizer, 2013).

In contrast to SG, there appears to be no stimulation of productivity at the IS station where low rates of NPP and N uptake were measured (Table 2.1). Interestingly, the f-ratio at IS was higher

than at all the other summer stations except SG. Numerous studies have observed elevated biological activity near ice shelves, which is typically attributed to the alleviation of iron limitation due to local iron inputs associated with melting sea ice (Aguilar-Islas et al. 2008; Tovar-Sánchez et al. 2010; Gerringa et al. 2012; 2015; Herraiz-Borrenguero et al. 2016). That this was not the case at IS is probably because sampling occurred too late in the season to capture the period of intense sea-ice melt. In other words, by the time of our sampling in late January, any iron supplied from melting sea ice to the waters near the ice shelf had already been consumed by an earlier phytoplankton bloom. This is consistent with the observation that POC concentrations were highest at IS while NPP was lowest. The high f-ratio at IS can be attributed to the fact that the MLD was significantly shallower than the euphotic zone, allowing enough light into the mixed layer to favour NO_3^- consumption even though total N uptake was low. The implication is that iron (rather than light) exerted the dominant control on productivity at the Fimble Ice Shelf at the time of our sampling, but by limiting rather than stimulating phytoplankton growth.

In sum, the data show that, unsurprisingly, the Southern Ocean is more productive in summer than winter in terms of NPP and carbon export potential (the latter inferred from ρNO_3^-). However, the new production paradigm as a framework for computing the potential for export production is ill-suited for the wintertime Southern Ocean because of the high proportion of NH_4^+ uptake that occurs in the absence of carbon fixation. The new production paradigm may adequately describe new and regenerated N uptake and carbon export potential in summer, with the caveats that 1) regenerated DON consumption cannot be ignored and 2) the rate of euphotic zone nitrification must be low relative to ρNO_3^-. This latter requirement is examined in detail below.

2.4.2 The seasonal cycle of nitrification in the Southern Ocean surface layer

Rates of surface layer nitrification were low in summer and high in winter, consistent with expectations for a region governed by high hydrographic seasonality. In winter, the mixed layer is deep (up to 150-200 m) relative to the base of the euphotic zone (<100 m; Table 2.1) and incident radiation is low. This means that light inhibition of nitrifying microorganisms (Horrigan et al. 1981; Olson 1981b; Guerrero and Jones 1996; Merbt et al. 2012; Qin et al. 2014) is alleviated and phytoplankton spend long periods in the dark, rendering them far less competitive for NH_4^+ (Ward 1985; 2005; Smith et al. 2014; Wan et al. 2018). Despite our

observation of elevated NH_4^+ oxidation in winter, NH_4^+ uptake (likely by heterotrophic bacteria) occurs at double the $NH_4^+{}_{ox}$ rate at three out of four stations (Table 2.1). This suggests that the NH_4^+ regeneration flux must be high in autumn following the period of high NPP and/or high in winter (i.e., at the time of our sampling) in order to support significant rates of NH_4^+ uptake and oxidation and still yield a relatively high mixed-layer NH_4^+ concentration. When the mixed layer shoals in summer, surface layer nitrification is no longer favorable because nitrifiers are more likely to experience light inhibition and phytoplankton, now released from light limitation, will outcompete the slow-growing nitrifiers for NH_4^+. Indeed, the surface layer-integrated NH_4^+ uptake rates are 6-50 times higher than the concurrently-measured NH_4^+ oxidation rates in summer.

Direct measurements of nitrification south of 40°S are limited, with only two studies focused on the open Southern Ocean (Olson, 1981a; Bianchi et al. 1997). Nonetheless, our summer rates (0.7 to 30.1 nM d^{-1} for $NH_4^+{}_{ox}$ and 0.3 to 36.8 nM d^{-1} for $NO_2^-{}_{ox}$) fall within the range reported previously for the open and coastal Southern Ocean and other high latitude regions. For example, Olson (1981a) measured low rates of NH_4^+ oxidation (6 to 8.9 nM d^{-1} and 0 to 12.9 nM d^{-1}) during mid-summer and spring in the Ross and Scotia Seas, respectively, and Tolar et al. (2016) report average summertime mixed-layer NH_4^+ oxidation rates of 13 ± 3 nM d^{-1} for experiments conducted on the continental shelf and slope west of the Antarctic Peninsula. Similarly, low summertime NH_4^+ oxidation rates (0-30 nM d^{-1}) have been measured throughout the euphotic zone of the Pacific Arctic Ocean (55°N to 68°N) (Shiozaki et al. 2016) and in the surface of the Chukchi and Beaufort Seas (0-11 nM d^{-1}) (Christman et al. 2011; Baer et al. 2014). In contrast, Cavagna et al. (2015) measured mixed-layer nitrification rates of 0-3000 nM d^{-1} in the spring on the Kerguelen Plateau (although most values were <1000 nM d^{-1} and almost all the higher rates occurred below the euphotic zone). However, given that this region is highly iron (and silicate) fertilized and characterized by elevated productivity (de Baar et al. 1995; Blain et al. 2001; 2007), the high rates of NO_3^- production are unlikely to be representative of the open Southern Ocean.

There are no direct measurements of nitrification from the open Southern Ocean in winter with which to compare my data (0.7 to 334 nM d^{-1} for $NH_4^+{}_{ox}$ and 0 to 342 nM d^{-1} for $NO_2^-{}_{ox}$). Tolar et al. (2016) report NH_4^+ oxidation rates from the upper 150 m off the West Antarctic Peninsula in late winter (September) of 62 ± 16 nM d^{-1}, but given the coastal nature of this sampling site, the rates cannot be taken to reflect the open Southern Ocean. Bianchi et al. (1997) measured

NH_4^+ and NO_2^- oxidation across the Indian open Southern Ocean in autumn (April and May) and report rates over the upper 100 m of 24-84 nM d^{-1} and 9.6-72 nM d^{-1}, respectively. These are within the range of the winter rates measured here, albeit at the low end. The lower rates may in part derive from the fact that Bianchi et al. (1997) only sampled the upper 100 m of the water column, yet the mixed layer would have been deeper than this at many of their stations (Dong et al. 2008; Sallée et al. 2010) and nitrification rates tend to be higher towards the base of the mixed layer. Another possibility is that in autumn, phytoplankton, now iron-limited and unable to efficiently consume NO_3^- (Hutchins et al. 2001; Tagliabue et al. 2012) but still experiencing sufficient light levels to photosynthesize, assimilate predominantly NH_4^+ (El-Sayed, 1987; Jacques 1991; Goeyens et al. 1995; Priddle et al. 1998), largely outcompeting nitrifiers for this substrate. In any case, the available data (including those reported here) suggest that low light and reduced competition for NH_4^+ create conditions in the Southern Ocean's winter mixed layer that favor nitrification. In the summer by contrast, light inhibition and rapidly growing phytoplankton allow for rates of surface nitrification that are insignificant relative to both wintertime nitrification and summertime autotrophic NO_3^- consumption. This seasonal pattern is also evident in the available Southern Ocean NO_3^- isotope data that show assimilation to be the major biological process acting on the surface NO_3^- pool in summer (DiFiore et al. 2009; Kemeny et al. 2016; Fripiat et al. 2019) with nitrification dominating in winter (Smart et al. 2015).

The NO_2^- concentrations over the upper ~200 m of the water column showed no trend with depth and are similar in summer and winter (~0.2 µM) despite the large seasonal differences in $NH_4^+{}_{ox}$ and $NO_2^-{}_{ox}$ (see *Appendix A2.3*). This has been observed previously in high-latitude surface waters (Fripiat et al. 2019; Zakem et al. 2018) and is in contrast to the oxygenated oligotrophic ocean where NO_2^- builds up at the base of the euphotic zone as a primary NO_2^- maximum (Lomas and Lipschultz 2006; Ward 2008). The accumulation of NO_2^- throughout the upper water column poleward of 45° has been explained as deriving from the upward mixing in winter of NO_3^-+NO_2^- that cannot be depleted by phytoplankton due to iron and/or light limitation and that is then available to nitrifying organisms (Zakem et al. 2018). In other words, NH_4^+ and NO_2^- oxidizing organisms should coexist in Southern Ocean surface waters with iron/light-limited phytoplankton. Our data suggest that the situation is more nuanced than this. Open Southern Ocean phytoplankton always experience some degree of iron limitation (Moore et al. 2007; Tagliabue et al. 2012), which becomes more pronounced over the growing season (Tagliabue et al. 2014; Ryan-Keogh et al. 2018; Mtshali et al. 2019). Despite this,

nitrification is insignificant relative to autotrophic NO_3^- and NH_4^+ uptake in the euphotic zone in summer, with higher rates observed only in the dark sub-euphotic zone waters. By contrast, in winter when the mixed layer deepens below the base of the euphotic zone, phytoplankton growth is minimal despite the entrainment of iron from the subsurface (Tagliabue et al. 2014; Mtshali et al. 2019) and nitrification rates are high. These observations suggest that light exerts a stronger control than iron on potential phytoplankton-nitrifier co-existence in Southern Ocean surface waters.

2.4.3 Estimates of the f-ratio and implications for the new production paradigm

Southern Ocean f-ratios calculated previously from ^{15}N uptake experiments range from 0.03 to 0.70, with similar values reported for the Indian, Atlantic and Pacific sectors, and most of the available data generated for the summer (Table 2.2). Using equation 2.2, relatively high summertime surface layer-integrated f-ratios are calculated (range of 0.29 to 0.87, average of 0.66 if all stations are considered and 0.58 if only stations 1-4 are considered). Taken at face value, these f-ratios imply that ~60% of summertime NPP is available for export into the ocean interior. However, the AZ rate data suggest that a form of regenerated DON may support as much as 30-45% of NPP. Accounting for this decreases the station 3 and 4 f-ratios to 0.40 ± 0.24 and 0.55 ± 0.28, respectively ($f\text{-ratio}_{(corrected)}$ (DON) in Table 2.1), significantly reducing the carbon export potential implied by the AZ measurements of NO_3^- and NH_4^+ uptake alone.

Very low wintertime f-ratios are calculated (0.03-0.11), driven by NH_4^+ uptake rates that are 11 to 45 times higher than the coincident ρNO_3^-, in line with previous winter estimates for the same region (0.03-0.29; Table 2.2). These latter values were interpreted as indicating that most wintertime NPP in the Southern Ocean is regenerated. However, as discussed above, our winter rates of NH_4^+ uptake (and those of Cota et al. (1992) and Philibert et al. (2015)) are anomalously high and almost entirely decoupled from concurrently-measured rates of NPP, which is best explained as reflecting high rates of heterotrophic bacterial NH_4^+ uptake. Given the available data, it is not possible to disentangle the relative contribution of heterotrophs versus autotrophs to NH_4^+ assimilation in the winter Southern Ocean. Even if NPP and autotrophic N uptake are assumed to be tightly coupled such that any NH_4^+ consumption in excess of the stoichiometric quantity required to support NPP (minus the contribution from NO_3^- uptake) is due to heterotrophic bacteria, it is unknown whether phytoplankton consume some quantity of DON during the winter and/or heterotrophic bacteria are responsible for some portion of the

measured NO_3^- uptake (Kirchman 1994; Kirchman and Wheeler 1998; Fouilland et al. 2007). The implication of these uncertainties is that wintertime NH_4^+ consumption in the Southern Ocean cannot be equated to regenerated production, and any calculation of the f-ratio predicated on this assumption will be inaccurate.

Euphotic zone nitrification represents an additional complication to calculations of the f-ratio, and not accounting for it can yield significant overestimates of this parameter and the carbon export flux (Yool et al. 2007). Unlike in the case of DON, the *in situ* production of NO_3^- in surface waters would not be detectable as a "missing" N source because phytoplankton do not distinguish between new and regenerated NO_3^- during assimilation. However, our concurrent measurements of N uptake and NH_4^+ and NO_2^- oxidation can be used to estimate the fraction of NO_3^- consumption deriving from surface nitrification, and the f-ratio (equation 2.2) can be corrected for nitrification following (Fernández et al., 2005):

$$\text{f ratio}_{(\text{corrected})} = \frac{V_{NO3} - V_{\text{nitrification}}}{V_{NO3} + V_{NH4}} \qquad (2.5)$$

One might assume that the best approximation of $V_{\text{nitrification}}$ (i.e., the rate of nitrification) is $NO_2^-{}_{ox}$, as this is the step in the nitrification pathway that actually produces NO_3^-. However, since the pathway that is rate-limiting for nitrification is not clear, $NH_4^+{}_{ox}$ may be an equally good indicator of the *in situ* nitrification rate (Yool et al. 2007). The f-ratio is thus corrected using both $NH_4^+{}_{ox}$ and $NO_2^-{}_{ox}$ in order to yield the broadest possible range of corrected values. Subtracting measured nitrification from nitrate uptake may not yield the most accurate estimates of the f-ratio$_{(\text{corrected})}$, particularly at high rates of nitrification (Yool et al. 2007). However, it is the best option available given the data I have in hand. Moreover, high rates of surface-layer nitrification were measured in winter only, leading me to conclude that the f-ratio cannot be computed with any confidence for this season (see below), regardless of how one corrects for nitrification.

In summer, surface-integrated $NH_4^+{}_{ox}$ and $NO_2^-{}_{ox}$ are low at all stations, but they are not zero. The f-ratios decline by 0.9-5.2% (average of 2.8 ± 1.8%) using $NH_4^+{}_{ox}$ and 0.8-9.4% (average of 4.6 ± 3.9%) using $NO_2^-{}_{ox}$ as a proxy for nitrification. This is in keeping with Southern Ocean NO_3^- isotope studies that have estimated surface layer nitrification to account for <10% of the NO_3^- consumed by phytoplankton during summer (Trull et al. 2008; DiFiore et al. 2009). To a

first approximation, therefore, equating NO_3^- uptake to new (and export) production appears to be reasonable for the Southern Ocean in summer, although regenerated DON assimilation requires consideration. Indeed, accounting for the possibility of DON uptake in summer decreases the f-ratio far more than *in situ* nitrification at stations 3 and 4. The combined effect of DON consumption and surface nitrification is to decrease the fraction of NPP potentially available for export in the summer from 66 ± 21% to 54 ± 21% if all stations are considered, and from 58 ± 22% to 42 ± 12% if only stations 1-4 are included.

For winter, a comparison of mixed layer-integrated $NH_4^+{}_{ox}$ and $NO_2^-{}_{ox}$ with ρNO_3^- suggests that on average, 16 ± 14 times more NO_3^- is regenerated than is consumed by phytoplankton (18 ± 14 times if $NH_4^+{}_{ox}$ and 14 ± 9 times if $NO_2^-{}_{ox}$ is used as a proxy for nitrification; Table 2.1). This suggests that, from a mass balance perspective, none of the carbon produced in Southern Ocean surface waters in winter is exported into the ocean interior (Dugdale and Goering, 1967; Eppley and Peterson, 1979). Moreover, that nitrification can account for >100% of ρNO_3^- at all stations, coupled with the evidence for heterotrophic bacterial assimilation of NH_4^+, renders wintertime calculations of the f-ratio meaningless. In Table 2.1, f-ratios that have been "corrected" for nitrification according to equation 2.5 ($f\text{-ratio}_{(corrected)}$ ($NH_4^+{}_{ox}$) and $f\text{-ratio}_{(corrected)}$ ($NO_2^-{}_{ox}$)) are presented. However, for winter, this exercise is intended only to illustrate the failure of the new production paradigm as a framework for understanding carbon production and export; the winter $f\text{-ratios}_{(corrected)}$, which are all negative, have no quantitative meaning.

Based on measurements of NO_3^- isotope ratios, Smart et al. (2015) concluded that the AZ winter mixed layer is conducive to nitrification because of the highly seasonal nature of these polar waters. Our dataset extends this characterization to include the PFZ and SAZ. Indeed, it is the strong seasonal cycle – a discrete summertime period of mixed-layer NO_3^- drawdown followed by a low-light winter period characterized by high rates of mixed-layer nitrification – that appears to render the new production paradigm appropriate for estimating carbon export potential in summer. However, this is complicated in the AZ by the fact that the winter mixed layer, in the form of the T_{min}, is an important NO_3^- source to surface waters in summer (DiFiore et al. 2010; Smart et al. 2015). While the T_{min} continuously exchanges NO_3^- with underlying deep waters (i.e., CDW; NO_3^- originating from this deep water mass is truly "new" to the surface layer), our data and those of Smart et al. (2015) suggest that a significant fraction of the T_{min} NO_3^- pool is produced in the winter mixed layer. The implication is that summertime

phytoplankton growth is fueled, at least in part, by NO_3^- regenerated in surface waters in winter. Similarly, an uncertain quantity of the NO_3^- in the upper SAZ is sourced via equatorward Ekman transport from the AZ (Gordon et al. 1977; Sigman et al. 1999; Lourey and Trull 2001; Wang et al. 2001; DiFiore et al. 2006; Moore et al. 2006), such that N cycling in the AZ mixed layer, including nitrification, may affect the carbon budget of the SAZ.

So far, I have examined N cycling in the summer and winter Southern Ocean separately, estimating carbon export potential and the f-ratio for each season in isolation. In addition, I have relied on the original new production paradigm assumption that fluxes into and out of the euphotic zone can be used to constrain new and export production (Dugdale and Goering 1967). However, CO_2 regenerated from organic matter that is exported from the summer euphotic zone and remineralized above the depth of deep winter mixing (~150 m in the AZ/PFZ and ~200 m in the SAZ in the Atlantic sector; Sallée et al. 2010; Du Plessis et al. 2017) may escape back to the atmosphere in winter, thus not constituting export on an annual basis. Moreover, nitrate produced via nitrification in the winter mixed layer that is then supplied to the summertime surface (e.g., from the T_{min}) cannot be considered truly "new," nor can its consumption be taken as indicative of carbon export potential. Accounting for these complications in order to estimate annual export production from my data is not straightforward given 1) the uncertainty surrounding the quantity of NO_3^- supplied to AZ surface waters from the T_{min} vs. CDW, particularly since the T_{min} is constantly exchanging with CDW (DiFiore et al. 2010; Smart et al. 2015), 2) the uncertainty associated with NO_3^- transport from the AZ to the SAZ (DiFiore et al. 2006), and 3) how little is known about the upper Southern Ocean N cycle in late summer, autumn, and early spring.

Integrating the summer and winter rate data to the maximum depth of winter mixing yields annual estimates of the f-ratio$_{(corrected)}$ of ≤0 at all but station 4, where the calculated value is 0.19. Only stations 1-4 are included in this exercise as there are no winter data for the SG and IS stations. A major weakness of this approach, as evidenced by the fact that it suggests the Southern Ocean supports no carbon export on an annual basis, is that it assumes that the periods dominated by mixed-layer NO_3^- uptake versus nitrification are of equal length and well-represented by our data. This is highly unlikely. NO_3^- uptake could be higher in spring and early summer when the mixed layer shoals and iron becomes available to phytoplankton – that is, the period of maximum NO_3^- drawdown may not have been captured. By contrast, the interval of maximum nitrification may have been sampled in winter given that the MLD at all

stations was very similar to the maximum expected depth (Sallée et al. 2010; Du Plessis et al. 2017) and solar radiation was near its lowest. Without a more highly temporally-resolved dataset, these uncertainties cannot be addressed.

If instead, the wintertime f-ratios are set to zero and averaged over summer and winter, the annual f-ratios become 0.26, 0.15, 0.36, and 0.39 for stations 1 through 4, respectively. These values might be considered an upper bound on the annual f-ratio since they do not account for mixed-layer nitrification rates that are higher than (rather than equal to) ρNO_3^- in winter. They are nonetheless comparable to annual average estimates of the export ratio computed using empirically-derived algorithms that require only NPP and SST data – 0.11-0.32, 0.14-0.36, 0.19-0.41, and 0.19-0.42 for stations 1 through 4, respectively (e.g., see equations 2.2 and 2.3 in Laws et al. (2000) and equation 2.2 in Henson et al. (2011)). These crude f-ratio estimates are also similar to annual values derived from a variety of geochemical measurements for the region south of 40°S (0.28-0.43; Lourey and Trull 2001; DiFiore et al. 2006; Reuer et al. 2007; Emerson 2014; Johnson et al. 2017).

The exercise above is not intended to yield an "accurate" estimate of the annual f-ratio for the Atlantic Southern Ocean, but instead to highlight the difficulty of extrapolating ^{15}N-based measurements of new and regenerated production beyond the specific temporal and environmental conditions that they represent. Averaging over summer and winter, while an improvement, does not solve this problem since it assumes that the annual cycle is well-represented by two snapshots of upper Southern Ocean N dynamics. Moreover, the biogeochemical implications of one season for another (e.g., nitrification in the winter mixed layer, which becomes the summertime T_{min} layer) are difficult to constrain without additional seasonal data and improved estimates of NO_3^- exchange between the T_{min} and CDW in the AZ/PFZ, the SAZ summer mixed layer and thermocline, and the AZ and SAZ surface layers. Nonetheless, measurements of N uptake and nitrification such as those presented here provide important insights into the fertility and biogeochemical functioning of the upper Southern Ocean ecosystem on a seasonal basis. In this regard, and given the severe paucity of such data, our winter measurements are particularly important.

2.5 Conclusions and implications

Rates of NPP, N uptake, and nitrification were investigated across the Atlantic Southern Ocean in winter and summer. Mid-summer was characterized by relatively high rates of NO_3^--fuelled primary production, with a minimal contribution of nitrification to the surface NO_3^- pool. Comparison of the specific rates of carbon and N uptake reveal the possibility of regenerated DON consumption in summer, at least in the PFZ and AZ. The winter was dominated by high rates of heterotrophic NH_4^+ consumption and nitrification in the mixed layer. During this season, low light availability, driven by both a decrease in solar radiation and deep mixing, limits phytoplankton growth and renders nitrifiers and heterotrophic bacteria more competitive. Despite the clear temporal separation of NO_3^- assimilation and regeneration in the Southern Ocean mixed layer, I ultimately conclude that the new production paradigm (and associated f-ratio) as a framework for estimating new production and carbon export potential, which considers fluxes into and out of the euphotic zone, should be applied with caution.

Interpretation of these data relies heavily on knowledge of the degree of coupling between NPP and N uptake in surface waters, highlighting the value of parallel carbon and N cycle measurements. Our co-generated NPP and N uptake data show that the upper ocean N cycle is dominated by heterotrophic NH_4^+ uptake (and nitrification) in winter, which has implications for the rate and seasonality of NH_4^+ regeneration. Summing the average rates of NH_4^+ consumption and oxidation across the study region yields a daily surface layer NH_4^+ demand of 23.5 mmol N m^{-2} (or ~170 nM d^{-1}, assuming an average MLD of 140 m). In addition, the ambient NH_4^+ concentration in winter is high relative to the summer and to other open ocean regions (mixed-layer average of 663 nM). Combined, these two observations imply that NH_4^+ regeneration occurs at an elevated rate, either concurrently with the high rates of wintertime NH_4^+ uptake and oxidation or prior to this in late summer and/or autumn. Under these conditions, the Southern Ocean mixed layer likely becomes net heterotrophic and thus a source of CO_2 to the atmosphere.

It seems unlikely that there is sufficient high-quality biomass available in winter to yield the NH_4^+ regeneration rates required to support the measured NH_4^+ uptake and oxidation rates. For a start, the rates of autotrophic productivity are low in winter, which means that little fresh organic matter is being generated. Indeed, the elevated C:N ratio of winter biomass indicates that the organic material is fairly degraded. Moreover, the fact that heterotrophic bacteria have

turned to NH_4^+ to support some fraction of their N nutrition may be indicative of the poor quality of the organic matter available to them. I thus hypothesize that much of the NH_4^+ available in winter is regenerated prior to this season, likely following the period of elevated phytoplankton growth. This is consistent with studies of NO_3^- and PON isotopes, which suggest that intense N recycling is pervasive in the late summer/autumn (Lourey et al. 2003; Smart et al. 2015), as well as with studies from coastal Antarctica (e.g., Henley et al. 2017). If the NH_4^+ available in winter is mostly produced prior to this season, one would expect NH_4^+ to accumulate in Southern Ocean surface waters in autumn. While there is some indication from late summer studies that this may be the case (Koike et al. 1986; Owens et al. 1991; Bianchi et al. 1997; Sambrotto and Mace, 2000; Kemeny et al. 2018), the seasonally-resolved dataset required to test this hypothesis, as for the annual cycle of new and regenerated production, currently does not exist.

Chapter 3: The kinetics of ammonium uptake and oxidation across the African sector of the Southern Ocean

A version of this chapter has been included as a manuscript entitled "*The kinetics of ammonium uptake and oxidation across the African sector of the Southern Ocean*" submitted for review in Limnology and Oceanography.

Mdutyana, M., Sun, X., Burger, J.M., Flynn, R.F., Smith, S., van Horsten, N.R., Roychoudhury, A.N., Planquette, H., Bucciarelli, E., Thomalla, S.J., Ward, B.B., and Fawcett, S.E. The kinetics of ammonium uptake and oxidation across the African sector of the Southern Ocean. *Limnology and Oceanography*. *Under review*

Abstract

Central to the Southern Ocean's disproportionate role in setting atmospheric CO_2 is the seasonal alternation between upward mixing of nutrients and their subsequent consumption by phytoplankton. Active nutrient cycling within the mixed layer, including the release of ammonium (NH_4^+) and its removal by phytoplankton and nitrifiers, also has implications for Southern Ocean CO_2 drawdown, yet remains poorly understood. Kinetic experiments were conducted across the Southern Ocean's African sector to investigate the dependence of NH_4^+ uptake (summer, winter) and oxidation (winter) on NH_4^+ concentration. NH_4^+ uptake followed a Michaelis-Menten function in both seasons with V_{max} decreasing poleward, apparently controlled mainly by light in winter and temperature in summer. The half-saturation constant (K_m) increased poleward with increasing ambient NH_4^+ concentration ($[NH_4^+]_{amb}$) and was three-fold higher in winter (150-405 nM) than summer (41-115 nM), suggesting that summertime phytoplankton are adapted to low-NH_4^+ conditions while winter communities typically receive a higher NH_4^+ supply. NH_4^+ oxidation showed a high affinity for NH_4^+ (K_m of 28-137 nM), suggesting a dominant role for ammonia-oxidizing archaea, and followed a Michaelis-Menten curve only when $[NH_4^+]_{amb}$ was ≤90 nM. V_{max} was near-constant across the region regardless of $[NH_4^+]_{amb}$, temperature, or light. Coincident mixed-layer iron and NH_4^+ oxidation measurements lead to the hypothesis that iron availability may (co-)limit V_{max}. If verified, this suggestion has implications for models that parameterize nitrification as a linear function of $[NH_4^+]_{amb}$. Additionally, iron depletion in the surface Southern Ocean may limit the role of mixed-layer nitrification, which is significant in winter, in offsetting phytoplankton CO_2 drawdown annually.

3.1. Introduction

The global ocean absorbs ~30% of anthropogenic carbon dioxide (CO_2) emissions, with the Southern Ocean south of 35°S accounting for ~40% of the oceanic CO_2 sink (Devries, 2014; Gruber et al. 2019). The extent of CO_2 drawdown in this region is largely set by the balance between macronutrient (i.e., nitrate and phosphate) recharge in winter and nutrient consumption in summer (Sarmiento and Toggweiler, 1984; Gregor et al. 2018). Nitrate (NO_3^-) remains replete in open Southern Ocean surface waters throughout the growing season due to a combination of iron and light (and possibly, temperature; Boyd et al. 2010; Strzepek et al. 2019) limitation of phytoplankton (Martin, 1990; Sunda and Huntsman, 1997). Since phytoplankton growth fueled by deep NO_3^- must be balanced by the export of organic matter out of surface waters on an annual basis (Dugdale and Goering 1967), the high concentration of unconsumed mixed-layer NO_3^- represents a "leak" in the global ocean's biological pump – by consuming NO_3^- more completely, Southern Ocean phytoplankton could theoretically lower atmospheric CO_2 (Sarmiento and Toggweiler, 1984; Sigman and Boyle, 2000).

Because of its role in setting the efficiency of the biological pump, NO_3^- cycling has been the focus of considerable research effort in the Southern Ocean, with less attention paid to the active cycling of nitrogen (N) in the seasonally-varying mixed layer, including the release of ammonium (NH_4^+) and its subsequent removal via phytoplankton uptake and nitrification. High ammonium concentrations ([NH_4^+]) appear to accumulate in the Southern Ocean mixed layer during winter (Henley et al. 2020; Mdutyana et al. 2020; Weir et al. 2020) even though NH_4^+ removal processes – NH_4^+ uptake (by phytoplankton and possibly heterotrophic bacteria) and NH_4^+ oxidation (the first step in the nitrification pathway) – are active during this season (Philibert et al. 2015; Smart et al. 2015; Mdutyana et al. 2020). That high NH_4^+ concentrations persist in the winter mixed layer despite elevated rates of NH_4^+ removal implies that NH_4^+ regeneration outpaces NH_4^+ uptake and oxidation, turning the Southern Ocean mixed layer net heterotrophic, a condition under which it becomes a biological source of CO_2 to the atmosphere. In addition, since some fraction of the NO_3^- produced by mixed-layer nitrification in winter will support phytoplankton growth the following summer (Mdutyana et al. 2020), the annual rate of NH_4^+ (and nitrite; NO_2^-) oxidation relative to NO_3^- assimilation determines net biological CO_2 drawdown (Dugdale and Goering 1967).

To better understand NH_4^+ dynamics in the winter Southern Ocean mixed layer and the implications for nutrient cycling and CO_2 drawdown, I focus on the biogeochemical processes

that consume NH_4^+. Mixed-layer NH_4^+ has two possible fates; assimilation by phytoplankton (and possibly heterotrophic bacteria; Kirchman et al., 1991; 1994; Mdutyana et al. 2020) and conversion to NO_2^- by ammonia oxidizing archaea and bacteria (AOA and AOB, respectively). Across much of the global ocean, the expectation is that NH_4^+ assimilation will outpace NH_4^+ oxidation in the upper mixed layer (Ward, 1985, 2005; Smith et al. 2014) even though phytoplankton and ammonia oxidizers appear to have a similar affinity for NH_4^+ (e.g., Kanda et al. 1985; Sahlsten, 1987; Harrison et al. 1996; Rees et al. 2006; Martens-Habbena et al. 2009; Newell et al. 2013; Zhang et al. 2020). This expectation arises from culture and *in situ* experiments showing photosensitivity among ammonia oxidizers, which both directly limits mixed-layer NH_4^+ oxidation and renders ammonia oxidizers less competitive than phytoplankton for NH_4^+ (Hooper & Terry, 1974; Olson, 1981b; Ward, 1985, 2005; Horrigan and Springer, 1990; Merbt et al. 2012; Qin et al. 2014; Smith et al. 2014). However, I recently measured high rates of NH_4^+ oxidation throughout the mixed layer, including in surface (~5 m) waters, across the wintertime Southern Ocean (between the Subantarctic Zone (SAZ) and the edge of the Marginal Ice Zone (MIZ)), coincident with fairly high rates of NH_4^+ assimilation and, with the possible exception of in the MIZ, in the presence of light (Chapter 2; Mdutyana et al. 2020). This implies that the controls on NH_4^+ consumption in winter Southern Ocean surface waters are more complex than light availability and competition between phytoplankton and ammonia oxidizers for NH_4^+.

The dependence of a biogeochemical process (e.g., NH_4^+ uptake or oxidation) on the availability of a particular substrate (e.g., NH_4^+) can be examined in the open ocean through experiments designed to yield a hyperbolic Michaelis-Menten relationship, provided that the rate of that process is limited by the substrate under investigation (e.g., MacIsaac and Dugdale, 1969; Ward and Kilpatrick, 1990; Harrison et al. 1996; Cochlan & Bronk, 2001; Horak et al. 2013; Newell et al., 2013; Peng et al. 2016). The kinetic parameters derived from the resultant Michaelis-Menten function – the maximum rate of substrate transformation (V_{max}) and the half-saturation constant (K_m), which is the substrate concentration at which the reaction rate (V) = $V_{max}/2$ – reveal important information about the physiological capabilities of, and constraints upon, the organisms consuming the substrate. The K_m for NH_4^+ uptake is estimated to be low, although it varies considerably with ocean region and ambient [NH_4^+] (K_m = 25-429 nM; Sahlsten, 1987; Harrison et al. 1996; Cochlan and Bronk, 2001; Rees et al. 2006). For NH_4^+ oxidation, the K_m has so far been successfully determined from very few ocean regions, with existing estimates from studies of natural populations suggesting that it must be <200 nM, and

potentially an order of magnitude lower (Olson, 1981b; Hashimoto et al. 1983; Ward and Kilpatrick 1990; Horak et al., 2013; Newell et al., 2013; Peng et al. 2016; Zhang et al., 2020). Culture work has yielded a similarly low K_m for AOA (133 nM), while the K_m for NH_4^+ oxidation by AOB has been estimated to be two- to three orders of magnitude higher (>10-100 μM; Martens-Habbena et al. 2009).

Central to the application of Michaelis-Menten kinetics is the idea that substrate concentration is the proximate limiting factor on the rate of substrate consumption (Dugdale, 1967; Eppley et al. 1969). This assumption seems reasonable in the case of NH_4^+, which is typically present in open ocean waters at very low concentrations (Rees et al. 1999; Gruber, 2008; Paulot et al. 2015). Indeed, there is considerable evidence of NH_4^+ uptake rates increasing with increasing ambient [NH_4^+], including in the Southern Ocean (Thomalla et al. 2011; Mdutyana et al. 2020). The situation is less clear for NH_4^+ oxidation, which is perhaps to be expected given the low K_m associated with this pathway (Martens-Habbena et al. 2009; Horak et al. 2013; Newell et al. 2013; Peng et al. 2016; Xu et al. 2019). Additional environmental factors such as temperature, light, community composition, and/or interactions with other nutrients (e.g., iron) can also influence the rates of NH_4^+ uptake and oxidation. For instance, phytoplankton consumption of NH_4^+, while less energy-intensive than NO_3^- uptake (Dortch 1990), is nonetheless affected by light availability (Kanda et al. 1985; Ward, 1985a) and has been shown to increase at higher temperatures (Kanda et al. 1985; Smith and Harrison, 1991; Harrison et al. 1996; Baer et al. 2014). Additionally and potentially coincidentally, smaller phytoplankton, which often dominate warmer, nutrient-poor regions, appear to prefer NH_4^+ over more oxidized N forms (Mulholland and Lomas, 2008 and references therein), and NH_4^+ can also be assimilated by heterotrophic bacteria (Kirchman et al. 1991; 1994; Allen et al. 2002; Bradley et al. 2010).

NH_4^+ oxidation appears less affected by temperature than NH_4^+ uptake (Horak et al. 2013; Baer et al. 2014), possibly because ammonia oxidizers are adapted to the temperatures that they typically experience (e.g., Thamdrup and Fleischer, 1998; Ward, 2008; Horak et al. 2013; 2018). In estuaries and rivers, salinity exerts an important, at times dominant, control on NH_4^+ oxidation rates (e.g., Somville, 1984; Iriarte et al. 1997; Rysgaard et al. 1999; Bernhard et al. 2007). In the open ocean, however, salinity is relatively invariant, at least on the scales relevant to the response time of bacteria and archaea. AOA greatly outnumber AOB over the upper few hundred meters of the ocean (e.g., Beman et al. 2008; Newell et al. 2011; Peng et al. 2016; Pajares et al. 2019) and the similarity of culture-based AOA K_m values (Martens-Habbena et

al. 2009) to *in situ* estimates (Horak et al. 2013; Newell et al. 2013; Wan et al. 2018; Xu et al. 2019; Zhang et al. 2020) is consistent with AOA being the dominant ammonia oxidizers in all open ocean systems investigated to-date (e.g., Newell et al. 2011; Peng et al. 2016). A recent culture study of the globally-abundant AOA, *Nitrosomopumilus maritimus* SCM1, found that elevated iron concentrations are required for this organism to oxidize NH_4^+ and that its affinity for iron is low (Shafiee et al. 2019). Iron availability may thus influence the rates of NH_4^+ oxidation in regions such as the Southern Ocean where mixed-layer iron concentrations are nearly always <0.2 nM (Tagliabue et al. 2012).

To better understand the controls on the high mixed-layer NH_4^+ concentrations that seem to persist in the winter Southern Ocean, I conducted a series of kinetics experiments across the African (i.e., east Atlantic/west Indian) sector in winter (NH_4^+ uptake and oxidation) and summer (NH_4^+ uptake only, given the evidence for negligible NH_4^+ oxidation in the Southern Ocean mixed layer in summer; Mdutyana et al. 2020) (Figure 3.1). To contextualize these findings, I also measured NH_4^+ uptake and oxidation rates with depth (0-200 m) during winter, along with NH_4^+ and dissolved iron concentrations. Our results confirm that NH_4^+ accumulates in the polar Southern Ocean mixed layer in winter and suggest that the maximum rate of its removal in these waters is not controlled by NH_4^+ availability but by other environmental drivers such as light, temperature, and possibly iron.

3.2 Materials and Methods

3.2.1 Field experiments

3.2.1.1 Sampling location

Two cruises were undertaken onboard the R/V *SA Agulhas II* – a winter cruise in July 2017 from Cape Town, South Africa, to the MIZ (encountered at 61.7°S; De Jong et al. 2018) that returned along the WOCE IO6 line (30°E) (VOY25; Figure 3.1a) and a summer cruise in December 2018 from Cape Town to Antarctica along the GoodHope line (WOCE A12; 0°E)

(VOY35; Figure 3.1b). During winter, samples were collected on both legs of the cruise while in summer, samples were collected on the southward leg only.

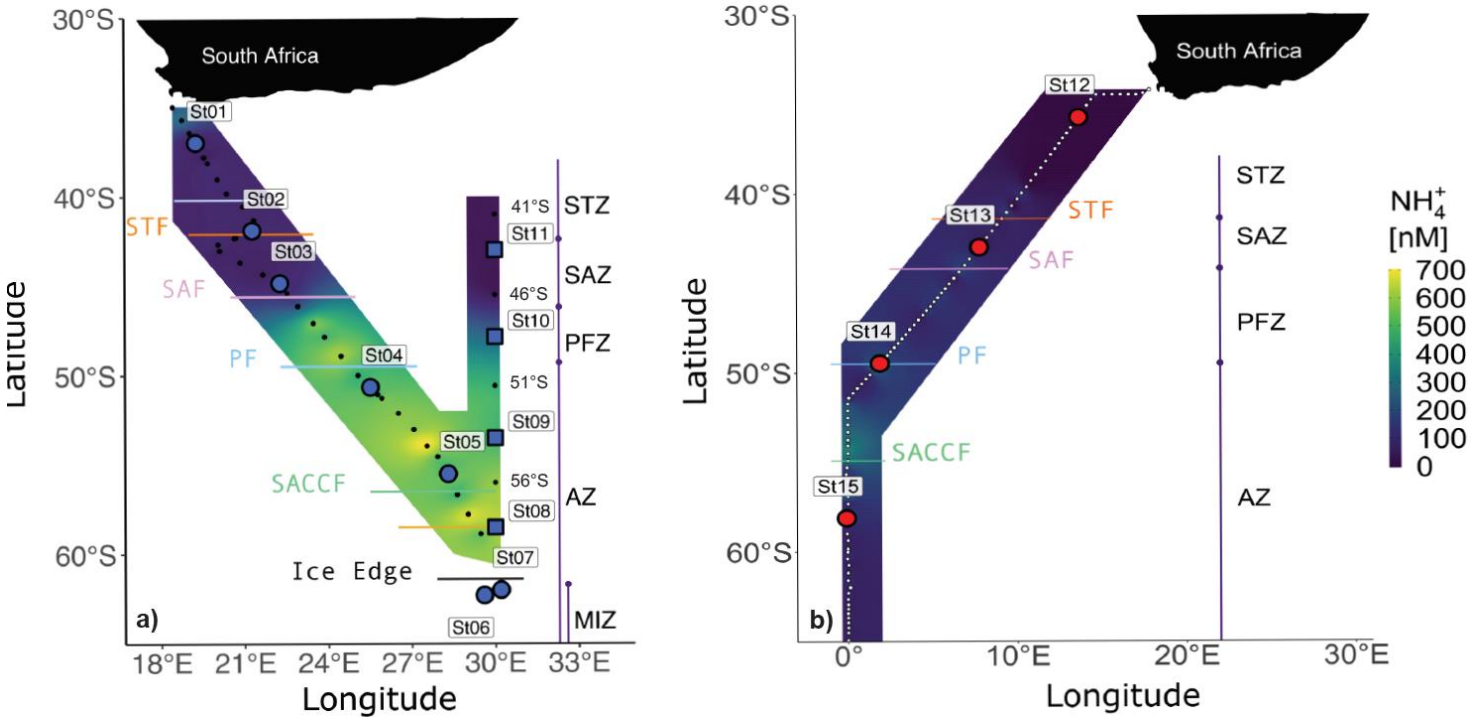

Figure 3.1: Maps showing the cruise track (small black and white symbols), experimental station positions (large blue and red symbols), and locations of ancillary surface sampling in a) winter and b) summer, overlaid on surface (~7 m) ammonium concentration ([NH_4^+]; colours). For both seasons, the small dots (black in winter and white in summer) indicate the surface stations, the circles indicate the kinetics experiment stations (blue in winter, red in summer) and the blue squares show the locations of the depth-profile experiments conducted in winter. The solid horizontal lines denote the frontal positions at the time of sampling, with the major zones of the Southern Ocean indicated by the vertical lines and dots – STZ, Subtropical Zone; STF, Subtropical Front; SAZ, Subantarctic Zone; SAF, Subantarctic Front; PFZ, Polar Frontal Zone; PF, Polar Front; AZ, Antarctic Zone; SACCF, Southern Antarctic Circumpolar Front; MIZ, Marginal Ice Zone. The underway system was turned off during the sampling of the MIZ; hence, the winter NH_4^+ concentration map does not extend to St 06 and 07.

3.2.1.2 Incubation experiments

In winter, kinetics experiments were conducted between 37°S and 55°S (NH_4^+ uptake) or 62°S (NH_4^+ oxidation) on the southward leg of VOY25 (St 01 to St 07), and the depth distribution of NH_4^+ uptake and oxidation was investigated at four stations along the WOCE I06 transect between 59°S and 41°S on the northward leg (St 08 to St 11; Figure 3.1a). In summer, kinetic experiments were conducted between 36°S and 58°S for NH_4^+ uptake only (St 12 to St 14; Figure 3.1b).

Incubation experiments were terminated after 3-6 hours (NH_4^+ uptake) and 23-30 hours (NH_4^+ oxidation). These experiments were not carried out under trace metal-clean conditions, so trace-metal contamination cannot be ruled out. However, previous work conducted under ultra

clean conditions has shown no effect of iron addition over 24 hours on NH_4^+ oxidation (Shafiee et al. 2019) or NH_4^+ uptake (e.g., during seawater incubations conducted in the Southern Ocean (Timmermans et al. 1998; Cochlan et al. 2002) and Subarctic Pacific (Kudo et al. 2005; 2009)).

NH_4^+ uptake and oxidation kinetics: At the kinetics stations, seawater (25 L) was collected via the ship's underway system (intake at ~7 m), transferred to a carboy that was gently shaken to homogenize the contents, then screened through 200 µm nylon mesh to remove zooplankton grazers and dispensed into 1 L acid-washed polycarbonate bottles for NH_4^+ uptake (winter and summer) and 250 mL acid-washed high density polyethylene (HDPE) opaque bottles for NH_4^+ oxidation (winter only). Bottles were rinsed three times with sample water prior to filling. For NH_4^+ uptake, duplicate bottles (eight sets in winter and seven in summer) were amended with $^{15}NH_4Cl$ to yield $^{15}NH_4^+$ concentrations ranging from 50 nM to 7500 nM (winter) or 50 nM to 3500 nM (summer). For NH_4^+ oxidation, seven sets of duplicate bottles were amended with $^{15}NH_4Cl$ to yield $^{15}NH_4^+$ concentrations ranging from 10 nM to 1500 nM. In addition, because the ambient NO_2^- concentrations were expected to be low (Zakem et al. 2018; Fripiat et al. 2019; Mdutyana et al. 2020), all NH_4^+ oxidation bottles were amended with 200 nM $^{14}NO_2^-$ to act as an "isotope trap" for the $^{15}NO_2^-$ produced by NH_4^+ oxidation.

Depth distribution of NH_4^+ uptake and oxidation: In winter, seawater was collected at St 08 to St 11 using a CTD-rosette equipped with 24 12-L Niskin bottles and transferred through 200 µm mesh into acid-washed polycarbonate bottles for NH_4^+ uptake and opaque HDPE bottles for NH_4^+ oxidation. NH_4^+ uptake was investigated at five depths (10 m, 25 m, 50 m, 75 m and 200 m), with experiment bottles incubated under light conditions corresponding to water column irradiance levels of 55%, 30%, 10%, 1%, and 0% of surface photosynthetically active radiation (PAR). The 200-m (0% PAR) samples were incubated in opaque bottles. The NH_4^+ oxidation experiments were conducted using water collected from six depths (10 m, 25 m, 50 m, 75 m, 200 m, and 500 m). For both NH_4^+ uptake and oxidation, duplicate bottles from each depth were amended with 200 nM $^{15}NH_4^+$, with 200 nM $^{14}NO_2^-$ added to the oxidation bottles.

Following ^{15}N-tracer addition, the kinetics and depth-profile experiments were processed in the same way. NH_4^+ uptake bottles were incubated in custom-built on-deck incubators equipped with neutral density screens and supplied with running surface seawater to simulate *in situ* light and temperature conditions. Temperature was monitored throughout the incubations, which lasted 3-6 hours. Experiments were terminated by gently vacuum filtering the incubated water through pre-combusted (450°C for 8 hours) 0.3 µm glass fibre filters (GF-

75s; Sterlitech) to collect the particulate organic N (PON). Filters were stored in combusted (500°C for 5 hours) foil envelopes and frozen at -80°C until analysis. The NH_4^+ oxidation bottles from the upper 75 m were incubated in the on-deck incubators and the 200 m and 500 m samples were incubated in a cold-room set at ~2˚C. From each bottle, initial (T_0) subsamples were collected in 50 mL centrifuge tubes immediately after the addition of $^{15}NH_4^+$+$^{14}NO_2^-$ and final (T_f) subsamples were taken when the incubations were terminated 23-30 hours later. Subsamples were filtered and stored frozen at -20°C until analysis.

3.2.1.3 Hydrographic and biogeochemical measurements

The positions of the major hydrographic fronts were determined from temperature and salinity data measured by the ship's hull-mounted thermosalinograph (~7 m), augmented in winter by temperature, salinity, and oxygen concentrations measured by the CTD sensors (Orsi et al. 1995; Belkin and Gordon 1996; Pollard et al. 2002; Read et al. 2002). For the return leg of VOY25 (winter), the mixed layer depth was determined for each Niskin (up)cast as the depth between 10 m and 400 m at which the Brunt Väisälä Frequency squared (i.e., N^2) reached a maximum (Schofield et al. 2015; Carvalho et al. 2017).

Seawater samples were collected every two (summer) or four (winter) hours from the ship's underway system on the southward leg of the cruises for the determination of NH_4^+ concentrations (Figure 3.1). During the winter return leg, surface NH_4^+ samples were collected from Niskin bottles fired at 10 m at eight hydrocast stations along the WOCE IO6 line. Samples were also collected at nine additional depths over the upper 500 m at the four depth-distribution stations for NO_2^- and NO_3^-, and at all the hydrocast stations for NH_4^+ (see Figure 3.2 for sampling depths). For NO_2^- and NO_3^-, unfiltered seawater was collected in duplicate 50 mL polypropylene centrifuge tubes that were stored frozen at -20°C until analysis.

For NH_4^+, 40 mL of unfiltered seawater were collected in duplicate HDPE bottles that had been 'aged' with orthophthaldialdehyde working reagent (OPA-WR) and Milli-Q water prior to the cruise. These samples were measured shipboard (see below). At the four winter depth-distribution stations, samples were also collected for the analysis of dissolved iron (DFe) and copper (DCu) concentrations following GEOTRACES protocols (Cutter et al. 2018) and using a trace metal-clean CTD rosette and GO-FLO bottles. The GO-FLO bottles were transferred into a class 100 clean laboratory for subsampling, wherein seawater was filtered through 0.2

µm Sartobran capsule filters into acid-cleaned low-density polyethylene bottles. The samples were then acidified to pH 1.7 via the addition of hydrochloric acid (Ultrapur, Merck) and stored double-bagged until analysis.

3.2.2 Laboratory analyses

3.2.2.1 Nutrient concentrations

NH_4^+ concentrations were analysed shipboard via the fluorometric method (Holmes et al. 1999, as updated by Taylor et al. 2007) using a Turner Designs Trilogy fluorometer, and corrected for the matrix effect (ME) deriving from the calibration of seawater samples to Milli-Q standards (detection limit of <20 nM, precision of ±10 nM, ME ≤10%). Ambient NO_2^- concentrations were also measured shipboard using the colorimetric method of Grasshoff et al. (1983) and a Thermo Scientific Genesys 30 Visible spectrophotometer (detection limit of 20 nM and precision of ±20 nM). NO_3^-+NO_2^- concentrations were measured ashore using a Lachat Quick-Chem flow injection autoanalyzer (Egan, 2008) in a configuration with a detection limit of 200 nM and precision of ±300 nM. The concentration of NO_3^- was then determined by subtracting NO_2^- from NO_3^-+NO_2^-. Aliquots of a certified reference material (JAMSTEC) were included in each NO_2^- and NO_3^-+NO_2^- run to ensure measurement accuracy.

DFe and DCu concentrations were measured using a sea*FAST* pico inline pre-concentration (x50) system (Elemental Scientific Inc., ESI) and sector field inductively coupled plasma mass spectrometer (SF-ICP-MS, Element XR Thermo Scientific) (Lagerström et al. 2013). A spike of 1 µg L^{-1} indium was used as an internal standard to correct for instrument drift. The detection limit, defined as three times the standard deviation of the blanks, was 0.042 nM (n = 7) and 0.705 nM (n = 13) for DFe and DCu, respectively. Analytical error was determined through the repeat analysis of calibration standards and was then applied (as a percentage) to the sample concentrations determined during each batch run. The mean percentage error for samples was 3.67 ± 1.89% and 2.37 ± 1.98% (mean ± SD, n = 183 and n = 132) for DFe and DCu, respectively. For DFe, analyses of GEOTRACES SAFe S and SAFe D1 reference seawater of 0.104 ± 0.004 nM (mean ± SD, n = 2) and 0.975 ± 0.120 nM (mean ± SD, n = 9), respectively, agree with consensus values (0.093 ± 0.008 nM and 0.933 ± 0.023 nM). Similarly, for DCu, analyses of SAFe S and SAFe D1 reference seawater of 0.561 ± 0.02 nM (mean ± SD, n = 5) and 2.047 ± 0.392 nM (mean ± SD, n = 9) agree with consensus values (0.520 ± 0.050 nM and

2.280 ± 0.150 nM, respectively). North Pacific GSP and GSC reference seawater, calibrated against the SAFe reference seawater, was used as an internal standard.

3.2.2.2 NH_4^+ uptake rates

On shore, the GF-75 filters were oven-dried at 45°C for 24 hours, then pelletized into tin cups. The concentration and isotopic composition of the PON was analyzed using a Delta V Plus isotope ratio mass spectrometer (IRMS) coupled to a Flash 2000 elemental analyser, with a detection limit of 1 μg N and precision of ±0.005 At%. Blanks (combusted unused filters) and laboratory running standards (Merck gel, Valine, Choc, NH_4Cl) calibrated to international reference materials were run after every five samples. The transport rates of NH_4^+ uptake (ρNH_4^+; nM d^{-1}) were calculated according to the equations of Dugdale and Wilkerson (1986) (*see equations 2.1a-2.1c*) assuming a day-length between 7 and 10 hours for winter and 14 and 18 hours for summer, dependent on the station latitude. The specific NH_4^+ uptake rates (V_{NH4+}; h^{-1}) were then computed by normalizing the hourly ρNH_4^+ values to the measured PON concentrations.

3.2.2.3 NH_4^+ oxidation rates

The azide method of McIlvin and Altabet (2005), as amended by Peng et al. (2015), was used to convert NO_2^- to N_2O gas that was then measured by IRMS. Briefly, a 1:1 mixture of 2 M sodium azide and 20% acetic acid buffer was prepared daily and purged with helium gas (He) for 20 minutes to remove any N_2O produced from NO_2^- present in the reagents. Samples were aliquoted into gas-tight vials that were flushed with He for 10 minutes, after which 0.4 mL of sodium azide/acetic acid buffer was added to each vial. Vials were incubated for 1 hour at room temperature, then sample pH was adjusted to >12 via the addition of 10 M sodium hydroxide.

The concentration of N_2O and ratio of $^{45}N_2O/^{44}N_2O$ (where the ^{15}N atom in $^{45}N_2O$ derives from $^{15}NO_2^-$ produced by $^{15}NH_4^+$ oxidation) were measured using a Delta V Plus IRMS with a custom-built purge-and-trap front end (Sigman et al. 2001; McIlvin and Casciotti 2011; Weigand et al. 2016) with a detection limit of 0.2 nmol N and precision in $\delta^{15}N$ of 0.2‰ ($\delta^{15}N$, in ‰ vs. air, = $(^{15}N/^{14}N_{sample}/^{15}N/^{14}N_{air} - 1) \times 1000$). The $\delta^{15}N$ of NO_2^- was derived from $^{45}N_2O/^{44}N_2O$ following Peng et al. (2015), and then the rate of NH_4^+ oxidation ($NH_4^+{}_{ox}$; nM d^{-1}) was calculated as:

$$NH_4^+{}_{ox} = \frac{\Delta[^{15}NO_2^-]}{f^{15}_{NH_4^+} \times T} \quad (3.1)$$

where $\Delta(^{15}NO_2^-)$ is the change in the concentration of $^{15}NO_2^-$ (nM) between the start and end of the incubation, calculated from the difference in the measured $\delta^{15}N$ of NO_2^- in the T_f and T_0 samples, $f^{15}_{NH_4}$ is the fraction of ^{15}N-labelled NH_4^+ substrate at the start of the incubation, and T is the incubation length (days) (Peng et al. 2015). All $^{15}NO_2^-$ produced during the incubations was assumed to derive from $^{15}NH_4^+$ oxidation. The detection limit was calculated for each experiment as the NO_2^- production rate necessary to cause a 2‰ increase in the $\delta^{15}N$ of NO_2^- relative to the T_0 value (Santoro et al. 2013). The detection limit, which is sensitive to $f^{15}_{NH_4}$ and the NO_2^- concentration at the end of the incubation, ranged from 0.02 to 0.11 nM d^{-1}.

3.2.2.4 Kinetic parameter estimation

The kinetic parameters V_{max} and K_m were derived using the Michaelis-Menten equation:

$$V = \frac{V_{max} \times S}{K_m + S} \quad (3.2)$$

where V is the measured NH_4^+ uptake or oxidation rate, V_{max} is the maximum rate of substrate transformation for a given set of conditions, achieved when enzymes or organisms are saturated by substrate, S is the substrate (i.e., ambient + tracer NH_4^+) concentration, and K_m is the half-saturation constant (i.e., the NH_4^+ concentration at which $V = V_{max}/2$). The affinity (α) of phytoplankton for S is calculated as V_{max}/K_m.

The Michaelis-Menten function was fit to the measured NH_4^+ concentration and uptake or oxidation rate data using a non-linear optimization approach that gives equal weight to each datapoint (drc package in R; Ritz et al. 2015). For NH_4^+ uptake kinetics experiments, the specific rate (i.e., V_{NH4+}) is typically reported as it speaks to inherent cellular capacity while the transport rate (ρNH_4^+) is indicative of the community response (Table 3.1). More practically, computing V_{NH4+} allows NH_4^+ uptake kinetic constants to be compared across regions with disparate PON concentrations. Here, I plot and discuss V_{NH4+} (h^{-1}) versus $[NH_4^+]$ (Figure 3.3, 3.4 and 3.5), but report both the maximum V_{NH4+} (V_{max}; h^{-1}) and ρNH_4^+ (ρ_{max} nM d^{-1}) for each experiment and show the Michaelis-Menten curves for ρNH_4^+ in the appendix B (Figure B3.1 and B3.2). For NH_4^+ oxidation, I report only $NH_4^+{}_{ox}$ (nM d^{-1}).

Table 3.1: A selection of previously measured kinetic parameters (V_{max} and K_m), including results from the current study, associated with NH_4^+ uptake from different regions of the open ocean. PON concentrations are reported here in nM for ease of calculating ρ_{max} from V_{max}. For the kinetic parameters derived in the present study, values in parentheses are the standard errors associated with the Michaelis-Menten model (as computed using the drc package in R; Ritz et al. 2015), while the 95% confidence intervals (CIs) are shown in square brackets (computed using the nlstools package in R; Baty et al. 2015). *nd* indicates no data.

Region	Season	Latitude	Longitude	$[NH_4^+]$ (nM)	PON (nM)	V_{max}	K_m (nM)	Affinity	Reference
Indian Southern Ocean: St 01	Winter	37°S	19°E	90	488 (37)	7.9 (0.3)	327 (50)	0.02	This study
Indian Southern Ocean: St 02	Winter	42°S	21°E	72	483 (81)	3.4 (0.2)	150 (39)	0.02	
Indian Southern Ocean: St 03	Winter	45°S	22°E	44	430 (92)	3.9 (0.3)	211 (65)	0.02	
Indian Southern Ocean: St 04	Winter	51°S	26°E	468	344 (23)	3.1 (0.4)	405 (202)	0.01	
Indian Southern Ocean: St 05	Winter	56°S	28°E	521	356 (74)	1.2 (0.2)[a]	nd	nd	
Atlantic Southern Ocean: St 12	Summer	36°S	14°E	below detection	557 (106)	8.0 (0.1)	41 (4.3)	0.20	
Atlantic Southern Ocean: St 13	Summer	43°S	8°E	88	926 (250)	4.1 (0.3)	79 (29)	0.05	
Atlantic Southern Ocean: St 14	Summer	50°S	2°E	138	1030 (175)	3.5 (0.2)	110 (27)	0.03	
Atlantic Southern Ocean: St 15	Summer	58°S	0,1°W	109	1018 (134)	1.5 (0.0)	115 (16)	0.01	
Ross Sea	Early Spring	77°S	176°E	0.0		1.0 (0.0)	40 (10)	0.03	Cochlan and Bronk (2001)
Ross Sea	Summer	77°S	176°E	0.0		4.0 (0.3)	333 (98)	0.01	
Ross Sea	Summer	78°S	176°W	130		4.8 (0.3)	131 (32)	0.04	
Ross Sea	Late Spring	77°S	178°W	20		3.4 (0.2)	153 (43)	0.02	
North Atlantic (oceanic)	Autumn	28-43°N	20-58°W	below detection		9.2	30 (22)	0.3	Harrison et al. (1996)
North Atlantic (coastal)	Autumn	28-43°N	20-58°W	160		18	198 (148)	0.09	
North Atlantic (oceanic)	Spring	28-43°N	20-58°W	60		9.4	25 (11)	0.36	
North Atlantic (coastal)	Spring	28-43°N	20-58°W	90		7.2	52 (30)	0.13	
Canary Basin	Spring	22-31°N	23-12°W	below detection		9.3	40 (18)	0.23	
Eastern Tropical Atlantic Province	Winter	2-15°S	0-10°E	37-61		10-26[b]	19-49	0.32-0.64	Rees et al. (2006)
Canary Coastal Province	Summer	15°N	15°W	327		139[b]	429	0.32	
North Atlantic Tropical Province	Summer	28°N	15°W	33		11[b]	33	0.34	
North Atlantic Drift Province	Summer	45°N	1°W	53		25[b]	81	0.31	
North Pacific Ocean	Winter			nd		2.7-14	50-410	0.01-0.18	Kanda et al. (1985)
Central North Pacific Gyre	Summer	28°N	155°W	nd		0.02	30	0.0007	Sahlsten (1987)
Offshore Oyashio	Spring	38-43°N	143-151°E	nd		11-20[b]	25-600	0.02-0.56	Shiomoto et al. (1994)
Offshore Oyashio	Summer	38-43°N	143-151°E	nd		19-38[b]	23-110	0.34-1.0	

Note that V_{max} values are reported as $x10^{-3}$ h^{-1} and K_m values as nM
Values in the brackets are standard errors
nd indicates no data
[a] *V_{avg}; see text for details*
[b] *Rates reported as ρ_{max} (nM h^{-1})*

3.3 Results

3.3.1 Hydrography and nutrient concentrations

In winter, kinetic experiments were conducted in all the major zones of the Southern Ocean (taken to be the waters south of 35°S): the Subtropical Zone (STZ) north of the Subtropical Front (STF), the Subantarctic Zone (SAZ) between the Subantarctic Front (SAF) and the STF, the Polar Frontal Zone (PFZ) between the Polar Front (PF) and the SAF, the Antarctic Zone (AZ) between the PF and the Marginal ice Zone (MIZ), with the Southern Antarctic Circumpolar Current Front (SACCF) dividing the permanently ice-free waters of the northern AZ from the seasonally ice-covered southern AZ, and the MIZ (Figure 3.1a). Summertime kinetics experiments were conducted at similar latitudes, although no measurements were made south of 58°S (i.e., the MIZ in winter), and no CTD casts were conducted (Figure 3.1b). Sea surface temperatures (SST) decreased southwards from 16°C at 37°S (St 01) to -1.1°C at 62°S (Stations 06 and 07) in winter and from 20°C at 36°S (St 12) to 1°C at 58°S (St 15) in summer. For the eight winter hydrocast stations, mixed layer depth (MLD) averaged 143 m in the AZ, 146 m in the PFZ, 205 m in the SAZ, and 113 m in the STZ (Figure 3.2a). These depths are within the reported climatological ranges of MLDs for the African sector of the Southern Ocean in winter (Sallée et al. 2010).

Wintertime underway ambient NH_4^+ concentrations ($[NH_4^+]_{amb}$) ranged from 44 nM to 700 nM (transect average of 297 ± 232 nM) and increased southwards, with the sharpest increase apparent just south of the SAF, beyond which $[NH_4^+]_{amb}$ remained consistently high (550 ± 68 nM between 47°S and 62°S; Figure 3.1a). Summer surface $[NH_4^+]_{amb}$ ranged from undetectable to 338 nM (transect average of 97 ± 88 nM), with the highest concentrations encountered between the PF and the SACCF (198 ± 88 nM; Figure 3.1b). In winter, $[NH_4^+]_{amb}$ was relatively homogenous throughout the mixed layer at each station and ranged from 14 ± 5.0 nM in the STZ to 427 ± 44 nM in the southern AZ (Figure 3.2b). The winter hydrocast station NO_2^- concentrations showed no clear latitudinal trend and ranged from 77 ± 9 nM (St 09; 54°S) to 175 ± 12 nM (St 08; 59°S) in the mixed layer, over which they were fairly constant at a given station (Figure 3.2c). The NO_3^- concentrations were lowest in the SAZ mixed layer (St 11 at 43°S; 10 ± 1.0 µM) and highest in the southern AZ (St 08; 28 ± 0.2 µM) (Figure 3.2d). For a more detailed discussion of the NO_3^- concentration data, see Weir et al. (2020).

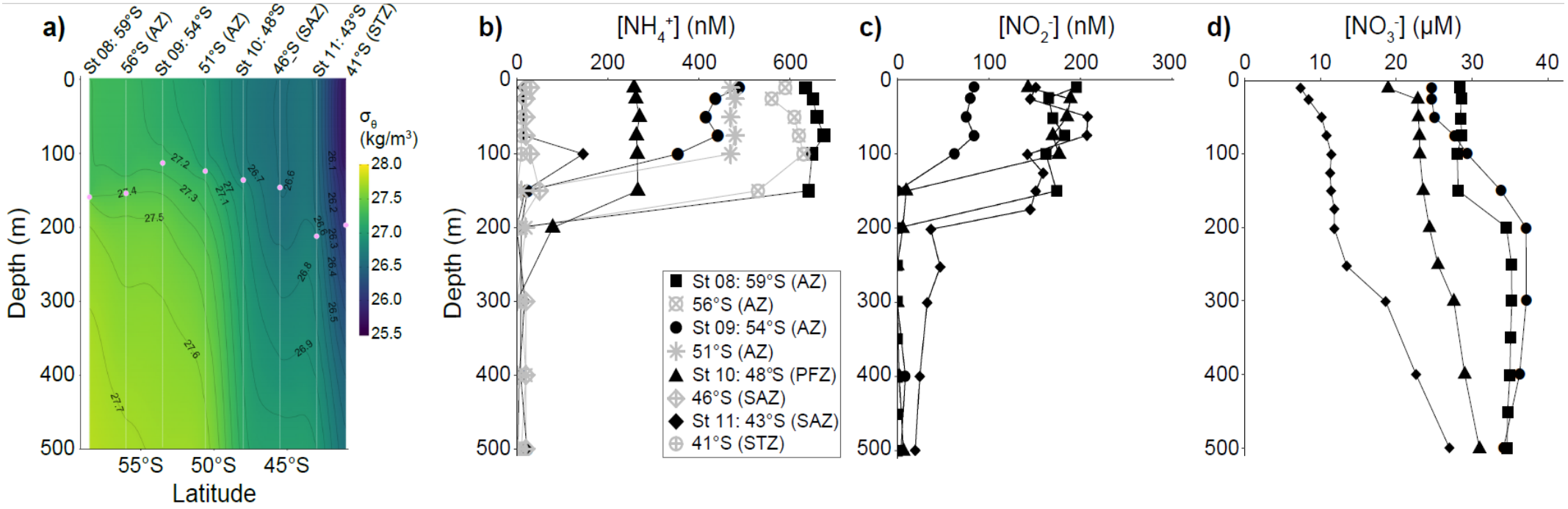

Figure 3.2: Water column (0-500 m) profiles of a) potential density and concentrations of b) ammonium (NH_4^+), c) nitrite (NO_2^-), and d) nitrate (NO_3^-) sampled on the northbound leg of the winter cruise (VOY25). In panel a, the vertical white lines show the positions of all the hydrocast stations, with the four depth profile stations (St 08-11) labeled above the panel, and the pink dots show the mixed layer depths. In panel b, the grey symbols indicate stations where samples for NH_4^+ uptake and oxidation rates were not collected and measured, while black symbols indicate stations where samples were collected and rates were measured.

The average surface (~7 m) PON concentrations at the kinetics stations decreased slightly from north to south in winter, from 0.49 ± 0.04 μM at 37°S to 0.34 ± 0.02 μM at 51°S, while in summer, PON concentrations increased two-fold from north to south, from 0.56 ± 0.11 μM at 36°S to 1.02 ± 0.13 μM at 58°S (Table 3.1).

3.3.2 Kinetics of NH_4^+ uptake

In winter, four out of five stations (the southernmost station at 55°S being the exception) showed a Michaelis-Menten relationship between NH_4^+ uptake rate and [NH_4^+] (Figure 3.3 and S1). The derived values of V_{max} generally decreased southwards, from 7.9 x10^{-3} h^{-1} (ρ_{max} of 38 ± 1.0 nM d^{-1}) at 37°S (STZ; St 01) to 3.2 x10^{-3} h^{-1} (ρ_{max} of 6.7 ± 1.3 nM d^{-1}) at 51°S (PFZ; St 04) (Table 3.1; Table B3.1, appendix B, which includes 95% confidence intervals (CI) for all derived parameters). At 55°S (AZ; St 05), V_{NH4+} did not vary with [NH_4^+], averaging 1.2 ± 0.2 x10^{-3} h^{-1} (ρ_{NH4+} of 3.2 ± 0.5 nM d^{-1}) (Figure 3.3e). Estimates of K_m generally increased with latitude, ranging from 150 ± 39 nM (95% CI of 54 to 274 nM) at 42°S (St 02) to 405 ± 202 nM (95% CI of 48 to 924 nM) at 51°S (St 04), with the estimate of 327 ± 50 nM (95% CI of 204 to 448 nM) derived for the northernmost STZ station (St 01) emerging as an exception (Figure 3.3a).

In summer, NH_4^+ uptake at all four stations was well-described by a Michaelis-Menten function, with V_{max} and K_m decreasing and increasing southwards, respectively (Figure 3.4 and S3.2; Table 3.1). V_{max} ranged from 8.0 x10^{-3} h^{-1} at 36°S (STZ; St 12) to 1.5 x10^{-3} h^{-1} at 58°S (AZ; St 15) (ρ_{max} of 80 ± 4.9 nM d^{-1} to 32 ± 1.1 nM d^{-1}) while K_m ranged from 41 ± 4.3 nM (95% CI of 30 to 52 nM) to 115 ± 16 nM (95% CI of 74 to 157 nM) (Table B3.1, appendix B).

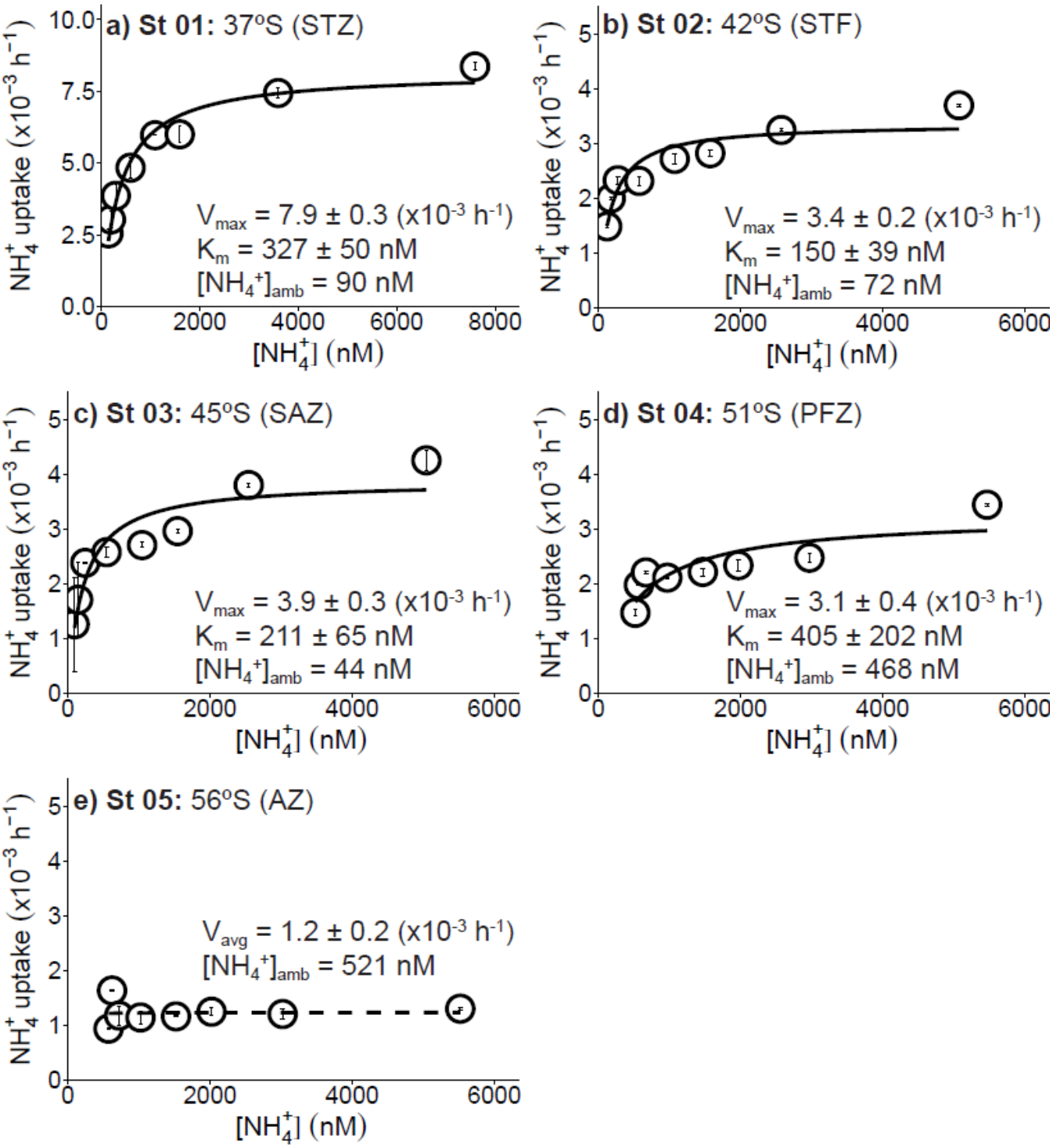

Figure 3.3: The dependence of NH_4^+ uptake rates on $[NH_4^+]$ at the surface (~7 m) in winter at a) St 01: 37°S (STZ), b) St 02: 42°S (STF), c) St 03: 45°S (SAZ), d) St 04: 51°S (PFZ), and e) St 05: 55°S (AZ). The solid line shows the Michaelis-Menten fit, with the derived values of V_{max} and K_m, as well as the ambient ammonium concentration ($[NH_4^+]_{amb}$), indicated on each panel. At St 05, a Michaelis-Menten relationship was not observed; here, the dashed horizontal line indicates the average NH_4^+ uptake rate (V_{avg}). Error bars show the standard error of replicate experiments, each measured at least twice. Where errors bars are not visible, they are smaller than the data markers.

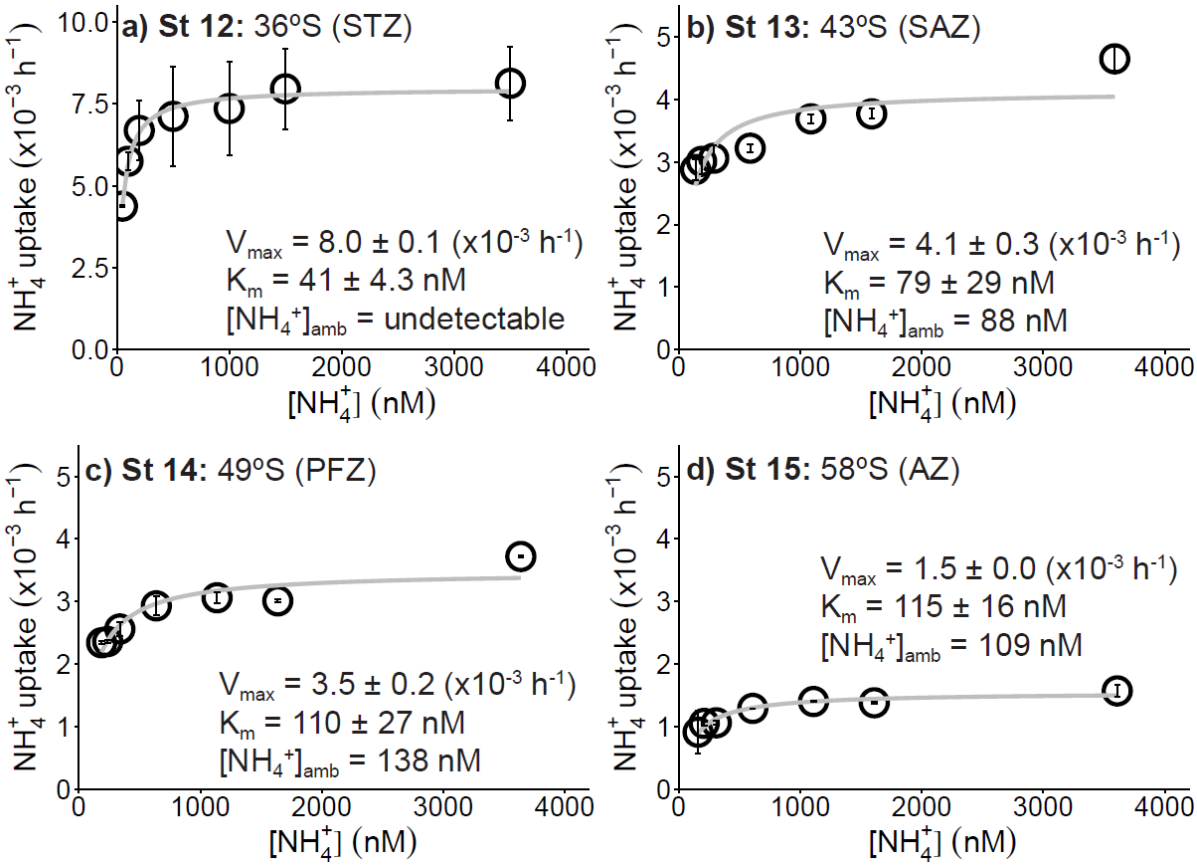

Figure 3.4: The dependence of ammonium uptake rates on [NH_4^+] at the surface (~7 m) in summer at a) St 12: 36°S (STZ), b) St 13: 43°S (SAZ), c) St 14: 49°S (PFZ), and d) St 15: 58°S (AZ). The solid line shows the Michaelis-Menten fit, with the derived values of V_{max} and K_m, as well as the ambient ammonium concentration ([NH_4^+]$_{amb}$), indicated on each panel. Error bars show the standard error of replicate experiments, each measured at least twice. Where errors bars are not visible, they are smaller than the data markers.

3.3.3 Kinetics of NH_4^+ oxidation

The kinetic constants for NH_4^+ oxidation (experiments only conducted in winter) could be derived at three out of seven stations (the three northernmost stations, all with [NH_4^+]$_{amb}$ ≤ 90 nM; Figure 3.5a-c). At the other stations, the $NH_4^+{}_{ox}$ rates remained roughly constant even as [NH_4^+] increased (Figure 3.5d-g and Table 3.2; "non-MM stations"). The estimates of V_{max} for the three northern stations were similar, ranging from 19 ± 1.9 nM d^{-1} at 42°S (STF; St 02) to 23 ± 2.1 nM d^{-1} at 37°S (STZ; St 02) (average of 21 ± 1.5 nM d^{-1}), while the average $NH_4^+{}_{ox}$ rates at the non-MM stations (V_{avg}) ranged from 14 ± 2.6 nM d^{-1} at 62°S (MIZ; St 07) to 22 ± 3.8 nM d^{-1} at 51°S (PFZ; St 04) (Table 3.2). The values of K_m ranged from 28 ± 21 nM (95% CI of -23.8 to 79.9 nM) at 42°S (St 02) to 137 ± 40 nM (95% CI of 39 to 235 nM) at 37°S (St 01) (Table B3.1).

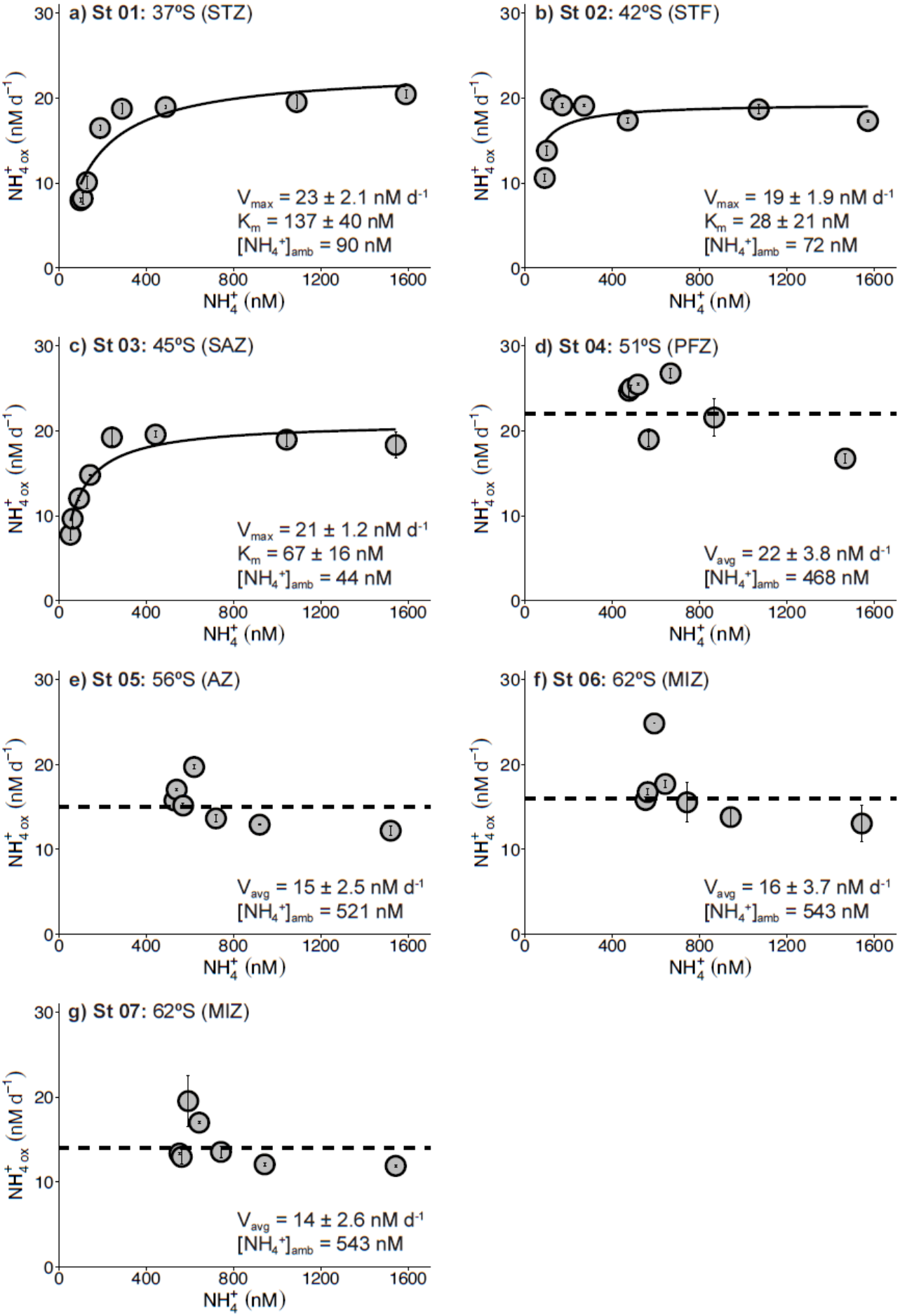
a) St 01: 37ºS (STZ)
V_{max} = 23 ± 2.1 nM d^{-1}
K_m = 137 ± 40 nM
$[NH_4^+]_{amb}$ = 90 nM
b) St 02: 42ºS (STF)
V_{max} = 19 ± 1.9 nM d^{-1}
K_m = 28 ± 21 nM
$[NH_4^+]_{amb}$ = 72 nM
c) St 03: 45ºS (SAZ)
V_{max} = 21 ± 1.2 nM d^{-1}
K_m = 67 ± 16 nM
$[NH_4^+]_{amb}$ = 44 nM
d) St 04: 51ºS (PFZ)
V_{avg} = 22 ± 3.8 nM d^{-1}
$[NH_4^+]_{amb}$ = 468 nM
e) St 05: 56ºS (AZ)
V_{avg} = 15 ± 2.5 nM d^{-1}
$[NH_4^+]_{amb}$ = 521 nM
f) St 06: 62ºS (MIZ)
V_{avg} = 16 ± 3.7 nM d^{-1}
$[NH_4^+]_{amb}$ = 543 nM
g) St 07: 62ºS (MIZ)
V_{avg} = 14 ± 2.6 nM d^{-1}
$[NH_4^+]_{amb}$ = 543 nM
NH_4^+ ox (nM d^{-1})
NH_4^+ (nM)
0
10
20
30
400
800
1200
1600

Figure 3.5 (previous page)**:** The dependence of NH_4^+ oxidation rates on $[NH_4^+]$ at the surface (~7 m) in winter at a) St 01: 37°S (STZ), b) St 02: 42°S (STF), c) St 03: 45°S (SAZ), d) St 04: 51°S (PFZ), e) St 05: 55°S (AZ), f) St 06: 62°S (MIZ), and g) St 07: 62°S (MIZ). The solid line shows the Michaelis-Menten fit, with the derived values of V_{max} and K_m, as well as the ambient ammonium concentrations ($[NH_4^+]_{amb}$), indicated on each panel. At St 04-07, a Michaelis-Menten relationship was not observed; here, the dashed horizontal line indicates the average NH_4^+ oxidation rate (V_{avg}), taken to approximate V_{max} (see text for details). Error bars show the standard error of replicate experiments, each measured at least twice. Where errors bars are not visible, they are smaller than the data markers.

3.3.4 Potential implications of isotopic dilution of $^{15}NH_4^+$ by co-occurring $^{14}NH_4^+$ regeneration

As $^{15}NH_4^+$ and $^{14}NH_4^+$ are converted to $^{15}NO_2^-$ and $^{14}NO_2^-$ during NH_4^+ oxidation during incubation experiments, $^{14}NH_4^+$ is concurrently produced by heterotrophic bacterial remineralization of organic N. If unaccounted for, the $^{14}NH_4^+$ produced in the nitrification bottles, which will change (i.e., dilute) $f_{NH_4}^{15}$, may cause the NH_4^+ oxidation rates to be underestimated (*sensu* Glibert et al. 1982 for NH_4^+ uptake). The implications of isotope dilution vary as a function of the initial quantity of ^{15}N tracer added and the ambient $[NH_4^+]$, with the kinetics experiments to which the lowest ^{15}N tracer amendments were made being most vulnerable to change. Without coincident measurements of $^{14}NH_4^+$ regeneration rates, the NH_4^+ oxidation rates cannot be confidently corrected for isotope dilution; however, the sensitivity of the derived kinetic parameters to isotope dilution can be evaluated, at least hypothetically.

The NH_4^+ oxidation rates computed for the kinetics experiments at St 01, St 02, and St 03 are corrected for $^{14}NH_4^+$ isotope dilution according to the approach of Glibert et al. (1982; 1985) and Mulholland and Bernhardt (2005) by assuming an $^{14}NH_4^+$ regeneration rate of 20 nM d^{-1} (the average (and only) rate measured in the open Southern Ocean in summer; Goeyens et al. 1991), then re-derived V_{max} and K_m from these "corrected" rates (Figure B3.4, appendix B). The kinetic constants were altered differently by isotope dilution, with V_{max} being negligibly influenced while the K_m values were strongly affected, which is expected given that K_m is sensitive to the lowest rates of substrate transformation. K_m decreased at St 01 from 137 ± 40 nM (95% CI of 41 to 236 nM) to 108 ± 33 nM (95% CI of 27 to 189 nM), at St 02 from 28 ± 21 nM (95% CI of -19 to 74 nM) to 11 ± 16 nM (95% CI of -29 to 52 nM) and at St 03 from 67 ± 16 nM (95% CI of 29 to 105 nM) to 41 ± 9.4 nM (95% CI of 15 and 66 nM). In sum, K_m decreased by 22 to 59%, with the largest decrease at the stations with the lowest original K_m values. While such (hypothetical) changes to K_m are not trivial, the corrected values overlap

with the 95% CIs computed for our "uncorrected" K_m estimates. Moreover, the exercise above demonstrates that accounting for regeneration would not change our general observation of a low K_m for NH_4^+ oxidation in the Southern Ocean. Hereafter, only the uncorrected values are discussed since without coincident measurements of NH_4^+ regeneration, the NH_4^+ oxidation rates cannot be appropriately corrected for isotope dilution. I note that isotope dilution is potentially also a concern for NH_4^+ uptake rate estimates (Glibert et al. 1982) but given the short duration of the NH_4^+ uptake experiments, the effect was likely minor. For the depth-profile rate measurements, the initial $^{15}NH_4^+$ additions were so high as to negate the influence of isotope dilution (i.e., as for our estimates of V_{max}).

Table 3.2: A selection of previously measured kinetic parameters (V_{max} and K_m) and results from the current study, associated with NH_4^+ oxidation from different regions of the open ocean. For the kinetic parameters derived in the present study, values in parentheses are the standard errors associated with the Michaelis-Menten model (as computed using the drc package in R; Ritz et al. 2015), while the 95% confidence intervals (CIs) are shown in square brackets (computed using the nlstools package in R; Baty et al. 2015). *nd* indicates no data.

Region	Season	Latitude	Longitude	$[NH_4^+]$ (nM)	Sampled depth (m)	V_{max} (nM d^{-1})	K_m (nM)	Reference
Indian Southern Ocean: St 1	Winter	37°S	19°E	90	7	23 (2.1)	137 (40)	This study
Indian Southern Ocean: St 2	Winter	42°S	21°E	72	7	19 (1.9)	28 (21)	
Indian Southern Ocean: St 3	Winter	45°S	22°E	44	7	21 (1.2)	67 (16)	
Indian Southern Ocean: St 4	Winter	50°S	26°E	468	7	22 (3.8)[a]	nd	
Indian Southern Ocean: St 5	Winter	55°S	28°E	521	7	15 (2.5)[a]	nd	
Indian Southern Ocean: St 6	Winter	62°S	30°E	543	50	16 (3.7)[a]	nd	
Indian Southern Ocean: St 7	Winter	62°S	30°E	543	50	14 (2.6)[a]	nd	
Sargasso Sea	Winter	32°N	64°W	8.1	100	2.6 (1.1)	65 (41)	Newell et al. (2013)
Hood Canal in Puget Sound	Summer	47°N	123°W	60	50	nd	98 (14)	Horak et al. (2014)
Eastern Tropical South Pacific	Winter	14°S	80°W	nd	75	25 (1.3)	27 (4.4)	Peng et al. (2016)
Western Pacific Ocean	Autumn	30°N	148°E	nd	150	98 (20)	81 (66)	Zhang et al. (2020)
Pacific Ocean	Spring	26°N	134°E	32	5	0.19 (0.02)	172 (60)	Xu et al. 2019
Pacific Ocean	Spring	26°N	134°E	29	40	0.50 (0.03)	97 (20)	
Pacific Ocean	Spring	30°N	144°E	80	40	0.53 (0.05)	76 (25)	
Pacific Ocean	Spring	34°N	150°E	39	50	13 (0.4)	247 (22)	
Pacific Ocean	Spring	36°N	144°E	205	30	35 (4.6)	210 (81)	
East China Sea: Coastal	Spring	31°N	125°E	96	20	71 (6.7)	89 (29)	
South China Sea	Summer	21°N	120°E	nd	30-78	45-128	62-168	Wan et al. (2018)

Note that V_{max} values are reported as nM d^{-1} and K_m values as nM. Values in the brackets are standard errors.

nd indicates no data.

Values in brackets are standard errors.

[a]*V_{avg}; see text for details.*

3.3.5 Depth profiles of NH_4^+ uptake and oxidation in winter

The NH_4^+ uptake rates were fairly low throughout the upper 75 m (the approximate depth of the euphotic zone) at all depth-profile stations (St 08 to St 11). The rates reached a maximum of 6.26 nM d^{-1} at 25 m in St 08 and 6.94, 18.0, and 14.5 nM d^{-1} at 50 m at stations 09, 10, and 11, respectively, before declining to undetectable values below the 1% light depth (Figure 3.6a). Averaged over the euphotic zone, the uptake rates were lower at the stations south of PF, 3.6 ± 2.1 nM d^{-1} (St 08) and 5.1 ± 1.6 nM d^{-1} (St 09), compared to those north of PF, 11.5 ± 4.7 nM d^{-1} (St 10) and 11.8 ± 2.2 nM d^{-1} (St 11). The specific NH_4^+ uptake rates (V_{NH4+}) ranged from 0.9 to 3.2 x10^{-3} h^{-1} (0.005 to 0.04 d^{-1}), with upper 75 m averages that ranged from 1.39 ± 0.44 x10^{-3} h^{-1} (0.009 ± 0.003 d^{-1}) at St 08 to 5.48 ± 0.70 x10^{-3} h^{-1} (0.026 ± 0.003 d^{-1}) at St 10 and were lower to the north of the PF.

The $NH_4^+{}_{ox}$ rates were relatively homogenous throughout the upper 75 m at each station, with maximum rates of 21 and 17 nM d^{-1} measured at 50 m at St 09 and 10, respectively, while St 08 and 11 showed maximum rates of 15 and 24 nM d^{-1}, respectively, at 75 m. The mean of the euphotic zone rates were similar (average of 14 ± 2.8 nM d^{-1}; range of 12.6 ± 3.3 to 16.5 ± 3.4 nM d^{-1}) at all but the northernmost station (St 11; 21 ± 2.8 nM d^{-1}) (Figure 3.6b). The rates were lower at 200 m (range of 3.5 to 15 nM d^{-1}) and decreased to an average of 3.4 ± 0.6 nM d^{-1} by 500 m.

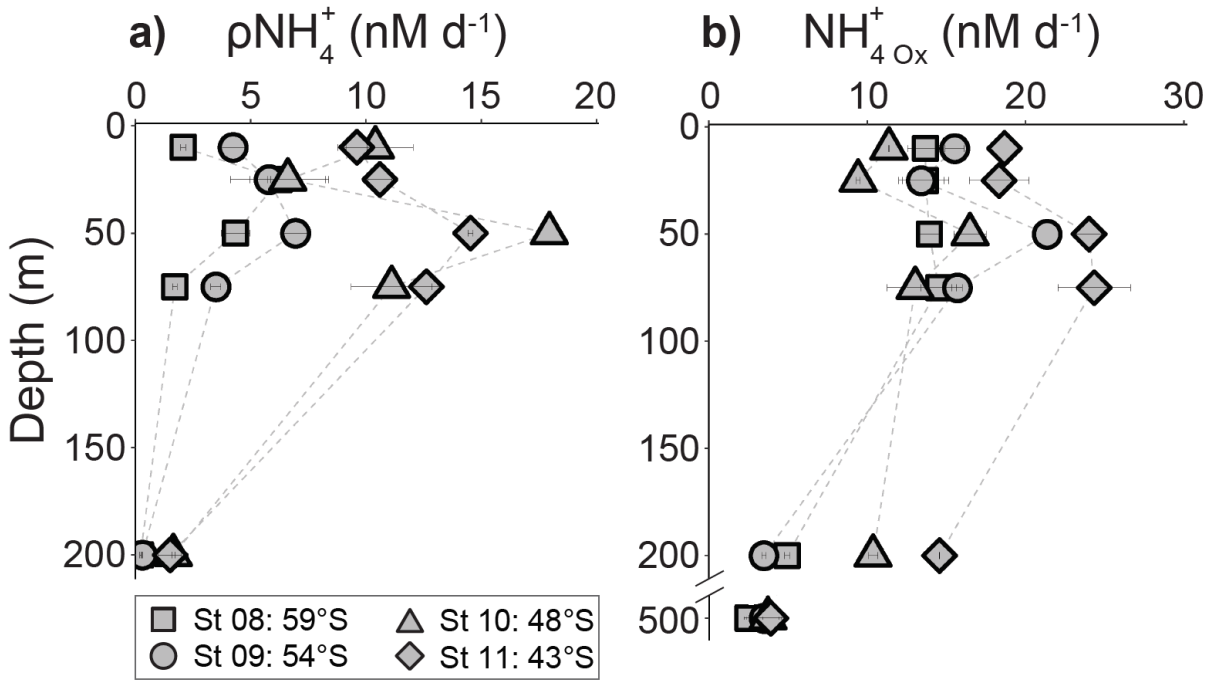

Figure 3.6: Wintertime upper water column rates of a) NH_4^+ uptake (0-200 m) and b) NH_4^+ oxidation (0-200 m and 500 m) measured at the depth profile stations. Here, the NH_4^+ uptake rates are shown as transport rates (nM d^{-1}) rather than specific rates, with the specific rates noted in the text. Error bars show the standard error of replicate experiments, each measured at least twice. Where error bars are not visible, they are smaller than the data markers. The dashed lines connecting the data points are included only to guide the eye and should not be taken to indicate interpolation with depth, particularly between 75 m and 200 m.

3.4 Discussion

The high-resolution [NH_4^+] measurements presented here reveal that NH_4^+ accumulates in the upper Southern Ocean during winter, particularly in the PFZ and AZ (Figure 3.1a and Figure 3.2b; Henley et al. 2020; Mdutyana et al. 2020). That the [NH_4^+] is near-homogeneous throughout the mixed layer at all hydrocast stations suggests that the residence time of NH_4^+, which is set by the relative rates of its production and consumption, is longer than the timescale of winter surface-layer mixing. While little is known of the seasonal cycle of NH_4^+ in the Southern Ocean, I suggest that the heterotrophic breakdown of late-summer/autumn phytoplankton biomass supplies much of the NH_4^+ that accumulates in the winter mixed layer. This conclusion is based in part on the observation of mixed-layer PON concentrations of 0.5-2.5 μM in late-summer versus 0.3-0.8 μM in winter (Table 3.1; DiFiore et al. 2009; Joubert et al. 2011; Mdutyana et al. 2020; Smart et al. 2020), as well as the (extremely limited and only available for summer) estimates of NH_4^+ regeneration rates in the Southern Ocean mixed layer that can reach as high as 50-100 nM d^{-1} (Goeyens et al. 1991).

The integrated mixed-layer NH_4^+ uptake and oxidation rates at the time of our sampling were 0.3-1.8 mmol m^{-2} d^{-1} and 1.4-4.5 mmol m^{-2} d^{-1}, respectively, yielding a combined mixed-layer NH_4^+ removal rate of 1.7 to 6.3 mmol m^{-2} d^{-1}. Dividing these values by the integrated mixed-layer NH_4^+ concentrations suggests a biological turnover time for NH_4^+ of 14-38 days for the stations south of the SAF, with station St 11 in the SAZ characterized by a turnover time of 1.1 days. Dividing the mixed-layer NH_4^+ consumption rates at each depth by the coincident NH_4^+ concentrations yields a similar picture, with average turnover times for St 08 to St 10 of 12-37 days and for St 11 of 0.4 days. This exercise suggests that the residence time of NH_4^+ in the winter mixed layer of the Southern Ocean south of the SAF is on the order of a month, and possibly longer given that the NH_4^+ consumption rates were determined via the addition of 200 nM $^{15}NH_4^+$, which likely stimulated uptake (see below). The mixed-layer [NH_4^+] declines to <200 nM across the Southern Ocean by early summer (Figure 3.1b; Sambrotto and Mace, 2000; Henley et al., 2020; Mdutyana et al. 2020), which indicates that between winter and late spring, the rate of NH_4^+ consumption must increase and/or the rate of its production must decline. Wintertime NH_4^+ regeneration rates are likely to be low relative to other seasons given the limited supply of PON (Cota et al. 1992; Philibert et al. 2015; Mdutyana et al. 2020; Smart et al. 2020) and will remain low in spring until productivity ramps up in response to increased light availability (Arrigo et al. 2008; Thomalla et al. 2011). As long as elevated mixed-layer [NH_4^+] persists, the upper Southern Ocean ecosystem is net heterotrophic and thus a biological source of CO_2 to the atmosphere.

Our measured rates of NH_4^+ uptake (V_{max} and depth-profile) increase northwards as the NH_4^+ concentration decreases, while the NH_4^+ oxidation rates are similar across the transect (Figure 3.6, 3.7a, and 3.8a). The differing trends in NH_4^+ uptake versus oxidation imply that photosynthetic NH_4^+ uptake, and thus the limitations thereon, exerts the ultimate control on the accumulation of NH_4^+ in the winter Southern Ocean mixed layer. Below, the results are evaluated in the context of existing estimates of the kinetic parameters associated with NH_4^+ uptake and oxidation, and possible drivers of the observed trends are then examined.

3.4.1 Southern Ocean kinetic parameters in the context of existing knowledge

Estimates of V_{max} for NH_4^+ uptake (ranging between 1.5 and 8.0 x10^{-3} h^{-1}) are similar at similar latitudes in winter and summer (Figure 3.7a and b), indicating that seasonal differences in the absolute NH_4^+ uptake rates (i.e., ρNH_4^+) are due primarily to changes in biomass (i.e., PON)

rather than to variations in per cell uptake rates. Our V_{max} values are also similar to estimates from other oceanic regions (1.0 to 9.2 $x10^{-3}$ h^{-1}; Table 3.1; Harrison et al. 1996; Cochlan and Bronk, 2001; Rees et al. 2006), with the exception of coastal systems where V_{max} is generally higher (7.2 to 18 $x10^{-3}$ h^{-1}; Harrison et al. 1996), likely because coastal $[NH_4^+]_{amb}$ is often elevated (Rodrigues and Williams, 2002; McCarthy et al. 2009; Heiss and Fulweiler, 2016) and coastal phytoplankton tend to be larger than those inhabiting open ocean waters (Deppeler and Davidson 2017).

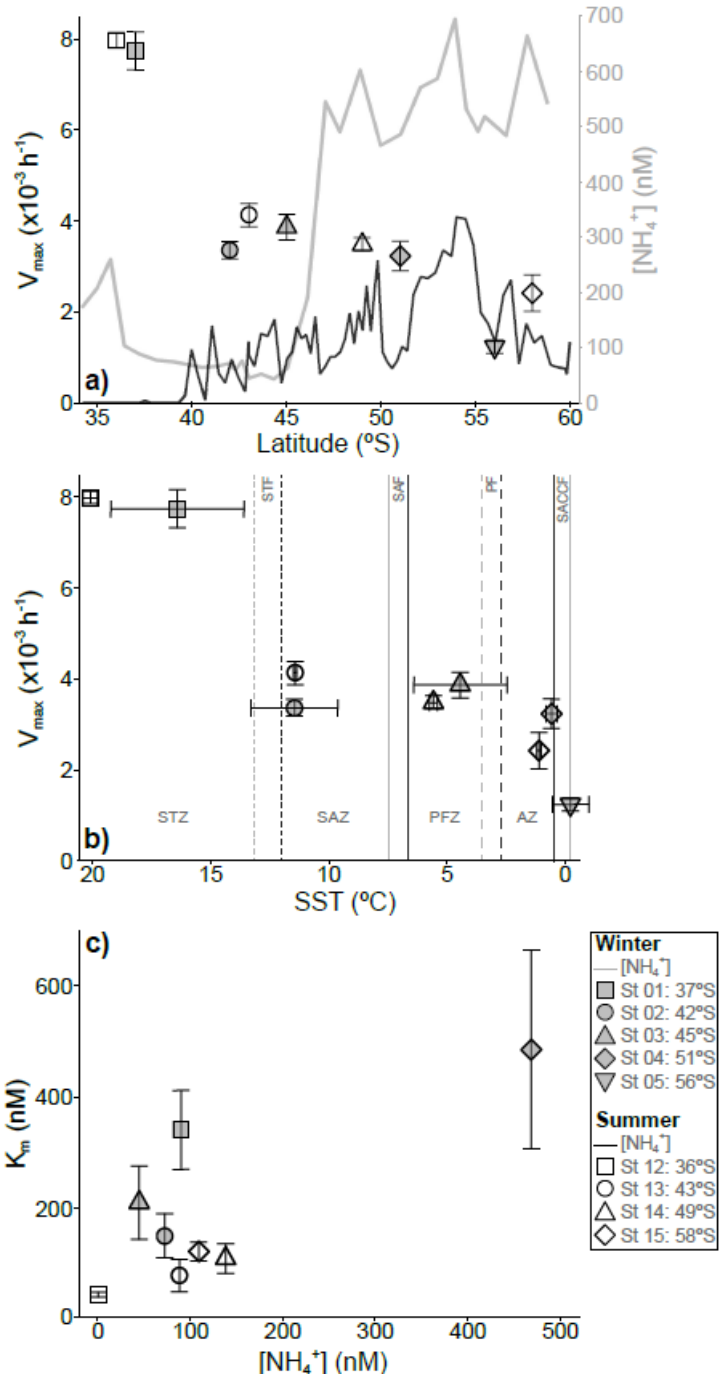

Figure 3.7 (previous page)**:** Potential controls on the kinetic parameters associated with NH_4^+ uptake. V_{max} is shown as a function of a) latitude and b) SST, and c) K_m as a function of $[NH_4^+]_{amb}$. Open symbols represent summer and filled symbols represent winter. In panel a, the left-hand y-axis (black) applies to V_{max} and the right-hand y-axis (grey) to $[NH_4^+]_{amb}$; the latter parameter, measured for samples collected from the ship's underway intake every four (winter) or two (summer) hours is shown by the solid grey (winter) and black (summer) lines. In panel b, the vertical lines represent the frontal positions in winter (grey) and summer (black), with the fronts and zones of the Southern Ocean labelled on the plot: STZ, Subtropical Zone; STF, Subtropical Front; SAZ, Subantarctic Zone; SAF, Subantarctic Front; PFZ, Polar Frontal Zone; PF, Polar Front; AZ, Antarctic Zone; SACCF, Southern Antarctic Circumpolar Front. Vertical error bars show the propagated error associated with V_{max} (panel a) and K_m (panel c) computed using the drc package in R (Ritz et al. 2015), while the symbols and horizontal error bars on panel b indicate the average (± standard deviation) SST experienced by the samples during the 23- to 30-hour incubations.

Estimates of the K_m for NH_4^+ uptake by Southern Ocean phytoplankton range between 41 nM and 405 nM, with clear seasonal differences – winter is characterized by over three-fold higher K_m values (150-405 nM) than summer (41-115 nM) (Table 3.1; Figure 3.7c). The K_m for phytoplankton in the oligotrophic ocean has been shown to be <100 nM (Kanda et al. 1985; Sahlsten, 1987; Harrison et al. 1996; Rees et al. 2006), while high latitude and coastal phytoplankton communities are typically characterized by higher K_m values (up to 600 nM; Shiomoto et al. 1994; Harrison et al. 1996; Cochlan and Bronk, 2001; Rees et al. 2006). This difference can be explained by the higher $[NH_4^+]_{amb}$ often encountered in coastal and higher latitude regions, including the Southern Ocean (Shiomoto et al. 1994; Rees et al. 2006). While similar estimates of V_{max} were derived for the summer and winter Southern Ocean, the seasonal difference in K_m reveals that the affinity of summertime phytoplankton for NH_4^+ is at least three-times that of the winter community. The subsequent summer-to-winter decrease in affinity coincides with a three-fold rise in the average $[NH_4^+]_{amb}$.

The kinetic parameters reported here for NH_4^+ uptake are, to our knowledge, the first for the open Southern Ocean, although not for its coastal waters – Cochlan and Bronk (2001) estimated similar values of V_{max} (1.0 to 4.8 $x10^{-3}$ h^{-1}) and K_m (40 to 333 nM) for the Ross Sea in spring and summer. However, our NH_4^+ oxidation kinetic parameters are the first such data for the Southern Ocean. For winter Southern Ocean waters north of the PF (37-45°S) where $[NH_4^+]_{amb}$ is low (≤90 nM), V_{max} ranges from 19-23 nM d^{-1}, which is higher than the V_{max} reported for the Sargasso Sea (Newell et al. 2013), subtropical North Pacific (Xu et al. 2019), and Hood Canal in Puget Sound (Horak et al. 2013), similar to rates from the Eastern Tropical South Pacific (Peng et al. 2016), and lower than estimates from the East and South China Sea and far western Pacific (Wan et al. 2018; Xu et al. 2019; Zhang et al. 2020) (Table 3.2). I note, however, that ammonia oxidizers were collected from the surface Southern Ocean (~7 m) in this study, while most other data are for communities collected at or near the base of the mixed

layer. It is possible that V_{max} would be higher near the base of the winter Southern Ocean mixed layer given our previous work showing NH_4^+ oxidation rates >50 nM d^{-1} at this depth (Mdutyana et al. 2020). The only other near-surface measurement of V_{max}, from 5 m in the subtropical North Pacific, yields an estimate of <1 nM d^{-1} (Xu et al. 2019). I thus suggest that the unique conditions of the winter Southern Ocean are reasonably favourable for NH_4^+ oxidation (Mdutyana et al. 2020).

Our estimates of the K_m for NH_4^+ oxidation range from 28-137 nM, similar to reported K_m values from the open ocean and culture studies (27-247 nM; Table 3.2; Olson 1981; Martens-Habbena et al. 2009; Horak et al. 2013; Newell et al. 2013; Qin et al. 2014; Peng et al. 2016; Wan et al. 2018; Zhang et al. 2020). The very high affinity of ammonia oxidizers for NH_4^+ in our study indicates that AOA dominate NH_4^+ oxidation in the shallow Southern Ocean, as has been shown elsewhere (e.g., Horak et al. 2013; Newell et al. 2013; Peng et al. 2016; Shiozaki et al. 2016). Indeed, the K_m reported for cultured and natural assemblages of AOB ranges from 8 μM to 14 mM (Knowles et al. 1965; Ward, 1987; Stehr et al. 1995; Martens-Habbena et al. 2009; Martens-Habbena and Stahl, 2011), orders of magnitude higher than that estimated here and for the cultured AOA, *N. maritimus* SCM1 (133 nM; Martens-Habbena et al. 2009). The hypothesized dominance of AOA over AOB in the shallow Southern Ocean is further supported by the fact that 1) V_{max} is first achieved at an $[NH_4^+]$ of 122 nM to 290 nM and 2) a Michaelis-Menten relationship cannot be derived for stations where $[NH_4^+]_{amb}$ was ≥468 nM (St 04-St 07; from 51ºS to the MIZ; Figure 3.4), indicating the saturation of NH_4^+ oxidation by $[NH_4^+]_{amb}$. Very similar average rates (V_{avg}) are observed at these stations, as well as at the depth-profile stations (St 08-St 11) where the mixed-layer ambient+tracer $[NH_4^+]$ ranged from 236 nM to 852 nM. It thus appears that an $[NH_4^+]$ of 200-300 nM is saturating for mixed-layer NH_4^+ oxidation (and AOA) in the Southern Ocean.

3.4.2 The biogeochemical controls on NH_4^+ consumption across the Southern Ocean

Below, I explore the environmental parameters that may control NH_4^+ consumption (uptake and oxidation) in the Southern Ocean mixed layer. I begin by summarising the relationships observed between the empirically-derived kinetic parameters and potentially important environmental variables, and then discuss their implications.

3.4.2.1 Controls on NH_4^+ uptake

For all experiments conducted in summer and all but one in winter (St 05 at 55ºS), NH_4^+ uptake is well-described by the Michaelis-Menten function (Figures 3.3 and 3.4). This implies that *in situ* NH_4^+ uptake rates across the Southern Ocean are limited by substrate availability when $[NH_4^+]_{amb}$ is <1000 nM in summer and <2000 nM in winter. The alleviation of substrate limitation does not, however, yield the same estimates of V_{max} and/or K_m at all stations, raising the question of what controls these parameters. In both seasons, V_{max} decreases with increasing latitude, increasing $[NH_4^+]_{amb}$, and decreasing SST, with the sharpest decrease occurring between 36°S and 43°S, followed by a more gradual decline towards the south (Figure 3.7a and b). K_m shows a generally positive relationship with latitude (Figure B3.3a, appendix B), SST (Figure B3.3b, appendix B), and $[NH_4^+]_{amb}$ (Figure 3.7c), although I have no estimates of K_m for 138 nM < $[NH_4^+]_{amb}$ < 468 nM because of the strong $[NH_4^+]_{amb}$ gradient in the PFZ, particularly in winter (Figure 3.1a and 3.2b). While $[NH_4^+]_{amb}$ in each Southern Ocean zone is on average three-fold higher in winter than summer, for the same $[NH_4^+]_{amb}$, K_m is two- to four-times higher in winter (e.g., compare St 02 (42ºS) in winter ($[NH_4^+]_{amb}$ of 72 nM and K_m of 150 nM) to St 13 (43ºS) in summer ($[NH_4^+]_{amb}$ of 88 nM and K_m of 79 nM); Table 3.1). The implication of this observation is that summertime phytoplankton are adapted to a lower $[NH_4^+]_{amb}$, while winter communities are accustomed to a sustained higher supply of NH_4^+ (Kanda et al. 1985; Harrison et al. 1996; Rees et al. 2006).

The apparent relationship of V_{max} to latitude could be driven by a number of factors, including $[NH_4^+]_{amb}$, light, and temperature. Since V_{max} decreases southwards as $[NH_4^+]_{amb}$ increases in both seasons, the availability of NH_4^+ is not the primary determinant of the maximum rate of its consumption by phytoplankton. Despite the relatively low energy requirement associated with NH_4^+ assimilation (Dortch, 1990), light is nonetheless expected to exert a strong control on V_{max} in winter, although not in summer when the Southern Ocean is light-replete (Venables and Moore 2010) due to both the amount of solar radiation that surface waters receive and the fairly shallow mixed layers that characterize this season (summer MLDs range from 20-130 m; Dong et al. 2008; Sallée et al.2010; du Plessis et al. 2017; 2019). Given the shallow MLDs, it is even possible that summer phytoplankton are light-inhibited at the surface, thus yielding the north-south decline in V_{max}. However, our water samples were collected from 7 m where light had already been attenuated to ~55% of surface PAR and were subsequently incubated at this light level. Light inhibition is thus unlikely to explain our observations.

V_{max} decreases with decreasing SST in both seasons, although the decline is more consistent in summer, with the winter estimates of V_{max} remaining roughly constant between the STF and SACCF despite a >10ºC change in SST (Figure 3.7b). For summer, an average Q_{10}, which is a measure of the proportional increase in reaction rate for a 10ºC rise in temperature, of 1.9 is calculated for the transect (from an SST of 1.3ºC (AZ) to 5.9ºC (PFZ), Q_{10} = 2.3; from an SST of 5.9ºC (PFZ) to 11.5ºC (SAZ), Q_{10} = 1.3; from an SST of 11.5ºC (SAZ) to 19.6ºC (STZ), Q_{10} = 2.1). These Q_{10} values imply that temperature does exert a control on V_{max} (Harrison et al., 1996; Kanda et al., 1985; Baer et al., 2014; Smith and Harrison, 1991), and that this control is strongest south of the PFZ. By contrast, the average Q_{10} for winter is ~1, except between 55ºS and 50ºS (SST and V_{max} increase from 0.5ºC to 1.8ºC and 1.2 $x10^{-3}$ h^{-1} to 3.1 $x10^{-3}$ h^{-1}, respectively) where it reaches an unrealistically high value (>100). Culture experiments have shown NH_4^+ uptake to be fairly insensitive to temperature (Reay et al. 1999), while *in situ* data from the Arctic, where the SST overlaps with that of the Southern Ocean, indicate a role for temperature (Baer et al. 2014). Our data suggest that the dominant control on the maximum NH_4^+ uptake rate attainable by Southern Ocean phytoplankton could be temperature in summer but is more likely to be light in winter. The effects of these parameters may be direct (e.g., higher SST leading to higher rates of enzyme function; Clayton and Ahmed, 1986; Lomas and Glibert, 1999a; Lomas and Gilbert, 1999b) or indirect insofar as seasonal changes in light or SST drive changes in the phytoplankton species present in the water column.

The Southern Ocean phytoplankton community varies seasonally due to changes in environmental conditions (e.g., light, temperature) and macronutrient- and trace metal (e.g., iron) availability (Boyd, 2002; Smith and Lancelot, 2004; Viljoen et al. 2019). Thus, although not measured directly in this study, community composition likely plays a role in the observed differences in the kinetic parameters, as well as in the derived Q_{10} values (e.g., Suzuki and Takahashi 1995; Stawiarski et al. 2016). Small phytoplankton tend to favour NH_4^+ over NO_3^- as their primary N source (Dortch, 1990; Berg et al. 2003; Heil et al. 2007) and are expected to express a high affinity for this substrate (Koike et al. 1983; Dortch 1990). In winter, nanoflagellates dominate Southern Ocean surface waters (Clarke and Leakey, 1996; Weir et al. 2020), with larger phytoplankton such as diatoms becoming more abundant in summer, although the smaller groups remain productive (Viljoen et al. 2018; 2019). Since diatoms specialize in NO_3^- assimilation (Litchman et al., 2006; Fawcett and Ward, 2011), which in the Southern Ocean is controlled by a combination of iron and light availability (Martin, 1990; Sunda and Huntsman 1997; Sedwick et al. 1999; Moore et al. 2013), it is likely that NH_4^+

uptake remains the purview of smaller phytoplankton for most of the year (Stolte et al. 1994; Trull and Armand, 2001; Karsh et al. 2003). This may explain our similar V_{max} estimates for winter and summer (Table 3.1). I suggest that the two- to three-fold seasonal increase in biomass mainly reflects the growth of larger, NO_3^--consuming cells in spring/summer, with a significant portion of this biomass exported from the euphotic zone by the end of the growing season (Tréguer et al. 1995; Rigual-Hernández et al. 2016). By contrast, smaller cells contribute far less to biomass and are primarily incorporated into the microbial loop that dominates NH_4^+ consumption throughout the year, at rates that are dependent on light (mainly in winter), SST (mainly in summer, when NH_4^+ availability will also play a role), and possibly iron availability. I note, however, that V_{max} for the NH_4^+ consumers may be higher in summer than our data suggest given that this parameter is calculated for total sampled biomass (i.e., total PON), much of which may have been generated via the assimilation of NO_3^- rather than NH_4^+; without size-fractionated/population-specific measurements, this uncertainty cannot be addressed. Regardless, the data reveal that at the whole-community level, the maximum capacity of Southern Ocean phytoplankton for NH_4^+ uptake is similar in summer and winter, although apparently controlled by different environmental parameters.

Iron plays a critical role in shaping Southern Ocean phytoplankton communities (Boyd et al. 2000; Coale et al. 2003; Wojtasiewicz et al. 2019). While NH_4^+ uptake has no direct iron requirement, iron is necessary for photosynthetic and electron transport chains (Raven et al. 1999; Morel and Price, 2003), as well as for the synthesis of chlorophyll (Chereskin and Castelfranco 1982). Mixed-layer iron concentrations in the open Southern Ocean appear to be slightly higher in winter than summer (Tagliabue et al. 2014; Mtshali et al. 2019), which may partially offset wintertime light limitation of photosynthesis (Viljoen et al. 2018) and by extension, NH_4^+ uptake. DFe concentrations were measured coincident with rates of NH_4^+ uptake at the winter depth-profile stations. A positive relationship between mixed-layer ρNH_4^+ and DFe was observed ($R^2 = 0.37$; $p = 0.013$; Figure 3.9a), suggesting that iron may influence phytoplankton growth on NH_4^+, presumably via the iron requirement of photosynthesis. As there are no DFe data from the kinetics stations, the potential role of iron in the observed latitudinal gradient in V_{max} cannot be evaluated. That said, a large global compilation of DFe measurements focused on the Southern Ocean suggests minimal differences in mixed-layer iron concentrations among its latitudinal zones (Tagliabue et al. 2012).

3.4.2.2 Controls on NH_4^+ oxidation

Kinetic parameters associated with NH_4^+ oxidation could only be determined at the three northernmost stations, with $NH_4^+{}_{ox}$ apparently saturated at $[NH_4^+]_{amb}$ at the other four stations (Figure 3.5; Table 3.2). The $NH_4^+{}_{ox}$ rates at these non-MM stations, averaged over the range of NH_4^+ substrate additions (i.e., V_{avg}), are thus taken as equivalent to V_{max}. For St 01-St 03, V_{max} ranges from 19 ± 1.9 nM d^{-1} to 23 ± 2.1 nM d^{-1}, while V_{avg} at St 04-St 07 ranges from 14 ± 2.6 nM d^{-1} to 22 ± 3.8 nM d^{-1}. No consistent trends are observed in the maximum NH_4^+ oxidation rate (V_{max} and V_{avg}) with latitude or SST, although V_{avg} is slightly lower at the higher latitude stations (St 05-St 07) where SST is lowest (Figure 3.8). This decline does not coincide with the sharp rise in $[NH_4^+]_{amb}$, which occurs between 45ºS and 47ºS, north of St 04 (Figure 3.8a). The decoupling of V_{max} (or V_{avg}) and $[NH_4^+]_{amb}$ implies that the maximum rate of $NH_4^+{}_{ox}$ is not controlled by $[NH_4^+]_{amb}$, consistent with our recent work from the Atlantic Southern Ocean that showed no relationship of mixed-layer $NH_4^+{}_{ox}$ to $[NH_4^+]_{amb}$ at concentrations ≥400 nM (Mdutyana et al. 2020). Additionally, at St 01-St 03, V_{max} is first achieved at a substrate concentration of 122 to 290 nM (Figure 3.5a-c), indicating that when $[NH_4^+]_{amb}$ is >122-290 nM, the primary control on $NH_4^+{}_{ox}$ is no longer substrate availability. No change in V_{max} and V_{avg} is observed between St 01 and St 04 (~1450 km apart) despite a >15ºC change in SST, while south of the PF where SST is <0°C, V_{avg} is 32% lower than at the stations with SSTs >0°C (Figure 3.8). That said, the Q_{10} value calculated by averaging the rate and SST data from the stations south versus north of where SST = 0°C is 1.35, suggesting a minimal (but perhaps not negligible when SST is <0.6ºC, the average value measured at St 04) temperature effect. Our findings are consistent with previous work, including from the Indian sector of the Southern Ocean (Bianchi et al. 1997) and the Arctic (Baer et al. 2014), showing that temperature has little influence on the *in situ* rates of nitrification because nitrifiers are generally well-adapted to the environment in which they are found (Ward, 2008; Horak et al. 2013; 2018).

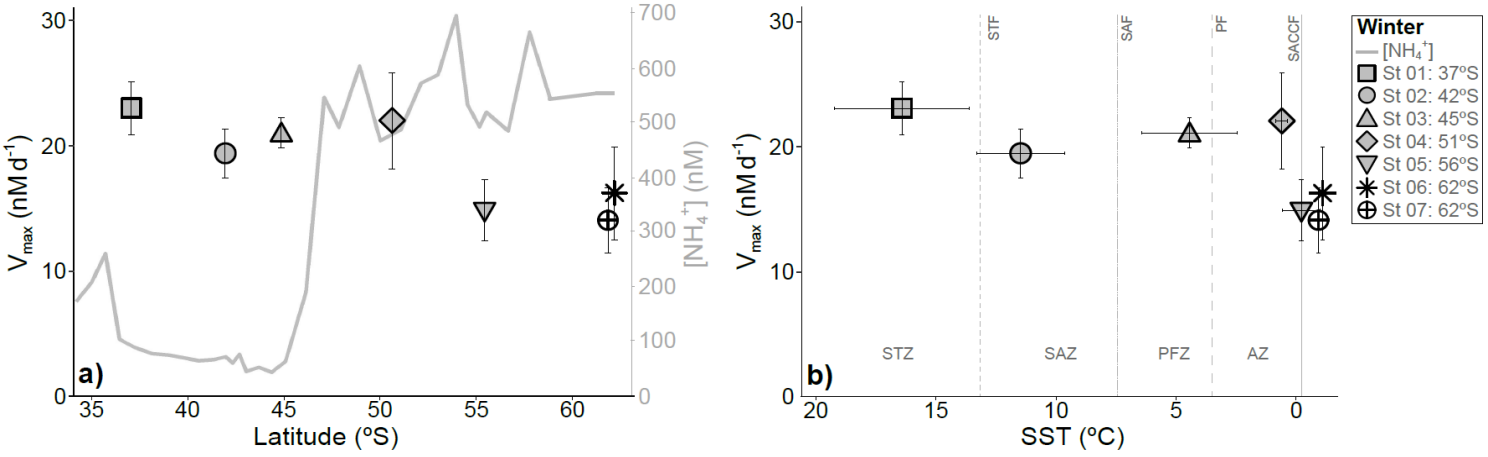

Figure 3.8: Potential controls on the kinetic parameters associated with NH_4^+ oxidation. V_{max} is shown as a function of a) latitude and b) SST. In panel a, the left-hand y-axis (black) applies to V_{max} and the right-hand y-axis (grey) to $[NH_4^+]_{amb}$; the latter parameter, measured from the ship's underway intake every four hours, is shown by grey lines on the plot. Vertical error bars show the propagated error associated with V_{max} (panel a and b) computed using the drc package in R (Ritz et al. 2015), while the symbols and horizontal error bars on panel b indicate the average (± standard deviation) SST experienced by the samples during the 23- to 30-hour incubations. Fronts and zones labelled on the plot are as in Figure 3.7.

Inhibition of nitrification by light in the open ocean has been widely documented, with $NH_4^+{}_{ox}$ generally expected to rise as light declines (Olson, 1981b; Ward, 2005; Peng et al. 2018; Lu et al. 2020). Indeed, I have previously attributed elevated wintertime Southern Ocean mixed-layer nitrification rates to the low-light conditions encountered during this season (Mdutyana et al. 2020). Photosensitivity seems to be more pronounced for AOA than AOB at low light (Merbt et al. 2012b), although the AOA response is apparently strain-specific (Beman et al. 2008; Luo et al. 2014; Qin et al. 2014). Our estimates of V_{max} and V_{avg} show no evidence of differential light inhibition, with the lowest V_{avg} measured at the stations with the lowest light availability (Figure 3.8a) – here, latitude is used as a proxy for light availability, which is reasonable given the observed negative relationship of average daily PAR to latitude in July 2017 (https://oceancolor.gsfc.nasa.gov/l3/) and the fact that ammonia oxidizers respond slowly to changes in the ambient light field (Lu et al. 2020). While our $NH_4^+{}_{ox}$ experiments were conducted in dark bottles, this is unlikely to have artefactually increased the measured rates given the evidence for very slow to no recovery of AOA from light inhibition in the dark (Merbt et al. 2012), along with our prior results showing no light inhibition in the surface Southern Ocean for samples incubated under simulated *in situ* wintertime light conditions (Mdutyana et al. 2020). A further consideration is that the light effect may be indirect in the sense that at low light, phytoplankton are less competitive for NH_4^+ (Ward, 1985, 2005b; Smith et al. 2014; Zakem et al. 2018). However, plotting the V_{max} for NH_4^+ uptake versus the V_{max} and V_{avg} for

$NH_4^+{}_{ox}$ for kinetics experiments conducted at the same stations (filled symbols in Figure 3.9b) and ρNH_4^+ versus $NH_4^+{}_{ox}$ at all overlapping depths for the depth-profile stations (open symbols in Figure 3.9b) reveals a weak positive relationship between NH_4^+ uptake and oxidation. This is the opposite of the relationship expected for competition between phytoplankton and ammonia oxidizers (Wan et al. 2018) and is also unsurprising given the evidence that $[NH_4^+]_{amb}$ is not the primary control on the V_{max} of either group. This raises the question of what, if not $[NH_4^+]_{amb}$, light, SST, or competition with phytoplankton, controls the maximum rate of NH_4^+ oxidation in shallow Southern Ocean waters?

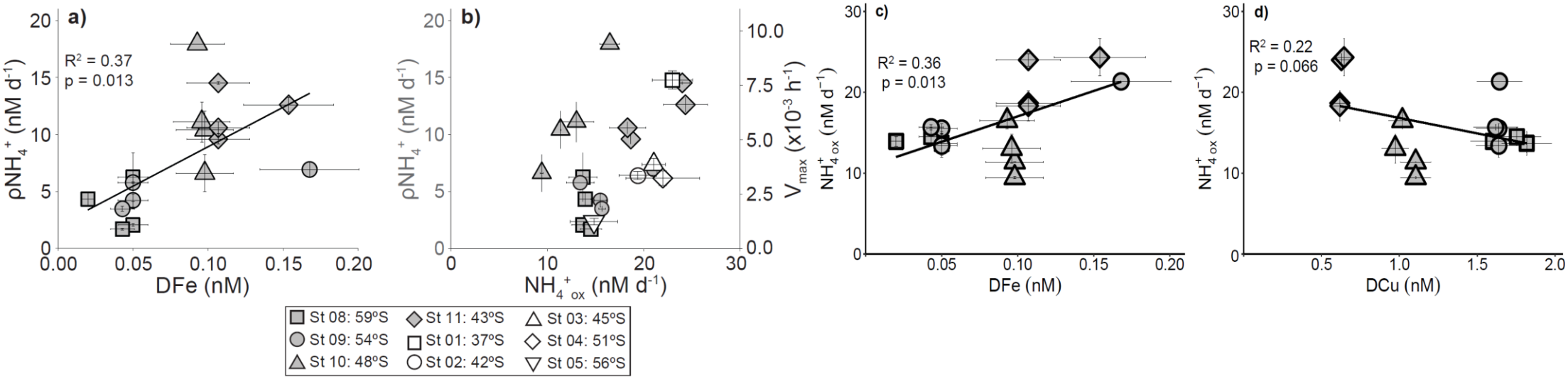

Figure 3.9: a) Depth profile (St 08-11) (0-75 m) measured rates of NH_4^+ uptake (nM d^{-1}) plotted against the coincident dissolved iron concentrations (DFe), b) NH_4^+ uptake rates (nM d^{-1}) plotted against the concurrently-measured NH_4^+ oxidation rates at the depth profile (0-75 m; filled symbols, left-hand y-axis) and wintertime V_{max} or V_{avg} for NH_4^+ uptake (h^{-1}) plotted against NH_4^+ oxidation (nM d^{-1}) at kinetic stations 1-5 (open symbols; right-hand y-axis). Also shown are the measured depth profile rates (0-75 m) of NH_4^+ oxidation plotted against coincident measurements of c) DFe and d) DCu. Error bars show the standard error of replicate experiments/collections, each measured at least twice.

3.4.3 A hypothesized role for iron in limiting NH_4^+ oxidation

It is well known that iron limits primary production and N uptake across the Southern Ocean (Martin, 1990; Boyd et al. 2007), but far less attention has been paid to iron as a potential control on nitrification despite the general recognition that NH_4^+ oxidation (at least by AOB) requires this trace element (Meiklejohn, 1953; Morel and Price, 2003). A recent culture study demonstrated that the growth of the globally abundant marine AOA, *N. maritimus* SCM1, is strongly dependent on the availability of inorganic iron (Shafiee et al. 2019). In addition, the affinity of this AOA for iron appears to be low, as inferred from an estimated K_m for inorganic iron uptake that is 10- to 100-times greater than the K_m derived for most phytoplankton and heterotrophic bacteria. While the K_m expressed by AOA in the environment could well be lower than that measured in culture, one implication of these findings is that NH_4^+ oxidation may be iron-limited in the mixed layer of some ocean regions, including the Southern Ocean (Shafiee et al. 2019). A positive relationship is observed between DFe and $NH_4^+{}_{ox}$ ($R^2 = 0.36$; $p = 0.013$; Figure 3.9c) for samples collected throughout the mixed layer at the depth-profile stations, consistent with the notion that iron may exert a control on nitrification (Figure 3.9c; here, $NH_4^+{}_{ox}$ is likely similar to V_{max} at each depth/station because the rates were measured following the addition of 200 nM $^{15}NH_4^+$, which is a higher than the derived K_m for NH_4^+ oxidation). Unfortunately, there are no DFe measurements that coincide with our kinetic experiments and so cannot draw a stronger conclusion. Nonetheless, given the work of Shafiee et al. (2019) suggesting that AOA will be uncompetitive for iron under open ocean conditions and the fact that higher rates of $NH_4^+{}_{ox}$ are observed at higher DFe (even at the same station), it seems plausible that iron may play a role in determining the rate of NH_4^+ oxidation attainable by nitrifiers in the iron-limited upper Southern Ocean.

NH_4^+ oxidation is a multi-step pathway that involves the oxidation of NH_4^+ to hydroxylamine (NH_2OH), catalyzed by the ammonia monooxygenase (AMO) enzyme (Arp et al. 2002; Vajrala et al. 2013), and the subsequent oxidation of NH_2OH (via nitric oxide; NO) to NO_2^- (Walker et al. 2010; Vajrala et al. 2013; Kozlowski et al. 2016; Caranto and Lancaster, 2017). AOA and AOB each possess a variant of AMO, both of which appear to contain mono- and di-nuclear copper centers (Lieberman and Rosenzweig 2005). In addition, AOA have a number of copper-containing metalloenzymes that are hypothesized to be involved in electron transfer (Hallam et al. 2006; Wei et al. 2006; Walker et al. 2010; Blainey et al. 2011; Amin et al. 2013). By contrast, AOB rely on iron-rich *cytochrome c* proteins, particularly for the oxidation of NH_2OH to NO, which is catalyzed by the heme-rich hydroxylamine oxidoreductase (HAO) complex

(Arp et al. 2002; Walker et al. 2010). No genes have yet been discovered in the open ocean that encode an analogous HAO in AOA (e.g., Hallam et al. 2006; Wei et al. 2006; Walker et al. 2010 ; Blainey et al. 2011; Mosier et al. 2012; Amin et al. 2013).

Given the above, one might expect the iron requirement of AOA to be fairly low, particularly compared to that of AOB, although I note that little is known of the affinity of AOB for iron. However, recent proteomic studies have shown that the iron-sulphur (Fe-S) protein, ferredoxin, is highly expressed in *N. maritimus* SCM1 (Qin et al. 2018) and the AOA, *Candidatus* Nitrosopelagicus brevis (Santoro et al. 2015; Carini et al. 2018). Because ferredoxin is co-expressed with key AMO modules, it has been hypothesized that Fe-S proteins may be important for AOA electron transport (Shafiee et al. 2019) in addition to copper proteins. *Ca* N. brevis also has genes encoding iron-specific membrane uptake proteins, while other marine AOA, including *N. maritimus* SCM1, instead possess genes homologous to non-specific metal transporters (Shafiee et al. 2019). Taken together, the available data strongly suggest that AOA in the upper Southern Ocean will have a high iron requirement and may thus be vulnerable to iron limitation. Elevated nitrification rates have been observed in the mixed layer of the naturally iron-fertilized waters surrounding Kerguelen Island (Cavagna et al. 2015; Fripiat et al. 2015) and South Georgia (Mdutyana et al. 2020), consistent with this hypothesis. While the idea that iron availability limits nitrification in the upper Southern Ocean requires direct testing, the alleviation of such a limitation may explain the high NH_4^+ oxidation rates (26-151 nM d^{-1}) that I measured previously in the lower mixed layer of the Atlantic Southern Ocean in winter (Chapter 2; Mdutyana et al. 2020). As light is attenuated with depth in the water column and phytoplankton growth declines, AOA will become more competitive for the limited available iron, the consumption of which should allow them to oxidize the relatively large ambient NH_4^+ pool more rapidly provided they are not (co-)limited by another resource.

It is possible that mixed-layer NH_4^+ removal may be (co-)limited by copper given that this trace metal is a cofactor in AMO and is involved in electron transfer (Walker et al. 2010; Amin et al. 2013; Santoro et al. 2015) – indeed, copper limitation has been shown to restrict the growth of AOA in culture (Amin et al. 2013). DCu concentrations in the Southern Ocean mixed layer are similar to other ocean regions (Dieu and Sohrin 2013; Minami et al. 2015; Zheng et al. 2017), typically ranging between 0.5 and 2 nM and increasing towards the south (Monteiro and Orren, 1985; Ellwood et al. 2008; Heller and Croot, 2015; Cloete et al. 2019). One might thus expect copper limitation, if pertinent, to have a greater effect on NH_4^+ oxidation rates in northern Southern Ocean waters. However, plotting mixed-layer $NH_4^+{}_{ox}$ as a function of DCu

shows the opposite trend, with the highest rates of $NH_4^+{}_{ox}$ occurring at the lowest DCu concentrations (R^2 = 0.22; p = 0.066; Figure 3.9d). The implication is that NH_4^+ oxidation is not copper-limited in the winter Southern Ocean, with the relationship shown in Figure 3.9d driven mainly by the strong zonal gradient in mixed-layer DCu concentrations.

A possible role for copper in Southern Ocean NH_4^+ removal more broadly cannot be ruled out, however, particularly in summer when mixed-layer DCu (and DFe) concentrations decline (Ellwood 2008; Lai et al. 2008; Boye et al. 2012; Cloete et al. 2019; Viljoen et al. 2019). Iron-limited phytoplankton generally have a high requirement for copper because they employ a multicopper oxidase as part of their high-affinity iron transport system (Peers et al. 2005; Wells et al. 2005; Maldonado et al. 2006). It has also been proposed based on culture work that under iron limitation, phytoplankton may use a copper aminase enzyme to access NH_4^+ (Palenik and Morel 1991); if this occurs in the Southern Ocean, it would further increase the requirement of phytoplankton for copper and complicate the interactions among the copper, iron, and N cycles. Additionally, Southern Ocean diatoms, which dominate south of the SAF in summer and winter (Wright et al. 2010 ; Petrou et al. 2016; Rembauville et al. 2017; Weir et al. 2020), may have an extra copper requirement given culture data showing that iron-limited diatoms synthesize plastocyanin, a copper-containing protein involved in electron transfer that substitutes for the iron-rich cytochrome c_6 (Peers et al. 2005; Peers and Price, 2006). Finally, the available data show that Southern Ocean NH_4^+ oxidation rates are highest just below the mixed layer throughout the year (Olson, 1981b; Bianchi et al. 1997; Mdutyana et al. 2020); here, light levels are low, iron, copper, and NH_4^+ concentrations decrease sharply (but not necessary coincidentally), and there is the possibility of competition with phytoplankton for resources. While very little is known of the potential for copper to limit photosynthetic NH_4^+ uptake in the Southern Ocean and NH_4^+ oxidation in the open ocean more broadly, copper bioavailability and cycling, and copper-iron interactions, may have implications for the Southern Ocean's N cycle that have to-date been overlooked.

3.5 Conclusions and implications

The Southern Ocean is a quintessential HNLC region where surface-layer NO_3^- concentrations are replete throughout the year. Here, I show that NH_4^+ accumulates in the winter mixed layer of the Southern Ocean's African sector along with the elevated NO_3^-, particularly south of the SAF, in part because the organisms involved in its removal (i.e., phytoplankton and ammonia

oxidizers) are limited in the maximum NH_4^+ consumption rates that they can achieve. What is not yet clear is whether NH_4^+ production outpaces NH_4^+ removal in winter, or whether NH_4^+ production occurs predominantly in late-summer and autumn following the period of maximum phytoplankton growth, with the subsequent net removal of NH_4^+ taking place throughout the autumn and winter. In each zone of the winter Southern Ocean, the maximum specific NH_4^+ uptake rate for phytoplankton is similar in summer and winter, but appears to be dominantly controlled by light availability in winter and temperature in summer. The affinity of phytoplankton for NH_4^+ across the Southern Ocean is variable, and is significantly higher in summer than winter, suggesting that the summertime NH_4^+ supply is low compared to that of winter when phytoplankton are adapted to conditions of sustained higher availability. Across more than 25 degrees of latitude and all the zones of the Southern Ocean, the kinetic parameters associated with NH_4^+ oxidation are low and near-invariant. The very low estimates of K_m, akin to values measured in oligotrophic waters, strongly suggest that as in other ocean regions, AOA rather than AOB dominate NH_4^+ oxidation in the upper Southern Ocean (Beman et al. 2008; Newell et al. 2011; Peng et al. 2016; Pajares et al. 2019). V_{max} is achieved at low $[NH_4^+]_{amb}$ and changes little with light, temperature, $[NH_4^+]_{amb}$, or competition with phytoplankton for substrate. I thus hypothesize that dissolved iron availability may exert a control on the NH_4^+ oxidation rate, particularly when ambient NH_4^+ concentrations are >200 nM (i.e., in polar Southern Ocean waters).

There are a number of implications of these findings. First, the observation of low and invariant maximum NH_4^+ oxidation rates that show little sensitivity to temperature or $[NH_4^+]_{amb}$ is relevant for biogeochemical models that parameterize nitrification as a linear function of $[NH_4^+]_{amb}$, scaled for temperature (e.g., Vichi et al. 2007). Additionally, no biogeochemical model currently allows for an iron (or copper) control on nitrification. While deeper investigation is required to confirm the role of iron in both NH_4^+ and NO_2^- oxidation (nitrite oxidoreductase, the enzyme that catalyzes the oxidation of NO_2^- to NO_3^-, has a substantial iron requirement; Meincke et al. 1992; Lücker et al. 2010), it is nonetheless worth considering the potential consequences for upper-ocean biogeochemistry (modelled and observed) of this putative control. For instance, in regions where $[NH_4^+]_{amb}$ is elevated relative to the K_m for NH_4^+ oxidation, competition between phytoplankton and ammonia oxidizers for iron may contribute to the distribution and functioning of these two groups, particularly in the lower mixed layer where their niches are most likely to overlap and in high-latitude regions in winter where the surface light flux is low. Moreover, it is likely that the iron supply to Southern Ocean

surface waters will increase in future (IPCC, 2019; Henley et al. 2020 and references therein), with models predicting that phytoplankton productivity will rise significantly in response (Bopp et al. 2013; Leung et al. 2015; Fu et al. 2016; Moore et al. 2018). However, no model can adequately capture the numerous complex interactions among changing environmental variables and the microbial community (Hutchins and Boyd, 2016; Strzepek et al. 2019). An improved parameterization of nitrification, the pathway that links the reduced and oxidized N cycles, would constitute an important step forward in understanding the response of upper Southern Ocean biogeochemistry to global change.

Second, if mixed-layer NH_4^+ oxidation is limited by iron availability, then the iron-deplete conditions of the surface Southern Ocean may restrict the extent to which surface nitrification can offset CO_2 drawdown by phytoplankton. Nitrification is the dominant biological process occurring in the Southern Ocean mixed layer in winter, producing regenerated NO_3^- (Smart et al. 2015; Mdutyana et al. 2020). Some fraction of this NO_3^- is supplied to and consumed by phytoplankton in spring and summer (Mdutyana et al. 2020) because the winter mixed layer evolves into both the summer mixed layer and the underlying layer that exchanges NO_3^- with the upper ocean throughout the spring and summer (Whitworth and Nowlin 1987; Difiore et al. 2010). However, unlike for NO_3^- mixed up into the euphotic zone from below the depth of winter mixing, phytoplankton growth on regenerated NO_3^- does not equate to net atmospheric CO_2 removal (*sensu* the new production paradigm; Dugdale and Goering, 1967; Yool et al. 2007). Thus, the controls on the production of regenerated NO_3^- in the Southern Ocean mixed layer directly affect the strength of its biological pump, with higher rates of mixed-layer nitrification potentially weakening export production.

Third, these data and those of others show that the affinity of ammonia oxidizers for NH_4^+ is very high (Horak et al. 2013; Newell et al. 2013; Peng et al. 2016; Xu et al. 2019; Zhang et al. 2020). That these organisms achieve their V_{max} at such low concentrations of $[NH_4^+]_{amb}$ (at times <150 nM) introduces a potential methodological issue that is illustrated by my own measurements of $NH_4^+{}_{ox}$ with depth (Figure 3.6b). Most studies of NH_4^+ oxidation that use the isotope tracer method involve the addition of at least 50-200 nM $^{15}NH_4^+$ (e.g., Santoro et al. 2013; Peng et al. 2018; Shiozaki et al. 2019; Mdutyana et al. 2020). In waters with low $[NH_4^+]_{amb}$, the addition of such concentrations can stimulate NH_4^+ oxidation to rates in excess of those occurring in the environment, oftentimes approaching V_{max}. This appears to be the case for the depth-profile stations where the ambient+tracer NH_4^+ concentration was always >200 nM and the measured mixed-layer NH_4^+ oxidation rates were similar to the estimates of

V_{max}. This result underscores the importance when conducting such experiments of adding as little $^{15}NH_4^+$ as possible, preferably following the analysis of $[NH_4^+]_{amb}$ (Ward, 2011). Alternately, measured NH_4^+ oxidation rates can be corrected for $^{15}NH_4^+$ addition (e.g., Horak et al. 2013), although this relies on knowing K_m with a high degree of certainty.

Finally, increasing atmospheric CO_2 concentrations are causing the ocean to warm and acidify (IPCC, 2019), with consequences for the Southern Ocean N cycle that are difficult to predict. Warming is likely to increase the rate of biological reactions (e.g., phytoplankton growth; Eppley, 1972; Sherman et al. 2016; Moore et al. 2018), although the effect on nitrification is unclear, with my data and those of others suggesting a minimal response of ammonia oxidizers to a change in temperature (Horak et al. 2013; Baer et al. 2014). It is possible, therefore, that in a warmer Southern Ocean, phytoplankton will become more competitive than ammonia oxidizers at the depths where they overlap, particularly given the prediction of a general warming-driven shift towards smaller phytoplankton (Constable et al. 2014; Petrou et al. 2016; Deppeler and Davidson 2017) that are more adept at NH_4^+ acquisition and potentially less vulnerable to light limitation (e.g., Banse, 1976). Changes in phytoplankton community composition are also likely to change the photosynthetic iron demand and possibly iron remineralization dynamics (Ellwood et al. 2014; Boyd 2019; Bressac et al. 2019), the latter affected by the extent to which the microbial loop is upregulated relative to the biological pump, itself contingent upon community composition (e.g., the prevalence of large diatoms versus nanoflagellates; Deppeler and Davidson, 2017; Tréguer et al. 2018; Boyd, 2019; Henley et al. 2020). Additionally, a decrease in upper ocean pH will alter iron speciation, with as-yet uncertain implications for its availability to phytoplankton and other microbes (Shi et al., 2010; Hutchins and Boyd, 2016). Finally, acidification has been shown to have a detrimental effect on nitrification (Beman et al. 2011; Shiozaki et al. 2019) because the equilibrium between seawater NH_4^+ and ammonia (NH_3; the substrate for oxidation; Suzuki et al. 1974) shifts towards NH_4^+ at lower pH. By contrast, the effect of declining pH and higher seawater CO_2 on phytoplankton growth is less clear (e.g., Mackey et al. 2015). If we are to better predict future changes in the Southern Ocean N cycle, and by extension its role in CO_2 cycling, climate, and global ocean productivity, an improved understanding of the controls on nitrification in shallow Southern Ocean waters is required.

Chapter 4: Controls on nitrite oxidation in the upper Southern Ocean: insights from winter kinetics experiments across the Indian sector

Abstract

Measurements of the upper ocean nitrogen (N) cycle can be used to understand atmospheric CO_2 drawdown by biology. In the Southern Ocean in winter, nitrification is the dominant mixed-layer N cycle process, with some of the nitrate (NO_3^-) produced therefrom persisting to fuel productivity during the subsequent growing season, potentially weakening the spring/summer biological CO_2 sink. To better understand the controls on Southern Ocean nitrification, NO_2^- oxidation kinetics experiments were conducted in surface waters across the Indian sector (37-62ºS; 19-30ºE) in winter 2017. While all experiments yielded a Michaelis-Menten relationship with substrate concentration, the NO_2^- oxidation rates only increased significantly once the NO_2^- concentration exceeded 115 ± 2.3 to 245 ± 18 nM, suggesting that NO_2^- oxidizers require a minimum (i.e., "threshold") NO_2^- concentration to produce NO_3^-. The half saturation constant ranged from 134 ± 8 to 403 ± 24 nM, indicating a relatively high affinity of Southern Ocean NO_2^- oxidizers for NO_2^-, in contrast to results from culture experiments. Despite this high affinity of NO_2^- oxidizers, NO_2^- concentrations are rarely <150 nM in the Southern Ocean's mixed layer, regardless of season. Over the upper 75 m, the measured ammonium oxidation rates that were two- to seven-fold higher than the coincident rates of NO_2^- oxidation, indicating that NO_2^- oxidation is the rate-limiting step for nitrification in the winter Southern Ocean. This, combined with a possible NO_2^- concentration threshold for NO_2^- oxidation, may explain the non-zero NO_2^- that persists throughout the Southern Ocean's mixed layer. I hypothesize that the apparent threshold NO_2^- requirement of NO_2^- oxidizers is indicative of NO_2^- substrate undersaturation of the heme-rich NO_2^- oxidoreductase enzyme, perhaps driven by the limited availability of iron in Southern Ocean surface waters.

4.1 Introduction

The cycling of nitrogen (N) in the upper ocean is central to the role that phytoplankton and bacteria play in atmospheric carbon dioxide (CO_2) consumption and production. Annually, the Southern Ocean accounts for ~35% of total oceanic CO_2 removal (DeVries et al. 2017; Gruber et al. 2019; Watson et al. 2020) and absorbs ~40% of anthropogenic CO_2 (Khatiwala et al. 2009; Hauck et al. 2015; Gruber et al. 2019; Watson et al. 2020). The contribution of biology to CO_2 drawdown can be evaluated using the new production paradigm, among other approaches. This framework defines phytoplankton growth on nitrate (NO_3^-) supplied from below the euphotic zone as "new production" and phytoplankton growth on ammonium (NH_4^+) recycled within the euphotic zone as "regenerated production" (Dugdale and Goering 1967). Over appropriate timescales, new production is equivalent to "export production", the latter referring to the organic matter produced by phytoplankton that escapes recycling in surface waters and sinks into the ocean interior, thereby sequestering atmospheric CO_2 at depth (Dugdale and Goering 1967; Eppley and Peterson 1979; Volk and Hoffert 1985; Raven and Falkowski 1999). However, the occurrence of nitrification in the euphotic zone, which produces regenerated NO_3^-, complicates applications of the new production paradigm since phytoplankton growth fuelled by this NO_3^- will drive no net removal of CO_2 (Yool et al. 2007).

In the Southern Ocean, nitrification appears to be largely confined to the dark waters below the euphotic zone during the summertime period of maximum NO_3^- consumption by phytoplankton (DiFiore et al. 2009; Mdutyana et al. 2020). By contrast, the Southern Ocean winter is characterized by elevated mixed-layer nitrification, coincident with low rates of NO_3^- uptake (Smart et al. 2015; Mdutyana et al. 2020). Some of the NO_3^- regenerated in the winter mixed layer will be supplied to phytoplankton during the proceeding spring and summer growing season, with negative implications for CO_2 removal on an annual basis. That said, there is evidence that ammonia oxidizing archaea, the organisms that are dominantly responsible for NH_4^+ oxidation (the first step in the nitrification pathway; (Beman et al. 2008; Newell et al. 2011; Peng et al. 2016) have a high iron requirement (Shafiee et al. 2019), such that NH_4^+ oxidation may at times experience iron limitation (Shafiee et al. 2019; Figure 3.9c). If this limitation is verified and proves widespread in the environment, one implication is that

the iron-deplete conditions of the surface Southern Ocean may restrict mixed-layer nitrification and by extension, its potential role in impeding autotrophic CO_2 drawdown.

Nitrification is a chemoautotrophic process involving two pathways facilitated by different groups of microorganisms. The first is NH_4^+ oxidation, which involves the oxidation of NH_4^+ via hydroxylamine and nitric oxide to NO_2^- (Walker et al. 2010; Vajrala et al. 2013; Kozlowski et al. 2016b; Caranto and Lancaster 2017) by ammonia oxidizing archaea and bacteria (AOA and AOB, respectively; collectively, ammonia oxidizing organisms, AOO). The second step is the oxidation of NO_2^- to NO_3^- by nitrite oxidizing bacteria (NOB), a polyphyletic group of microbes that is not well-understood in the ocean (Watson et al. 1986; Beman et al. 2013; Daims et al. 2016; Pachiadaki et al. 2017; Sun et al. 2021). In general, there are limited data on NO_2^- oxidation, with only a handful of rate measurements available for the Southern Ocean (Olson 1981a; Bianchi et al. 1997; Mdutyana et al. 2020). Such measurements are critical, however, if we are to better understand the controls on nitrification in the Southern Ocean mixed layer and the connection between NO_3^- production by NOB and its subsequent removal by phytoplankton.

One approach for investigating the controls on NO_2^- oxidation is through experiments designed to yield a hyperbolic Michaelis-Menten relationship between NO_2^- oxidation rate and NO_2^- concentration. Useful kinetic parameters can be derived from this relationship, such as the maximum oxidation rate (V_{max}) and the half-saturation constant (K_m), with the latter indicating the NO_2^- concentration at which the oxidation rate equals $V_{max}/2$. Estimates of K_m reveal information about the efficiency of NOB in acquiring substrate NO_2^-, while V_{max} is indicative of the maximum rate of NO_2^- oxidation that can be achieved under a particular set of conditions. In the ocean, direct measurements of NO_2^- oxidation kinetic parameters are extremely limited (Olson 1981; Sun et al. 2017, 2021; Zhang et al. 2020), with no estimates available for the Southern Ocean. K_m values derived from culture studies of NOB (ranging from 9-544 µM; Nowka et al. 2015; Ushiki et al. 2017) are orders of magnitude higher than the existing estimates for NOB in coastal waters and oxygen deficient zones (ranging from 0.07-0.51 µM; Olson 1981; Sun et al. 2017; Zhang et al. 2020), emphasizing the gaps in our understanding of this pathway and the organisms that catalyse it.

Generally, the distribution of NO_2^- in the upper low-latitude oxygenated ocean shows a peak near the base of the mixed layer (known as the primary nitrite maximum; PNM), with much lower concentrations above and below this depth (Lomas and Lipschultz 2006). By contrast, at higher latitudes including in the Southern Ocean, the NO_2^- concentration remains elevated (100-400 nM) and fairly invariant throughout the mixed layer in all seasons (Zakem et al. 2018; Fripiat et al. 2019; Mdutyana et al. 2020). One potential explanation for this NO_2^- accumulation is a decoupling of the NH_4^+ and NO_2^- oxidation rates, with NO_2^- oxidation being the rate-limiting step in the nitrification pathway, contrary to expectations for oxygenated marine waters (Kendall 1998; Walker et al. 2010; Vajrala et al. 2013). However, this idea has yet to be examined using observations.

To better understand the controls on NO_2^- oxidation (and thus, nitrification) in the Southern Ocean, I conducted a series of NO_2^- oxidation kinetics experiments in wintertime surface waters across the Indian sector. At every station (seven in total) along a transect from 37-62°S (the Subtropical Zone to the Marginal Ice Zone), the NO_2^- oxidation rate increased with increasing NO_2^- concentration, as per the expected Michaelis-Menten relationship. The derived K_m values were low and increased with increasing ambient NO_2^- concentration. Additionally, there appeared to be a minimum NO_2^- concentration that was required before the NO_2^- oxidation rate increased significantly (i.e., a "threshold" concentration), implying that the enzyme that catalyses NO_2^- oxidation to NO_3^- (nitrite oxidoreductase; NXR) may have been substrate-limited. Finally, rates of NH_4^+ oxidation measured coincident with NO_2^- oxidation over the euphotic zone suggest that NO_2^- oxidation is the rate-limiting step for nitrification across the Southern Ocean in winter.

4.2 Materials and Methods

4.2.1. Sampling site and experimental design

A winter cruise was undertaken onboard the R/V *SA Agulhas II* in July 2017 from Cape Town, South Africa, to the marginal ice zone (MIZ; encountered at 61.7°S; de Jong et al. 2018), returning to South Africa along the WOCE I06 transect (30ºE) (Figure 4.1). Sampling was conducted on two legs – between 37°S and 62°S on the southbound leg (Leg 1) and between

59°S and 41°S on the return leg along the WOCE I06 line (Leg 2). During Leg 1, only surface samples were collected, while on Leg 2, the deployment of hydrocasts allowed for depth-profile sampling.

Hydrography and nutrient collections: The positions of the major hydrographic fronts (the Subtropical Front, STF; Subantarctic Front, SAF; Polar Front, PF; and Southern Antarctic Circumpolar Current Front, SACCF; Figure 4.1) were determined from temperature and salinity measured by the ship's hull-mounted thermosalinograph (~7 m), augmented by temperature, salinity, and oxygen concentrations measured on Leg 2 by the CTD sensors (Orsi et al. 1995; Belkin and Gordon 1996; Pollard et al. 2002; Read et al. 2002). For the hydrocast stations, the mixed layer depth was determined for each Niskin (up)cast as the depth between 10 m and 400 m of maximum Brunt Väisälä frequency squared (i.e., N^2) (Schofield et al. 2015; Carvalho et al. 2017).

Nutrient concentrations: Seawater samples were collected every four hours from the ship's underway system (~7 m intake) on Leg 1 for the determination of NO_2^- concentrations (Figure 4.1a). During Leg 2, samples were collected from Niskin bottles fired remotely between the surface and 500 m at eight hydrocast stations for the analysis of NO_2^-, NO_3^-, and NH_4^+ concentrations (see Figure 4.1b and c for station locations and sampling depths). For NO_2^- and NO_3^-, unfiltered seawater was collected in duplicate 50 mL polypropylene centrifuge tubes that were analysed shipboard within 24 hours of collection (NO_2^-) or stored frozen at -20°C until analysis (NO_3^-). Seawater samples for NH_4^+ were collected unfiltered in duplicate "aged" high-density polyethylene (HDPE) bottles and analysed shipboard within 24 hours of collection.

NO_2^- oxidation kinetics experiments: On Leg 1, seawater samples were collected from the surface via the ship's underway system at seven stations spanning the different zones of the Southern Ocean (the Subtropical Zone (STZ) to the north of the STF, at the STF, the Subantarctic Zone (SAZ) between the STF and SAF, the Polar Frontal Zone (PFZ) between the SAF and PF, the Open Antarctic Zone (OAZ) between the PF and SACCF, and the Marginal Ice Zone (MIZ) south of the SACCF; St 01 to St 07 in Figure 4.1a). At each station, 25 L of seawater were collected in a single carboy that was gently shaken to homogenize the contents

before the seawater was sieved through a 200 µm nylon mesh to remove zooplankton grazers and then dispensed into 250 mL acid-washed opaque HDPE bottles. All the bottles were rinsed three times with sample water prior to filling. Eight sets of duplicate 250 mL bottles were amended with $Na^{15}NO_2$ to yield $^{15}NO_2^-$ concentrations ranging from 10 nM to 1500 nM.

Depth distribution of NO_2^- oxidation rates: On Leg 2, seawater was collected at four stations (one each in the Polar Antarctic Zone (PAZ; just north of the edge of the MIZ), OAZ, PFZ, and SAZ; St 08 to St 11 in Figure 4.1a-c) using a CTD-rosette equipped with 24 12-litre Niskin bottles. Seawater from six depths (10 m, 25 m, 50 m, 75 m, 200 m, and 500 m) was pre-filtered (200 µm nylon mesh) and transferred into rinsed 250 mL acid-washed opaque HDPE bottles. Duplicate bottles from each depth were amended with $Na^{15}NO_2$ to yield a final $^{15}NO_2^-$ concentration of 200 nM. From all incubation bottles (for kinetics and depth distribution), initial (T_0) subsamples were collected in 50 mL centrifuge tubes immediately after the addition of $^{15}NO_2^-$. The HDPE bottles from the upper 75 m were then incubated in custom-built on-deck incubators supplied with running surface seawater, while those from 200 m and 500 m were incubated in a ~2ºC cold room. The incubations lasted 23-30 hours and were terminated via the collection of final (T_f) subsamples (50 mL). All subsamples were filtered (0.2 µm) and stored frozen at -20°C until analysis.

Depth distribution of NO_3^- uptake rates: To assess the extent to which mixed-layer NO_2^- oxidation supports wintertime NO_3^- uptake by phytoplankton, NO_3^- uptake experiments were also conducted over the upper 75 m (the approximate depth of the euphotic zone) at St 08 to St 11 on Leg 2. Seawater was collected from four depths – 10 m, 25 m, 50 m, and 75 m – in duplicate 2 L clear polycarbonate bottles following filtration (200 µm nylon mesh) to remove large grazers. $Na^{15}NO_3$ was added to each bottle to yield a final $^{15}NO_3^-$ concentration of 3 µM, and the bottles were then transferred to custom-built deck-board incubators equipped with neutral density screens that allowed for the penetration of 55%, 30%, 10%, and 1% of surface photosynthetically active radiation (PAR). The bottles were kept at near *in situ* temperature by a supply of continuously-running seawater from the underway system. Samples were incubated for 3-6 hours, and incubations were terminated by filtering the bottle contents through a pre-combusted (450°C for 8 hours) 0.3 µm glass fibre filter (GF-75; Sterlitech) that was

subsequently enclosed in a foil envelop (pre-combusted at 500°C for 5 hours) and stored at -80°C until analysis.

4.2.2 Laboratory analyses

4.2.2.1 Nutrient concentrations

Samples were analysed for NO_2^- concentrations onboard the ship using the colorimetric method of Grasshoff et al. (1983) and a Thermo Scientific Genesys 30 Visible spectrophotometer (detection limit of 20 nM, precision of ±20 nM). NO_3^-+NO_2^- concentrations were measured ashore using a Lachat Quick-Chem flow injection autoanalyzer (Egan, 2008) in a configuration with a detection limit of 0.2 µM and precision of ±0.3 µM. The concentration of NO_3^- was determined by subtracting NO_2^- from NO_3^-+NO_2^-. Aliquots of a certified reference material (JAMSTEC) were included in each NO_2^- and NO_3^-+NO_2^- run to ensure measurement accuracy. The NH_4^+ concentrations were also determined shipboard using the fluorometric method of Holmes et al. (1999); the methodological details and resulting data are discussed at length in chapter 3.

4.2.2.2 NO_2^- oxidation rates

The denitrifier-isotope ratio mass spectrometer (IRMS) method (Sigman et al. 2001; McIlvin and Casciotti 2011) was used to measure the $\delta^{15}N$ of NO_3^- ($\delta^{15}N\text{-}NO_3^-$) produced from $^{15}NO_2^-$ oxidation for both the kinetics and depth profile experiments ($\delta^{15}N$, in ‰ vs. air, = $(^{15}N/^{14}N_{sample}/^{15}N/^{14}N_{air} - 1) \times 1000$). Samples were measured using a Delta V Plus IRMS with a custom-built purge-and-trap front end (McIlvin and Casciotti 2011) in a configuration with a detection limit of 0.2 nmol of N and a precision in $\delta^{15}N$ of 0.2‰. Prior to isotope analysis, samples were treated with sulfamic acid (15 mM) for 1 hour to remove $^{15}NO_2^-$ remaining at the end of the experiments, after which sample pH was adjusted to ~7-8 via the addition of 2 M NaOH. To account for inefficiencies in $^{15}NO_2^-$ removal, both T_f and T_0 samples were treated with sulfamic acid and analysed for $\delta^{15}N\text{-}NO_3^-$ (more accurately, $\delta^{15}N\text{-}NO_3^-$+$NO_2^-$), with the difference between them taken as the $^{15}NO_3^-$ enrichment due to $^{15}NO_2^-$ oxidation (Peng et al. 2015). International reference materials (IAEA-N3, USGS 34, USGS 32) were used to calibrate the measured $\delta^{15}N\text{-}NO_3^-$.

The rate of NO_2^- oxidation ($NO_2^-{}_{ox}$; nM d^{-1}) was calculated following Peng et al. (2015) as:

$$NO_{2\,ox}^{-} = \frac{\Delta[^{15}NO_3^-]}{f_{NO_2^-}^{15} \times T} \quad (4.1)$$

Where $\Delta(^{15}NO_3^-)$ is the change in the concentration of $^{15}NO_3^-$ between the start and end of the incubation due to NO_2^- oxidation, calculated from the difference in the measured $\delta^{15}N\text{-}NO_3^-$ between the T_f and T_0 samples, $f_{NO_2}^{15}$ is the fraction of the NO_2^- substrate pool labelled with ^{15}N at the start of the incubation, and T is the incubation length (days). Detection limits for $NO_2^-{}_{ox}$ rates ranged from 0.11 to 0.36 nM d^{-1}, calculated according to Santoro et al. (2013) and Mdutyana et al. (2020).

4.2.2.3. Kinetic model

Kinetic parameters are typically calculated using the Michaelis-Menten (MM) equation for enzyme kinetics (Monod 1942):

$$V = \frac{V_{max} \times S}{K_m + S} \quad (4.2)$$

where V is the measured reaction rate, V_{max} is the maximum reaction rate achievable under *in situ* conditions, S is the substrate concentration, and K_m is the half-saturation constant, defined as the substrate concentration at which $V = V_{max}/2$.

The MM equation (equation 4.2) is a rectangular hyperbola, meaning that the asymptotes along the x- and y-axes are perpendicular. By definition, when S (the x-axis variable) is equal to zero, V (the y-axis variable) is also zero, forcing equation 4.2 through the origin. In the case of NO_2^- oxidation, the assumption that once $S > 0$, $V > 0$ is appropriate in waters where the ambient NO_2^- concentration is near-zero or where NO_2^- is non-zero but considerably lower than the K_m. In the Southern Ocean, mixed-layer NO_2^- concentrations are typically always ≥150 nM (Cavagna et al. 2015; Zakem et al. 2018; Fripiat et al. 2019; Mdutyana et al. 2020) and forcing the MM model through the origin results in a poor fit to the measurements (red line in Figure C4.1). This poor fit, in turn, leads to clearly inaccurate estimates of the kinetic parameters, particularly K_m (Table C4.1, appendix C).

While not typical for studies of NO_2^- oxidation kinetics in the ocean, researchers have taken to modifying the standard form of non-linear regression models, including the MM equation, to better fit observations (e.g., Birch 1999; Tsoularis and Wallace 2002; Archontoulis and Miguez 2014). For application to this dataset, equation 4.2 has been modified to allow V = 0 at S > 0 by subtracting a location parameter, C, from S (Figure 4.2; Archontoulis and Miguez 2014). In other words, the y-intercept (i.e., where V = 0) is set equal to C rather than to zero, which yields equation 4.3:

$$V = \frac{V_{max} \times (S-C)}{K_{m*} + (S-C)} \quad (4.3)$$

Using a non-linear, least-squares optimization method (Scipy lmfit package, Python 3.7.6), I solved equation 4.3 for V_{max}, K_{m*}, and C. The value of K_{m*} derived thus is relative to C, such that the substrate concentration at which V =V_{max}/2 (i.e., K_m) is actually equal to K_{m*} + C (Supplemental Information). Mechanistically, C represents a "threshold" substrate concentration; when S ≤ C, V = 0. All kinetic parameters are reported as the best fit plus 95% confidence interval (i.e., mean ± 2σ; Table C4.1, appendix C).

4.2.2.4 Revising the depth distribution of NO_2^- oxidation using K_m

For the NO_2^- oxidation experiments conducted at the Leg 2 hydrocast stations, the $Na^{15}NO_2$ was added to yield a final $^{15}NO_2^-$ concentration of 200 nM at all the sampled depths. However, at low ambient NO_2^- concentrations (< ~1 μM), an amendment of this magnitude may stimulate NO_2^- oxidation, leading to an overestimation of the *in situ* rates. Therefore, the measured $NO_2^-{}_{ox}$ rates were revised using the derived K_m values as per Rees et al. (1999), Diaz and Raimbault (2000), and Horak et al. (2013):

$$\mathrm{corr}NO_{2_{Ox}}^- = \frac{NO_{2_{Ox}}^-}{\frac{[NO_2^-]_{total}}{K_m + [NO_2^-]_{total}} \times \frac{K_m + [NO_2^-]_{amb}}{[NO_2^-]_{amb}}} \quad (4.4)$$

Here, $corrNO_2^-{}_{ox}$ is the revised rate of $NO_2^-{}_{ox}$, $NO_2^-{}_{ox}$ is the measured NO_2^- oxidation rate (equation 4.1), $[NO_2^-]_{amb}$ is the ambient NO_2^- concentration measured at each depth, $[NO_2^-]_{total}$ refers to [$^{15}NO_2^-$ tracer] + $[NO_2^-]_{amb}$, and K_m is the derived half-saturation constant. Given the observed relationship between K_m and $[NO_2^-]_{amb}$ (see section 4.2 below), a K_m was estimated for each sample depth from the equation resulting from the linear regression of all derived K_m values on $[NO_2^-]_{amb}$. $CorrNO_2^-{}_{ox}$ was also computed using the K_m derived from the Leg 1

kinetics experiment located nearest each hydrocast station, with very similar results. The values of corr$NO_2^-{}_{ox}$ presented here were computed using K_m values derived from the linear regression equation. Rates of NH_4^+ oxidation measured coincident with $NO_2^-{}_{ox}$ on Leg 2 (Figure 3.6b) were similarly revised (to yield corr$NH_4^+{}_{ox}$) using the K_m values derived from kinetics experiments conducted during Leg 1 (Figure 3.5a-c) – for St 08 and 09, K_m =137 nM, for St 09, K_m = 67 nM, and for St 11, K_m = 28 nM.

4.2.2.5. Isotopic dilution of $^{15}NO_2^-$ by co-occurring NH_4^+ oxidation

The focus of this study is the second step in the nitrification pathway. However, not only will NO_2^- have been consumed in the incubation bottles (i.e., oxidized to NO_3^-), it will also have been produced by NH_4^+ oxidation, the first step in the nitrification pathway. For all of the NO_2^- oxidation rate experiments (kinetics and depth profiles), the coincident rates of NH_4^+ oxidation were measured (Figure 3.6b), and these data can be used to account for any dilution of the $^{15}NO_2^-$ pool by $^{14}NO_2^-$ produced from $^{14}NH_4^+$ oxidation (following the approach of Glibert et al. 1982, 1985; Mulholland and Bernhardt 2005). Because the ambient NO_2^- concentrations were reasonably high (mean of 157 ± 54 nM, range of 64 to 226 nM for all the depths at which experiments were conducted; Figure 4.1a-b) and the NH_4^+ oxidation rates were fairly low (mean of 13.4 ± 4.0 nM d-1, range of 7.8 to 22.0 nM d-1; see Figure 4.3f-j for the depth profile rates and Chapter 3 for the kinetics station rates), isotopic dilution was minor. Below the mixed layer where the ambient NO_2^- concentrations were near-zero, so too were the NH_4^+ oxidation rates, which again resulted in minimal dilution of the $^{15}NO_2^-$ pool. Accounting for isotope dilution increased the NO_2^- oxidation rates by 0 to 12% (mean of 3.9 ± 0.3% and median of 3.7 ± 0.3%) which is within the experimental error associated with the rate measurements; the effect of isotope dilution is thus considered negligible.

4.2.2.6. Nitrate uptake rates

On shore, the GF-75 filters were oven-dried at 45°C for 24 hours, then pelletized into tin cups following the removal of unused peripheral filter. The concentration and isotopic composition of the particulate organic N (PON) captured on the filters was analyzed using a Delta V Plus IRMS coupled to a Flash 2000 elemental analyser, with a detection limit of 1 µg N and precision of ±0.005 At%. Blanks (combusted unused filters + tin capsules) and laboratory running standards calibrated to international reference materials were run after every ten

samples. The absolute rates of NO_3^- uptake (ρNO_3^-; nM d^{-1}) were calculated after blank correction according to the equations of Dugdale and Wilkerson (1986) assuming a day-length between 7 and 10 hours, dependent on the station latitude. The specific NO_3^- uptake rates (V_{NO3^-}; h^{-1}) were then computed by normalizing ρNO_3^- to the associated measured PON concentration.

To compute the fraction of the mixed-layer NO_3^- pool consumed by phytoplankton that derived from *in situ* nitrification, ρNO_3^- and $corrNO_2^-{}_{ox}$ were trapezoidally-integrated over the mixed layer following Mdutyana et al. (2020), and the integrated values of $corrNO_2^-{}_{ox}$ were then divided by integrated ρNO_3^-.

4.3 Results

4.3.1. Hydrography and nutrient concentrations

The positions of the major hydrographic fronts during both legs of the cruise are shown in Figure 4.1a. At the hydrocast stations (Leg 2), the mixed layer depth (MLD) averaged 143 m in the OAZ, 146 m in the PFZ, 205 m in the SAZ, and 113 m in the STZ. These depths are within the reported climatological range for the Indian Ocean sector in winter (Sallée et al. 2010). Underway ambient NO_2^- concentrations (Leg 1) ranged from 74 nM to 232 nM (transect average of 168 ± 48 nM; median of 177 nM) and generally increased with latitude, albeit with a high degree of variability (Figure 4.1a; Figure C4.2). The ambient NO_2^- concentrations at the hydrocast stations were fairly constant throughout the mixed layer, decreasing rapidly to values below detection by 150-200 m (Figure 4.1b). Mixed-layer NO_2^- showed no clear latitudinal trend, mainly because of the anomalously low concentrations measured at St 09 (54°S; mixed-layer average of 64 ± 30 nM). The NO_3^- concentrations were also near-homogenous throughout the mixed layer, decreasing from 28.4 ± 0.2 µM at the southernmost station (St 08; 59°S) to 3.7 ± 1.1 µM at the northernmost station (41°S), and increasing below the mixed layer as expected (Figure 4.1c).

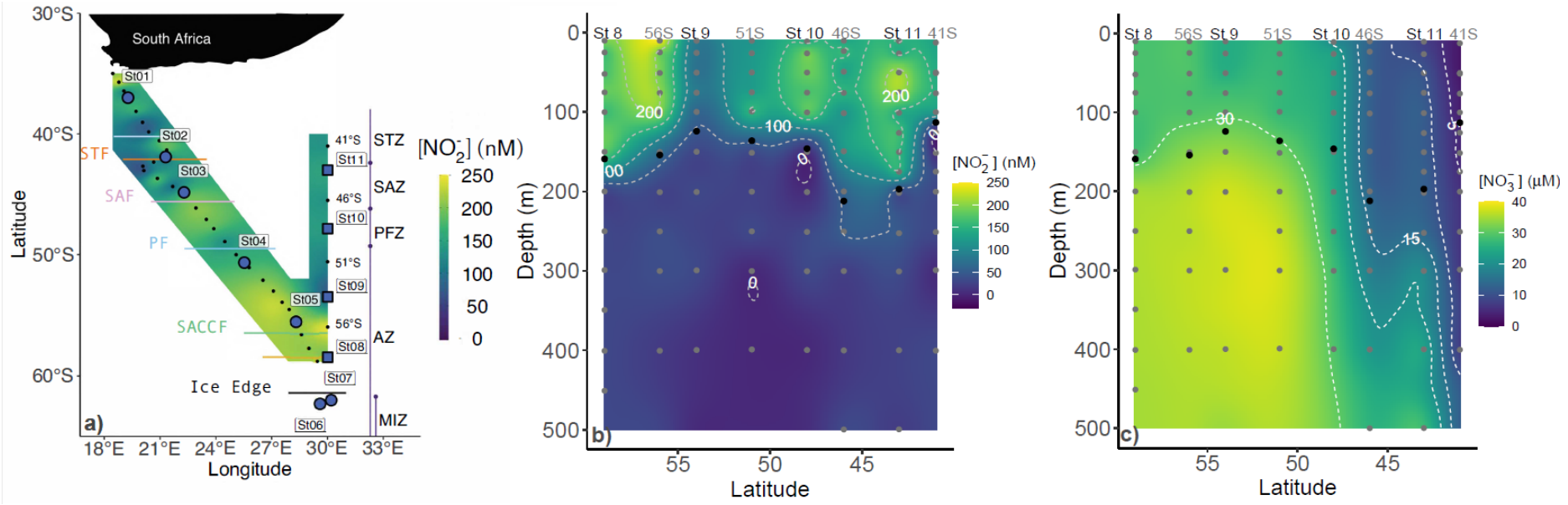

Figure 4.1: a) Map of the cruise track showing the kinetics experiments station positions (large circle symbols) and locations of the underway stations sampled during Leg 1 (small symbols), overlaid on the measured surface (~7 m) nitrite concentrations ($[NO_2^-]$). Additionally, the locations of the hydrocast stations occupied during Leg 2 are shown, with the stations at which depth distribution experiments were conducted indicated by the large square symbols. The coloured horizontal lines denote the frontal positions at the time of sampling and the major zones of the Southern Ocean are indicated by the vertical lines and dots – STZ, Subtropical Zone; STF, Subtropical Front; SAZ, Subantarctic Zone; SAF, Subantarctic Front; PFZ, Polar Frontal Zone; PF, Polar Front; AZ, Antarctic Zone; SACCF, Southern Antarctic Circumpolar Front; MIZ, Marginal Ice Zone. Also shown are water column (0-500 m) profiles of the concentrations of b) nitrite (NO_2^-) and c) nitrate (NO_3^-) sampled during Leg 2. The vertical grey dots indicate the sampling depths at all the hydrocast stations (eight in total), with the four stations at which depth distribution experiments were conducted (St 08 to St 11) labeled above the panel. The black dots show the mixed layer depth.

4.3.2. NO_2^- oxidation rates

4.3.2.1. Kinetics experiments

At all the kinetics stations (St 01 to St 07; Leg 1), an MM curve could be fit to the NO_2^- oxidation rate *versus* substrate measurements using equation 4.3 (Figure 4.2). The derived kinetic parameters varied across the transect (Table 4.1). The maximum NO_2^- oxidation rate (V_{max}) ranged from 5.2 ± 0.1 nM d^{-1} (mean of 9.1 ± 1.1 nM d^{-1} for St 02 and St 03) at the STF (St 02; Figure 4.2b) to 13 ± 0.4 nM d^{-1} in the AZ (St 05; Figure 4.2e), with a transect average of 9.0 ± 1.1 nM d^{-1}. V_{max} increased southwards between the 29 and the AZ, before decreasing in the MIZ to 8.2 ± 0.1 nM d^{-1} at St 06 (Figure 4.2f) and 6.6 ± 0.3 nM at St 07 (Figure 4.2g). The half-saturation constant, K_m, increased from 134 ± 8.0 nM at the STF (St 02; Figure 4.2b) to 403 ± 24 nM in the MIZ (St 06; Figure 4.2f), with a transect average of 277 ± 31 nM. The value of C increases southwards from 115 ± 2.3 nM at the STF (St 02; Figure 4.2b) to 254 ± 18 nM in the AZ (St 05; Figure 4.2e) and then decreased to 163 ± 11 nM at MIZ at St 06 (Figure 4.2f) before increasing to 237 ± 10 nM at St 07 (Figure 4.2g). On average across the transect, C was 181 ± 45 nM.

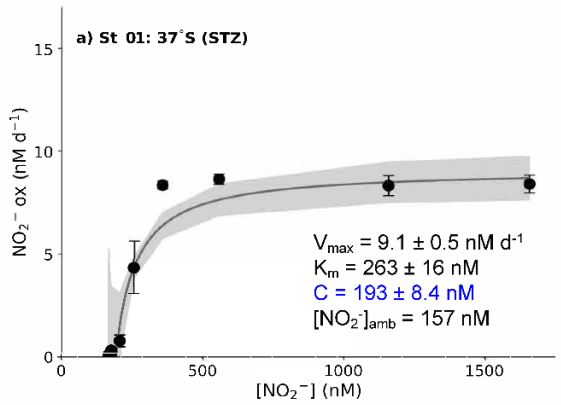
a) St 01: 37°S (STZ)
V_{max} = 9.1 ± 0.5 nM d^{-1}
K_m = 263 ± 16 nM
C = 193 ± 8.4 nM
[NO_2^-]$_{amb}$ = 157 nM
NO_2^- ox (nM d^{-1})
[NO_2^-] (nM)

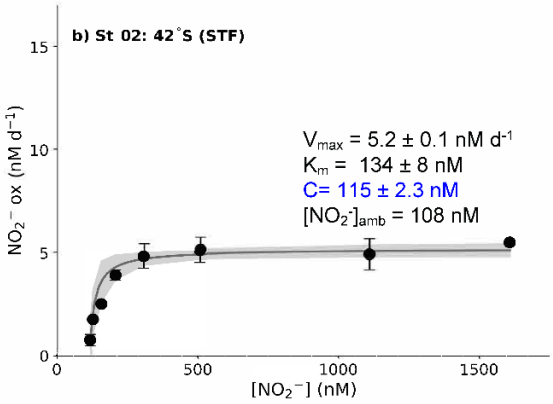
b) St 02: 42°S (STF)
V_{max} = 5.2 ± 0.1 nM d^{-1}
K_m = 134 ± 8 nM
C= 115 ± 2.3 nM
[NO_2^-]$_{amb}$ = 108 nM
NO_2^- ox (nM d^{-1})
[NO_2^-] (nM)

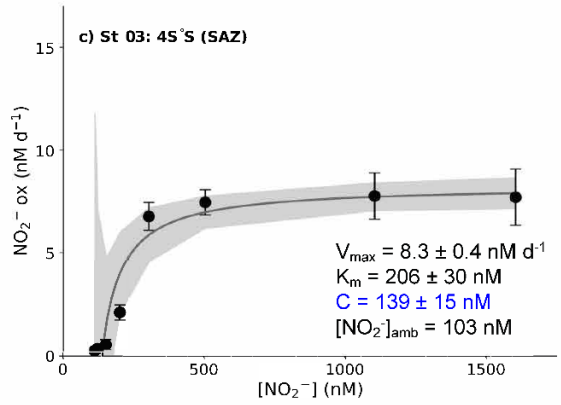
c) St 03: 45°S (SAZ)
V_{max} = 8.3 ± 0.4 nM d^{-1}
K_m = 206 ± 30 nM
C = 139 ± 15 nM
[NO_2^-]$_{amb}$ = 103 nM
NO_2^- ox (nM d^{-1})
[NO_2^-] (nM)

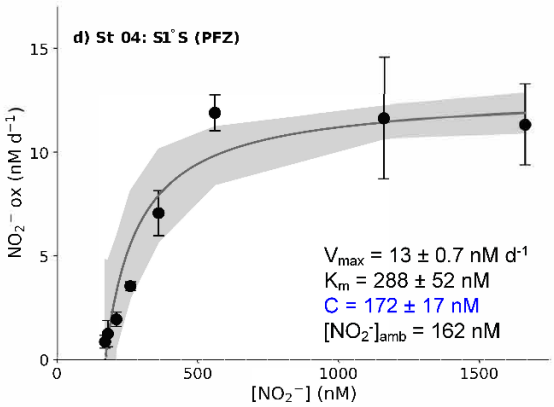
d) St 04: 51°S (PFZ)
V_{max} = 13 ± 0.7 nM d^{-1}
K_m = 288 ± 52 nM
C = 172 ± 17 nM
[NO_2^-]$_{amb}$ = 162 nM
NO_2^- ox (nM d^{-1})
[NO_2^-] (nM)

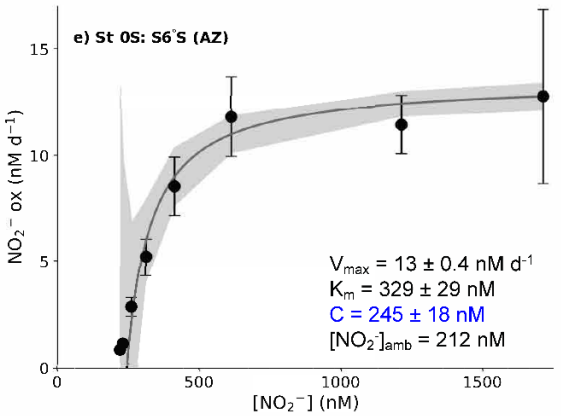
e) St 05: 56°S (AZ)
V_{max} = 13 ± 0.4 nM d^{-1}
K_m = 329 ± 29 nM
C = 245 ± 18 nM
[NO_2^-]$_{amb}$ = 212 nM
NO_2^- ox (nM d^{-1})
[NO_2^-] (nM)

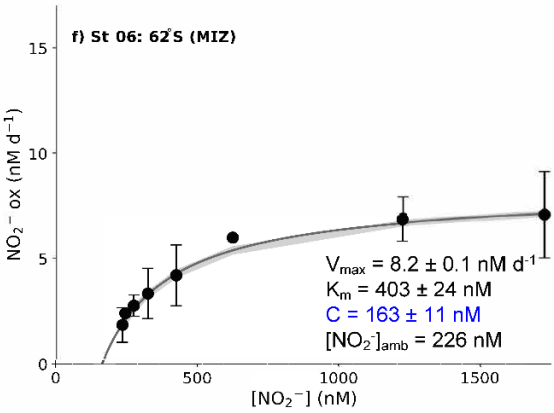
f) St 06: 62°S (MIZ)
V_{max} = 8.2 ± 0.1 nM d^{-1}
K_m = 403 ± 24 nM
C = 163 ± 11 nM
[NO_2^-]$_{amb}$ = 226 nM
NO_2^- ox (nM d^{-1})
[NO_2^-] (nM)

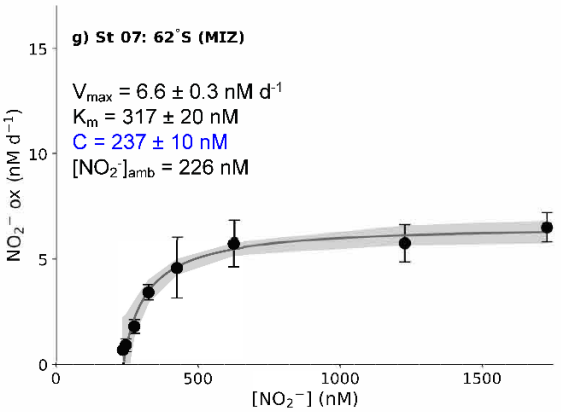
g) St 07: 62°S (MIZ)
V_{max} = 6.6 ± 0.3 nM d^{-1}
K_m = 317 ± 20 nM
C = 237 ± 10 nM
[NO_2^-]$_{amb}$ = 226 nM
NO_2^- ox (nM d^{-1})
[NO_2^-] (nM)

Figure 4.2: Kinetics experiments: the dependence of NO_2^- oxidation rates on the nitrite concentration ($[NO_2^-]$) at the surface (~7 m) in winter at a) St 01: 37°S (STZ), b) St 02: 42°S (STF), c) St 03: 45°S (SAZ), d) St 04: 51°S (PFZ), e) St 05: 55°S (OAZ), f) St 06: 62°S (MIZ), and g) St 07: 62°S (MIZ). The solid lines show the Michaelis-Menten best fit, with the derived values of V_{max}, K_m and C, as well as the ambient concentration of nitrite ($[NO_2^-]_{amb}$), indicated on each panel. Error bars indicate the standard error of replicate experiments, each measured at least twice. Where errors bars are not visible, they are smaller than the data markers. The grey shaded area shows the 95% confidence interval.

4.3.2.2. Depth distributions

The NO_2^- oxidation rates calculated using equation 4.1 were low and largely invariant over the upper 75 m (the approximate depth of the euphotic zone), ranging from 1.9 to 9.7 nM d^{-1} (averaging 4.9 ± 2.4 nM d^{-1}; filled symbols in Figure 4.3b-e). All stations showed a maximum NO_2^- oxidation rate at 200 m (roughly coincident with or just below the base of the mixed layer), ranging between 11 and 28 nM d^{-1} (average of 18 ± 7.0 nM d^{-1}). The NO_2^- oxidation rates displayed a latitudinal gradient, with lower rates in the AZ (St 08 and 09) than in the PFZ (St 10) and SAZ (St 11).

Revising the NO_2^- oxidation rates according to equation 4.4 decreased the 0-75 m rates by between 13 and 26% (i.e., $corrNO_2^-{}_{ox}$ ranged from 1.6 to 8.5 nM d^{-1} and averaged 4.0 ± 2.0 nM d^{-1} over the upper 75 m; open symbols in Figure 4.3b-e). The largest decrease (of between 39 and 68%) occurred at 200 m and 500 m, coinciding with very low ambient NO_2^- concentrations (Figure 4.3a); nonetheless, at all but St 08, the 200 m maximum NO_2^- oxidation rate remained, although its magnitude was lower. The coincidentally-measured and revised NH_4^+ oxidation rates showed a similar pattern, with the largest decrease occurring at the depths with the lowest ambient NH_4^+ concentrations (Figure 4.3f-j) – over the upper 75 m, the rates decreased by 1 to 9% at St 08 to St 10 (mixed-layer $[NH_4^+]_{amb}$ averaged 263 ± 4.3 to 655 ± 15 nM; Figure 4.3f), while St 11 experienced an average decrease of 40 ± 23% (mixed-layer $[NH_4^+]_{amb}$ averaged 13 ± 1.6 nM). Similar to the NO_2^- oxidation rates, the NH_4^+ oxidation rates decreased most at 200 m and 500 m, between 33% and 70%. Hereafter, the revised NO_2^- and NH_4^+ oxidation rates ($corrNO_2^-{}_{ox}$ and $corrNH_4^+{}_{ox}$, respectively) are used when referring to the depth distributions of these processes, including in the Figures. I note, however, that the corrected rates still may not be entirely accurate since K_m was not derived individually for each depth at each station (Horak et al. 2013). Nonetheless, because of the high concentration of the ^{15}N-tracer amendments relative to all derived K_m values, I am confident that the corrected rates are more representative of *in situ* conditions than the rates computed using equation 4.1.

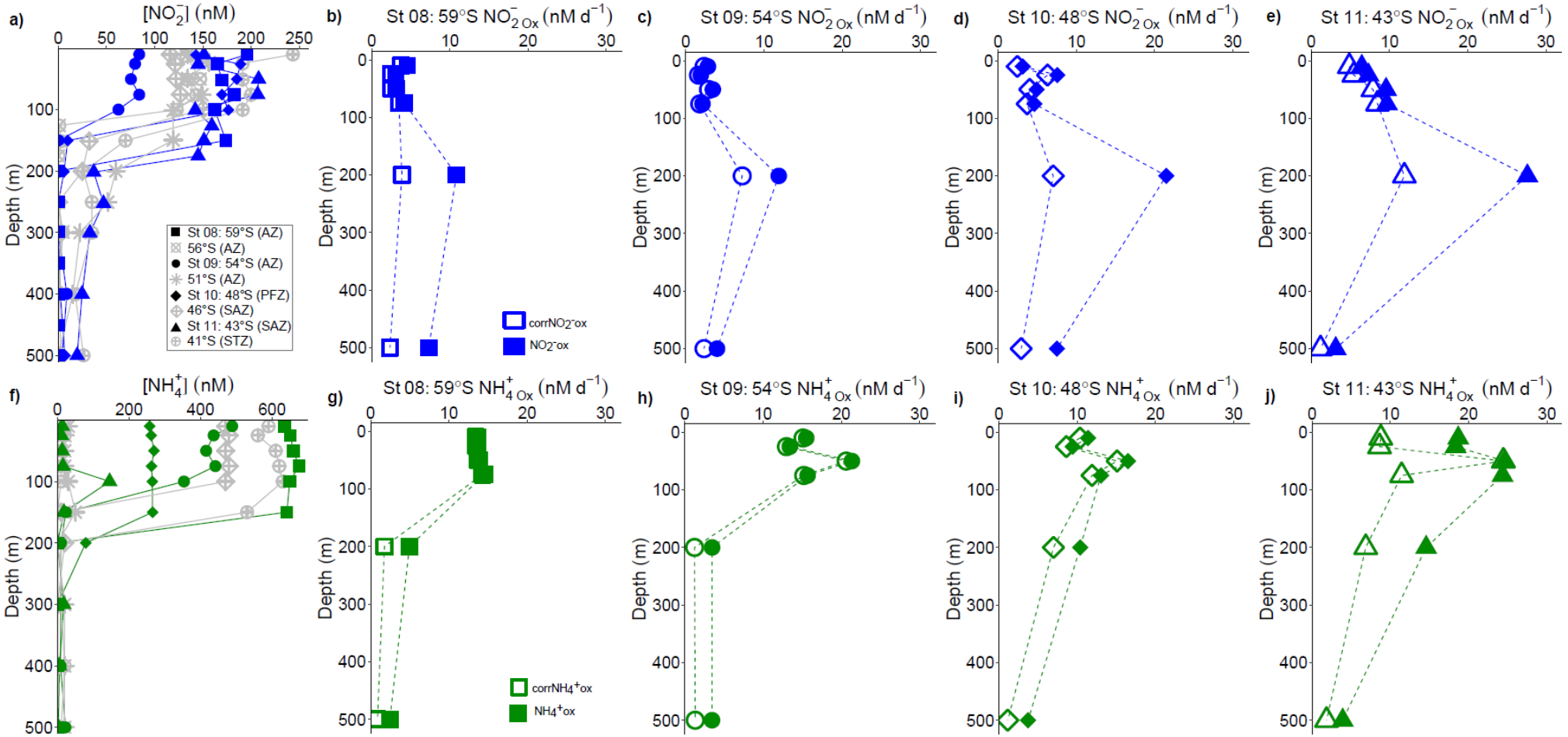

Figure 4.3: Depth distribution experiments: water column (0-500 m) profiles of the concentration of a) nitrite ($[NO_2^-]$) and f) ammonium ($[NH_4^+]$), and rates of NO_2^- and NH_4^+ oxidation at b and g) St 08: 59°S (AZ), c and h) St 09: 54°S (AZ), d and i) St 10: 48°S (PFZ), and e and j) St 11: 43°S (SAZ). In panels a and f, the blue and green symbols indicate the stations at which oxidation rates were measured while the grey symbols show data from the stations where no experiments were conducted. In panels b-e and g-j, open symbols represent oxidation rates revised for possible stimulation due to ^{15}N-tracer additions ($corrNO_2^-ox$ and $corrNH_4^+ox$; equation 4.4) and closed symbols show the uncorrected rates (equation 4.1). Error bars indicate the standard error of replicate experiments, each measured at least twice. Where error bars are not visible, they are smaller than the data markers. The dashed lines connecting the data points are included only to guide the eye and should not be taken to indicate interpolation with depth.

4.3.3 NO_3^- uptake rates

The rates of NO_3^- uptake (ρNO_3^-) were low and relatively homogenous over the upper 75 m at each station (Figure C4.3a, appendix C). Average euphotic zone ρNO_3^- increased northwards, from 2.9 ± 1.1 nM d^{-1} at St 08 in the PAZ to 12 ± 2.0 nM d^{-1} at St 11 in the SAZ, with a transect average of 6.2 ± 3.4 nM d^{-1}. The euphotic zone PON concentrations also increased northwards, from 0.24 ± 0.02 µM at St 08 to 0.47 ± 0.08 µM at St 11 (Figure C4.3b, appendix C). As a result of the coincident northward rise in ρNO_3^- and PON, combined with the southward decline in daylight hours, the euphotic zone-averaged specific NO_3^- uptake rates (V_{NO3}) were similar at all stations, ranging from 1.3 ± 0.5 × 10^{-3} h^{-1} (0.010 ± 0.004 d^{-1}; St 09) to 2.6 ± 0.4 × 10^{-3} h^{-1} (0.024 ± 0.004 d^{-1}; St 11), with a transect average of 1.9 ± 0.7 × 10^{-3} h^{-1} (0.016 ± 0.007 d^{-1}; Table C4.2, appendix C). Kinetic parameters associated with NO_3^- uptake could only be measured at two stations (St 01: 37°S and St 02: 42°S); average V_{max} of 0.8 ± 0.5 × 10^{-3} h^{-1}, K_m of 4.25 ± 1.45 µM, and C value of 2.5 ± 0.6 µM (Figure C4.4a and b).

Integrated over the mixed layer, $corrNO_2^-{}_{ox}$ accounted for an average of 122% of ρNO_3^- (range of 63% at St 09 in the OAZ to 237% at St 08; Table C4.2, appendix C), as has been observed previously in the wintertime Southern Ocean (Chapter 2; Mdutyana et al. 2020). These data confirm that most of the mixed-layer NO_3^- consumed by phytoplankton in winter, and likely also a significant fraction assimilated in spring, supports regenerated rather than new production, thus impeding the biological CO_2 sink (Yool et al. 2007; Mdutyana et al. 2020).

4.4 Discussion

The oxidation of NO_2^-, the ultimate step in the nitrification pathway, is important in the cycling of oceanic N because it produces NO_3^-, the most oxidized and dominant form of N that controls phytoplankton growth across most of the global ocean. Experiments designed to measure the kinetics of NO_2^- oxidation, as conducted here, allow for an examination of the major controls on marine nitrification. Across all the major zones of the wintertime Southern Ocean, the addition of NO_2^- to collections of surface seawater stimulated NO_2^- oxidation following a Michaelis-Menten relationship, suggesting that substrate availability plays a dominant role in the rate of NO_3^- production in the Southern Ocean's winter mixed layer. Curiously, an apparent minimum substrate requirement of NO_2^- oxidation (i.e., a "threshold" NO_2^- concentration; 115 to 245 nM) was also observed, in contrast to expectations for a "classical" Michaelis-Menten

relationship (i.e., V is assumed to increase as soon as S > 0; Monod 1942). Below, I examine my findings in the context of existing estimates of NO_2^- oxidation kinetic parameters and then evaluate the potential drivers of the observed trends. I also discuss possible reasons for the apparent requirement of Southern Ocean NOB for a threshold ambient NO_2^- concentration and consider the implications thereof for the regional N cycle.

4.4.1 Southern Ocean NO_2^- oxidation kinetic parameters in the context of existing estimates

Measurements of NO_2^- oxidation rates are limited in the Southern Ocean, with only two studies that have directly measured this pathway in open-ocean waters (Bianchi et al. 1997; Mdutyana et al. 2020). For NO_2^- oxidation kinetics, there are no data at all for the Southern Ocean. This scarcity of Southern Ocean measurements is unsurprising given that *in situ* NO_2^- oxidation kinetics studies are generally limited; indeed, to my knowledge, there are only two studies from the coastal ocean (Olson 1981a; Zhang et al. 2020b) and two from the Eastern Tropical North Pacific oxygen deficient zone (ETNP ODZ; with experiments conducted across a range of ambient oxygen concentrations; Sun et al. 2017, 2021). By contrast, there exist numerous estimates of NO_2^- oxidation kinetic parameters determined from studies using cultured marine NOB (e.g., Sorokin et al. 2012; Nowka et al. 2015; Jacob et al. 2017; Kits et al. 2017; Zhang et al. 2020). In general, culture experiments suggest far higher kinetic constants compared to the limited *in situ* observations from the ocean, particularly in the case of K_m (i.e., culture-based estimates of 9-544 µM; Blackburne et al. 2007; Nowka et al. 2015; Ushiki et al. 2017).

The high K_m values derived for cultured NOB suggest that the affinity of these organisms for NO_2^- is low, yet this is not what is observed in the environment. For the Southern Ocean, I report high substrate affinities of NOB, with values of K_m ranging from 134 to 403 nM, which is largely within the range documented for coastal waters (27-506 nM; Zhang et al. 2020) and the oxygenated open ocean (27-506 nM; Olson 1981; Zhang et al. 2020) (Table **4.**1). In the low- to zero-oxygen waters of the ETNP ODZ, similarly low K_m values have been reported (254 ± 161 nM; Sun et al. 2017), as have values >5 µM (Sun et al. 2021). These latter estimates were associated with ambient NO_2^- concentrations >1 µM. The relationship between ambient NO_2^- concentration and K_m is explored in detail in section 4.2 below, although for low ambient NO_2^- concentrations only given that (some of) the environmental factors affecting NO_2^- oxidation at high ambient NO_2^- (e.g., in the ODZs) are likely to be unique. For example, oxygen has been shown to decrease the rate of NO_2^- oxidation in these regions (Sun et al. 2017, 2021), and novel clades of NOB have been detected (Sun et al. 2021).

Table 4.1: Kinetic parameters (V_{max}, K_m and C) associated with NO_2^- oxidation experiments conducted across the Indian sector of the Southern Ocean in winter 2017. Included here is the best fit and 95% confidence interval ("CI") for each kinetic parameter derived using a non-linear, least-squares optimization method (Scipy lmfit package, Python 3.7.6).

Station name	**Latitude**	**Longitude**	**$[NO_2^-]_{amb}$ (nM)**	**V_{max} (nM d^{-1})**	**95%:CI (nM d^{-1})**	**K_m (nM)**	**95%:CI (nM)**	**C (nM)**	**95%:CI (nM)**
St 01	37°S	19°E	157	9.1	7.9 to 10	263	192 to 350	193	144 to 206
St 02	42°S	21°E	108	5.2	4.8 to 5.5	134	109 to 163	115	105 to 119
St 03	45°S	22°E	103	8.3	7.4 to 9.3	206	15 to 373	139	-11 to 163
St 04	50°S	26°E	162	13	11 to 15	288	104 to 538	172	68 to 204
St 05	55°S	28°E	212	14	13 to 15	329	183 to 458	245	138 to 272
St 06	62°S	30°E	226	8.2	7.8 to 8.6	403	320 to 499	163	129 to 187
St 07	62°S	30°E	226	6.6	6.0 to 7.4	317	234 to 395	237	190 to 255

Across the Southern Ocean transect, V_{max} ranged from 5 to 14 nM d^{-1}, which is quite low compared to existing estimates from other regions, although such a comparison is not particularly informative as my rates (and typically those of others) are not normalized for NOB abundance. The estimates of V_{max} are also low compared to a previous study of mixed-layer nitrification in the wintertime Southern Ocean (Mdutyana et al. 2020). This difference may in part be due to the fact that my kinetics experiments were conducted using surface (~7 m) seawater (and thus, the surface NOB community that had been exposed to surface conditions, including elevated light), yet the highest rates of NO_2^- oxidation often occur near the base of the mixed layer, including in the Southern Ocean (Figure 4.3b-e; Sun et al. 2017; Peng et al. 2018; Mdutyana et al. 2020). The opposite pattern has also been observed, however, with deeper samples yielding a lower V_{max} than samples collected in shallow waters (Sun et al. 2017; Zhang et al. 2020).

Table 4.2: A selection of previously derived K_m values from other regions of the open ocean, along with the concurrently-measured ambient concentrations of nitrite ($[NO_2^-]_{amb}$).

Region	$[NO_2^-]$ (nM)	Sampled depth (m)	Km (nM)	SE	Reference
Indian Southern Ocean: St 01: 37°S	157	7	263	16	This study
Indian Southern Ocean: St 02: 42°S	108	7	134	8	This study
Indian Southern Ocean: St 03: 45°S	103	7	206	30	This study
Indian Southern Ocean: St 04:51°S	162	7	288	52	This study
Indian Southern Ocean: St 05: 56°S	212	7	329	29	This study
Indian Southern Ocean: St 06: 62°S	226	50	403	24	This study
Indian Southern Ocean: St 07: 62°S	226	50	317	20	This study
Southern California Bight	20	60	70	nd	Olson 1981
Eastern Tropical North Pacific	100	53	281	151	Sun et al. 2017
Eastern Tropical North Pacific	50	170	227	55	Sun et al. 2017
South China Sea	51	110	195	33	Zhang et al. 2020
South China Sea	71	95	175	37	Zhang et al. 2020
South China Sea	31	150	49	15	Zhang et al. 2020
South China Sea	185	75	506	82	Zhang et al. 2020
South China Sea	34	200	27	11	Zhang et al. 2020
Subtropical South Atlantic	14	150	74	29	Fawcett et al. in prep
Subtropical South Atlantic	152	150	167	4,3	Fawcett et al. in prep

4.4.2 Environmental drivers of the NO_2^- oxidation kinetic parameters

I report maximum NO_2^- oxidation rates that generally increase towards the south and with decreasing SST (recognizing that these two parameters co-vary), although St 01 in the STZ and St 06 and 07 in the MIZ deviate from this trend (Figure 4.4a and b; $R^2 = 0.019$; $p = 0.77$ and 0.12; $p = 0.45$, respectively). Changes in the NOB community across the transect may account for some of the observed variability in V_{max} given that the NO_2^- oxidation rates are not normalized for organism abundance. Nonetheless, taking latitude as a qualitative proxy for light (both light intensity, and the duration (i.e., number of hours) of light supply), it is perhaps unsurprising that the maximum NO_2^- oxidation rates increase southwards given that NOB are known to be at least partially inhibited by light (Olson 1981b; Ward 2005a; Peng et al. 2018). This hypothesis does not hold for the stations in the MIZ, however, at which V_{max} decreases sharply despite these waters receiving the least light (less than 5 hours of weak sunlight, versus ~9 hours at 37ºS to ~7 hours at 55ºS). The temperatures at the MIZ stations were <0°C, which raises the possibility of a temperature effect on V_{max}. Indeed, I previously observed a strong decline in the V_{max} associated with NH_4^+ oxidation at SSTs <0°C in the Southern Ocean, while at SSTs ranging from 0.6°C to 16°C, V_{max} was invariant (Figure 3.8b in Chapter 3).

Marine nitrification has been reported to be largely unaffected by temperature variations (Bianchi et al. 1997; Horak et al. 2013; Baer et al. 2014), although NH_4^+ and NO_2^- oxidation may respond differently to similar changes in temperature. For example, marine NOB incubated at temperatures ranging from 10°C to 35°C responded far more slowly to an increase in temperature than co-incubated AOA, resulting in an accumulation of NO_2^- in the incubation bottles (Schaefer and Hollibaugh 2017). By contrast, no robust relationship is observed between temperature and the maximum rate of NH_4^+ oxidation occurring *in situ* across all zones of the Southern Ocean (Chapter 3), a finding that is consistent with previous studies of NH_4^+ oxidation from the Arctic and temperate coastal ocean (Horak et al. 2013; Baer et al. 2014) and that suggests ammonia oxidizers are generally well-adapted to the environment in which they are found (Ward et al. 2007; Horak et al. 2013, 2018). Far less work has been done to assess the response of NOB to temperature changes. Heterotrophic bacteria in an Arctic polynya have been shown to be more impacted by temperature changes when ambient nutrients are replete (Yager and Deming 1999); it is possible that this is also the case for NOB. In the absence of experiments specifically designed to test the response of Southern Ocean NOB communities to temperature, it is difficult to disentangle the effect on NO_2^- oxidation of temperature from

that of light (and possibly other parameters that co-vary with latitude across the Southern Ocean, such as substrate and/or micronutrient availability).

Plotting V_{max} as a function of the ambient substrate concentration ($[NO_2^-]_{amb}$) reveals a strong positive relationship for all but the MIZ stations (Figure 4.4c; $R^2 = 0.73$; $p = 0.065$ if the MIZ stations are excluded). In particular, the STZ station (St 01) that appeared anomalous in the plots of V_{max} versus latitude and SST is consistent with the other non-MIZ stations when evaluated in V_{max} versus $[NO_2^-]_{amb}$ space. The positive relationship of V_{max} to $[NO_2^-]_{amb}$ could be taken as evidence that NO_2^- availability exerts a strong control on the maximum achievable rate of NO_2^- oxidation and that NOB are thus well-adapted to their environment. However, I note that V_{max} varies four-fold while $[NO_2^-]_{amb}$ only changes by a factor of two, and that $[NO_2^-]_{amb}$ is also correlated with latitude ($R^2 = 0.51$, $p = 1.1x10^{-5}$ for all surface $[NO_2^-]_{amb}$ data; Figure C4.2, appendix C). Additionally, previous wintertime Southern Ocean NO_2^- oxidation rates (albeit not V_{max}) showed no relationship with the ambient NO_2^- concentration (Bianchi et al. 1997; Mdutyana et al. 2020). The extent to which V_{max} is directly controlled by $[NO_2^-]_{amb}$ is thus unclear, and it is likely that NOB community composition, light availability, and temperature also play a role, with SST perhaps becoming more important at very low temperatures (i.e., in the MIZ).

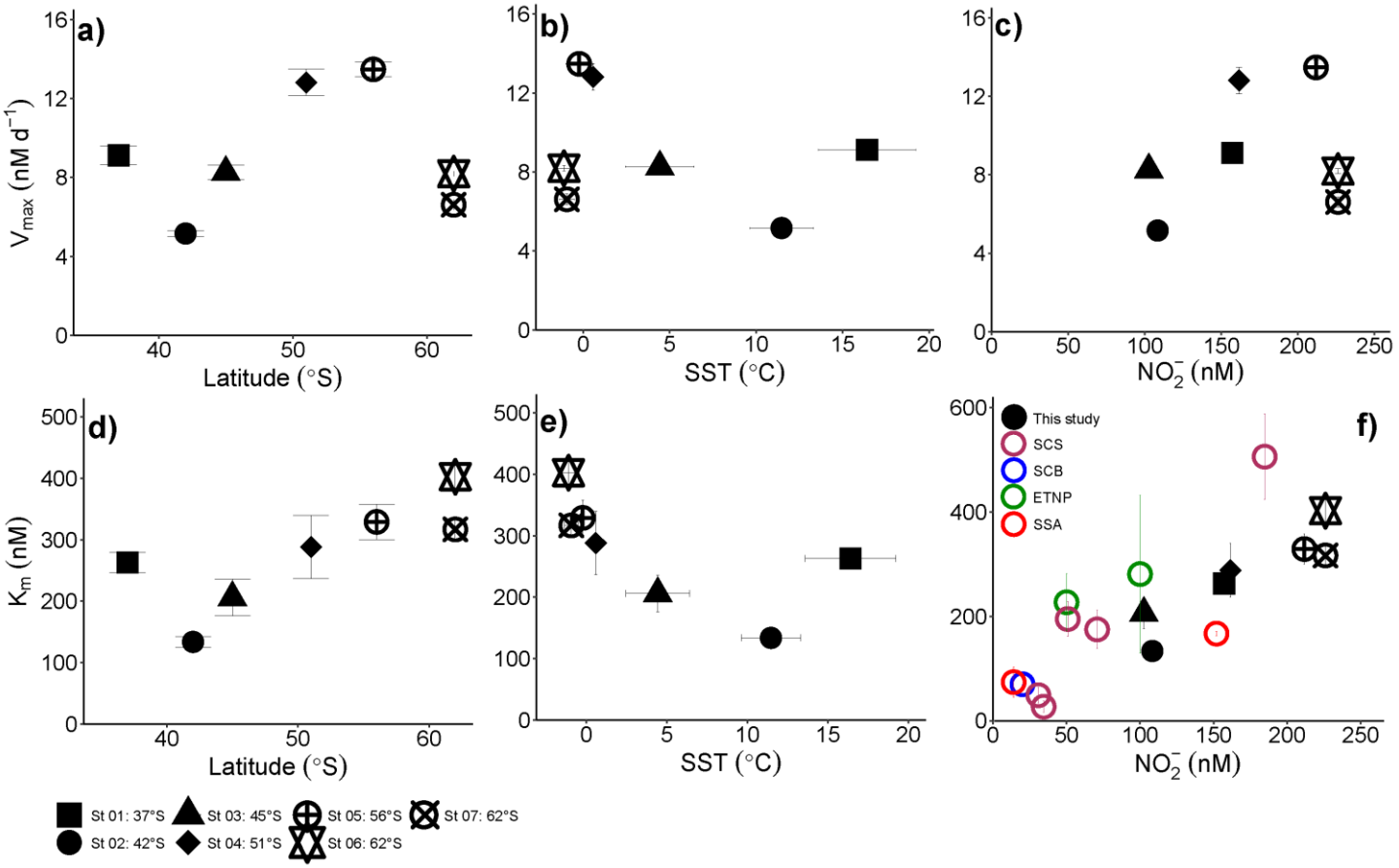

Figure 4.4: Potential controls on the kinetic parameters associated with NO_2^- oxidation. V_{max} and K_m are shown as a function of a and d) latitude, b and e) SST, and c and f) $[NO_2^-]_{amb}$. Vertical error bars show the propagated error associated with V_{max} and K_m computed using a non-linear, least-squares optimization method (Scipy lmfit package, Python 3.7.6), while the symbols and horizontal error bars on panels b and e indicate the average (± standard deviation) SST experienced by the samples during the 24-hour incubations (given that the incubator was cooled using running surface seawater). In panel f, black symbols show data from kinetics stations sampled during this study, purple symbols show K_m values from the South China Sea (SCS; Zhang et al. 2020), the blue symbol shows the K_m value derived for the South California Bight (SCB; Olson 1981a), the green symbol shows K_m values from Eastern Tropical North Pacific oxygen deficient zone (ETNP; Sun et al. 2017), and the red symbols show K_m values derived for the Subtropical South Atlantic (SSA; Fawcett et al. unpubl.).

My estimates of K_m reveal that NOB in the wintertime Southern Ocean have a high affinity for NO_2^- that appears to decrease (i.e., the K_m rises) at higher latitudes (i.e., lower light) and lower temperatures, with St 01 in the STZ again emerging as an exception (Figure 4.4d and e; R^2 = 0.86, p = 0.0075 and 0.86, p = 0.0076, respectively). However, plotting K_m as a function of $[NO_2^-]_{amb}$ for my data only reveals a strong positive relationship (R^2 = 0.83, p = 0.0044; Figure 4.4f; black data points), implying that NO_2^- availability rather than temperature or light exerts the dominant control on K_m. This trend further indicates that NOB are well-adapted to the environment (or Southern Ocean region) in which they are found. Southern Ocean mixed-layer NO_2^- concentrations are almost never <150 nM, regardless of the season (Zakem et al. 2018; Fripiat et al. 2019; Mdutyana et al. 2020), yet the relationship of K_m to $[NO_2^-]_{amb}$ also holds at far lower NO_2^- concentrations. The coloured data points in Figure 4.4f show K_m as a function of $[NO_2^-]_{amb}$ for four additional regions where a Michaelis-Menten relationship of NO_2^- oxidation rate to NO_2^- concentration was observed and where $[NO_2^-]_{amb}$ was <250 nM (two coastal ocean sites, the South China Sea (SCS; Zhang et al. 2020) and Southern California Bight (SCB; Olson 1981); one oligotrophic ocean site, the subtropical South Atlantic (SSA; Fawcett et al. unpubl.); and two stations from the ETNP ODZ, where oxygen concentrations ranged from 0 μM to 16.8 μM (Sun et al. 2017)). The robust positive relationship of K_m to $[NO_2^-]_{amb}$ that emerges when these previous results are combined with my Southern Ocean data (Figure 4.4f; R^2 = 0.68, p = 5.2 x10^{-5}) strongly implicates $[NO_2^-]_{amb}$ as the dominant control on the K_m of NO_2^- oxidation in the ocean, particularly at low $[NO_2^-]_{amb}$.

The production of NO_2^- by ammonia oxidation has been hypothesized to be subject to iron limitation, with AOB relying on iron-rich *cytochrome c* proteins (Arp et al. 2002; Walker et al. 2010) and AOA apparently characterized by a low affinity for inorganic iron (Shafiee et al. 2019). NOB also contain iron-rich enzymes, such as nitrite oxidoreductase, which is responsible for converting NO_2^- to NO_3^- (Meincke et al. 1992; Spieck et al. 1998). While there are no iron data with which to compare the kinetic parameters, dissolved iron concentrations ([DFe]) were measured at the hydrocast stations (St 08 to St 11). The revised depth-specific NO_2^- oxidation rates at these stations are weakly positively correlated with [DFe] (R^2 = 0.35, p = 0.016; Figure 4.5), indicating a potential role for iron in controlling NO_2^- oxidation. Combined with the evidence that iron may also constrain marine NH_4^+ oxidation (Shafiee et al. 2019; Thesis Chapter 3), this observation implies that mixed-layer nitrification in the Southern Ocean may be iron-limited. Since phytoplankton consumption of regenerated NO_3^-

yields no net removal of atmospheric CO_2 (Yool et al. 2007), an iron-related control on mixed-layer nitrification would help to limit to a degree at which this process can weaken the Southern Ocean's biological pump.

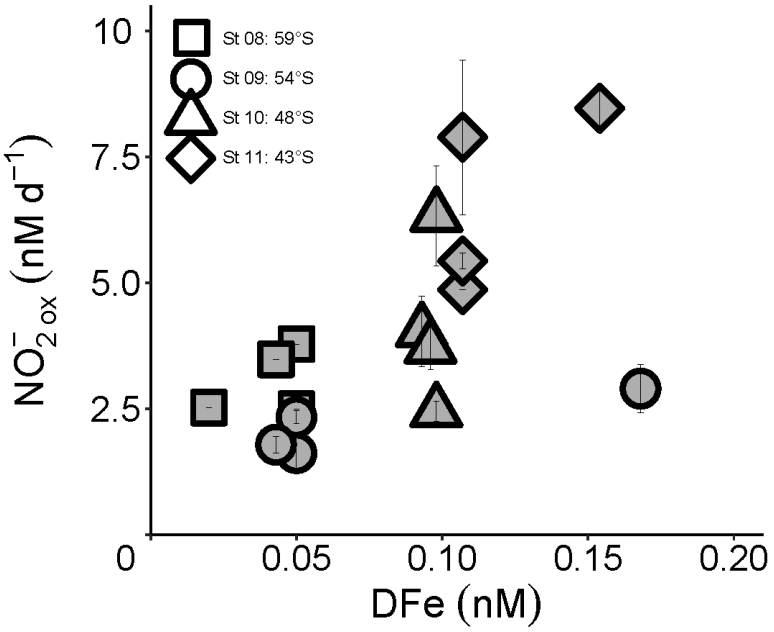

Figure 4.5: Euphotic zone (0-75 m) rates of NO_2^- oxidation measured at the depth distribution stations (St 08 to St 11) plotted against coincident dissolved iron concentrations (DFe). Error bars indicate the standard error of replicate experiments/collections, each measured at least twice. Where errors bars are not visible, they are smaller than the data markers.

4.4.3 Persistence of elevated NO_2^- concentrations throughout the Southern Ocean mixed layer

While still limited, there is growing evidence that marine AOA have a very high affinity for NH_4^+ (more correctly, ammonia (NH_3), the substrate for NH_4^+ oxidation; Table 3.2; Martens-Habbena et al. 2009; Horak et al. 2013; Newell et al. 2013; Peng et al. 2016). Marine NOB also appear able to consume low concentrations of substrate, based on the few *in situ* studies conducted to-date, including this one (Figure 4.4f; Olson 1981; Sun et al. 2017; Zhang et al. 2020). This high substrate affinity is perhaps unsurprising given that NO_2^- concentrations are generally near-zero throughout the oxygenated ocean, rising modestly to values typically <0.5 µM at the PNM in (sub)tropical waters (Lomas and Lipschultz 2006; Zakem et al. 2018) and <0.4 µM throughout the upper ocean in (sub)polar regions (Zakem et al. 2018). The average surface NO_2^- concentration measured during Leg 1 of the cruise was 168 ± 48 nM (Figure 4.1a) and the average mixed-layer concentration for Leg 2 was 137 ± 57 nM (Figures 4.1b and 4.3a).

Similar concentrations have been observed previously across the Southern Ocean, including in other seasons (Cavagna et al. 2015; Fripiat et al. 2019; Mdutyana et al. 2020). Thus, while NO_2^- oxidation in Southern Ocean surface waters is characterized by a low K_m, the affinity of NOB for NO_2^- is apparently not high enough to completely remove the available NO_2^-. The persistence of elevated NO_2^- concentrations in the mixed layer at high latitudes has been attributed to the inability of iron- and/or light-limited phytoplankton to fully consume NO_2^- transported to the surface with NO_3^- during deep mixing events (Zakem et al. 2018). However, subsurface NO_2^- concentrations in the Southern Ocean are typically below detection (Figure 4.1b and 4.3a; Olsen et al. 2016), so it is unclear how deep mixing could supply measurable NO_2^- to the euphotic zone.

A second possible source of elevated mixed-layer NO_2^- is efflux following partial NO_3^- reduction to NO_2^- by phytoplankton (Lomas and Lipschultz 2006), which has been extensively documented in laboratory and field studies (see Collos 1998 for a review). The release of NO_2^- by phytoplankton has been hypothesized to result from light limitation of intracellular NO_2^- reduction (Vaccaro and Ryther 1960; Kiefer et al. 1976), short-term increases in irradiance to which phytoplankton cannot adapt (Lomas and Lipschultz 2006), iron limitation of NO_3^- assimilation (Milligan and Harrison 2000), and/or release of phytoplankton from NO_3^- limitation following a period of starvation (Sciandra and Amara 1994). While it is conceivable that some of these mechanisms may be ongoing in the Southern Ocean, they all require the initial uptake of NO_3^- by phytoplankton. This process occurs in the winter mixed layer at rates that are too low to support NO_2^- efflux to the extent that NO_2^- would accumulate to concentrations of 100-300 nM (e.g., Figure C4.3, appendix C; Philibert et al. 2015; Mdutyana et al. 2020) while simultaneously being removed by NO_2^- oxidation. Additionally, a reasonable correlation between the NH_4^+ oxidation rates and $[NO_2^-]_{amb}$ ($R^2 = 0.46$; $p = 0.00027$; Figure C4.5, appendix C) was observed, which implies that NO_2^- derives predominantly from NH_4^+ oxidation rather than phytoplankton efflux.

A third potential explanation for elevated mixed-layer NO_2^- is thus a decoupling of NH_4^+ and NO_2^- oxidation, which appears to be widespread in the environment (e.g., Ward and Zafiriou 1988; Beman et al. 2013). In the oxygenated ocean, NH_4^+ oxidation has been considered the rate-limiting step in the nitrification pathway because NO_2^- seldom accumulates in the mixed

layer (Kendall 1998; Kowalchuk and Stephen 2001; Walker et al. 2010; Vajrala et al. 2013). However, direct observations (i.e., rate measurements) from numerous oceanic regions show contrasting results, with NO_2^- oxidation sometimes outpacing NH_4^+ oxidation (Horrigan et al. 1990; Dore and Karl 1996; Bristow et al. 2015; Peng et al. 2018), while in other cases, NH_4^+ oxidation is dominant (Ward and Kilpatrick 1991; Clark et al. 2008; Kalvelage et al. 2013). The limited data available from previous investigations in the Southern Ocean show no clear trend (Bianchi et al. 1997; Mdutyana et al. 2020). In the present study, the mixed-layer NO_2^- oxidation rates, corrected for possible stimulation due to tracer addition, are two- to seven-times lower than the coincidentally measured (and corrected) NH_4^+ oxidation rates (Figures 4.3 and 4.6). Additionally, the maximum rates of NO_2^- oxidation (V_{max}) derived for the surface NOB community (~5 to 13 nM d^{-1}; Figure 4.2) are on average half those determined for NH_4^+ oxidation (14 to 23 nM d^{-1}; Figure 3.5a-g). At the time of sampling, therefore, NO_2^- oxidation was rate-limiting to nitrification, which likely accounts for at least some of the NO_2^- accumulated in the Southern Ocean's winter mixed layer.

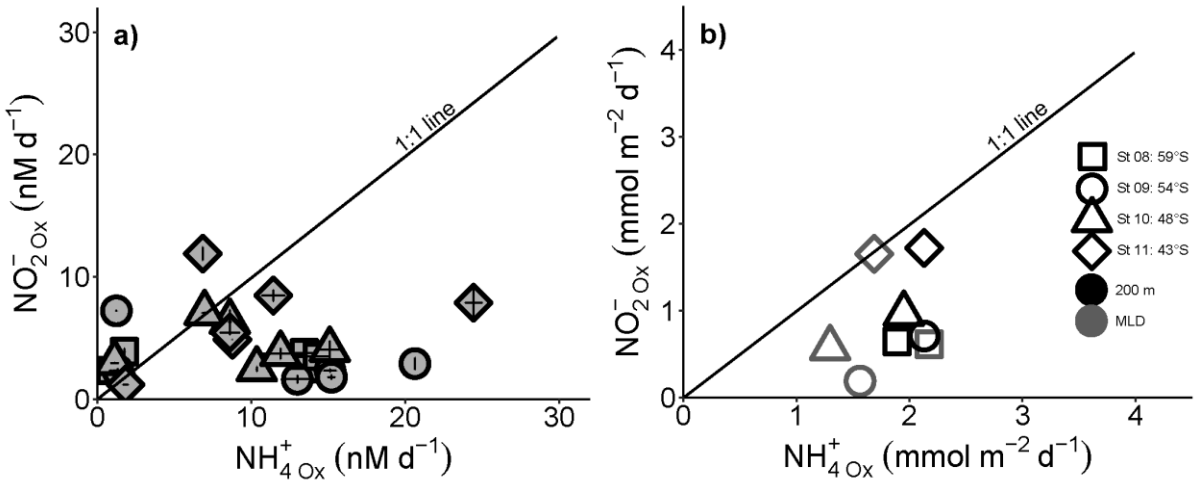

Figure 4.6: The relationship between the measured rates of NO_2^- and NH_4^+ oxidation for a) each experiment depth in the upper water column (0-500 m) and b) integrated over the mixed layer (grey symbols) and upper 200 m (black symbols). Error bars on panel a indicate the standard error of replicate experiments, each measured at least twice, while on panel b, error bars show the propagated error. Where errors bars are not visible, they are smaller than the data markers. The black diagonal line on both panels has a slope 1, which is expected if the rates of NH_4^+ and NO_2^- oxidation are tightly coupled.

If a decoupling of NH_4^+ and NO_2^- oxidation is dominantly responsible for the accumulation of NO_2^-, an obvious question is why these rates are not balanced. Environmental factors like temperature, light, and/or pH may play a role (Ward 2008; Heiss and Fulweiler 2017), as may iron limitation and the different ecophysiologies of NH_4^+ and NO_2^- oxidizers. AOA have been

shown to adapt more rapidly than NOB to a change in temperature (Schaefer and Hollibaugh 2017); however, the seasonal SST variations within the various zones of the Southern Ocean are fairly small and the study showing the differential response of AOA and NOB was conducted at temperatures far higher than those experienced in much of the Southern Ocean.

With regards to light, there is evidence from culture and field studies that NOB are more photosensitive than AOA and AOB (Bock 1965; Olson 1981b; Qin et al. 2014). My data are consistent with this notion insofar as the V_{max} associated with NO_2^- oxidation in surface waters rises with increasing latitude (and thus decreasing light; Figure 4.4a) while the V_{max} derived for NH_4^+ oxidation remains largely unchanged across >30 degrees of latitude (Figure 3.8a). However, the ambient NO_2^- concentration in Southern Ocean surface waters is also significantly correlated with latitude (Figure C4.2, appendix C) while the NH_4^+ concentration is not, such that the differing trends in V_{max} may have more to do with substrate availability than photoinhibition.

Physical mixing, particularly deep winter overturning, might also contribute to a decoupling of the NH_4^+ and NO_2^- oxidation steps. In coastal waters, deep winter mixing has been shown to dilute the nitrifying organism community, particularly NOB, leading to low rates of NO_2^- oxidation while NH_4^+ oxidation rates remain elevated, ultimately causing NO_2^- accumulation in the upper layer (Haas et al. 2021). While the differential effect of mixing may play a role in NO_2^- accumulation in the open Southern Ocean, it is unlikely that the entire NO_2^- reservoir can be ascribed to this process. The rates of NH_4^+ oxidation are only slightly higher than those of NO_2^- oxidation in the winter mixed layer (Figure 4.3). Additionally, the mixed layer NH_4^+ concentrations are elevated (Chapter 3; Figure 2.2b and Figure 3.2b), which indicates that NH_4^+ oxidizers are limited by something other than NH_4^+ substrate, preventing them from catalysing higher rates of NO_2^- production (and thus NO_2^- accumulation).

A number of studies have shown the negative effect of decreasing pH on NH_4^+ oxidation in the ocean (e.g., Huesemann et al. 2002; Beman et al. 2011; Kitidis et al. 2011), driven by the reduction in the proportion of NH_3 relative to NH_4^+ at lower pH. By contrast, NO_2^- oxidation may increase as pH declines (Fulweiler et al. 2011; Heiss and Fulweiler 2017), although such

a correlation has only been observed in one coastal region. While a differential response of AOA/AOB and NOB to pH would decouple NH_4^+ and NO_2^- oxidation, the resultant trend should be one of higher NO_2^- accumulation in the northern Southern Ocean where surface pH is higher in winter and lower NO_2^- accumulation to the south where pH is lower (Key et al. 2004; McNeil and Matear 2008) – this is not the observed meridional pattern.

Nitrite oxidoreductase (NXR), the enzyme possessed by NOB that is responsible for aerobic NO_2^- oxidation to NO_3^-, is an iron-sulfur molybdoprotein (Sundermeyer-Klinger et al. 1984; Meincke et al. 1992; Lücker et al. 2010). As such, NO_2^- oxidation has a significant iron requirement (Saito et al. 2020; Bayer et al. 2021), intimated by the relationship observed between the NO_2^- oxidation rates and DFe (Figure 4.5). Additionally, NO_2^- accumulation at the PNM in the California Current has been hypothesized to be caused by iron limitation of NOB (Santoro et al. 2013). AOB also require iron, in particular for the oxidation of hydroxylamine, which is catalyzed by the heme-rich hydroxylamine oxidoreductase (HAO) complex (Arp et al. 2002; Walker et al. 2010). By contrast, AOA, the dominant marine NH_4^+ oxidizers, rely mainly on copper-containing proteins to mediate NH_4^+ oxidation (Walker et al. 2010; Amin et al. 2013; Santoro et al. 2015). In the iron-limited Southern Ocean, it is thus possible that iron scarcity more strongly limits NO_2^- than NH_4^+ oxidation. However, recent culture and proteomic work suggests that AOA may actually have a high iron requirement (Santoro et al. 2015; Carini et al. 2018; Qin et al. 2018; Shafiee et al. 2019). Additionally, I have previously hypothesized an iron-related control on NH_4^+ oxidation in the Southern Ocean (see Chapter 3.4.3). Deeper investigation is thus required to characterize the role of iron in controlling the relative rates of NH_4^+ and NO_2^- oxidation, and the implications for the complete nitrification pathway.

A further consideration is differences in the ecology of AOA and NOB. Marine NOB are an order of magnitude less abundant than AOA (e.g., Füssel et al. 2012; Beman et al. 2013b; Pachiadaki et al. 2017; Damashek et al. 2019; Kitzinger et al. 2020) and roughly three-times larger (Watson and Waterbury 1971; Könneke et al. 2005; Martens-Habbena et al. 2009; Pachiadaki et al. 2017), and while their affinity for NO_2^- appears to be high, the *in situ* K_m values derived to-date are not as low as those reported for NH_4^+ oxidation (Horak et al. 2013; Peng et al. 2016; Xu et al. 2019; Zhang et al. 2020; Table 3.2), as expected given their larger size (Aksnes and Egge 1991; Litchman et al. 2007; Zakem et al. 2018). Additionally, the

theoretical energy gain from NO_2^- oxidation is lower than from NH_4^+ oxidation (Bock and Wagner 2006), and it has been estimated that NOB must consume three-times as much N as NH_4^+ oxidizers to produce the same amount of biomass (Zakem et al. 2018). Nonetheless, a recent study from the Gulf of Mexico showed that NOB from the phylum *Nitrospinae*, the dominant NO_2^- oxidizers in the ocean, grow five-times faster than AOA and produce roughly four-times as much biomass despite their lower abundance, in part because they can support up to half of their cellular N requirement using organic N compounds such as urea (Kitzinger et al. 2020). This study was conducted in hypoxic shelf waters, however, such that the applicability of its findings to the Southern Ocean is unclear. Nevertheless, it seems likely that the very different life strategies of NH_4^+ and NO_2^- oxidizers play a role in decoupling the steps of nitrification in the Southern Ocean.

Thus far, I have focused on possible bottom-up controls on NH_4^+ versus NO_2^- oxidation. A further consideration, grounded in resource limitation theory, is that since nitrifiers require a subsistence concentration of substrate (R*) to maintain their population, those with the lowest R* will outcompete all other organisms limited by the same resource provided that their V_{max} is greater than their loss rate due to grazing and/or viral lysis (Zakem et al. 2018). Because NOB are considerably larger than AOA (Watson and Waterbury 1971; Könneke et al. 2005; Martens-Habbena et al. 2009; Pachiadaki et al. 2017), they will have a higher R* (i.e., minimum NO_2^- requirement) than AOA even before grazing pressure is factored in. Their large size also means that NOB are more likely to be grazed than AOA, which will further increase their R* (according to its definition provided above), as will the fact that their maximum growth rates are slow and thus could easily be lower than their loss rates. Taken together, these factors may increase R*, potentially resulting in the accumulation of NO_2^- in the water column. These factors may also help to explain why the K_m for NO_2^- oxidation, in the Southern Ocean and elsewhere, is considerably higher than that derived for NH_4^+ oxidation (Figure 3.5a-c; Table 3.2, Chapter 3). Additionally, the fact that NOB will be preferentially grazed over AOA likely contributes to NO_2^- oxidation being the rate-limiting step of nitrification.

That NO_2^- oxidation was rate-limiting at the time of sampling does not necessarily explain the accumulation of NO_2^- in the Southern Ocean mixed layer year-round. Neither NH_4^+ nor NO_2^- oxidation occur at elevated rates in summer or autumn (Bianchi et al. 1997; Mdutyana et al.

2020), yet the elevated NO_2^- concentrations persist during these seasons (Cavagna et al. 2015; Fripiat et al. 2019; Mdutyana et al. 2020). To fit a Michaelis-Menten curve to my experimental data required amending the classical equation (equation 4.2) to allow for a positive x-intercept (i.e., a non-zero S value at which V was still zero, denoted as the C parameter in equation 4.3) (Archontoulis and Miguez 2014). Additionally, at most stations, the NO_2^- oxidation rates did not increase substantially following the initial two or three substrate amendments (i.e., in Figure 4.2, the slope of the relationship between V and S is less steep for the initial two to three values of S than at higher values). Practically, these findings suggest that Southern Ocean NOB require a minimum (i.e., threshold) NO_2^- concentration, below which, NO_2^- becomes limiting. Coupled with weak drawdown of NO_2^- in the Southern Ocean by iron- and/or light-limited phytoplankton during their incomplete consumption of the NO_3^-+NO_2^- pool, a threshold substrate requirement of NOB can explain the year-round persistence of non-zero mixed-layer NO_2^- since it implies that there is no mechanism by which NO_2^- can be completely exhausted.

I hypothesize that the NO_2^- concentration threshold is indicative of an undersaturation by substrate NO_2^- of NXR, which is a membrane-bound enzyme (Sundermeyer-Klinger et al. 1984; Lücker et al. 2010) that occurs in two forms: 1) with the substrate-binding subunit (NxrA) orientated outwards into the periplasmic space, as in *Nitrospira* and *Nitrospina* (Spieck et al. 1998; Lücker et al. 2010; 2013; Koch et al. 2015; Daims et al. 2016) and 2) with NxrA orientated inward towards the cytoplasm, as in *Nitrococcus* and *Nitrobacter* (Spieck et al. 1996; Starkenburg et al. 2006; Sorokin et al. 2012). The dominant genera of NOB in the ocean are *Nitrospina* and *Nitrospira* (Füssel et al. 2012; Beman et al. 2013), with a recent metaproteomic study identifying *Nitrospina* NXR as the most abundant microbial protein in the mesopelagic zone of the Central Tropical Pacific (Saito et al. 2020). If *Nitrospina* (and/or *Nitrospira*) is similarly abundant across the Southern Ocean, as has been intimated for the Pacific Subantarctic (Raes et al. 2020), the fact that its NXR is contained within the periplasmic space means that substrate undersaturation is possible. This is in contrast to NOB with a cytoplasmic NXR that must first transport NO_2^- across the cell membrane and into the cytoplasm, where is can accumulate to saturating concentrations before being oxidized (Daims et al. 2016). These NOB (i.e., *Nitrococcus* and *Nitrobacter*) have a lower NO_2^- affinity that those with a periplasmic NXR (Schramm et al. 1999; Nowka et al. 2015), with the latter group thus better suited to regions of low NO_2^-. Nonetheless, my data suggest the NXR in the Southern Ocean,

likely associated with *Nitrospina* and *Nitrospira* (Raes et al. 2020), is substrate-limited, resulting in a perennial background concentration of NO_2^- throughout the mixed layer.

Nitrospina and *Nitrospira* are ubiquitous in the ocean (Füssel et al. 2012; Beman et al. 2013), which raises the question of why a similar NO_2^- concentration threshold has not been reported from other regions. This may partly be due to the very limited number of NO_2^- oxidation kinetics experiments that have to-date been conducted in the open ocean and/or to the fact that a classic Michaelis-Menten function is usually imposed upon kinetics data, with V assumed to increase as soon as S > 0. Additionally, depending on the maximum substrate concentration added during kinetics experiments, it can be difficult to discern a possible threshold NO_2^- concentration by simply examining the resultant plots. Inspection of published Michaelis-Menten curves reveals the possibility of a non-zero C value (i.e., V = 0 at S > 0) in some cases, including in the ETNP ODZ (Sun et al. 2021) and associated with the PNM in the South China Sea (Zhang et al. 2020b), similar to my observations (Figure 4.2). However, there are other published curves that clearly do intercept the origin in V versus S space (Olson 1981a; Sun et al. 2017), possibly reflecting a different NOB community (e.g., dominated by *Nitrococcus*). Alternately, environmental factors unique to the Southern Ocean, such as light, temperature, and/or iron availability, may be instrumental in driving the NO_2^- threshold and associated elevated mixed-layer NO_2^- concentrations that I observe. Indeed, iron limitation of NXR could be implicit in its undersaturation. Indeed, using NXR concentrations, estimates of NXR specific activity, and direct measurements of *in situ* NO_2^- oxidation rates, Saito et al. (2020) deduced that *Nitrospina* NXR is undersaturated in the iron-limited tropical Pacific. This finding is consistent with the mechanism I invoke to explain the apparent NO_2^- concentration threshold in the Southern Ocean, as well as with the existence of such a threshold indicating *Nitrospina* (and/or *Nitrospira*) dominance of the *in situ* NOB community (Raes et al. 2020).

4.5 Concluding remarks

This study presents the first NO_2^- oxidation kinetics experiments for the Southern Ocean, conducted during winter 2017. All the experiments were well-described by the Michaelis-Menten equation, provided that a location parameter, C, was included. V_{max} ranged from 5.2 ± 0.1 to 14 ± 0.4 nM d^{-1} and K_m ranged from 134 ± 8 to 403 ± 24 nM, with the latter parameter

showing a strong positive relationship with $[NO_2^-]_{amb}$. The positive derived values of C (range of 115 ± 2.3 to 245 ± 18 nM) are interpreted to indicate a $[NO_2^-]_{amb}$ threshold below which NOB are NO_2^- limited, and I hypothesize that this threshold indicates substrate limitation of NXR, possibly exacerbated by the low ambient iron concentrations characteristic of the upper Southern Ocean. From depth profile measurements, I deduce that the rate-limiting step of nitrification in the winter season is NO_2^- oxidation, as NH_4^+ oxidation was up to seven-times higher than coincident rates of NO_2^- oxidation in the mixed layer. Despite this, NO_3^- production from NO_2^- accounted for 63-237% of the NO_3^- consumed by phytoplankton, as observed previously in the Atlantic sector of the wintertime Southern Ocean (Mdutyana et al. 2020).

NO_2^- oxidation, as the ultimate step that connects reduced N to its most oxidized form (NO_3^-), is important throughout the water column, but particularly in the upper layer where the supply of reduced N is highest. The production of NO_3^- within the mixed layer from *in situ* nitrification can complicate the application of the new production paradigm as a framework for estimating export production (Yool et al. 2007; Mdutyana et al. 2020), which advocates for additional measurements of this pathway over the upper ~200 m. Additionally, it is becoming increasingly clear that we lack a mechanistic understanding of the controls on nitrification (both NH_4^+ and NO_2^- oxidation), which renders it challenging to model both its magnitude and distribution, and to assess how these may change in future. In particular, further study of the role of iron in controlling nitrification (i.e., NO_2^- and NH_4^+ oxidation) in the open ocean is required, particularly in the Southern Ocean where the mixed layer's biological N cycle is dominated by nitrification in winter (Smart et al. 2015; Mdutyana et al. 2020) and surface-layer iron is very low throughout the year (Tagliabue et al. 2012).

Chapter 5: Knowledge gaps and future directions

Each research chapter of this thesis includes a detailed conclusions and implications section. Below, rather than repeating these conclusions and implications, I focus on some of the knowledge gaps in Southern Ocean N cycling that my work has highlighted, possible future research directions, and the impact of global warming on Southern Ocean N cycling and the biological pump given my findings regarding the environmental controls on mixed-layer N cycle processes.

5.1 Knowledge gaps in N cycling in the Southern Ocean

It is indisputable that a clear picture of the contribution of biology to carbon drawdown in the Southern Ocean requires consideration of iron. The role of iron in controlling the uptake of NO_3^-, carbon export and phytoplankton distributions has been extensively researched in the Southern Ocean (e.g., Van Leeuwe et al. 1997; Hutchins et al. 2001; Prakash et al. 2010; Ryan-Keogh et al. 2017; 2018; Viljoen et al. 2018; 2019) while its role in the uptake and cycling of NH_4^+ has been largely overlooked. In part, this is because iron is not directly required for the transport and assimilation of NH_4^+ (Morel and Price 2003), but it *is* critical for photosynthesis (Raven et al. 1999; Shi et al. 2007). There is also no published research on the role of iron in nitrification by natural nitrifier populations. In this thesis, I have relied heavily on a recent culture study demonstrating that NH_4^+ oxidation by a single strain of AOA requires high concentrations of iron (Shafiee et al. 2019) in order to argue for the potentially significant role of iron in controlling NH_4^+ oxidation rates and NH_4^+ concentrations across the Southern Ocean. However, the results of a single culture study are by no means unequivocal, and there are often significant discrepancies between the findings of culture/laboratory studies and *in situ* experiments (e.g., Martens-Habbena et al. 2009; Newell et al. 2013; Peng et al. 2016). The possibility of an iron control on NO_2^- oxidation is less controversial as it is well-known that the enzyme in NOB that oxidizes NO_2^- to NO_3^- has a significant iron requirement (Walker et al. 2010; Daims et al. 2016). Nonetheless, little has been done *in situ* to investigate this putative driver (Saito et al. 2020). Taken together, the findings described in this thesis, combined with those reported in previous laboratory and field studies (e.g., Arp et al. 2002; Walker et al. 2010; Cavagna et al. 2015; Santoro et al. 2015; Carini et al. 2018; Qin et al. 2018; Shafiee et al. 2019;

Saito et al. 2020), strongly indicate the potential for iron to limit both steps of nitrification in regions with low concentrations of iron, including the Southern Ocean.

While phytoplankton community composition has been fairly well-documented in the Southern Ocean, albeit predominantly during summer (Wright et al. 2010; Gibberd et al. 2013; Mendes et al. 2015; Viljoen et al. 2018; 2019), nitrifier community composition and distributions across the different frontal zones is unknown, with only a single study to-date that reports nitrifier species abundance (Raes et al. 2020). While the Raes et al. (2020) study no doubt provides valuable new information, the authors only sampled two depths (the surface and the base of the mixed layer) and only in winter. Moreover, they report extremely high (one might argue unrealistically high) rates of total nitrification (NH_4^+ to NO_3^- oxidation; as high as 1440 nM d^{-1}) at both the surface and the MLD (i.e., there was no significant depth-related difference in the rates), which contradicts our understanding of the depth distribution of nitrification (and all known controls thereon, including iron).

There is clearly much that remains unknown regarding regenerated NO_3^- production in the shallow Southern Ocean. With regards to NH_4^+ oxidation, population dominance by either AOB or AOA has important implications for the cycling of NH_4^+ as AOA have been observed to display a considerably higher affinity for NH_4^+ than AOB (Martens-Habbena et al. 2009; Peng et al. 2016). This indicates that these organisms may directly (and efficiently) compete with phytoplankton for NH_4^+, especially at depths or in seasons where phytoplankton growth is limited by light (Zakem et al. 2018), assuming of course that the AOA are not (co)limited by another resource. The work described in Chapters 2 and 3 of this thesis begins to address some of these complexities, but there is still much to learn. Likewise, the hypothesis outlined in Chapter 4 that the NXR enzyme associated with certain NOB is undersaturated in the shallow waters, as has been suggested for the tropical Pacific using entirely different data (Saito et al. 2020), has the potential to fill another important gap in our understanding of N cycling insofar as it provides an explanation for i) why NH_4^+ oxidation may not always be the rate-limiting step in the nitrification pathway (Kendall 1998; Walker et al. 2010; Vajrala et al. 2013); ii) why NO_2^- concentrations are elevated in high-latitude surface waters year-around, and iii) why rates of nitrification can be low in shallow waters even when the environmental conditions (e.g., light levels) suggest that they should not be.

Given the significant implications of nitrification for both N and carbon cycling, there is a clear need for *in situ* observations and careful experiments designed to explore the knowledge gaps outlined above. Nitrification rate measurements (including kinetics) in the Southern Ocean are currently few and far between, and there is still a lot of information needed, such as nitrifier community composition across the different frontal zones, both in the mixed layer and below, and during different seasons, particularly the transitional seasons of autumn and spring when nitrification and phytoplankton N uptake are most likely to overlap (temporally and spatially). To further investigate the mixed-layer accumulation of NH_4^+ and NO_2^-, the extent to which mixed-layer nitrification acts against the Southern Ocean's biological CO_2 sink, and the ecological niches of phytoplankton versus nitrifiers in the Southern Ocean, the role of iron in limiting nitrification should be investigated coincident with its implications for other mixed-layer N cycle processes. An important component of this involves empirically determining the effects of changing iron availability on the rates of N uptake and regeneration, nitrifier and phytoplankton community composition, and the physiological capabilities of Southern Ocean microorganisms.

The work presented in this thesis has also underscored some methodological issues that require consideration during future field campaigns. A recurrent problem is that the NH_4^+ simultaneously regenerated within the euphotic zone during uptake and oxidation experiments dilutes the $^{15}N/^{14}N$ ratio of the ambient NH_4^+ pool (Glibert et al. 1982). This isotope dilution can result in the calculation of lower rates than those actually occurring in the environment – the implications of underestimating NH_4^+ transformation rates for deriving kinetic parameters and estimating regenerated production are discussed at length in this thesis. The best way of mitigating this issue is by conducting coincident experiments designed to quantify to the rate of NH_4^+ regeneration. The experiments themselves are fairly straightforward, and leverage the fact that remineralization dilutes an ^{15}N-labeled NH_4^+ pool with ^{14}N over time (Lipschultz 2008 and references therein). While far less common than analyses of PON, NO_2^- and NO_3^- isotope ratios (with the latter two species measured after conversion to N_2O; Sigman et al. 2001; McIlvin and Altabet 2005), measurements of the $^{15}N/^{14}N$ ratio of NH_4^+ have become considerably easier in recent years. Using a basic solution of hypobromite, NH_4^+ can be quantitatively oxidized to NO_2^- (Zhang et al. 2007), after which the NO_2^- is processed as described in Chapters 2 and 3 of this thesis (McIlvin and Altabet 2005; Peng et al. 2015). From the NH_4^+ isotope ratios, preferably measured for more than one time point during the

experiments, NH_4^+ regeneration rates can be computed and used to correct the NH_4^+ uptake and oxidation rates for isotope dilution (Glibert et al. 1982; Goeyens et al. 1991; Clark et al. 2007).

Measurements of NH_4^+ regeneration would also be valuable for their own sake, particularly as warming changes the balance between productivity supported by upward mixing of new nutrients and that fuelled by the microbial loop (Henley et al. 2020 and references therein). There is currently only one study from the Southern Ocean that reports rates of NH_4^+ regeneration (Goeyens et al. 1991); however, it was not conducted in the open Southern Ocean but in the coastal waters of the Weddell Sea. As described in Chapter 3 of this thesis, there are regions of the Southern Ocean that host unusually elevated mixed-layer NH_4^+ concentrations in winter (and perhaps at other times of year) – the extent to which this condition exists because of high remineralisation of organic matter or because of limitations on the processes removing NH_4^+ is not yet clear. Direct measurements of NH_4^+ regeneration rates would go a long way towards closing this knowledge gap in the cycling of N in the upper Southern Ocean.

5.2 The upper Southern Ocean N cycle under climate change

Iron as an essential trace metal in the uptake of NO_3^- is well-documented in the Southern Ocean (Van Leeuwe et al. 1997; Hutchins et al. 2001; Prakash et al. 2010; Ryan-Keogh et al. 2017; 2018; Viljoen et al. 2018; 2019). The delivery and cycling of iron are being altered by climate-driven shifts in Southern Ocean physics, chemistry and biology (Bowie et al. 2009; Lin et al. 2011; Boyd et al. 2012a; Tagliabue et al. 2014; Lannuzel et al. 2016; Meehl et al. 2019), with the general prediction being that iron concentrations will rise in the future (Boyd et al. 2012; Henley et al. 2020 and references therein), theoretically allowing biological processes that require iron to increase their activities (Bopp et al. 2013; Boyd et al. 2015) – in reality, however, the biological response will be contingent on a multitude of overlapping factors. NO_3^- uptake in the Southern Ocean should be enhanced under higher iron concentrations (Martin et al. 1990), which should also favour the growth of diatoms (assuming replete silicate concentrations; Hutchins et al. 2001), leading to elevated atmospheric CO_2 drawdown and sequestration (Armstrong et al. 2009; Cavan et al. 2015; Viljoen et al. 2018; 2019). However, iron is not the only control on Southern Ocean N cycling and productivity. The strong coupling

between iron and photosynthetic physiology means that phytoplankton growth is often co-limited by iron and light (Moore et al. 2013), with the interplay between them manifesting in complex ways (e.g., Strzepek et al. 2012, 2019; Viljoen et al. 2018; Andrew et al. 2019; Trimborn et al. 2019). For instance, a reduction in stratification associated with declining sea ice or wind intensification (as predicted for the open AZ; Meijers 2014; Armour et al. 2016; Rintoul 2018) will result in phytoplankton being mixed over a greater depth range, thus spending more time under light limitation, which can increase their iron demand (Strzepek et al. 2019b). It has also been hypothesized that warming may increase the iron demand of phytoplankton (Rose et al. 2009), while higher iron availability could render phytoplankton more tolerant of warming (Andrew et al. 2019).

The projected increase in iron concentrations also has implications for nitrification. While yet to be confirmed in the environment, Shafiee et al. (2019) demonstrated in culture that iron is important for NH_4^+ oxidation by AOA, a finding also implicated in recent proteomic studies (Santoro et al. 2015; Carini et al. 2018; Qin et al. 2018), and it has long been recognized that AOB require iron for their hydroxylamine oxidoreductase enzyme (Meiklejohn 1953; Arp et al. 2002; Morel and Price 2003; Walker et al. 2010). NO_2^- oxidizers also have iron complexes that they use for the oxidation of NO_2^- to NO_3^- (Walker et al. 2010), so may too be vulnerable to iron limitation. If iron concentrations rise in the near future, increased euphotic zone nitrification, particularly in winter, may become more important in offsetting carbon drawdown by phytoplankton annually, although this depends on the response of phytoplankton to changes in iron supply, as well as on the influence of changing light levels and temperature on both phytoplankton and nitrifiers. It is clear that to better understand the implications of changes in iron availability for the N cycle (and by extension, the biological controls on CO_2), The role of iron in mixed-layer N cycling must first be characterized at high resolution under environmentally-relevant conditions. We currently have a reasonable idea of the effect of iron on NO_3^- utilization, but little to no understanding of its influence (direct or indirect) on reduced N consumption, production, and oxidation, or on the interactions among N cycle pathways.

The temperature increase predicted for the future global ocean will have significant implication for primary production and the composition of phytoplankton communities (Sherman et al. 2016; Deppeler and Davidson 2017 and references therein). At a first order, warmer

temperatures should increase the metabolic mechanisms of phytoplankton (Eppley 1972; Moore et al. 2018), such that ocean warming may lead to increased atmospheric CO_2 drawdown via higher phytoplankton growth rates. However, Southern Ocean phytoplankton are adapted to lower temperatures and experience thermal stress at low temperatures (e.g., Andrew et al. 2019), although unlike tropical phytoplankton, their optimum growth temperatures appear to be slightly higher than their *in situ* temperatures (Thomas et al. 2012). Nonetheless, thermal stress has been shown to hinder the growth of some Southern Ocean phytoplankton (e.g., the diatom *P. inermis* and the haptophyte *P. antarctica*; Boyd et al. 2013; Andrew et al. 2019), and warming is likely to cause a shift in the phytoplankton community composition, which has implications for exportable carbon (e.g., Hutchins and Boyd 2016; Sherman et al. 2016; Zhu et al. 2016; Deppeler and Davidson 2017 and references therein). A shift towards larger species and more diatom-dominated populations should increase the potential for CO_2 drawdown (Armstrong et al. 2009; Tréguer et al. 2018; Boyd 2019) while a shift towards small species is likely to enhance the microbial loop (e.g., Constable et al. 2014; Petrou et al. 2016; Deppeler and Davidson 2017), decreasing biological CO_2 drawdown. Additionally, a shift towards small phytoplankton species may result in enhanced competition with AOA and AOB for NH_4^+ and other scarce resources, possibly constraining mixed-layer nitrification (Mdutyana et al. 2020). Increased temperatures have been shown to decouple the two steps of nitrification, potentially explaining short-term accumulations of NO_2^- in coastal regions (Bristow et al. 2015; Schaefer and Hollibaugh 2017).

In the Southern Ocean, the effect of rising temperatures on nitrification rates has not been directly tested. Here, warming may lead to either a rise or a decline in nitrification rates given the evidence from NO_3^- isotope ratios (DiFiore et al. 2009; Smart et al. 2015) and direct measurements (Mdutyana et al. 2020; Raes et al. 2020) for much higher rates of nitrification in winter than in summer. If winter temperatures rise slightly (but not beyond the temperature optima of the extant nitrifiers), nitrification rates could increase. By contrast, enhanced thermal stratification may decrease winter mixed-layer nitrification rates by increasing photoinhibition of nitrifiers – in this case, the temperature effect is indirect. Another possibility is that the upregulation of the microbial loop driven by a shift towards smaller phytoplankton-dominated assemblages (e.g., Deppeler and Davidson 2017) may increase nitrification rates by providing a greater flux of limiting substrate. At present, however, far too little is known of the controls

on nitrification in the Southern Ocean to warrant speculation as to how this process is likely to change.

Ocean pH is decreasing with climate change because of enhanced CO_2 absorption (i.e., "ocean acidification"; Doney et al. 2009; Feely et al. 2009), with the Southern Ocean expected to experience ocean acidification more rapidly and intensely than other oceanic regions (Orr et al. 2005; Fabry et al. 2009; Jiang et al. 2015; Figuerola et al. 2021). Ocean acidification has several implications for the biological processes involved in the cycling of N, in part because ocean acidification affects biodiversity (Doney et al. 2009). Lower-pH surface waters have consequences for the formation (and dissolution) of calcite and aragonite shells (e.g., of coccolithophores, pteropods, and foraminifera), with aragonite and calcite undersaturation events already observed in the Southern Ocean and predicted to become more frequent (Orr et al. 2005; McNeil and Matear 2008; Feely et al. 2009; Bednaršek et al. 2012a; b; Hauri et al. 2016; Jones et al. 2017; Kerr et al. 2018). Any ocean acidification-related changes in phytoplankton community composition (which are likely to be complex) will directly impact the efficiency of the biological carbon pump. For instance, under high CO_2 (low pH), phytoplankton in the Ross Sea have been observed to shift from a community dominated by *P. antarctica* and pennate diatoms to one dominated by large, chain-forming centric diatoms (Tortell et al. 2008; Feng et al. 2010) that contribute more to carbon export (e.g., Petrou et al. 2019). By contrast, in coastal East Antarctica, primary productivity was observed to decrease under higher CO_2 and the phytoplankton community shifted towards smaller species that are less effective carbon exporters (Hancock et al. 2018; Westwood et al. 2018). In addition, ocean acidification has the potential to affect new production (and thus carbon export potential) as a result of its apparent enhancement of bacterial activity (i.e., the microbial loop) (Maas et al. 2013; Westwood et al. 2018; Petrou et al. 2019). As such, regenerated production fuelled by recycled NH_4^+ may become relatively more dominant under lower pH conditions.

We clearly still have much to learn regarding the implications of ocean acidification for phytoplankton productivity and diversity and thus N and carbon cycling in the Southern Ocean (Mackey et al. 2015; Henley et al. 2020 and references therein). A decrease in upper ocean pH will also alter iron speciation, with uncertain implications for its subsequent availability to phytoplankton and other microbes (Shi et al. 2010; Hutchins and Boyd 2016), including

nitrifiers. Nitrification will additionally be directly affected by ocean acidification, with acidic conditions shown to negatively affect nitrification rates (Beman et al. 2011; Shiozaki et al. 2019). This is because acidification alters the equilibrium between NH_4^+ and NH_3, decreasing the availability of NH_3, the substrate for NH_4^+ oxidation (Chapter 3). A more acidic ocean may thus be one that supports less nitrification, thereby reducing the NO_3^- supply in the upper ocean, with potentially large-scale consequences for marine productivity and N cycling. In the context of the work presented in this thesis, the scenarios outlined above underscore the need for more nuanced definitions of new and regenerated production if we are to keep relying on N cycle measurements to provide quantitative insights into a rapidly changing ocean carbon cycle.

References cited

Aguilar-Islas, A. M., R. D. Rember, C. W. Mordy, and J. Wu. 2008. Sea ice-derived dissolved iron and its potential influence on the spring algal bloom in the Bering Sea. Geophysical Research Letters. doi:10.1029/2008GL035736

Aksnes, D. L., and J. K. Egge. 1991. A_theoretical_model_for_nutrient_uptake_in_phytoplankton. Marine Ecology Progress Series **70**: 65--72.

Alderkamp, A. C., M. M. Mills, G. L. van Dijken, and others. 2012. Iron from melting glaciers fuels phytoplankton blooms in the Amundsen Sea (Southern Ocean): Phytoplankton characteristics and productivity. Deep-Sea Research Part II: Topical Studies in Oceanography **71**–**76**: 32–48. doi:10.1016/j.dsr2.2012.03.005

Allen, A. E., M. H. Howard-Jones, M. G. Booth, M. E. Frischer, P. G. Verity, D. A. Bronk, and M. P. Sanderson. 2002. Importance of heterotrophic bacterial assimilation of ammonium and nitrate in the Barents Sea during summer. Journal of Marine Systems **38**: 93–108. doi:10.1016/S0924-7963(02)00171-9

Altabet, M. A., and R. Francois. 2001. Nitrogen isotope biogeochemistry of the Antarctic polar frontal zone at 170°W. Deep-Sea Research Part II: Topical Studies in Oceanography. doi:10.1016/S0967-0645(01)00088-1

Amin, S. A., J. W. Moffett, W. Martens-Habbena, and others. 2013. Copper requirements of the ammonia-oxidizing archaeon Nitrosopumilus maritimus SCM1 and implications for nitrification in the marine environment. Limnology and Oceanography **58**: 2037–2045. doi:10.4319/lo.2013.58.6.2037

Andrew, S. M., H. T. Morell, R. F. Strzepek, P. W. Boyd, and M. J. Ellwood. 2019. Iron Availability Influences the Tolerance of Southern Ocean Phytoplankton to Warming and Elevated Irradiance. Frontiers in Marine Science **6**: 1–12. doi:10.3389/fmars.2019.00681

Archontoulis, S. V., and F. E. Miguez. 2014. Nonlinear regression models and applications in agricultural research. Agronomy Journal **107**: 786–798. doi:10.2134/agronj2012.0506

Ardyna, M., L. Lacour, S. Sergi, and others. 2019. Hydrothermal vents trigger massive phytoplankton blooms in the Southern Ocean. Nature Communications **10**: 1–8. doi:10.1038/s41467-019-09973-6

Armour, K. C., J. Marshall, J. R. Scott, A. Donohoe, and E. R. Newsom. 2016. Southern Ocean warming delayed by circumpolar upwelling and equatorward transport. Nature Geoscience **9**: 549–554. doi:10.1038/ngeo2731

Armstrong, R. A., C. Lee, J. I. Hedges, S. Honjo, and S. G. Wakeham. 2001. A new, mechanistic model for organic carbon fluxes in the ocean based on the quantitative association of POC with ballast minerals. Deep-Sea Research Part II: Topical Studies in Oceanography **49**: 219–236. doi:10.1016/S0967-0645(01)00101-1

Armstrong, R. A., M. L. Peterson, C. Lee, and S. G. Wakeham. 2009. Settling velocity spectra and the ballast ratio hypothesis. Deep-Sea Research Part II: Topical Studies in Oceanography **56**: 1470–1478. doi:10.1016/j.dsr2.2008.11.032

Arp, D. J., L. A. Sayavedra-Soto, and N. G. Hommes. 2002. Molecular biology and biochemistry of ammonia oxidation by Nitrosomonas europaea. Archives of Microbiology **178**: 250–255. doi:10.1007/s00203-002-0452-0

Arrigo, K. R., G. L. van Dijken, and S. Bushinsky. 2008. Primary production in the Southern Ocean, 1997-2006. Journal of Geophysical Research: Oceans **113**: 1997–2006. doi:10.1029/2007JC004551

Arrigo, K. R., G. R. DiTullio, R. B. Dunbar, D. H. Robinson, M. VanWoert, D. L. Worthen, and M. P. Lizotte. 2000. Phytoplankton taxonomic variability in nutrient utilization and primary production in the Ross Sea. Journal of Geophysical Research: Oceans **105**: 8827–8846. doi:10.1029/1998jc000289

Arrigo, K. R., and C. R. McClain. 1994. Spring phytoplankton production in the western Ross Sea. Science **266**. doi:10.1126/science.266.5183.261

Arrigo, K. R., D. H. Robinson, D. L. Worthen, R. B. Dunbar, G. R. DiTullio, M. VanWoert, and M. P. Lizotte. 1999. Phytoplankton community structure and the drawdown of nutrients and CO2 in the Southern Ocean. Science **283**: 365–367. doi:10.1126/science.283.5400.365

Assmy, P., V. Smetacek, M. Montresor, and others. 2013. Thick-shelled, grazer-protected diatoms decouple ocean carbon and silicon cycles in the iron-limited Antarctic Circumpolar Current. Proceedings of the National Academy of Sciences of the United States of America **110**: 20633–20638. doi:10.1073/pnas.1309345110

Atkinson, A., M. J. Whitehouse, J. Priddle, G. C. Cripps, P. Ward, and M. A. Brandon. 2001. South Georgia, Antarctica: A productive, cold water, pelagic ecosystem. Marine Ecology Progress Series. doi:10.3354/meps216279

de Baar, H., A. Buma, R. Nolting, G. Cadee, G. Jacques, and P. Treguer. 1990a. On iron limitation of the Southern Ocean:

experimental observations in the Weddell and Scotia Seas. Marine Ecology Progress Series **65**: 105–122. doi:10.3354/meps065105

de Baar, H., A. Buma, R. Nolting, G. Cadee, G. Jacques, and P. Treguer. 1990b. On iron limitation of the Southern Ocean: experimental observations in the Weddell and Scotia Seas. Marine Ecology Progress Series **65**: 105–122. doi:10.3354/meps065105

de Baar, H. J. W., U. Bathmannt, V. Smetacek, B. M. Löscher, and C. Veth. 1995. Importance of iron for plankton blooms and carbon dioxide drawdown in the Southern Ocean. Nature. doi:10.1038/373412a0

Baer, S. E., T. L. Connelly, R. E. Sipler, P. L. Yager, and D. A. Bronk. 2014. Effect of temperature on rates of ammonium uptake and nitrification in the western coastal Arctic during winter, spring, and summer. Global biogeochemical cycles **28**: 1455–1466. doi:10.1111/1462-2920.13280

Bagwell, J. 2009. TRANSCRIPTIONAL RESPONSE OF NITROGEN UPTAKE AND ASSIMILATION IN MARINE DIATOMS; THALASSIOSIRA PSEUDONANA AND THALASSIOSIRA WEISSFLOGII. MSC: University of North Carolina Wilmington.

Baird, M. E., S. M. Emsley, and J. M. Mcglade. 2001. Modelling the interacting effects of nutrient uptake, light capture and temperature on phytoplankton growth. Journal of Plankton Research **23**: 829–840. doi:10.1093/plankt/23.8.829

Bakker, D. C. E., B. Pfeil, C. S. Landa, and others. 2016. A multi-decade record of high-quality fCO 2 data in version 3 of the Surface Ocean CO 2 Atlas (SOCAT). Earth System Science Data **8**: 383–413. doi:10.5194/essd-8-383-2016

Balch, W. M., D. T. Drapeau, B. C. Bowler, E. Lyczskowski, E. S. Booth, and D. Alley. 2011. The contribution of coccolithophores to the optical and inorganic carbon budgets during the Southern Ocean Gas Exchange Experiment: New evidence in support of the Great Calcite Belt hypothesis. Journal of Geophysical Research: Oceans **116**: 1–14. doi:10.1029/2011JC006941

Banse, K. 1976. RATES OF GROWTH, RESPIRATION AND PHOTOSYNTHESIS OF UNICELLULAR ALGAE AS RELATED TO CELL SIZE-A REVIEW1,2. Journal of Phycology. doi:10.1111/j.0022-3646.1976.00135.x

Banse, K. 1996. Low seasonality of low concentrations of surface chlorophyll in the Subantarctic water ring: Underwater irradiance, iron, or grazing? Progress in Oceanography **37**. doi:10.1016/S0079-6611(96)00006-7

Bathmann, U. V. 1998. Ecology and biogeochemistry in the Atlantic sector of the Southern Ocean During Austral Spring: The first JGOFS expedition aboard RV "Polarstern." Journal of Marine Systems **17**: 77–85. doi:10.1016/S0924-7963(98)00030-X

Baudoux, A. C., A. A. M. Noordeloos, M. J. W. Veldhuis, and C. P. D. Brussaard. 2006. Virally induced mortality of Phaeocystis globosa during two spring blooms in temperate coastal waters. Aquatic Microbial Ecology **44**: 207–217. doi:10.3354/ame044207

Bayer, B., M. A. Saito, M. R. McIlvin, S. Lücker, D. M. Moran, T. S. Lankiewicz, C. L. Dupont, and A. E. Santoro. 2021. Metabolic versatility of the nitrite-oxidizing bacterium Nitrospira marina and its proteomic response to oxygen-limited conditions. ISME Journal **15**: 1025–1039. doi:10.1038/s41396-020-00828-3

Bednaršek, N., J. Mozina, M. Vogt, C. O'Brien, and G. A. Tarling. 2012a. The global distribution of pteropods and their contribution to carbonate and carbon biomass in the modern ocean. Earth System Science Data **4**: 167–186. doi:10.5194/essd-4-167-2012

Bednaršek, N., G. A. Tarling, D. C. E. Bakker, and others. 2012b. Extensive dissolution of live pteropods in the Southern Ocean. Nature Geoscience **5**: 881–885. doi:10.1038/ngeo1635

Behrenfeld, M. J. 2010. Abandoning sverdrup's critical depth hypothesis on phytoplankton blooms. Ecology **91**: 977–989. doi:10.1890/09-1207.1

Behrenfeld, M. J., and A. J. Milligan. 2013. Photophysiological expressions of iron stress in phytoplankton. Annual Review of Marine Science **5**. doi:10.1146/annurev-marine-121211-172356

Belkin, I. M., and A. L. Gordon. 1996. Southern Ocean fronts from the Greenwich meridian to Tasmania. Journal of Geophysical Research C: Oceans. doi:10.1029/95JC02750

Beman, J. M., C. E. Chow, A. L. King, and others. 2011. Global declines in oceanic nitrification rates as a consequence of ocean acidification. Proceedings of the National Academy of Sciences of the United States of America **108**: 208–213. doi:10.1073/pnas.1011053108

Beman, J. M., J. Leilei Shih, and B. N. Popp. 2013. Nitrite oxidation in the upper water column and oxygen minimum zone of the eastern tropical North Pacific Ocean. ISME Journal **7**: 2192–2205. doi:10.1038/ismej.2013.96

Beman, J. M., B. N. Popp, and S. E. Alford. 2012. Quantification of ammonia oxidation rates and ammonia-oxidizing

archaea and bacteria at high resolution in the Gulf of California and eastern tropical North Pacific Ocean. Limnology and Oceanography **57**: 711–726. doi:10.4319/lo.2012.57.3.0711

Beman, J. M., B. N. Popp, and C. A. Francis. 2008. Molecular and biogeochemical evidence for ammonia oxidation by marine Crenarchaeota in the Gulf of California. ISME Journal **2**: 429–441. doi:10.1038/ismej.2007.118

Berg, G. M., M. Balode, I. Purina, S. Bekere, C. Béchemin, and S. Y. Maestrini. 2003. Plankton community composition in relation to availability and uptake of oxidized and reduced nitrogen. Aquatic Microbial Ecology **30**: 263–274. doi:10.3354/ame030263

Berges, J. A., D. E. Varela, and P. J. Harrison. 2002. Effects of temperature on growth rate, cell composition and nitrogen metabolism in the marine diatom Thalassiosira pseudonana (bacillariophyceae). Marine Ecology Progress Series **225**. doi:10.3354/meps225139

Berman-frank, I., P. Lundgren, Y. Chen, Z. Kolber, and B. Bergman. 2001. Segregation of Nitrogen Fixation and Oxygenic Photosynthesis in the Marine Cyanobacterium Trichodesmium. Science **1534**: 1534–1537. doi:10.1126/science.1064082

Bernhard, A. E., T. Donn, A. E. Giblin, and D. A. Stahl. 2005. Loss of diversity of ammonia-oxidizing bacteria correlates with increasing salinity in an estuary system. Environmental Microbiology **7**. doi:10.1111/j.1462-2920.2005.00808.x

Bernhard, A. E., Z. C. Landry, A. Blevins, J. R. De La Torre, A. E. Giblin, and D. A. Stahl. 2010. Abundance of ammonia-oxidizing archaea and bacteria along an estuarine salinity gradient in relation to potential nitrification rates. Applied and Environmental Microbiology **76**: 1285–1289. doi:10.1128/AEM.02018-09

Bernhard, A. E., J. Tucker, A. E. Giblin, and D. A. Stahl. 2007. Functionally distinct communities of ammonia-oxidizing bacteria along an estuarine salinity gradient. Environmental Microbiology **9**: 1439–1447. doi:10.1111/j.1462-2920.2007.01260.x

Bianchi, M., F. Feliatra, P. Tréguer, M. A. Vincendeau, and J. Morvan. 1997. Nitrification rates, ammonium and nitrate distribution in upper layers of the water column and in sediments of the Indian sector of the Southern Ocean. Deep-Sea Research Part II: Topical Studies in Oceanography **44**: 1017–1032. doi:10.1016/S0967-0645(96)00109-9

De Bie, M. J. M., A. G. C. L. Speksnijder, G. A. Kowalchuk, T. Schuurman, G. Zwart, J. R. Stephen, O. E. Diekmann, and H. J. Laanbroek. 2001. Shifts in the dominant populations of ammonia-oxidizing β-subclass Proteobacteria along the eutrophic Schelde estuary. Aquatic Microbial Ecology **23**: 225–236. doi:10.3354/ame023225

Biggs, T. E. G., J. Huisman, and C. P. D. Brussaard. 2021. Viral lysis modifies seasonal phytoplankton dynamics and carbon flow in the Southern Ocean. ISME Journal 1–8. doi:10.1038/s41396-021-01033-6

Birch, C. P. D. 1999. A new generalized logistic sigmoid growth equation compared with the Richards growth equation. Annals of Botany **83**: 713–723. doi:10.1006/anbo.1999.0877

Blackburne, R., V. M. Vadivelu, and Z. Yuan. 2007. Kinetic characterisation of an enriched Nitrospira culture with comparison to Nitrobacter. **41**: 3033–3042. doi:10.1016/j.watres.2007.01.043

Blain, S., B. Quéguiner, L. Armand, and others. 2007. Effect of natural iron fertilization on carbon sequestration in the Southern Ocean. Nature. doi:10.1038/nature05700

Blain, S., P. Tréguer, S. Belviso, and others. 2001. A biogeochemical study of the island mass effect in the context of the iron hypothesis: Kerguelen Islands, Southern Ocean. Deep-Sea Research Part I: Oceanographic Research Papers. doi:10.1016/S0967-0637(00)00047-9

Blainey, P. C., A. C. Mosier, A. Potanina, C. A. Francis, and S. R. Quake. 2011. Genome of a low-salinity ammonia-oxidizing archaeon determined by single-cell and metagenomic analysis. PLoS ONE **6**. doi:10.1371/journal.pone.0016626

Bock, E. 1965. Vergleichende Untersuchungen über die Wirkung sichtbaren Lichtes auf Nitrosomonas europaea und Nitrobacter winogradskyi. Archiv für Mikrobiologie. doi:10.1007/BF00406848

Bock, E., and M. Wagner. 2006. Ox i dat i on of Inorgan i c N i trogen Compound s a s an Energy Source,.

Booth, B. C. 1988. Size classes and major taxonomic groups of phytoplankton at two locations in the subarctic pacific ocean in May and August, 1984. Marine Biology **97**. doi:10.1007/BF00391313

Bopp, L., L. Resplandy, J. C. Orr, and others. 2013. Multiple stressors of ocean ecosystems in the 21st century: Projections with CMIP5 models. Biogeosciences **10**: 6225–6245. doi:10.5194/bg-10-6225-2013

Borrione, I., and R. Schlitzer. 2013. Distribution and recurrence of phytoplankton blooms around South Georgia, Southern Ocean. Biogeosciences **10**: 217–231. doi:10.5194/bg-10-217-2013

Bowie, A. R., D. Lannuzel, T. A. Remenyi, and others. 2009. Biogeochemical iron budgets of the Southern Ocean south of

Australia: Decoupling of iron and nutrient cycles in the subantarctic zone by the summertime supply. Global Biogeochemical Cycles **23**: 1–14. doi:10.1029/2009GB003500

Boyd, P., J. Laroche, M. Gall, R. Frew, R. M. L. Mckay, and A. Phytoplankton. 1999. Role of iron , light , and silicate in controlling algal biomass were studied during austral autumn and spring primary production (350-650 mg C m -2 d -1) were dominated by cells was little evidence of Fe-stressed algal. Geo **104**: 395–408. doi:10.1029/1999JC900009

Boyd, P. W. 2002. Environmental factors controlling phytoplankton processes in the Southern Ocean. Journal of Phycology **38**: 844–861. doi:10.1046/j.1529-8817.2002.t01-1-01203.x

Boyd, P. W. 2019. Physiology and iron modulate diverse responses of diatoms to a warming Southern Ocean. Nature Climate Change **9**: 148–152. doi:10.1038/s41558-018-0389-1

Boyd, P. W., K. R. Arrigo, R. Strzepek, and G. L. Van Dijken. 2012a. Mapping phytoplankton iron utilization: Insights into Southern Ocean supply mechanisms. Journal of Geophysical Research: Oceans **117**: 1–18. doi:10.1029/2011JC007726

Boyd, P. W., A. C. Crossley, G. R. DiTullio, F. B. Griffiths, D. A. Hutchins, B. Queguiner, P. N. Sedwick, and T. W. Trull. 2001. Control of phytoplankton growth by iron supply and irradiance in the subantarctic Southern Ocean: Experimental results from the SAZ Project. Journal of Geophysical Research: Oceans **106**: 31573–31583. doi:10.1029/2000jc000348

Boyd, P. W., and M. J. Ellwood. 2010. The biogeochemical cycle of iron in the ocean. Nature Geoscience **3**: 675–682. doi:10.1038/ngeo964

Boyd, P. W., T. Jickells, C. S. Law, and others. 2007. Mesoscale iron enrichment experiments 1993-2005: Synthesis and future directions. Science **315**: 612–617. doi:10.1126/science.1131669

Boyd, P. W., S. T. Lennartz, D. M. Glover, and S. C. Doney. 2015. Biological ramifications of climate-change-mediated oceanic multi-stressors. Nature Climate Change **5**: 71–79. doi:10.1038/nclimate2441

Boyd, P. W., T. A. Rynearson, E. A. Armstrong, and others. 2013. Marine Phytoplankton Temperature versus Growth Responses from Polar to Tropical Waters - Outcome of a Scientific Community-Wide Study. PLoS ONE **8**. doi:10.1371/journal.pone.0063091

Boyd, P. W., R. Strzepek, S. Chiswell, and others. 2012b. Microbial control of diatom bloom dynamics in the open ocean. Geophysical Research Letters **39**: 2–7. doi:10.1029/2012GL053448

Boyd, P. W., A. J. Watson, C. S. Law, and others. 2000. A mesoscale phytoplankton bloom in the polar Southern Ocean stimulated by iron fertilization. Nature **407**: 695–702. doi:10.1038/35037500

Boye, M., B. D. Wake, P. Lopez Garcia, J. Bown, A. R. Baker, and E. P. Achterberg. 2012. Distributions of dissolved trace metals (Cd, Cu, Mn, Pb, Ag) in the southeastern Atlantic and the Southern Ocean. Biogeosciences **9**: 3231–3246. doi:10.5194/bg-9-3231-2012

de Boyer Montégut, C., G. Madec, A. S. Fischer, A. Lazar, and D. Iudicone. 2004. Mixed layer depth over the global ocean: An examination of profile data and a profile-based climatology. Journal of Geophysical Research C: Oceans **109**: 1–20. doi:10.1029/2004JC002378

Bradley, P. B., M. P. Sanderson, M. E. Frischer, J. Brofft, M. G. Booth, L. J. Kerkhof, and D. A. Bronk. 2010. Inorganic and organic nitrogen uptake by phytoplankton and heterotrophic bacteria in the stratified Mid-Atlantic Bight. Estuarine, Coastal and Shelf Science **88**: 429–441. doi:10.1016/j.ecss.2010.02.001

Von Brand, T., N. W. Rakestraw, and C. E. Renn. 1937. Although the forniation of nitrate froni composted nitrogenous or ganic materials has been long known and practically applied, the current conception that specific biological agencies bring about these natural. 165–175.

Bressac, M., C. Guieu, M. J. Ellwood, and others. 2019. Resupply of mesopelagic dissolved iron controlled by particulate iron composition. Nature Geoscience **12**: 995–1000. doi:10.1038/s41561-019-0476-6

Bristow, L. A., T. Dalsgaard, L. Tiano, and others. 2016. Ammonium and nitrite oxidation at nanomolar oxygen concentrations in oxygen minimum zone waters. Proceedings of the National Academy of Sciences **113**: 10601–10606. doi:10.1073/pnas.1600359113

Bristow, L. A., N. Sarode, J. Cartee, A. Caro-Quintero, B. Thamdrup, and F. J. Stewart. 2015. Biogeochemical and metagenomic analysis of nitrite accumulation in the Gulf of Mexico hypoxic zone. Limnology and Oceanography **60**: 1733–1750. doi:10.1002/lno.10130

Broecker, W. S. 1982. Ocean chemistry during glacial time. Geochimica et Cosmochimica Acta **46**. doi:10.1016/0016-7037(82)90110-7

Bronk, D. A. 2002. Chapter 5 - Dynamics of DON, *In* Biogeochemistry of Marine Dissolved Oragnic Matter.

Bronk, D. A., P. M. Gilbert, T. C. Malone, S. Banahan, and E. Sahlsten. 1998. Inorganic and organic nitrogen cycling in Chesapeake Bay: Autotrophic versus heterotrophic processes and relationships to carbon flux. Aquatic Microbial Ecology **15**: 177–189. doi:10.3354/ame015177

Bronk, D. A., P. M. Glibert, and B. B. Ward. 1994. Nitrogen uptake, dissolved organic nitrogen release, and new production. Science **265**: 1843–6. doi:10.1126/science.265.5180.1843

Bronk, D. A., and B. B. Ward. 1999. Gross and net nitrogen uptake and DON release in the euphotic zone of Monterey Bay, California. Limnology and Oceanography **44**: 573–585. doi:10.4319/lo.1999.44.3.0573

Browning, T. J., E. P. Achterberg, A. Engel, and E. Mawji. 2021. Manganese co-limitation of phytoplankton growth and major nutrient drawdown in the Southern Ocean. Nature Communications **12**: 1–9. doi:10.1038/s41467-021-21122-6

Bruland, K. W. 1980. Oceanographic distributions of cadmium, zinc, nickel, and copper in the North Pacific. Earth and Planetary Science Letters **47**. doi:10.1016/0012-821X(80)90035-7

Brussaard, C. P. D., K. R. Timmermans, J. Uitz, and M. J. W. Veldhuis. 2008. Virioplankton dynamics and virally induced phytoplankton lysis versus microzooplankton grazing southeast of the Kerguelen (Southern Ocean). Deep-Sea Research Part II: Topical Studies in Oceanography **55**: 752–765. doi:10.1016/j.dsr2.2007.12.034

Brzezinski, M. A. 1988. Vertical distribution of ammonium in stratified oligotrophic waters. Limnology and Oceanography **33**: 1176–1182. doi:10.4319/lo.1988.33.5.1176

Brzezinski, M. A., M. L. Dickson, D. M. Nelson, and R. Sambrotto. 2003a. Ratios of Si, C and N uptake by microplankton in the Southern Ocean. Deep-Sea Research Part II: Topical Studies in Oceanography **50**: 619–633. doi:10.1016/S0967-0645(02)00587-8

Brzezinski, M. A., J. L. Jones, and M. S. Demarest. 2005. Control of silica production by iron and silicic acid during the Southern Ocean Iron Experiment (SOFeX). Limnology and Oceanography **50**: 810–824. doi:10.4319/lo.2005.50.3.0810

Brzezinski, M., J. Jones, K. Bidle, and F. Azam. 2003b. The Balance between Silica Production and Silica Dissolution in the Sea: Insights from Monterey Bay, …. Limnology and Oceanography **48**: 1846–1854.

Buchwald, C., A. E. Santoro, R. H. R. Stanley, and K. L. Casciotti. 2015. Nitrogen cycling in the secondary nitrite maximum of the eastern tropical North Pacific off Costa Rica. Global Biogeochemical Cycles. doi:10.1002/2015GB005187

Buesseler, K. O. 1998a. The decoupling of production and particulate export in the surface as a tracer of upper ocean Comparisons between production and. Global Biogeochemical Cycles **2**: 297–310.

Buesseler, K. O. 1998b. The decoupling of production and particulat export in the surface ocean. Global Biogeochemical Cycles **12**: 297–310.

Buma, A. G. J., H. J. W. de Baar, R. F. Nolting, and A. J. van Bennekom. 1991. Metal enrichment experiments in the Weddell-Scotia Seas: Effects of iron and manganese on various plankton communities. Limnology and Oceanography **36**: 1865–1878. doi:10.4319/lo.1991.36.8.1865

Buongiorno Nardelli, B., S. Guinehut, N. Verbrugge, Y. Cotroneo, E. Zambianchi, and D. Iudicone. 2017. Southern Ocean Mixed-Layer Seasonal and Interannual Variations From Combined Satellite and In Situ Data. Journal of Geophysical Research: Oceans **122**: 10042–10060. doi:10.1002/2017JC013314

Caldeira, K. 2000. The Role of the Southern Ocean in Uptake and Storage of Anthropogenic Carbon Dioxide. Science **287**: 620–622. doi:10.1126/science.287.5453.620

Campbell, W. H. 1999. NITRATE REDUCTASE STRUCTURE , FUNCTION AND REGULATION : Bridging the Gap between Biochemistry and Physiology. 277–303.

Caranto, J. D., and K. M. Lancaster. 2017. Nitric oxide is an obligate bacterial nitrification intermediate produced by hydroxylamine oxidoreductase. Proceedings of the National Academy of Sciences of the United States of America **114**: 8217–8222. doi:10.1073/pnas.1704504114

Cardoso, J. F. M. F., J. D. L. Van Bleijswijk, H. Witte, and F. C. Van Duyl. 2013. Diversity and abundance of ammonia-oxidizing Archaea and Bacteria in tropical and cold-water coral reef sponges. Aquatic Microbial Ecology **68**: 215–230. doi:10.3354/ame01610

Carini, P., C. L. Dupont, and A. E. Santoro. 2018. Patterns of thaumarchaeal gene expression in culture and diverse marine environments. Environmental Microbiology **20**: 2112–2124. doi:10.1111/1462-2920.14107

Carranza, M. M., and S. T. Gille. 2015. Southern Ocean wind-driven entrainment enhances satellite chlorophyll-a through the summer. Journal of Geophysical Research: Oceans. doi:10.1002/2014JC010203

Carvalho, F., J. Kohut, M. J. Oliver, and O. Schofield. 2017. Defining the ecologically relevant mixed-layer depth for Antarctica's coastal seas. Geophysical Research Letters. doi:10.1002/2016GL071205

Cassar, N., M. L. Bender, B. A. Barnett, S. Fan, W. J. Moxim, H. Levy, and B. Tilbrook. 2007. The southern ocean biological response to aeolian iron deposition. Science **317**: 1067–1070. doi:10.1126/science.1144602

Castellani, A. G., and C. F. Niven. 1955. Factors affecting the bacteriostatic action of sodium nitrite. Applied microbiology **3**. doi:10.1128/aem.3.3.154-159.1955

Cavagna, A. J., F. Fripiat, M. Elskens, and others. 2015. Production regime and associated N cycling in the vicinity of Kerguelen Island, Southern Ocean. Biogeosciences **12**: 6515–6528. doi:10.5194/bg-12-6515-2015

Cavan, E. L., F. A. C. Le Moigne, A. J. Poulton, G. A. Tarling, P. Ward, C. J. Daniels, G. M. Fragoso, and R. J. Sanders. 2015. Attenuation of particulate organic carbon flux in the Scotia Sea, Southern Ocean, is controlled by zooplankton fecal pellets. Geophysical Research Letters **42**: 821–830. doi:10.1002/2014GL062744

Cefarelli, A. O., M. Vernet, and M. E. Ferrario. 2011. Phytoplankton composition and abundance in relation to free-floating Antarctic icebergs. Deep-Sea Research Part II: Topical Studies in Oceanography **58**: 1436–1450. doi:10.1016/j.dsr2.2010.11.023

Chereskin, B. M., and P. A. Castelfranco. 1982. Effects of Iron and Oxygen on Chlorophyll Biosynthesis. Plant Physiology **69**: 112–116. doi:10.1104/pp.69.1.112

Chisholm, S. W., and F. M. M. Morel. 1991. What controls phytoplankton production in nutrient-rich areas of the open sea? Limonology And Oceanography **36**: U1507–U1511.

Christian, J. R., M. A. Verschell, R. Murtugudde, A. J. Busalacchi, and C. R. McClain. 2001. Biogeochemical modelling of the tropical Pacific Ocean. II: Iron biogeochemistry. Deep-Sea Research Part II: Topical Studies in Oceanography **49**. doi:10.1016/S0967-0645(01)00111-4

Christman, G. D., M. T. Cottrell, B. N. Popp, E. Gier, and D. L. Kirchman. 2011. Abundance, diversity, and activity of ammonia-oxidizing prokaryotes in the coastal arctic ocean in summer and winter. Applied and Environmental Microbiology **77**: 2026–2034. doi:10.1128/AEM.01907-10

Church, M. J., B. Wai, D. M. Karl, and E. F. DeLong. 2010. Abundances of crenarchaeal amoA genes and transcripts in the Pacific Ocean. Environmental Microbiology **12**: 679–688. doi:10.1111/j.1462-2920.2009.02108.x

Clark, D. R., A. P. Rees, and I. Joint. 2007. A method for the determination of nitrification rates in oligotrophic marine seawater by gas chromatography/mass spectrometry. Marine Chemistry **103**: 84–96. doi:10.1016/j.marchem.2006.06.005

Clark, D. R., A. P. Rees, I. Joint, S. Limnology, N. Jan, D. R. Clark, A. P. Rees, and I. Joint. 2008. Ammonium regeneration and nitrification rates in the oligo trophic Atlantic Ocean : Implications for new production estimates. Limnology and Oceanography **53**: 52–62.

Clarke, A., and R. J. G. Leakey. 1996. microbial community in a nearshore Antarctic marine ecosystem. **41**: 1281–1294.

Clayton, J., and S. Ahmed. 1986. Detection of glutamate synthase (GOGAT) activity in phytoplankton: evaluation of cofactors and assay optimization. Marine Ecology Progress Series **32**: 115–122. doi:10.3354/meps032115

Cloete, R., J. C. Loock, T. Mtshali, S. Fietz, and A. N. Roychoudhury. 2019. Winter and summer distributions of Copper, Zinc and Nickel along the International GEOTRACES Section GIPY05: Insights into deep winter mixing. Chemical Geology **511**: 342–357. doi:10.1016/j.chemgeo.2018.10.023

Coale, K. H., X. Wang, S. J. Tanner, and K. S. Johnson. 2003. Phytoplankton growth and biological response to iron and zinc addition in the Ross Sea and Antarctic Circumpolar Current along 170°W. Deep-Sea Research Part II: Topical Studies in Oceanography **50**: 635–653. doi:10.1016/S0967-0645(02)00588-X

Cochlan, W. P. 1986. Seasonal study of uptake and regeneration of nitrogen on the Scotian Shelf. Continental Shelf Research **5**. doi:10.1016/0278-4343(86)90076-2

Cochlan, W. P. 2008. Nitrogen Uptake in the Southern Ocean. Nitrogen in the Marine Environment 569–596. doi:10.1016/B978-0-12-372522-6.00012-8

Cochlan, W. P., and D. A. Bronk. 2001a. Nitrogen uptake kinetics in the Ross Sea, Antarctica. Deep-Sea Research Part II: Topical Studies in Oceanography **48**: 4127–4153. doi:10.1016/S0967-0645(01)00083-2

Cochlan, W. P., and D. A. Bronk. 2011. Effects of ammonium on nitrate utilization in the Ross Sea, Antarctica: Implications for *ƒ*-ratio estimates, *In*.

Cochlan, W. P., D. A. Bronk, and K. H. Coale. 2002. Trace metals and nitrogenous nutrition of Antarctic phytoplankton: Experimental observations in the Ross Sea. Deep-Sea Research Part II: Topical Studies in Oceanography **49**: 3365–

3390. doi:10.1016/S0967-0645(02)00088-7

Cochlan, W. P., and D. a Bronk. 2001b. Nitrogen uptake kinetics in the Ross Sea, Antarctica. Deep-Sea Research Part Ii-Topical Studies in Oceanography **48**: 4127–4153. doi:Doi 10.1016/S0967-0645(01)00083-2

Cochlan, W. P., N. M. Price, and P. J. Harrison. 1991. Effects of irradiance on nitrogen uptake by phytoplankton: comparison of frontal and stratified communities. Marine Ecology Progress Series **69**. doi:10.3354/meps069103

Coello-Camba, A., and S. Agustí. 2017. Thermal thresholds of phytoplankton growth in polar waters and their consequences for a warming polar ocean. Frontiers in Marine Science **4**: 1–12. doi:10.3389/fmars.2017.00168

Collos, Y. 1998. Nitrate uptake, nitrite release and uptake, and new production estimates. Marine Ecology Progress Series **171**: 293–301. doi:10.3354/meps171293

Collos, Y., and G. Slawyk. 1986. 13C and 15N uptake by marine phytoplankton-IV. Uptake ratios and the contribution of nitrate to the productivity of Antarctic waters (Indian Ocean sector). Deep Sea Research Part A, Oceanographic Research Papers. doi:10.1016/0198-0149(86)90029-4

Constable, A. J., J. Melbourne-Thomas, S. P. Corney, and others. 2014. Climate change and Southern Ocean ecosystems I: How changes in physical habitats directly affect marine biota. Global Change Biology **20**: 3004–3025. doi:10.1111/gcb.12623

Cordoba, F., J. Cardenas, and E. Fernandez. 1986. Kinetic Characterization of Nitrite Uptake and Reduction by Chlamydomonas reinhardtii. Plant Physiology **82**: 904–908. doi:10.1104/pp.82.4.904

Costa, E., J. Pérez, and J. U. Kreft. 2006. Why is metabolic labour divided in nitrification? Trends in Microbiology **14**: 213–219. doi:10.1016/j.tim.2006.03.006

Cota, G. F., W. O. Smith, D. M. Nelson, R. D. Muench, and L. I. Gordon. 1992. Nutrient and biogenic particulate distributions, primary productivity and nitrogen uptake in the Weddell-Scotia Sea marginal ice zone during winter. Journal of Marine Research **50**: 27. doi:http://dx.doi.org/10.1357/002224092784797764

Cox, P. M., R. A. Betts, C. D. Jones, and S. A. Spall. 2000. Nature_Co2-Gw. **408**: 184–187.

Croot, P. L., R. D. Frew, S. Sander, and others. 2007. Physical mixing effects on iron biogeochemical cycling: FeCycle experiment. Journal of Geophysical Research: Oceans **112**: 1–18. doi:10.1029/2006JC003748

Cullen, J. J. 2001. Primary Production Methods. Encyclopedia of Ocean Sciences 2277–2284. doi:10.1006/rwos.2001.0203

Cutter, G. A., J. G. Moffett, M. C. Nielsdóttir, and V. Sanial. 2018. Multiple oxidation state trace elements in suboxic waters off Peru: In situ redox processes and advective/diffusive horizontal transport. Marine Chemistry **201**: 77–89. doi:10.1016/j.marchem.2018.01.003

Daims, H., E. V. Lebedeva, P. Pjevac, and others. 2015. Complete nitrification by Nitrospira bacteria. Nature **528**: 504–509. doi:10.1038/nature16461

Daims, H., S. Lücker, and M. Wagner. 2016. A New Perspective on Microbes Formerly Known as Nitrite-Oxidizing Bacteria. Trends in Microbiology **24**: 699–712. doi:10.1016/j.tim.2016.05.004

Daims, H., J. L. Nielsen, P. H. Nielsen, K. H. Schleifer, and M. Wagner. 2001. In Situ Characterization of Nitrospira-Like Nitrite-Oxidizing Bacteria Active in Wastewater Treatment Plants. Applied and Environmental Microbiology **67**: 5273–5284. doi:10.1128/aem.67.11.5273-5284.2001

Daly, K. L., W. O. Smith, G. C. Johnson, and others. 2001. Hydrography, nutrients, and carbon pools in the Pacific sector of the Southern Ocean: Implications for carbon flux. Journal of Geophysical Research: Oceans **106**: 7107–7124. doi:10.1029/1999jc000090

Damashek, J., B. B. Tolar, Q. Liu, A. O. Okotie-Oyekan, N. J. Wallsgrove, B. N. Popp, and J. T. Hollibaugh. 2019. Microbial oxidation of nitrogen supplied as selected organic nitrogen compounds in the South Atlantic Bight. Limnology and Oceanography **64**: 982–995. doi:10.1002/lno.11089

Dang, H., X. W. Luan, R. Chen, X. Zhang, L. Guo, and M. G. Klotz. 2010. Diversity, abundance and distribution of amoA-encoding archaea in deep-sea methane seep sediments of the Okhotsk Sea. FEMS Microbiology Ecology **72**: 370–385. doi:10.1111/j.1574-6941.2010.00870.x

Davidson, I. R. 1991. Environmental Effects on Algal Photosynthesis: Temperature. Journal of Phycology **27**: 2–8. doi:10.1111/j.0022-3646.1991.00002.x

Deacon, G. E. R. 1982. Physical and biological zonation in the Southern Ocean. Deep Sea Research Part A, Oceanographic Research Papers **29**. doi:10.1016/0198-0149(82)90058-9

Dehairs, F., F. Fripiat, A. J. Cavagna, and others. 2015. Nitrogen cycling in the Southern Ocean Kerguelen Plateau area: Evidence for significant surface nitrification from nitrate isotopic compositions. Biogeosciences **12**: 1459–1482. doi:10.5194/bg-12-1459-2015

Delille, D. 2004. Abundance and function of bacteria in the Southern Ocean. Cellular and molecular biology (Noisy-le-Grand, France) **50**.

Demuynck, P., T. Tyrrell, A. Naveira Garabato, M. C. Moore, and A. P. Martin. 2019. Spatial Variations in Silicate-to-Nitrate Ratios in the Southern Ocean Surface Waters are Controlled in the Short Term by Physics Rather Than Biology. Biogeosciences Discussions 1–33. doi:10.5194/bg-2019-120

Deppeler, S. L., and A. T. Davidson. 2017. Southern Ocean phytoplankton in a changing climate. Frontiers in Marine Science **4**. doi:10.3389/fmars.2017.00040

Devries, T. 2014. The oceanic anthropogenic CO2 sink: Storage, air-sea fluxes, and transports over the industrial era. Global Biogeochemical Cycles **28**: 631–647. doi:10.1002/2013GB004739

DeVries, T., M. Holzer, and F. Primeau. 2017. Recent increase in oceanic carbon uptake driven by weaker upper-ocean overturning. Nature **542**: 215–218. doi:10.1038/nature21068

Diaz, F., and P. Raimbault. 2000. Nitrogen regeneration and dissolved organic nitrogen release during spring in a NW Mediterranean coastal zone (Gulf of Lions): Implications for the estimation of new production. Marine Ecology Progress Series **197**: 51–65. doi:10.3354/meps197051

DiFiore, P. J., D. M. Sigman, and R. B. Dunbar. 2009. Upper ocean nitrogen fluxes in the Polar Antarctic Zone: Constraints from the nitrogen and oxygen isotopes of nitrate. Geochemistry, Geophysics, Geosystems **10**. doi:10.1029/2009GC002468

Difiore, P. J., D. M. Sigman, K. L. Karsh, T. W. Trull, R. B. Dunbar, and R. S. Robinson. 2010. Poleward decrease in the isotope effect of nitrate assimilation across the Southern Ocean. Geophysical Research Letters **37**. doi:10.1029/2010GL044090

DiFiore, P. J., D. M. Sigman, T. W. Trull, M. J. Lourey, K. Karsh, G. Cane, and R. Ho. 2006. Nitrogen isotope constraints on subantarctic biogeochemistry. Journal of Geophysical Research: Oceans **111**: 1–19. doi:10.1029/2005JC003216

Doney, S. C., V. J. Fabry, R. A. Feely, and J. A. Kleypas. 2009. Ocean acidification: The other CO2 problem. Annual Review of Marine Science **1**: 169–192. doi:10.1146/annurev.marine.010908.163834

Dong, S., J. Sprintall, S. T. Gille, and L. Talley. 2008. Southern ocean mixed-layer depth from Argo float profiles. Journal of Geophysical Research: Oceans **113**: 1–12. doi:10.1029/2006JC004051

Dore, J. E., and D. A. I. Karl. 1996. Nitrification in the euphotic zone as a source for nitrite , nitrate , and nitrous oxide at Station ALOHA. **41**: 1619–1628.

Dortch, Q. 1990. The interaction between ammonium and nitrate uptake in phytoplankton. Marine Ecology Progress Series **61**: 183–201. doi:10.3354/meps061183

Downes, S. M., A. S. Budnick, J. L. Sarmiento, and R. Farneti. 2011. Impacts of wind stress on the Antarctic Circumpolar Current fronts and associated subduction. Geophysical Research Letters **38**: 3–8. doi:10.1029/2011GL047668

Ducklow, H. W., D. Eborah, K. Steinberg, and K. O. Buesseler. 2001a. Upper ocean carbon export and the biological pump. Oceanography **14**: 50–58. doi:10.5670/oceanog.2001.06

Ducklow, H. W., D. K. Steinberg, and K. O. Buesseler. 2001b. Upper ocean carbon export and the biological pump. Oceanography **14**: 50–58. doi:10.5670/oceanog.2001.06

Dugdale, R. C. 1967. Limitation in the Sea : DYNAMICS, IDENTIFICATION, AND SIGNIFICANCE. Limnology and Oceanography 685–695.

Dugdale, R. C., and J. J. Goering. 1967. Uptake of new and regenerated forms of nitrogen in primary productivity. Limnology and Oceanography **12**: 196–206. doi:10.4319/lo.1967.12.2.0196

Dugdale, R. C., and F. P. Wilkerson. 1986. the Use of N-15 To Measure Nitrogen Uptake in Eutrophic Oceans - Experimental Considerations. Limnology and Oceanography **31**: 673–689.

El-Sayed, S. Z. 1984. Productivity of Antarctic waters - a reappraisal. Marine phytoplankton and productivity. Proc. symposium, Taormina, 1983. doi:10.1029/ln008p0019

EL-SAYED, and S. Z. 1987. Biological productivity of Antarctic waters: present paradoxes and emerging paradigms. BIOMASS Scientific Series 7 1–22.

Ellwood, M. J. 2008. Wintertime trace metal (Zn, Cu, Ni, Cd, Pb and Co) and nutrient distributions in the Subantarctic Zone

between 40-52°S; 155-160°E. Marine Chemistry **112**: 107–117. doi:10.1016/j.marchem.2008.07.008

Ellwood, M. J., P. W. Boyd, and P. Sutton. 2008. Winter-time dissolved iron and nutrient distributions in the Subantarctic Zone from 40-52S; 155-160E. Geophysical Research Letters **35**: 2–7. doi:10.1029/2008GL033699

Ellwood, M. J., D. A. Hutchins, M. C. Lohan, and others. 2014. Iron stable isotopes track pelagic iron cycling during a subtropical phytoplankton bloom. Proceedings of the National Academy of Sciences of the United States of America **112**: E15–E20. doi:10.1073/pnas.1421576112

Emerson, S. 2014. Global Biogeochemical Cycles the biological carbon flux in the ocean. Global Biogeochemical Cycles 14–28. doi:10.1002/2013GB004680

Emerson, S., and J. Hedges. 2008. Chemical oceanography and the marine carbon cycle,.

Eppley, R. 1972. Temperature and phytoplankton growth in the sea. Fishery bulletin **70**: 1063–85.

Eppley, R. W., and B. J. Peterson. 1979. Particulate organic matter flux and planktonic new production in the deep ocean. Nature **282**: 677–680. doi:10.1038/282677a0

Eppley, R. W., J. N. Rogers, and J. J. Mccarthy. 1969. HALF-SATURATION CONSTANTS FOR UPTAKE OF NITRATE AND AMMONIUM BY MARINE PHYTOPLANKTON. Limonology And Oceanography **14**: 912–920.

Erguder, T. H., N. Boon, L. Wittebolle, M. Marzorati, and W. Verstraete. 2009. Environmental factors shaping the ecological niches of ammonia-oxidizing archaea. FEMS Microbiology Reviews **33**: 855–869. doi:10.1111/j.1574-6976.2009.00179.x

Evans, C., S. D. Archer, S. Jacquet, and W. H. Wilson. 2003. Direct estimates of the contribution of viral lysis. **30**: 207–219.

Evans, C., J. Brandsma, M. P. Meredith, D. N. Thomas, H. J. Venables, D. W. Pond, and C. P. D. Brussaard. 2021. Shift from carbon flow through the microbial loop to the viral shunt in coastal antarctic waters during austral summer. Microorganisms **9**: 1–13. doi:10.3390/microorganisms9020460

Evans, C., and C. P. D. Brussaard. 2012. Viral lysis and microzooplankton grazing of phytoplankton throughout the Southern Ocean. Limnology and Oceanography **57**: 1826–1837. doi:10.4319/lo.2012.57.6.1826

Fabry, V. J., J. B. McClintock, J. T. Mathis, and J. M. Grebmeier. 2009. Ocean acidification at high latitudes: The Bellwether. Oceanography **22**: 160–171. doi:10.5670/oceanog.2009.105

Fawcett, S. E., and B. B. Ward. 2011. Phytoplankton succession and nitrogen utilization during the development of an upwelling bloom. Marine Ecology Progress Series **428**: 13–31. doi:10.3354/meps09070

Feely, R. A., S. C. Doney, and S. R. Cooley. 2009. Ocean acidification: present conditions and future changes in a high-CO2 world. Oceanography **2**: 21–40. doi:10.1017/cbo9781139198776.020

Fenchel, T. 2008. The microbial loop - 25 years later. Journal of Experimental Marine Biology and Ecology **366**: 99–103. doi:10.1016/j.jembe.2008.07.013

Feng, Y., C. E. Hare, J. M. Rose, and others. 2010. Interactive effects of iron, irradiance and CO2 on Ross Sea phytoplankton. Deep-Sea Research Part I: Oceanographic Research Papers **57**: 368–383. doi:10.1016/j.dsr.2009.10.013

Fernández I., C., and P. Raimbault. 2007. Nitrogen regeneration in the NE Atlantic Ocean and its impact on seasonal new, regenerated and export production. Marine Ecology Progress Series **337**: 79–92. doi:10.3354/meps337079

Fernández, I. C., P. Raimbault, N. Garcia, P. Rimmelin, and G. Caniaux. 2005. An estimation of annual new production and carbon fluxes in the northeast Atlantic Ocean during 2001. Journal of Geophysical Research C: Oceans **110**: 1–15. doi:10.1029/2004JC002616

Fiala, M., and L. Oriol. 1990. Light-temperature interactions on the growth of Antarctic diatoms. Polar Biology **10**. doi:10.1007/BF00239374

Fielding, S., P. Ward, R. T. Pollard, S. Seeyave, J. F. Read, J. A. Hughes, T. Smith, and C. Castellani. 2007. Community structure and grazing impact of mesozooplankton during late spring/early summer 2004/2005 in the vicinity of the Crozet Islands (Southern Ocean). Deep-Sea Research Part II: Topical Studies in Oceanography **54**. doi:10.1016/j.dsr2.2007.06.016

Figuerola, B., A. M. Hancock, N. Bax, V. J. Cummings, R. Downey, H. J. Griffiths, J. Smith, and J. S. Stark. 2021. A Review and Meta-Analysis of Potential Impacts of Ocean Acidification on Marine Calcifiers From the Southern Ocean. Frontiers in Marine Science **8**. doi:10.3389/fmars.2021.584445

Flynn, R. F., J. M. Burger, K. Pillay, and S. E. Fawcett. 2018. Wintertime rates of net primary production and nitrate and ammonium uptake in the southern Benguela upwelling system. African Journal of Marine Science **40**: 253–266.

doi:10.2989/1814232X.2018.1502095

Fouilland, E., M. Gosselin, R. B. Rivkin, C. Vasseur, and B. Mostajir. 2007. Nitrogen uptake by heterotrophic bacteria and phytoplankton in Arctic surface waters. Journal of Plankton Research **29**: 369–376. doi:10.1093/plankt/fbm022

Francis, C. A., G. D. O'Mullan, and B. B. Ward. 2003. Diversity of ammonia monooxygenase (amoA) genes across environmental gradients in Chesapeake Bay sediments. Geobiology **1**. doi:10.1046/j.1472-4669.2003.00010.x

Francis, C. A., K. J. Roberts, J. M. Beman, A. E. Santoro, and B. B. Oakley. 2005. Ubiquity and diversity of ammonia-oxidizing archaea in water columns and sediments of the ocean. Proceedings of the National Academy of Sciences of the United States of America **102**: 14683–14688. doi:10.1073/pnas.0506625102

Franck, V. M., M. A. Brzezinski, K. H. Coale, and D. M. Nelson. 2000. Iron and silicic acid concentrations regulate Si uptake north and south of the Polar Frontal Zone in the Pacific Sector of the Southern Ocean. Deep-Sea Research Part II: Topical Studies in Oceanography **47**: 3315–3338. doi:10.1016/S0967-0645(00)00070-9

Freeman, N. M., N. S. Lovenduski, D. R. Munro, K. M. Krumhardt, K. Lindsay, M. C. Long, and M. Maclennan. 2018. The Variable and Changing Southern Ocean Silicate Front: Insights From the CESM Large Ensemble. Global Biogeochemical Cycles **32**: 752–768. doi:10.1029/2017GB005816

Fripiat, F., M. Elskens, T. W. Trull, and others. 2015. Significant mixed layer nitrification in a natural iron-fertilized bloom of the Southern Ocean. Global Biogeochemical Cycles. doi:10.1002/2014GB005051

Fripiat, F., A. S. Studer, G. H. Haug, and others. 2019. The isotope effect of nitrate assimilation in the Antarctic Zone: Improved estimates and paleoceanographic implications. Geochimica et Cosmochimica Acta **247**: 261–279. doi:10.1016/j.gca.2018.12.003

Frölicher, T. L., J. L. Sarmiento, D. J. Paynter, J. P. Dunne, J. P. Krasting, and M. Winton. 2015. Dominance of the Southern Ocean in anthropogenic carbon and heat uptake in CMIP5 models. Journal of Climate **28**: 862–886. doi:10.1175/JCLI-D-14-00117.1

Froneman, P. W., Laubscher, K.L., and Mcquaid, D. C. 2001. Size-fractionated Primary Production in the South Atlantic and Atlantic Sectors of the Southern Ocean. Journal of Plankton Research **23**: 611–622. doi:10.1093/plankt/23.6.611

Froneman, P. W., I. J. Ansorge, E. A. Pakhomovo, and J. R. E. Lutjeharms. 1999. Plankton community structure in the physical environment surrounding the Prince Edward Islands (Southern Ocean). Polar Biology **22**: 145–155. doi:10.1007/s003000050404

Froneman, P. W., and R. Perissinotto. 1996. Microzooplankton grazing and protozooplankton community structure in the South Atlantic and in the Atlantic sector of the Southern Ocean. Deep-Sea Research Part I: Oceanographic Research Papers **43**. doi:10.1016/0967-0637(96)00010-6

Froneman, P. W., R. Perissinotto, C. D. McQuaid, and R. K. Laubscher. 1995. Summer distribution of netphytoplankton in the Atlantic sector of the Southern Ocean. Polar Biology **15**: 77–84. doi:10.1007/BF00241045

Fu, W., J. T. Randerson, and J. Keith Moore. 2016. Climate change impacts on net primary production (NPP) and export production (EP) regulated by increasing stratification and phytoplankton community structure in the CMIP5 models. Biogeosciences **13**: 5151–5170. doi:10.5194/bg-13-5151-2016

Fulweiler, R. W., H. E. Emery, E. M. Heiss, and V. M. Berounsky. 2011. Assessing the Role of pH in Determining Water Column Nitrification Rates in a Coastal System. Estuaries and Coasts **34**: 1095–1102. doi:10.1007/s12237-011-9432-4

Füssel, J., P. Lam, G. Lavik, M. M. Jensen, M. Holtappels, M. Günter, and M. M. M. Kuypers. 2012. Nitrite oxidation in the Namibian oxygen minimum zone. ISME Journal **6**: 1200–1209. doi:10.1038/ismej.2011.178

Füssel, J., S. Lücker, P. Yilmaz, and others. 2017. Adaptability as the key to success for the ubiquitous marine nitrite oxidizer Nitrococcus. Science Advances **3**: 2–10. doi:10.1126/sciadv.1700807

Gandhi, N., R. Ramesh, A. H. Laskar, M. S. Sheshshayee, S. Shetye, N. Anilkumar, S. M. Patil, and R. Mohan. 2012. Zonal variability in primary production and nitrogen uptake rates in the southwestern Indian Ocean and the Southern Ocean. Deep Sea Research Part I: Oceanographic Research Papers **67**: 32–43. doi:10.1016/j.dsr.2012.05.003

Geider, R. J., and J. La Roche. 1994. The role of iron in phytoplankton photosynthesis, and the potential for iron-limitation of primary productivity in the sea. Photosynthesis Research **39**. doi:10.1007/BF00014588

Gerringa, L. J. A., A. C. Alderkamp, P. Laan, and others. 2012. Iron from melting glaciers fuels the phytoplankton blooms in Amundsen Sea (Southern Ocean): Iron biogeochemistry. Deep-Sea Research Part II: Topical Studies in Oceanography **71**–**76**: 16–31. doi:10.1016/j.dsr2.2012.03.007

Gibberd, M. J., E. Kean, R. Barlow, S. Thomalla, and M. Lucas. 2013. Phytoplankton chemotaxonomy in the Atlantic sector

of the Southern Ocean during late summer 2009. Deep-Sea Research Part I: Oceanographic Research Papers **78**: 70–78. doi:10.1016/j.dsr.2013.04.007

Glibert, P. M., M. R. Dennett, and J. C. Goldman. 1985. Inorganic carbon uptake by phytoplankton in Vineyard Sound, Massachusetts. II. Comparative primary productivity and nutritional status of winter and summer assemblages. Journal of Experimental Marine Biology and Ecology **86**. doi:10.1016/0022-0981(85)90025-5

Glibert, P. M., F. Lipschultz, J. J. Mccarthy, and M. a. Altabet. 1982. Isotope Dilution Models of Uptake and Remineralization of Ammonium By Marine Plankton. Limnology and Oceanography **27**: 639–650. doi:10.4319/lo.1982.27.4.0639

Glibert, P. M., F. P. Wilkerson, R. C. Dugdale, and others. 2016. Pluses and minuses of ammonium and nitrate uptake and assimilation by phytoplankton and implications for productivity and community composition, with emphasis on nitrogen-enriched conditions. Limnology and Oceanography **61**: 165–197. doi:10.1002/lno.10203

Goeyens, L., P. Tréguer, M. E. M. Baumann, W. Baeyens, and F. Dehairs. 1995. The leading role of ammonium in the nitrogen uptake regime of Southern Ocean marginal ice zones. Journal of Marine Systems **6**: 345–361. doi:10.1016/0924-7963(94)00033-8

Goeyens, L., P. Treguer, C. Lancelot, S. Mathot, S. Becquevort, J. Morvan, F. Dehairs, and W. Baeyens. 1991. Ammonium regeneration in the Scotia-Weddell Confluence area during spring 1988. Marine Ecology Progress Series **78**: 241–252. doi:10.3354/meps078241

González, M. L., V. Molina, L. Florez-Leiva, L. Oriol, A. J. Cavagna, F. Dehairs, L. Farias, and C. Fernandez. 2014. Nitrogen fixation in the Southern Ocean: a case of study of the Fe-fertilized Kerguelen region (KEOPS II cruise). Biogeosciences Discussions. doi:10.5194/bgd-11-17151-2014

Gordon, A. L., D. T. Georgi, and H. W. Taylor. 1977. Antarctic Polar Front Zone in the Western Scotia Sea - Summer 1975. Journal of Physical Oceanography **7**: 309–328. doi:10.1175/1520-0485(1977)007<0309:APFZIT>2.0.CO;2

Graham, R. M., and A. M. De Boer. 2013. The dynamical subtropical front. Journal of Geophysical Research: Oceans **118**: 5676–5685. doi:10.1002/jgrc.20408

Grasshoff K, Ehrhardt M, and, K. K. 1983. Methods of seawater analysis, Verlag Chemie, New York.

Gray, A. R., K. S. Johnson, S. M. Bushinsky, and others. 2018. Autonomous Biogeochemical Floats Detect Significant Carbon Dioxide Outgassing in the High-Latitude Southern Ocean. Geophysical Research Letters **45**: 9049–9057. doi:10.1029/2018GL078013

Gregor, L., S. Kok, and P. M. S. Monteiro. 2018. Interannual drivers of the seasonal cycle of CO2 in the Southern Ocean. Biogeosciences **15**: 2361–2378. doi:10.5194/bg-15-2361-2018

Grotti, M., F. Soggia, M. L. Abelmoschi, P. Rivaro, E. Magi, and R. Frache. 2001. Temporal distribution of trace metals in Antarctic coastal waters. Marine Chemistry **76**: 189–209. doi:10.1016/S0304-4203(01)00063-9

Gruber, N. 2008. The Marine Nitrogen Cycle. Nitrogen in the Marine Environment 1–50. doi:10.1016/B978-0-12-372522-6.00001-3

Gruber, N., D. Clement, B. R. Carter, and others. 2019a. The oceanic sink for anthropogenic CO 2 from 1994 to 2007. Science **363**: 1193–1199. doi:10.1126/science.aau5153

Gruber, N., M. Gloor, S. E. Mikaloff Fletcher, and others. 2009. Oceanic sources, sinks, and transport of atmospheric CO2. Global Biogeochemical Cycles **23**: 1–21. doi:10.1029/2008GB003349

Gruber, N., P. Landschützer, and N. S. Lovenduski. 2019b. The variable Southern Ocean Carbon Sink. Annual Review of Marine Science **11**: 159–186. doi:10.1126/sciadv.aav6471

Guerrero, M. A., and R. D. Jones. 1996. Photoinhibition of marine nitrifying bacteria. I. Wavelength-dependent response. Marine Ecology Progress Series **141**: 183–192. doi:10.3354/meps141183

Gwak, J. H., M. Y. Jung, H. Hong, and others. 2020. Archaeal nitrification is constrained by copper complexation with organic matter in municipal wastewater treatment plants. ISME Journal **14**: 335–346. doi:10.1038/s41396-019-0538-1

Haas, S., B. M. Robicheau, S. Rakshit, J. Tolman, C. K. Algar, J. LaRoche, and D. W. R. Wallace. 2021. Physical mixing in coastal waters controls and decouples nitrification via biomass dilution. Proceedings of the National Academy of Sciences of the United States of America **118**. doi:10.1073/pnas.2004877118

Hallam, S. J., K. T. Konstantinidis, N. Putnam, and others. 2006a. Genomic analysis of the uncultivated marine crenarchaeote Cenarchaeum symbiosum. Proceedings of the National Academy of Sciences of the United States of America **103**: 18296–18301. doi:10.1073/pnas.0608549103

Hallam, S. J., T. J. Mincer, C. Schleper, C. M. Preston, K. Roberts, P. M. Richardson, and E. F. DeLong. 2006b. Pathways of

carbon assimilation and ammonia oxidation suggested by environmental genomic analyses of marine Crenarchaeota. PLoS Biology **4**: 520–536. doi:10.1371/journal.pbio.0040095

Hanawa, K., and L. D.Talley. 2001. Chapter 5.4 Mode waters. International Geophysics **77**: 373–386. doi:10.1016/S0074-6142(01)80129-7

Hancock, A. M., A. T. Davidson, J. McKinlay, A. McMinn, K. G. Schulz, and R. L. Van Den Enden. 2018. Ocean acidification changes the structure of an Antarctic coastal protistan community. Biogeosciences **15**: 2393–2410. doi:10.5194/bg-15-2393-2018

Harrison, A. W. G., L. R. Harris, B. D. Irwin, B. O. Section, N. S. By, and W. G. Harrison. 1996. The kinetics of nitrogen utilization in the oceanic mixed layer: Nitrate and ammonium interactions at nanomolar concentrations. Limnology and Oceanography **41**: 16–32.

Harrison, W. G., and T. Platt. 1986. Photosynthesis-irradiance relationships in polar and temperate phytoplankton populations. Polar Biology **5**. doi:10.1007/BF00441695

Harrison, W., and L. Harris. 1986. Isotope-dilution and its effects on measurements of nitrogen and phosphorus uptake by oceanic microplankton. Marine Ecology Progress Series **27**: 253–261. doi:10.3354/meps027253

Hart, T. J. 1942. Phytoplankton periodicity in Antarctic surface waters (Discovery reports). Geographical Review **35**. doi:10.2307/211499

Hashimoto, L. K., W. A. Kaplan, S. C. Wofsy, and M. B. McElroy. 1983. Transformations of fixed nitrogen and N2O in the Cariaco Trench. Deep Sea Research Part A, Oceanographic Research Papers. doi:10.1016/0198-0149(83)90037-7

Hauck, J., C. Völker, D. A. Wolf-Gladrow, and others. 2015. On the Southern Ocean CO2 uptake and the role of the biological carbon pump in the 21st century. Global Biogeochemical Cycles **29**: 1451–1470. doi:10.1002/2015GB005140

Hauri, C., T. Friedrich, and A. Timmermann. 2016. Abrupt onset and prolongation of aragonite undersaturation events in the Southern Ocean. Nature Climate Change **6**: 172–176. doi:10.1038/nclimate2844

He, H., Y. Zhen, T. Mi, L. Fu, and Z. Yu. 2018. Ammonia-oxidizing archaea and bacteria differentially contribute to ammonia oxidation in sediments from adjacent waters of Rushan Bay, China. Frontiers in Microbiology **9**: 1–14. doi:10.3389/fmicb.2018.00116

Heil, C. A., M. Revilla, P. M. Glibert, and S. Murasko. 2007. Nutrient quality drives differential phytoplankton community composition on the southwest Florida shelf. Limnology and Oceanography **52**: 1067–1078. doi:10.4319/lo.2007.52.3.1067

Heiss, E. M., and R. W. Fulweiler. 2016. Coastal water column ammonium and nitrite oxidation are decoupled in summer. Estuarine, Coastal and Shelf Science **178**: 110–119. doi:10.1016/j.ecss.2016.06.002

Heiss, E. M., and R. W. Fulweiler. 2017. Erratum to “Coastal water column ammonium and nitrite oxidation are decoupled in summer” (Estuarine, Coastal and Shelf Science (2016) 178 (110–119) (S0272771417301981) (10.1016/j.ecss.2017.02.023)). Estuarine, Coastal and Shelf Science **193**: 37–45. doi:10.1016/j.ecss.2016.12.026

Heller, M. I., and P. L. Croot. 2015. Copper speciation and distribution in the Atlantic sector of the Southern Ocean. Marine Chemistry **173**: 253–268. doi:10.1016/j.marchem.2014.09.017

Henley, S. F., E. L. Cavan, S. E. Fawcett, and others. 2020. Changing Biogeochemistry of the Southern Ocean and Its Ecosystem Implications,.

Henley, S. F., R. E. Tuerena, A. L. Annett, A. E. Fallick, M. P. Meredith, H. J. Venables, A. Clarke, and R. S. Ganeshram. 2017. Macronutrient supply, uptake and recycling in the coastal ocean of the west Antarctic Peninsula. Deep-Sea Research Part II: Topical Studies in Oceanography **139**: 58–76. doi:10.1016/j.dsr2.2016.10.003

Hense, I., U. V. Bathmann, and R. Timmermann. 2000. Plankton dynamics in frontal systems of the Southern Ocean. Journal of Marine Systems **27**: 235–252. doi:10.1016/S0924-7963(00)00070-1

Hense, I., R. Timmermann, A. Beckmann, and U. V. Bathmann. 2003. Regional ecosystem dynamics in the ACC: Simulations with a three-dimensional ocean-plankton model. Journal of Marine Systems. doi:10.1016/S0924-7963(03)00063-0

Henson, S. A., R. Sanders, E. Madsen, P. J. Morris, F. Le Moigne, and G. D. Quartly. 2011. A reduced estimate of the strength of the ocean ’ s biological carbon pump. **38**: 10–14. doi:10.1029/2011GL046735

Herraiz-Borrenguero, L., D. Lannuzel, P. van de Merwe, A. Treverrow, and J. B. Pedro. 2016. Large flux of iron from the Amery Ice Shelf marine ice to Prydz Bay, East Antarctica. Journal of Geophysical Research: Oceans 1–14. doi:10.1002/2015JC011486.Received

Hiscock, M. R., V. P. Lance, A. M. Apprill, R. R. Bidigare, Z. I. Johnson, B. G. Mitchell, W. O. Smith, and R. T. Barber. 2008. Photosynthetic maximum quantum yield increases are an essential component of the Southern Ocean phytoplankton response to iron. Proceedings of the National Academy of Sciences of the United States of America **105**: 4775–4780. doi:10.1073/pnas.0705006105

Holl, C. M., and J. P. Montoya. 2005. Interactions between nitrate uptake and nitrogen fixation in continuous cultures of the marine diazotroph Trichodesmium (Cyanobacteria). Journal of Phycology **41**: 1178–1183. doi:10.1111/j.1529-8817.2005.00146.x

Holmes, R. M., A. Aminot, R. Kerouel, B. A. Hooker, and B. J. Peterson. 1999. A simple and precise method for measuring ammonium in marine and freshwater ecosystems. Canadian Journal of Fisheries and Aquatic Sciences **56**: 1801–1808. doi:10.1139/cjfas-56-10-1801

Holmes, T. M., K. Wuttig, Z. Chase, P. van der Merwe, A. T. Townsend, C. Schallenberg, M. Tonnard, and A. R. Bowie. 2019. Iron availability influences nutrient drawdown in the Heard and McDonald Islands region, Southern Ocean. Marine Chemistry **211**: 1–14. doi:10.1016/j.marchem.2019.03.002

Hooper, A. B., and K. R. Terry. 1974. Photoinactivation of ammonia oxidation in Nitrosomonas. Journal of Bacteriology **119**: 899–906.

Horak, R. E. A., W. Qin, A. D. Bertagnolli, and others. 2018. Relative impacts of light, temperature, and reactive oxygen on thaumarchaeal ammonia oxidation in the North Pacific Ocean. Limnology and Oceanography **63**: 741–757. doi:10.1002/lno.10665

Horak, R. E. A., W. Qin, A. J. Schauer, E. V. Armbrust, A. E. Ingalls, J. W. Moffett, D. A. Stahl, and A. H. Devol. 2013. Ammonia oxidation kinetics and temperature sensitivity of a natural marine community dominated by Archaea. ISME Journal **7**: 2023–2033. doi:10.1038/ismej.2013.75

Horrigan, S., F. Carlucci, and P. Williams. 1981. Light inhibition of nitrification in sea surface films. Journal of Marine Research **39:** 557–565.

Horrigan, S. G., J. P. Montoya, J. L. Nevins, J. J. McCarthy, H. Ducklow, R. Goericke, and T. Malone. 1990. Nitrogenous nutrient transformations in the spring and fall in the Chesapeake Bay. Estuarine, Coastal and Shelf Science **30**. doi:10.1016/0272-7714(90)90004-B

Horrigan, S. G., and A. L. Springer. 1990. Oceanic and estuarine ammonium oxidation: Effects of light. Association for the Sciences of Limnology and Oceanography **35**.

Hörstmann, C., E. Raes, P. L. Buttigieg, C. Lo Monaco, U. John, and A. Waite. 2021. Hydrographic fronts shape productivity, nitrogen fixation, and microbial community composition in the South Indian Ocean and the Southern Ocean. Biogeosciences Discussions 1–32. doi:10.5194/bg-2021-52

Hu, S., and W. O. Smith. 1998. The effects of irradiance on nitrate uptake and dissolved organic nitrogen release by phytoplankton in the Ross Sea. Continental Shelf Research **18**: 971–990. doi:10.1016/S0278-4343(98)00021-1

Huesemann, M. H., A. D. Skillman, and E. A. Crecelius. 2002. The inhibition of marine nitrification by ocean disposal of carbon dioxide. Marine Pollution Bulletin **44**: 142–148. doi:10.1016/S0025-326X(01)00194-1

Huisman, J., P. Van Oostveen, and F. J. Weissing. 1999. Critical depth and critical turbulence: Two different mechanisms for the development of phytoplankton blooms. Limnology and Oceanography **44**. doi:10.4319/lo.1999.44.7.1781

Hutchins, D. A., and P. W. Boyd. 2016. Marine phytoplankton and the changing ocean iron cycle. Nature Climate Change **6**: 1072–1079. doi:10.1038/nclimate3147

Hutchins, D. A., and K. W. Bruland. 1998. Iron-limited growth and Si:N ratios in a costal upwelling regime. Nature **393**: 561–564.

Hutchins, D. A., a. C. Crossley, G. R. DiTullio, F. B. Griffiths, P. W. Boyd, B. Queguiner, P. N. Sedwick, and T. W. Trull. 2001. Control of phytoplankton growth by iron and silicic acid availability in the subantarctic Southern Ocean: Experimental results from the SAZ Project. Journal of Geophysical Research **106**: 31573. doi:10.1029/2000JC000348

IPCC. 2019. IPCC Special Report on the Ocean and Cryosphere in a Changing Climate.

Iriarte, A., I. De Madariaga, F. Diez-Garagarza, M. Revilla, and E. Orive. 1997. Primary plankton production, respiration and nitrification in a shallow temperate estuary during summer. Journal of Experimental Marine Biology and Ecology. doi:10.1016/S0022-0981(96)02672-X

Irigoien, X., K. J. Flynn, and R. P. Harris. 2005. Phytoplankton blooms: A “loophole” in microzooplankton grazing impact? Journal of Plankton Research **27**: 313–321. doi:10.1093/plankt/fbi011

Jacob, J., B. Nowka, V. Merten, T. Sanders, E. Spieck, and K. Dähnke. 2017. Oxidation kinetics and inverse isotope effect

of marine nitrite-oxidizing isolates. Aquatic Microbial Ecology **80**: 289–300. doi:10.3354/ame01859

Jacques, G. 1991a. Is the concept of new production regenerated production valid for the Southern Ocean.

Jacques, G. 1991b. Is the concept of new production—regenerated production valid for the Southern Ocean? Marine Chemistry. doi:10.1016/S0304-4203(09)90022-6

Janssen, D. J., M. Sieber, M. J. Ellwood, and others. 2020. Trace metal and nutrient dynamics across broad biogeochemical gradients in the Indian and Pacific sectors of the Southern Ocean. Marine Chemistry **221**. doi:10.1016/j.marchem.2020.103773

Jiang, L. Q., R. A. Feely, B. R. Carter, D. J. Greeley, D. K. Gledhill, and K. M. Arzayus. 2015. Climatological distribution of aragonite saturation state in the global oceans. Global Biogeochemical Cycles **29**: 1656–1673. doi:10.1002/2015GB005198

Jickells, T. D., J. K. Moore, A. Oschlies, and others. 2017. A reevaluation of the magnitude and impacts of anthropogenic atmospheric nitrogen inputs on the ocean. Global Biogeochemical Cycles 289–305. doi:10.1002/2016gb005586

Jochem, F. J., S. Mathot, and B. Quéguiner. 1995. Size-fractionated primary production in the open Southern Ocean in austral spring. Polar Biology **15**: 381–392. doi:10.1007/BF00239714

Johnson, K. S., J. N. Plant, J. P. Dunne, L. D. Talley, and J. L. Sarmiento. 2017. Annual nitrate drawdown observed by SOCCOM profiling floats and the relationship to annual net community production. Journal of Geophysical Research: Oceans **122**: 6668–6683. doi:10.1002/2017JC012839

Jones, E. M., D. C. E. Bakker, H. J. Venables, and N. J. Hardman-Mountford. 2015. Seasonal cycle of CO2 from the sea ice edge to island blooms in the Scotia Sea, Southern Ocean. Marine Chemistry **177**: 490–500. doi:10.1016/j.marchem.2015.06.031

Jones, E. M., D. C. E. Bakker, H. J. Venables, and A. J. Watson. 2012. Dynamic seasonal cycling of inorganic carbon downstream of South Georgia, Southern Ocean. Deep-Sea Research Part II: Topical Studies in Oceanography **59**–**60**: 25–35. doi:10.1016/j.dsr2.2011.08.001

Jones, E. M., M. Fenton, M. P. Meredith, N. M. Clargo, S. Ossebaar, H. W. Ducklow, H. J. Venables, and H. J. W. de Baar. 2017. Ocean acidification and calcium carbonate saturation states in the coastal zone of the West Antarctic Peninsula. Deep-Sea Research Part II: Topical Studies in Oceanography **139**: 181–194. doi:10.1016/j.dsr2.2017.01.007

Jones, R. D., R. Y. Morita, H.-P. Koops, and S. W. Watson. 1988. A new marine ammonium-oxidizing bacterium, Nitrosomonas cryotolerans sp. nov. . Canadian Journal of Microbiology. doi:10.1139/m88-198

de Jong, E., M. Vichi, C. B. Mehlmann, C. Eayrs, W. De Kock, M. Moldenhauer, and R. R. Audh. 2018. Sea Ice conditions within the Antarctic Marginal Ice Zone in winter 2017, onboard the SA Agulhas II. Pangaea 2018. doi:10.1594/PANGAEA.885211

Joubert, W. R., S. J. Thomalla, H. N. Waldron, M. I. Lucas, M. Boye, F. A. C. Le Moigne, F. Planchon, and S. Speich. 2011. Nitrogen uptake by phytoplankton in the Atlantic sector of the Southern Ocean during late austral summer. Biogeosciences **8**: 2947–2959. doi:10.5194/bg-8-2947-2011

Kalvelage, T., G. Lavik, P. Lam, and others. 2013. Nitrogen cycling driven by organic matter export in the South Pacific oxygen minimum zone. Nature Geoscience **6**: 228–234. doi:10.1038/ngeo1739

Kamennaya, N. A., and A. F. Post. 2013. Distribution and expression of the cyanate acquisition potential among cyanobacterial populations in oligotrophic marine waters. Limnology and Oceanography **58**: 1959–1971. doi:10.4319/lo.2013.58.6.1959

Kanakidou, M., K. Tsigaridis, N. Mahowald, and others. 2012. Atmospheric fluxes of organic N and P to the global ocean. Global Biogeochemical Cycles **26**: 1–12. doi:10.1029/2011gb004277

Kanda, J., T. Saino, and A. Hattori. 1985. Nitrogen uptake by natural populations of phytoplankton and primary production in the Pacific Ocean: Regional variability of uptake capacity. Limnology and Oceanography **30**: 987–999. doi:10.4319/lo.1985.30.5.0987

Karl, D., R. Letelier, L. Tupas, J. Dore, J. Christian, and D. Hebel. 1997. The role of nitrogen fixation in biogeochemical cycling in the subtropical North Pacific Ocean. Nature **388**: 533–538. doi:10.1038/41474

Karsh, K. L., T. W. Trull, M. J. Lourey, and D. M. Sigman. 2003. Relationship of nitrogen isotope fractionation to phytoplankton size and iron availability during the Southern Ocean Iron RElease Experiment (SOIREE). Limnology and Oceanography **48**: 1058–1068. doi:10.4319/lo.2003.48.3.1058

Keith Moore, J., W. Fu, F. Primeau, and others. 2018. Sustained climate warming drives declining marine biological productivity. Science **359**: 113–1143. doi:10.1126/science.aao6379

Kemeny, P. C., E. R. Kast, M. P. Hain, and others. 2018. A Seasonal Model of Nitrogen Isotopes in the Ice Age Antarctic Zone: Support for Weakening of the Southern Ocean Upper Overturning Cell. Paleoceanography and Paleoclimatology. doi:10.1029/2018PA003478

Kemeny, P. C., M. A. Weigand, R. Zhang, B. R. Carter, K. L. Karsh, S. E. Fawcett, and D. M. Sigman. 2016. Enzyme-level interconversion of nitrate and nitrite in the fall mixed layer of the Antarctic Ocean. Global Biogeochemical Cycles **30**: 1069–1085. doi:10.1002/2015GB005350

Kendall, C. 1998. USGS -- Isotope Tracers -- Resources: Isotope Tracers in Catchment Hydrology -- Chapter 16. Isotope Tracers in Catchment Hydrology Elsevier Science B.V.

Kerr, R., C. Goyet, L. C. da Cunha, and others. 2018. Carbonate system properties in the Gerlache Strait, Northern Antarctic Peninsula (February 2015): II. Anthropogenic CO2 and seawater acidification. Deep-Sea Research Part II: Topical Studies in Oceanography **149**: 182–192. doi:10.1016/j.dsr2.2017.07.007

van Kessel, M. A. H. J., D. R. Speth, M. Albertsen, P. H. Nielsen, H. J. M. Op den Camp, B. Kartal, M. S. M. Jetten, and S. Lücker. 2015. Complete nitrification by a single microorganism. Nature **528**: 555–559. doi:10.1038/nature16459

Key, R. M., A. Kozyr, C. L. Sabine, and others. 2004. A global ocean carbon climatology: Results from Global Data Analysis Project (GLODAP). Global Biogeochemical Cycles **18**: 1–23. doi:10.1029/2004GB002247

Key, R. M., A. Olsen, S. van Heuven, and others. 2015. Global Ocean Data Analysis Project, Version 2 (GLODAPv2). ORNL/CDIAC- 162, NDP-093. Carbon Dioxide Information Analysis Center, Oak Ridge National Laboratory, US Dept. of Energy, Oak Ridge, Tennessee. doi: 10.3334/CDIAC/OTG.NDP093_GLODAPv2 **2**. doi:doi: 10.3334/CDIAC/OTG.NDP093_GLODAPv2 Here

Khatiwala, S., F. Primeau, and T. Hall. 2009. Reconstruction of the history of anthropogenic CO2 concentrations in the ocean. Nature **462**: 346–349. doi:10.1038/nature08526

Kiefer, D. A., R. J. Olson, and O. Holm-Hansen. 1976. Another look at the nitrite and chlorophyll maxima in the central North Pacific. Deep-Sea Research and Oceanographic Abstracts **23**. doi:10.1016/0011-7471(76)90895-0

Kim, B. K., H. M. Joo, J. Jung, B. Lee, and S. Y. Ha. 2020. In situ rates of carbon and nitrogen uptake by phytoplankton and the contribution of picophytoplankton in kongsfjorden, svalbard. Water (Switzerland) **12**: 1–22. doi:10.3390/w12102903

Kirchman, D. L. 1994. The uptake of inorganic nutrients by heterotrophic bacteria. Microbial Ecology **28**: 255–271. doi:10.1007/BF00166816

Kirchman, D. L., H. W. Ducklow, J. J. McCarthy, and C. Garside. 1994. Biomass and nitrogen uptake by heterotrophic bacteria during the spring phytoplankton bloom in the North Atlantic Ocean. Deep-Sea Research Part I. doi:10.1016/0967-0637(94)90081-7

Kirchman, D. L., Y. Suzuki, C. Garside, and H. W. Kucklos. 1991. High turnover rates of dissolved organic carbon during a spring phytoplankton bloom. Nature **352**: 612–614.

Kirchman, D. L., and P. A. Wheeler. 1998. Uptake of ammonium and nitrate by heterotrophic bacteria and phytoplankton in the sub-Arctic Pacific. **45**: 347–365.

Kirk, J. T. O. 1984. Dependence of relationship between inherent and apparent optical properties of water on solar altitude. Limnology and Oceanography **29**. doi:10.4319/lo.1984.29.2.0350

Kitidis, V., B. Laverock, L. C. McNeill, A. Beesley, D. Cummings, K. Tait, M. A. Osborn, and S. Widdicombe. 2011. Impact of ocean acidification on benthic and water column ammonia oxidation. Geophysical Research Letters **38**: 2–6. doi:10.1029/2011GL049095

Kits, K. D., C. J. Sedlacek, E. V. Lebedeva, and others. 2017. Kinetic analysis of a complete nitrifier reveals an oligotrophic lifestyle. Nature **549**: 269–272. doi:10.1038/nature23679

Kitzinger, K., H. K. Marchant, L. A. Bristow, and others. 2020. Single cell analyses reveal contrasting life strategies of the two main nitrifiers in the ocean. Nature Communications **11**. doi:10.1038/s41467-020-14542-3

Knap, A., A. Michaels, A. Close, H. Ducklow, and A. Dickson. 1996. Protocols for the Joint Global Ocean Flux Study (JGFOS) Core Measurements. JGOFS Reoprt Nr. 19, vi+170 pp 198.

Knapp, A., D. Capone, S. Bonnet, J. Dekaezemacker, and J. Sohm. 2012. Sensitivity of Trichodesmium erythraeum and Crocosphaera watsonii abundance and N2 fixation rates to varying NO3− and PO43− concentrations in batch cultures. Aquatic Microbial Ecology **66**: 223–236. doi:10.3354/ame01577

Knowles, G., A. L. Downing, and M. J. Barrett. 1965. Determination of Kinetic Constants for Nitrifying Bacteria in Mixed. Journal of general microbiology **38**: 263–278. doi:10.1099/00221287-38-2-263

Knox, F., and M. B. McElroy. 1984. Changes in atmospheric CO2: influence of the marine biota at high latitude. Journal of Geophysical Research **89**: 4629–4637. doi:10.1029/JD089iD03p04629

Koch, H., S. Lücker, M. Albertsen, and others. 2015. Expanded metabolic versatility of ubiquitous nitrite-oxidizing bacteria from the genus Nitrospira. Proceedings of the National Academy of Sciences of the United States of America **112**: 11371–11376. doi:10.1073/pnas.1506533112

Koike, I., O. Holm-hansen, and D. C. Biggs. 1986. Phytoplankton With Special Reference To Ammonium Cycling. Marine Ecology **30**: 105–116.

Kokkinakis, S. A., and P. A. Wheeler. 1987. Nitrogen uptake and phytoplankton growth in coastal upwelling regions. Limnology and Oceanography **32**: 1112–1123. doi:10.4319/lo.1987.32.5.1112

Könneke, M., A. E. Bernhard, J. R. De La Torre, C. B. Walker, J. B. Waterbury, and D. A. Stahl. 2005. Isolation of an autotrophic ammonia-oxidizing marine archaeon. Nature **437**: 543–546. doi:10.1038/nature03911

Korb, R. E., M. J. Whitehouse, S. E. Thorpe, and M. Gordon. 2005. Primary production across the Scotia Sea in relation to the physico-chemical environment. Journal of Marine Systems **57**: 231–249. doi:10.1016/j.jmarsys.2005.04.009

Korb, R. E., M. J. Whitehouse, and P. Ward. 2004. SeaWiFS in the southern ocean: Spatial and temporal variability in phytoplankton biomass around South Georgia. Deep-Sea Research Part II: Topical Studies in Oceanography **51**: 99–116. doi:10.1016/j.dsr2.2003.04.002

Kottmeier, S. T., and C. W. Sullivan. 1987. MARINE ECOLOGY -PROGRESS SERIES Late winter primary production and bacterial production in sea ice and seawater west of the Antarctic Peninsula. **36**: 287–298.

Kowalchuk, G. A., and J. R. Stephen. 2001. Ammonia-oxidizing bacteria: A model for molecular microbial ecology. Annual Review of Microbiology **55**: 485–529. doi:10.1146/annurev.micro.55.1.485

Kozlowski, J. A., M. Stieglmeier, C. Schleper, M. G. Klotz, and L. Y. Stein. 2016a. Pathways and key intermediates required for obligate aerobic ammonia-dependent chemolithotrophy in bacteria and Thaumarchaeota. ISME Journal **10**: 1836–1845. doi:10.1038/ismej.2016.2

Kozlowski, J. A., M. Stieglmeier, C. Schleper, M. G. Klotz, and L. Y. Stein. 2016b. Pathways and key intermediates required for obligate aerobic ammonia-dependent chemolithotrophy in bacteria and Thaumarchaeota. ISME Journal **10**: 1836–1845. doi:10.1038/ismej.2016.2

Krell, A., S. B. Schnack-Schiel, D. N. Thomas, G. Kattner, W. Zipan, and G. S. Dieckmann. 2005. Phytoplankton dynamics in relation to hydrography, nutrients and zooplankton at the onset of sea ice formation in the eastern Weddell Sea (Antarctica). Polar Biology **28**: 700–713. doi:10.1007/s00300-005-0733-6

Kristiansen, S., and T. Fabrot. 1991. Nitrogen uptake rates in phytoplankton and ice algae in the Barents Sea. Polar Research **10**. doi:10.1111/j.1751-8369.1991.tb00644.x

Kudela, R. M., and W. P. Cochlan. 2000. Nitrogen and carbon uptake kinetics and the influence of irradiance for a red tide bloom off southern California. Aquatic Microbial Ecology **21**: 31–47. doi:10.3354/ame021031

Kudela, R. M., W. P. Cochlan, and R. C. Dugdale. 1997. Carbon and nitrogen uptake response to light by phytoplankton during an upwelling event. Journal of Plankton Research **19**: 609–630. doi:10.1093/plankt/19.5.609

Kudo, I., Y. Noiri, W. P. Cochlan, K. Suzuki, T. Aramaki, T. Ono, and Y. Nojiri. 2009. Primary productivity, bacterial productivity and nitrogen uptake in response to iron enrichment during the SEEDS II. Deep-Sea Research Part II: Topical Studies in Oceanography **56**: 2755–2766. doi:10.1016/j.dsr2.2009.06.003

Kudo, I., Y. Noiri, K. Imai, Y. Nojiri, J. Nishioka, and A. Tsuda. 2005. Primary productivity and nitrogenous nutrient assimilation dynamics during the Subarctic Pacific Iron Experiment for Ecosystem Dynamics Study. Progress in Oceanography **64**: 207–221. doi:10.1016/j.pocean.2005.02.009

Kustka, A. B., S. A. Sañudo-Wilhelmy, E. J. Carpenter, D. Capone, J. Burns, and W. G. Sunda. 2003. Iron requirements for dinitrogen- And ammonium-supported growth in cultures of Trichodesmium (IMS 101): Comparison with nitrogen fixation rates and iron: Carbon ratios of field populations. Limnology and Oceanography **48**: 1869–1884. doi:10.4319/lo.2003.48.5.1869

De La Rocha, C. L., D. A. Hutchins, M. A. Brzezinski, and Y. Zhang. 2000. Effects of iron and zinc deficiency on elemental composition and silica production by diatoms. Marine Ecology Progress Series **195**: 71–79. doi:10.3354/meps195071

Lagerström, M. E., M. P. Field, M. Séguret, L. Fischer, S. Hann, and R. M. Sherrell. 2013. Automated on-line flow-injection ICP-MS determination of trace metals (Mn, Fe, Co, Ni, Cu and Zn) in open ocean seawater: Application to the GEOTRACES program. Marine Chemistry. doi:10.1016/j.marchem.2013.06.001

Lai, X., K. Norisuye, M. Mikata, T. Minami, A. R. Bowie, and Y. Sohrin. 2008. Spatial and temporal distribution of Fe, Ni,

Cu and Pb along 140°E in the Southern Ocean during austral summer 2001/02. Marine Chemistry **111**: 171–183. doi:10.1016/j.marchem.2008.05.001

Lam, P., G. Lavik, M. M. Jensen, and others. 2009. Revising the nitrogen cycle in the Peruvian oxygen minimum zone. Proceedings of the National Academy of Sciences of the United States of America **106**: 4752–4757. doi:10.1073/pnas.0812444106

Lancelot, C., S. Mathot, C. Veth, and H. de Baar. 1993. Factors controlling phytoplankton ice-edge blooms in the marginal ice-zone of the northwestern Weddell Sea during sea ice retreat 1988: Field observations and mathematical modelling. Polar Biology **13**: 377–387. doi:10.1007/BF01681979

Lancelot, C., A. De Montety, H. Goosse, S. Becquevort, V. Schoemann, B. Pasquer, and M. Vancoppenolle. 2009. Spatial distribution of the iron supply to phytoplankton in the Southern Ocean: A model study. Biogeosciences **6**: 2861–2878. doi:10.5194/bg-6-2861-2009

Landschützer, P., N. Gruber, F. A. Haumann, and others. 2015. Ocean carbon sink. Science **349**: 1221–1224. doi:10.1126/science.aab2620

Lannuzel, D., A. R. Bowie, P. C. van der Merwe, A. T. Townsend, and V. Schoemann. 2011. Distribution of dissolved and particulate metals in Antarctic sea ice. Marine Chemistry **124**: 134–146. doi:10.1016/j.marchem.2011.01.004

Lannuzel, D., V. Schoemann, J. de Jong, L. Chou, B. Delille, S. Becquevort, and J. L. Tison. 2008. Iron study during a time series in the western Weddell pack ice. Marine Chemistry **108**: 85–95. doi:10.1016/j.marchem.2007.10.006

Lannuzel, D., V. Schoemann, J. de Jong, J. L. Tison, and L. Chou. 2007. Distribution and biogeochemical behaviour of iron in the East Antarctic sea ice. Marine Chemistry **106**: 18–32. doi:10.1016/j.marchem.2006.06.010

Lannuzel, D., M. Vancoppenolle, P. Van Der Merwe, J. De Jong, K. M. Meiners, M. Grotti, J. Nishioka, and V. Schoemann. 2016. Iron in sea ice: Review & new insights. Elementa **4**: 1–19. doi:10.12952/journal.elementa.000130

Laperriere, S. M., M. Morando, D. G. Capone, T. Gunderson, J. M. Smith, and A. E. Santoro. 2021. Nitrification and nitrous oxide dynamics in the Southern California Bight. Limnology and Oceanography **66**: 1099–1112. doi:10.1002/lno.11667

Lara, E., D. Vaqué, E. L. Sà, and others. 2017. Unveiling the role and life strategies of viruses from the surface to the dark ocean. Science Advances **3**. doi:10.1126/sciadv.1602565

Laubscher, R. K., R. Perissinotto, and C. D. McQuaid. 1993. Phytoplankton production and biomass at frontal zones in the Atlantic sector of the Southern Ocean. Polar Biology **13**: 471–481. doi:10.1007/BF00233138

Law, C. S., E. R. Abraham, A. J. Watson, and M. Liddicoat. 2003. Vertical eddy diffusion and nutrient supply to the surface mixed layer of the Antarctic Circumpolar Current. Journal of Geophysical Research **108**: 1–14. doi:10.1029/2002jc001604

Laws, E. A., H. Ducklow, and J. J. McCarthy. 2000. Temperature effects on export production in the open ocean. Global Biogeochemical Cycles **14**: 1231–1246. doi:10.1029/1999GB001229

Lebedeva, E. V., M. Alawi, P. G. Jozsa, H. Daims, and E. Spieck. 2008. Physiological and phylogenetic characterization of a novel lithoautotrophic nitrite-oxidizing bacterium, “Candidatus Nitrospira bockiana.” International Journal of Systematic and Evolutionary Microbiology **58**: 242–250. doi:10.1099/ijs.0.65379-0

Lebedeva, E. V., S. Off, S. Zumbrägel, and others. 2011. Isolation and characterization of a moderately thermophilic nitrite-oxidizing bacterium from a geothermal spring. FEMS Microbiology Ecology **75**: 195–204. doi:10.1111/j.1574-6941.2010.01006.x

Van Leeuwe, M. A., R. Scharek, H. J. W. De Baar, J. T. M. De Jong, and L. Goeyens. 1997. Iron enrichment experiments in the Southern Ocean: Physiological responses of plankton communities. Deep-Sea Research Part II: Topical Studies in Oceanography **44**: 189–207. doi:10.1016/S0967-0645(96)00069-0

Lenton, A., B. Tilbrook, R. M. Law, and others. 2013. Sea-air CO2 fluxes in the Southern Ocean for the period 1990-2009. Biogeosciences **10**: 4037–4054. doi:10.5194/bg-10-4037-2013

Leung, S., A. Cabre, and I. Marinov. 2015. A latitudinally banded phytoplankton response to 21st century climate change in the Southern Ocean across the CMIP5 model suite. Biogeosciences **12**: 5715–5734. doi:10.5194/bg-12-5715-2015

Lewis, W. M., and D. P. Morris. 1986. Toxicity of Nitrite to Fish: A Review. Transactions of the American Fisheries Society **115**. doi:10.1577/1548-8659(1986)115<183:tontf>2.0.co;2

Li, J., D. B. Nedwell, J. Beddow, A. J. Dumbrell, B. A. McKew, E. L. Thorpe, and C. Whitby. 2015. amoA gene abundances and nitrification potential rates suggest that benthic ammonia-oxidizing bacteria and not archaea dominate N cycling in the Colne estuary, United Kingdom. Applied and Environmental Microbiology **81**: 159–165.

doi:10.1128/AEM.02654-14

Lieberman, R. L., and A. C. Rosenzweig. 2005. Crystal structure of a membrane-bound metalloenzyme that catalyses the biological oxidation of methane. Nature **434**: 177–182. doi:10.1038/nature03311

Lim, P. T., C. P. Leaw, G. Usup, A. Kobiyama, K. Koike, and T. Ogata. 2006. Effects of light and temperature on growth, nitrate uptake, and toxin production of two tropical dinoflagellates: Alexandrium tamiyavanichii and Alexandrium minutum (Dinophyceae). Journal of Phycology **42**. doi:10.1111/j.1529-8817.2006.00249.x

Lin, H., S. Rauschenberg, C. R. Hexel, T. J. Shaw, and B. S. Twining. 2011. Free-drifting icebergs as sources of iron to the Weddell Sea. Deep-Sea Research Part II: Topical Studies in Oceanography **58**: 1392–1406. doi:10.1016/j.dsr2.2010.11.020

Lipschultz, F. 2008. Isotope Tracer Methods for Studies of the Marine Nitrogen Cycle, *In* Nitrogen in the Marine Environment.

Litchman, E., C. A. Klausmeier, J. R. Miller, O. M. Schofield, and P. G. Falkowski. 2006. Multi-nutrient, multi-group model of present and future oceanic phytoplankton communities. Biogeosciences **3**: 585–606. doi:10.5194/bg-3-585-2006

Litchman, E., C. A. Klausmeier, O. M. Schofield, and P. G. Falkowski. 2007. The role of functional traits and trade-offs in structuring phytoplankton communities: Scaling from cellular to ecosystem level. Ecology Letters **10**: 1170–1181. doi:10.1111/j.1461-0248.2007.01117.x

Lomas, M. W. 2004. Nitrate reductase and urease enzyme activity in the marine diatom Thalassiosira weissflogii (Bacillariophyceae): Interactions among nitrogen substrates. Marine Biology **144**: 37–44. doi:10.1007/s00227-003-1181-x

Lomas, M. W., and P. M. Gilbert. 1999. Temperature regulation of nitrate uptake: A novel hypothesis about nitrate uptake and reduction in cool-water diatoms. Limnology and Oceanography **44**: 556–572. doi:10.4319/lo.1999.44.3.0556

Lomas, M. W., and P. M. Glibert. 1999a. Interactions between NH4/+ and NO3/- uptake and assimilation: Comparison of diatoms and dinoflagellates at several growth temperatures. Marine Biology **133**: 541–551. doi:10.1007/s002270050494

Lomas, M. W., and P. M. Glibert. 1999b. Interactions between NH4 and NO3 uptake and assimilation: Comparison of diatoms and dinoflagellates at several growth temperatures. Marine Biology **133**: 541–551. doi:10.1007/s002270050494

Lomas, M. W., and F. Lipschultz. 2006. Forming the primary nitrite maximum: Nitrifiers or phytoplankton? Limnology and Oceanography **51**: 2453–2467. doi:10.4319/lo.2006.51.5.2453

Lourantou, A., and N. Metzl. 2011. Decadal evolution of carbon sink within a strong bloom area in the subantarctic zone. Geophysical Research Letters **38**: 1–7. doi:10.1029/2011GL049614

Lourey, M. J., and T. W. Trull. 2001. Seasonal nutrient depletion and carbon export in the Subantarctic and Polar Frontal Zones of the Southern Ocean south of Australia. **106**.

Lourey, M. J., T. W. Trull, and D. M. Sigman. 2003. Sensitivity of δ 15 N of nitrate, surface suspended and deep sinking particulate nitrogen to seasonal nitrate depletion in the Southern Ocean . Global Biogeochemical Cycles **17**: n/a-n/a. doi:10.1029/2002gb001973

Lu, S., X. Liu, C. Liu, G. Cheng, and H. Shen. 2020. Influence of photoinhibition on nitrification by ammonia-oxidizing microorganisms in aquatic ecosystems. Reviews in Environmental Science and Biotechnology **2**. doi:10.1007/s11157-020-09540-2

Lücker, S., B. Nowka, T. Rattei, E. Spieck, and H. Daims. 2013. The genome of Nitrospina gracilis illuminates the metabolism and evolution of the major marine nitrite oxidizer. Frontiers in Microbiology **4**. doi:10.3389/fmicb.2013.00027

Lücker, S., M. Wagner, F. Maixner, and others. 2010. A Nitrospira metagenome illuminates the physiology and evolution of globally important nitrite-oxidizing bacteria. Proceedings of the National Academy of Sciences of the United States of America **107**: 13479–13484. doi:10.1073/pnas.1003860107

Luo, H., B. B. Tolar, B. K. Swan, C. L. Zhang, R. Stepanauskas, M. Ann Moran, and J. T. Hollibaugh. 2014. Single-cell genomics shedding light on marine Thaumarchaeota diversification. ISME Journal **8**: 732–736. doi:10.1038/ismej.2013.202

Lutjeharms, J. R. E., and I. J. Ansorge. 2001. The Agulhas Return Current. Journal of Marine Systems **30**: 115–138. doi:10.1016/S0924-7963(01)00041-0

Maas, E. W., C. S. Law, J. A. Hall, S. Pickmere, K. I. Currie, F. H. Chang, K. M. Voyles, and D. Caird. 2013. Effect of

ocean acidification on bacterial abundance, activity and diversity in the Ross Sea, Antarctica. Aquatic Microbial Ecology **70**: 1–15. doi:10.3354/ame01633

MacIsaac, J. J., and R. C. Dugdale. 1969. The kinetics of nitrate and ammonia uptake by natural populations of marine phytoplankton. Deep-Sea Research and Oceanographic Abstracts. doi:10.1016/0011-7471(69)90049-7

MacIsaac, J. J., and R. C. Dugdale. 1972. Interactions of light and inorganic nitrogen in controlling nitrogen uptake in the sea. Deep-Sea Research and Oceanographic Abstracts **19**. doi:10.1016/0011-7471(72)90032-0

Mackey, K. R. M., J. Morris, F. M. M. Morel, and S. A. Kranz. 2015. Response of Photosynthesis to Ocean Acidification Emerging Themes in Ocean Acidifcations Science. Oceanography **2828**: 74–91. doi:10.5670/oceanog.2015.33

Majkut, J. D., B. R. Carter, T. L. Frölicher, C. O. Dufour, K. B. Rodgers, and J. L. Sarmiento. 2014. An observing system simulation for Southern Ocean carbon dioxide uptake. Philosophical Transactions of the Royal Society A: Mathematical, Physical and Engineering Sciences **372**. doi:10.1098/rsta.2013.0046

Marinov, I., A. Gnanadesikan, J. R. Toggweiler, and J. L. Sarmiento. 2006. The Southern Ocean biogeochemical divide. Nature **441**: 964–967. doi:10.1038/nature04883

Martens-Habbena, W., P. M. Berube, H. Urakawa, J. R. De La Torre, and D. A. Stahl. 2009. Ammonia oxidation kinetics determine niche separation of nitrifying Archaea and Bacteria. Nature **461**: 976–979. doi:10.1038/nature08465

Martens-Habbena, W., and D. A. Stahl. 2011. Nitrogen metabolism and kinetics of ammonia-oxidizing archaea. Methods in Enzymology **496**: 465–487. doi:10.1016/B978-0-12-386489-5.00019-1

Martin-Jézéquel, V., M. Hildebrand, and A. Brzezinski Mark. 2000. Silicon metabolism in diatoms: implications for growth. Journal of Phycology **36**: 821–840. doi:10.1046/j.1529-8817.2000.00019.x

Martin, J. H. 1990. Glacial-interglacial CO2 change: The Iron Hypothesis. Paleoceanography **5**: 1–13. doi:10.1029/PA005i001p00001

Martin, J. H., S. E. Fitzwater, and R. M. Gordon. 1990. Iron deficiency limits phytoplankton growth in Antarctic waters. Global Biogeochemical Cycles **4**. doi:10.1029/GB004i001p00005

Martin, J. H., M. Gordon, and S. E. Fitzwater. 1991. The case for iron. Limnology and Oceanography **36**. doi:10.4319/lo.1991.36.8.1793

Martiny, A. C., J. A. Vrugt, and M. W. Lomas. 2014. Concentrations and ratios of particulate organic carbon, nitrogen, and phosphorus in the global ocean. Scientific Data **1**: 1–7. doi:10.1038/sdata.2014.48

Martiny, A. C., J. A. Vrugt, F. W. Primeau, and M. W. Lomas. 2013. Regional variation in the particulate organic carbon to nitrogen ratio in the surface ocean. Global Biogeochemical Cycles **27**: 723–731. doi:10.1002/gbc.20061

Massonnet, F., V. Guemas, N. S. Fuckar, and F. J. Doblas-Reyes. 2015. The 2014 High Record of Antarctic Sea Ice Extent. Bulletin of the American Meteorological Society **96**: 35–40.

Mateus, M. D. 2017. Bridging the gap between knowing and modeling viruses in marine systems-An upcoming frontier. Frontiers in Marine Science **3**: 1–16. doi:10.3389/FMARS.2016.00284

McCarthy, M. J., W. S. Gardner, P. J. Lavrentyev, F. J. Jochem, and C. J. Williams. 2009. Water Column Nitrogen Cycling and Microbial Plankton in Florida Bay. Contributions in Marine Science **38**: 49–62.

McCartney, M. S. 1975. Subantarctic mode water. EoS Trans. AGU **56**: 103–118.

McIlvin, M. R., and M. A. Altabet. 2005. Chemical conversion of nitrate and nitrite to nitrous oxide for nitrogen and oxygen isotopic analysis in freshwater and seawater. Analytical Chemistry **77**: 5589–5595. doi:10.1021/ac050528s

McIlvin, M. R., and K. L. Casciotti. 2011. Technical updates to the bacterial method for nitrate isotopic analyses. Analytical Chemistry **83**: 1850–1856. doi:10.1021/ac1028984

McNeil, B. I., and R. J. Matear. 2008. Southern Ocean acidification: A tipping point at 450-ppm atmospheric CO2. Proceedings of the National Academy of Sciences of the United States of America **105**: 18860–18864. doi:10.1073/pnas.0806318105

Mdutyana, M., S. J. Thomalla, R. Philibert, B. B. Ward, and S. E. Fawcett. 2020. The Seasonal Cycle of Nitrogen Uptake and Nitrification in the Atlantic Sector of the Southern Ocean. Global Biogeochemical Cycles 1–29. doi:10.1029/2019GB006363

Meehl, G. A., J. M. Arblaster, C. T. Y. Chung, M. M. Holland, A. DuVivier, L. A. Thompson, D. Yang, and C. M. Bitz. 2019. Sustained ocean changes contributed to sudden Antarctic sea ice retreat in late 2016. Nature Communications **10**: 1–9. doi:10.1038/s41467-018-07865-9

Meijers, A. J. S. 2014. The Southern Ocean in the Coupled Model Intercomparison Project phase 5. Philosophical Transactions of the Royal Society A: Mathematical, Physical and Engineering Sciences **372**. doi:10.1098/rsta.2013.0296

Meiklejohn, J. 1953. Iron and the nitrifying bacteria. Journal of general microbiology **8**: 58–65. doi:10.1099/00221287-8-1-58

Meincke, M., E. Bock, D. Kastrau, and P. M. H. Kroneck. 1992. Nitrite oxidoreductase from Nitrobacter hamburgensis: redox centers and their catalytic role. Archives of Microbiology **158**: 127–131. doi:10.1007/BF00245215

Mendes, C. R. B., R. Kerr, V. M. Tavano, F. A. Cavalheiro, C. A. E. Garcia, D. R. Gauns Dessai, and N. Anilkumar. 2015. Cross-front phytoplankton pigments and chemotaxonomic groups in the Indian sector of the Southern Ocean. Deep-Sea Research Part II: Topical Studies in Oceanography **118**: 221–232. doi:10.1016/j.dsr2.2015.01.003

Mengesha, S., F. Deharis, M. Fiala, M. Elskens, and L. Goeyens. 1998. Seasonal variation of phytoplankton community structure and nitrogen uptake regime in the Indian Sector of the Southern Ocean. Polar Biology **20**: 259–272.

Merbt, S. N., D. A. Stahl, E. O. Casamayor, E. Martí, G. W. Nicol, and J. I. Prosser. 2012a. Differential photoinhibition of bacterial and archaeal ammonia oxidation. FEMS Microbiology Letters **327**: 41–46. doi:10.1111/j.1574-6968.2011.02457.x

Merbt, S. N., D. A. Stahl, E. O. Casamayor, E. Martí, G. W. Nicol, and J. I. Prosser. 2012b. Differential photoinhibition of bacterial and archaeal ammonia oxidation. FEMS Microbiology Letters **327**: 41–46. doi:10.1111/j.1574-6968.2011.02457.x

Van Der Merwe, P., D. Lannuzel, A. R. Bowie, and K. M. Meiners. 2011. High temporal resolution observations of spring fast ice melt and seawater iron enrichment in East Antarctica. Journal of Geophysical Research: Biogeosciences **116**: 1–18. doi:10.1029/2010JG001628

Meskhidze, N., A. Nenes, W. L. Chameides, C. Luo, and N. Mahowald. 2007. Atlantic Southern Ocean productivity: Fertilization from above or below? Global Biogeochemical Cycles **21**: 1–9. doi:10.1029/2006GB002711

Metzl, N. 2009. Decadal increase of oceanic carbon dioxide in Southern Indian Ocean surface waters (1991-2007). Deep-Sea Research Part II: Topical Studies in Oceanography **56**: 607–619. doi:10.1016/j.dsr2.2008.12.007

Metzl, N., C. Brunet, A. Jabaud-Jan, A. Poisson, and B. Schauer. 2006. Summer and winter air-sea CO2 fluxes in the Southern Ocean. Deep-Sea Research Part I: Oceanographic Research Papers **53**: 1548–1563. doi:10.1016/j.dsr.2006.07.006

Michael Beman, J., B. N. Popp, and S. E. Alford. 2012. Quantification of ammonia oxidation rates and ammonia-oxidizing archaea and bacteria at high resolution in the Gulf of California and eastern tropical North Pacific Ocean. Limnology and Oceanography **57**: 711–726. doi:10.4319/lo.2012.57.3.0711

Milligan, A. J., and P. J. Harrison. 2000. Effects of non-steady-state iron limitation on nitrogen assimilatory enzymes in the marine diatom Thalassiosira weissflogii (Bacillariophyceae). Journal of Phycology **36**: 78–86. doi:10.1046/j.1529-8817.2000.99013.x

Minami, T., W. Konagaya, L. Zheng, S. Takano, M. Sasaki, R. Murata, Y. Nakaguchi, and Y. Sohrin. 2015. An off-line automated preconcentration system with ethylenediaminetriacetate chelating resin for the determination of trace metals in seawater by high-resolution inductively coupled plasma mass spectrometry. Analytica Chimica Acta **854**: 183–190. doi:10.1016/j.aca.2014.11.016

Minas, H. J., M. Minas, and T. T. Packard. 1986. Productivity in upwelling areas deduced from hydrographic and chemical fields. Limnology and Oceanography **31**: 1182–1206. doi:10.4319/lo.1986.31.6.1182

Mincer, T. J., M. J. Church, L. T. Taylor, C. Preston, D. M. Karl, and E. F. DeLong. 2007. Quantitative distribution of presumptive archaeal and bacterial nitrifiers in Monterey Bay and the North Pacific Subtropical Gyre. Environmental Microbiology. doi:10.1111/j.1462-2920.2007.01239.x

Mitchell, B. G., and O. Holm-Hansen. 1991. Observations of modeling of the Antartic phytoplankton crop in relation to mixing depth. Deep Sea Research Part A, Oceanographic Research Papers. doi:10.1016/0198-0149(91)90093-U

Le Moigne, F. A. C., M. Boye, A. Masson, R. Corvaisier, E. Grossteffan, A. Guéneugues, and P. Pondaven. 2013. Description of the biogeochemical features of the subtropical southeastern Atlantic and the Southern Ocean south of South Africa during the austral summer of the International Polar Year. Biogeosciences **10**: 281–295. doi:10.5194/bg-10-281-2013

Mongwe, N. P., N. Chang, and P. M. S. Monteiro. 2016. The seasonal cycle as a mode to diagnose biases in modelled CO2 fluxes in the Southern Ocean. Ocean Modelling **106**: 90–103. doi:10.1016/j.ocemod.2016.09.006

Mongwe, N. P., M. Vichi, and P. M. S. Monteiro. 2018. The seasonal cycle of pCO2 and CO2 fluxes in the Southern Ocean:

Diagnosing anomalies in CMIP5 Earth system models. Biogeosciences **15**: 2851–2872. doi:10.5194/bg-15-2851-2018

Monod, J. 1942. Recherches sur la croissance des cultures bacteriennes. Hermann and Cie, Paris.

Monteiro, M., J. Séneca, L. Torgo, D. F. R. Cleary, N. C. M. Gomes, A. E. Santoro, and C. Magalhães. 2017. Environmental controls on estuarine nitrifying communities along a salinity gradient. Aquatic Microbial Ecology **80**. doi:10.3354/ame01847

Monteiro, P. M. S., and M. J. Orren. 1985. Trace metals in the Southern Ocean: on the geochemistry of copper. Marine Chemistry. doi:10.1016/0304-4203(85)90045-3

Moore, C. M., M. M. Mills, K. R. Arrigo, and others. 2013. Processes and patterns of oceanic nutrient limitation. Nature Geoscience **6**: 701–710. doi:10.1038/ngeo1765

Moore, J. K., and M. R. Abbott. 2000. Phytoplankton chlorophyll distributions and primary production in the Southern Ocean. Journal of Geophysical Research: Oceans **105**: 28709–28722. doi:10.1029/1999jc000043

Moore, J. K., S. C. Doney, D. M. Glover, and I. Y. Fung. 2002. Iron cycling and nutrient-limitation patterns in surface waters of the world ocean. Deep-Sea Research Part II: Topical Studies in Oceanography **49**: 463–507. doi:10.1016/S0967-0645(01)00109-6

Moore, J. K., S. C. Doney, and K. Lindsay. 2004. Upper ocean ecosystem dynamics and iron cycling in a global three-dimensional model. Global Biogeochemical Cycles **18**: 1–21. doi:10.1029/2004GB002220

Morel, A. 1988. Optical modeling of the upper ocean in relation to its biogenous matter content (case I waters). Journal of Geophysical Research **93**. doi:10.1029/jc093ic09p10749

Morel, F. M. M., R. J. M. Hudson, and N. M. Price. 1991. Limitation of productivity by trace metals in the sea. Limnology and Oceanography **36**: 1742–1755. doi:10.4319/lo.1991.36.8.1742

Morel, F. M. M., and N. M. Price. 2003. The biogeochemical cycles of trace metals in the oceans. Science **300**: 944–947. doi:10.1126/science.1083545

Mosier, A. C., E. E. Allen, M. Kim, S. Ferriera, and C. A. Francis. 2012. Genome sequence of "candidatus nitrosopumilus salaria" BD31, an: Ammonia-oxidizing archaeon from the San Francisco Bay Estuary. Journal of Bacteriology **194**: 2121–2122. doi:10.1128/JB.00013-12

Mosier, A. C., and C. A. Francis. 2008. Relative abundance and diversity of ammonia-oxidizing archaea and bacteria in the San Francisco Bay estuary. Environmental Microbiology **10**. doi:10.1111/j.1462-2920.2008.01764.x

Mosseri, J., B. Quéguiner, L. Armand, and V. Cornet-Barthaux. 2008. Impact of iron on silicon utilization by diatoms in the Southern Ocean: A case study of Si/N cycle decoupling in a naturally iron-enriched area. Deep-Sea Research Part II: Topical Studies in Oceanography **55**: 801–819. doi:10.1016/j.dsr2.2007.12.003

Mtshali, T. N., N. R. van Horsten, S. J. Thomalla, and others. 2019. Seasonal Depletion of the Dissolved Iron Reservoirs in the Sub-Antarctic Zone of the Southern Atlantic Ocean. Geophysical Research Letters 1–10. doi:10.1029/2018GL081355

Muggli, D. L., and W. O. Smith. 1993. Regulation of nitrate and ammonium uptake in the Greenland Sea. Marine Biology **115**: 199–208. doi:10.1007/BF00346336

Mulholland, M. R., and P. W. Bernhardt. 2005. The effect of growth rate, phosphorus concentration, and temperature on N2 fixation, carbon fixation, and nitrogen release in continuous cultures of Trichodesmium IMS101. Limnology and Oceanography **50**: 839–849. doi:10.4319/lo.2005.50.3.0839

Mulholland, M. R., and M. W. Lomas. 2008. Nitrogen Uptake and Assimilation,.

Nelson, D. M., and W. O. Smith. 1986. Phytoplankton bloom dynamics of the western Ross Sea ice edge-II. Mesoscale cycling of nitrogen and silicon. Deep Sea Research Part A, Oceanographic Research Papers **33**. doi:10.1016/0198-0149(86)90042-7

Nelson, D., and W. Smith. 1991. Sverdrup revisited: Critical depths, maximum chlorophyll levels, and the control of Southern Ocean productivity by the irradiance-mixing regime. Limnol. Oceanog **36**: 1650–1661. doi:10.4319/lo.1991.36.8.1650

Newell, S. E., A. R. Babbin, A. Jayakumar, and B. B. Ward. 2011. Ammonia oxidation rates and nitrification in the Arabian Sea. Global Biogeochemical Cycles **25**: 1–10. doi:10.1029/2010GB003940

Newell, S. E., S. E. Fawcett, and B. B. Ward. 2013. Depth distribution of ammonia oxidation rates and ammonia-oxidizer community composition in the Sargasso Sea. Limnology and Oceanography **58**: 1491–1500. doi:10.4319/lo.2013.58.4.1491

Ngugi, D. K., J. Blom, I. Alam, and others. 2015. Comparative genomics reveals adaptations of a halotolerant thaumarchaeon in the interfaces of brine pools in the Red Sea. ISME Journal **9**: 396–411. doi:10.1038/ismej.2014.137

Ngugi, D. K., J. Blom, R. Stepanauskas, and U. Stingl. 2016. Diversification and niche adaptations of Nitrospina - like bacteria in the polyextreme interfaces of Red Sea brines. 1383–1399. doi:10.1038/ismej.2015.214

Nielsdóttir, M. C., T. S. Bibby, C. M. Moore, D. J. Hinz, R. Sanders, M. Whitehouse, R. Korb, and E. P. Achterberg. 2012. Seasonal and spatial dynamics of iron availability in the Scotia Sea. Marine Chemistry **130**–**131**: 62–72. doi:10.1016/j.marchem.2011.12.004

Nowka, B., H. Daims, and E. Spieck. 2015. Comparison of Oxidation Kinetics of Nitrite-Oxidizing Bacteria : Nitrite Availability as a Key Factor in Niche Differentiation. **81**: 745–753. doi:10.1128/AEM.02734-14

Olsen, A., A. Kozyr, S. K. Lauvset, and others. 2016. The Global Ocean Data Analysis Project version 2 (GLODAPv2) – an internally consistent data product for the world ocean. Earth System Science Data **8**: 297–323. doi:10.5194/essd-8-297-2016

Olson, R. 1980. Nitrate and ammonium uptake in Antarctic waters. Limnology and Oceanography **25**: 1064–1074. doi:10.4319/lo.1980.25.6.1064

Olson, R. 1981a. 15N tracer studies of the primary nitrite maximum. Journal of Marine Research **39**: 203–226.

Olson, R. 1981b. Differential Photoinhibition of Marine Nitrifying Bacteria - a Possible Mechanism for the Formation of the Primary Nitrite Maximum. Journal of Marine Research **39**: 227–238.

Orr, J. C., V. J. Fabry, O. Aumont, and others. 2005. Anthropogenic ocean acidification over the twenty-first century and its impact on calcifying organisms. Nature **437**: 681–686. doi:10.1038/nature04095

Orsi, A. H., G. C. Johnson, and J. L. Bullister. 1999. Circulation, mixing, and production of Antarctic Bottom Water. Progress in Oceanography **43**: 55–109. doi:10.1016/S0079-6611(99)00004-X

Orsi, A. H., T. Whitworth, and W. D. Nowlin. 1995a. On the meridional extent and fronts of the Antarctic Circumpolar Current. Deep-Sea Research Part I **42**: 641–673. doi:10.1016/0967-0637(95)00021-W

Orsi, H., T. Whitworth, and W. D. N. Jr. 1995b. On the meridional extent and fronts of the Antarctic Circumpolar Current Pronounced meridional gradients in surface properties separate waters of the Southern Ocean from the warmer and saltier waters of the subtropical circulations . Deacon (1933 , the S. Deep Sea Research **42**: 641–673. doi:10.1016/0967-0637(95)00021-W

Owens, N. J. P., J. Priddle, and M. J. Whitehouse. 1991. Variations in phytoplanktonic nitrogen assimilation around South Georgia and in the Bransfield Strait (Southern Ocean). Marine Chemistry. doi:10.1016/S0304-4203(09)90023-8

Paasche, E., I. Bryceson, and K. Tangen. 1984. INTERSPECIFIC VARIATION IN DARK NITROGEN UPTAKE BY DINOFLAGELLATES. Journal of Phycology **20**. doi:10.1111/j.0022-3646.1984.00394.x

Pachiadaki, M. G., E. Sintes, K. Bergauer, J. M. Brown, N. R. Record, B. K. Swan, and M. E. Mathyer. 2017. Major role of nitrite-oxidizing bacteria in dark ocean carbon fixation. **1051**: 1046–1051.

Paerl, H. W., L. E. Prufert-Bebout, and C. Guo. 1994. Iron-stimulated N2 fixation and growth in natural and cultured populations of the planktonic marine cyanobacteria Trichodesmium spp. Applied and Environmental Microbiology **60**: 1044–1047.

Pajares, S., and R. Ramos. 2019. Processes and Microorganisms Involved in the Marine Nitrogen Cycle: Knowledge and Gaps. Frontiers in Marine Science **6**. doi:10.3389/fmars.2019.00739

Pajares, S., M. F. Soto-Jiménez, and M. Merino-Ibarra. 2019. Molecular and isotopic evidence of the distribution of nitrogen-cycling microbial communities in the oxygen minimum zone of the Tropical Mexican Pacific. FEMS Microbiology Ecology **95**: 1–13. doi:10.1093/femsec/fiz143

Pakulski, J. D., R. Benner, R. Amon, B. Eadie, and T. Whitledge. 1995. Community metabolism and nutrient cycling in the Mississippi River plume: Evidence for intense nitrification at intermediate salinities. Marine Ecology Progress Series **117**: 207–218. doi:10.3354/meps117207

Pakulski, J. D., R. Benner, T. Whitledge, R. Amon, B. Eadie, L. Cifuentes, J. Ammerman, and D. Stockwell. 2000. Microbial metabolism and nutrient cycling in the Mississippi and Atchafalaya River plumes. Estuarine, Coastal and Shelf Science **50**: 173–184. doi:10.1006/ecss.1999.0561

Palenik, B., and F. M. M. Morel. 1991. Amine oxidases of marine phytoplankton. Applied and Environmental Microbiology **57**: 2440–2443. doi:10.1128/aem.57.8.2440-2443.1991

Parkinson, C. L. 2014. Global sea ice coverage from satellite data: Annual cycle and 35-yr trends. Journal of Climate **27**: 9377–9382. doi:10.1175/JCLI-D-14-00605.1

Paulot, F., D. J. Jacob, M. T. Johnson, and others. 2015. Global oceanic emission of ammonia: Constraints from seawater and atmospheric observations. Global Biogeochemical Cycles **29**: 1165–1178. doi:10.1002/2015GB005106

Peng, X., S. E. Fawcett, N. van Oostende, M. J. Wolf, D. Marconi, D. M. Sigman, and B. B. Ward. 2018. Nitrogen uptake and nitrification in the subarctic North Atlantic Ocean. Limnology and Oceanography. doi:10.1002/lno.10784

Peng, X., C. A. Fuchsman, A. Jayakumar, S. Oleynik, W. Martens-Habbena, A. H. Devol, and B. B. Ward. 2015. Ammonia and nitrite oxidation in the Eastern Tropical North Pacific. Global Biogeochemical Cycles **29**: 2034–2049. doi:10.1002/2015GB005278

Peng, X., C. A. Fuchsman, A. Jayakumar, M. J. Warner, A. H. Devol, and B. B. Ward. 2016. Revisiting nitrification in the Eastern Tropical South Pacific: A focus on controls. Journal of Geophysical Research: Oceans. doi:10.1002/2015JC011455

Penn, J., T. Weber, and C. Deutsch. 2016. Microbial functional diversity alters the structure and sensitivity of oxygen deficient zones. Geophysical Research Letters **43**: 9773–9780. doi:10.1002/2016GL070438

Petrou, K., K. G. Baker, D. A. Nielsen, A. M. Hancock, K. G. Schulz, and A. T. Davidson. 2019. Acidification diminishes diatom silica production in the Southern Ocean. Nature Climate Change **9**: 781–786. doi:10.1038/s41558-019-0557-y

Petrou, K., S. A. Kranz, S. Trimborn, C. S. Hassler, S. B. Ameijeiras, O. Sackett, P. J. Ralph, and A. T. Davidson. 2016. Southern Ocean phytoplankton physiology in a changing climate. Journal of Plant Physiology **203**: 135–150. doi:10.1016/j.jplph.2016.05.004

Philibert, R., H. Waldron, and D. Clark. 2015. A geographical and seasonal comparison of nitrogen uptake by phytoplankton in the Southern Ocean. Ocean Science **11**: 251–267. doi:10.5194/os-11-251-2015

Planas, D., S. Agustí, C. M. Duarte, T. C. Granata, and M. Merino. 1999. Nitrate uptake and diffusive nitrate supply in the Central Atlantic. Limnology and Oceanography **44**. doi:10.4319/lo.1999.44.1.0116

Planchon, F., D. Ballas, A. J. Cavagna, and others. 2015. Carbon export in the naturally iron-fertilized Kerguelen area of the Southern Ocean based on the 234Th approach. Biogeosciences **12**: 3831–3848. doi:10.5194/bg-12-3831-2015

Planquette, H., P. J. Statham, G. R. Fones, and others. 2007. Dissolved iron in the vicinity of the Crozet Islands, Southern Ocean. Deep-Sea Research Part II: Topical Studies in Oceanography **54**: 1999–2019. doi:10.1016/j.dsr2.2007.06.019

du Plessis, M., S. Swart, I. J. Ansorge, and A. Mahadevan. 2017a. Submesoscale processes promote seasonal restratification in the Subantarctic Ocean. Journal of Geophysical Research: Oceans. doi:10.1002/2016JC012494

du Plessis, M., S. Swart, I. J. Ansorge, and A. Mahadevan. 2017b. Submesoscale processes promote seasonal restratification in the Subantarctic Ocean. Journal of Geophysical Research: Oceans **122**: 1–22. doi:10.1002/2016JC012264.Received

Du Plessis, M., S. Swart, I. J. Ansorge, A. Mahadevan, and A. F. Thompson. 2019. Southern Ocean seasonal restratification delayed by submesoscale wind-front interactions. Journal of Physical Oceanography **49**: 1035–1053. doi:10.1175/JPO-D-18-0136.1

Pollard, R. T., M. I. Lucas, and J. F. Read. 2002. Physical controls on biogeochemical zonation in the Southern Ocean. Deep-Sea Research Part II: Topical Studies in Oceanography **49**: 3289–3305. doi:10.1016/S0967-0645(02)00084-X

Pollard, R. T., I. Salter, R. J. Sanders, and others. 2009. Southern Ocean deep-water carbon export enhanced by natural iron fertilization. Nature **457**: 577–580. doi:10.1038/nature07716

Pondaven, P., O. Ragueneau, P. Tre, A. Hauvespre, L. Dezileau, and J. L. Reyss. 2000. Resolving the ` opal paradox ' in the Southern Ocean. **405**: 168–172.

Prakash, S., R. Ramesh, M. S. Sheshshayee, R. Mohan, and M. Sudhakar. 2010. Effect of high level iron enrichment on potential nitrogen uptake by marine plankton in the Southern Ocean. Current Science **99**: 1400–1404.

Prakash, S., R. Ramesh, M. S. Sheshshayee, R. Mohan, and M. Sudhakar. 2015. Nitrogen uptake rates and f-ratios in the Equatorial and Southern Indian Ocean. Current Science **108**: 239–245.

Price, N. M., B. A. Ahner, and F. M. M. Morel. 1994. The equatorial Pacific Ocean: Grazer-controlled phytoplankton populations in an iron-limited ecosystem. Limnology and Oceanography **39**: 520–534. doi:10.4319/lo.1994.39.3.0520

Priddle, J., R. Leakey, C. Symon, M. Whitehouse, D. Robins, G. Cripps, E. Murphy, and N. Owens. 1995. Nutrient cycling by Antarctic marine microbial plankton. Marine Ecology Progress Series **116**: 181–198. doi:10.3354/meps116181

Priddle, J., D. B. Nedwell, M. J. Whitehouse, D. S. Reay, G. Savidge, L. C. Gilpin, E. J. Murphy, and J. C. Ellis-Evans. 1998. Re-examining the Antarctic Paradox: Speculation on the Southern Ocean as a nutrient-limited system. Annals of Glaciology **27**: 661–668.

Priddle, J., V. Smetacek, and U. Bathmann. 1992. Antarctic marine primary production, biogeochemical carbon cycles and

climatic change. Philosophical Transactions - Royal Society of London, B **338**: 289–297. doi:10.1098/rstb.1992.0149

Priscu, J. C., M. P. Lizotte, G. F. Cota, A. C. Palmisano, and C. W. Sullivan. 1991. Comparison of the irradiance response of photosynthesis and nitrogen uptake by sea ice microalgae. Marine Ecology Progress Series **70**. doi:10.3354/meps070201

Priscu, J. C., A. C. Palmisano, L. R. Priscu, and C. W. Sullivan. 1989. Temperature dependence of inorganic nitrogen uptake and assimilation in Antarctic sea-ice microalgae. Polar Biology **9**. doi:10.1007/BF00443231

Probyn, T. A., and S. J. Painting. 1985. Nitrogen uptake by size-fractionated phytoplankton populations in Antarctic surface waters1. Limnology and Oceanography **30**: 1327–1332. doi:10.4319/lo.1985.30.6.1327

Purkhold, U., A. Pommerening-Röser, S. Juretschko, M. C. Schmid, H. P. Koops, and M. Wagner. 2000. Phylogeny of all recognized species of ammonia oxidizers based on comparative 16S rRNA and amoA sequence analysis: Implications for molecular diversity surveys. Applied and Environmental Microbiology **66**: 5368–5382. doi:10.1128/AEM.66.12.5368-5382.2000

Qin, W., S. A. Amin, R. A. Lundeen, and others. 2018. Stress response of a marine ammonia-oxidizing archaeon informs physiological status of environmental populations. ISME Journal **12**: 508–519. doi:10.1038/ismej.2017.186

Qin, W., S. A. Amin, W. Martens-Habbena, and others. 2014. Marine ammonia-oxidizing archaeal isolates display obligate mixotrophy and wide ecotypic variation. Proceedings of the National Academy of Sciences of the United States of America **111**: 12504–12509. doi:10.1073/pnas.1324115111

Quéguiner, B. 2013. Iron fertilization and the structure of planktonic communities in high nutrient regions of the Southern Ocean. Deep-Sea Research Part II: Topical Studies in Oceanography **90**: 43–54. doi:10.1016/j.dsr2.2012.07.024

Raes, E. J., J. van de Kamp, L. Bodrossy, and others. 2020. N2 Fixation and New Insights Into Nitrification From the Ice-Edge to the Equator in the South Pacific Ocean. Frontiers in Marine Science **7**: 1–20. doi:10.3389/fmars.2020.00389

Rafter, P. A., D. M. Sigman, and K. R. M. Mackey. 2017. Recycled iron fuels new production in the eastern equatorial Pacific Ocean. Nature Communications **8**. doi:10.1038/s41467-017-01219-7

Ragueneau, O., P. Tréguer, A. Leynaert, and others. 2000. A review of the Si cycle in the modern ocean: Recent progress and missing gaps in the application of biogenic opal as a paleoproductivity proxy. Global and Planetary Change **26**: 317–365. doi:10.1016/S0921-8181(00)00052-7

Rakestraw, N. W., and A. Hollaender. 1936. Photochemical oxidation of ammonia in sea water. Science **84**. doi:10.1126/science.84.2185.442

Rani, S., H. W. Koh, S. K. Rhee, H. Fujitani, and S. J. Park. 2017. Detection and Diversity of the Nitrite Oxidoreductase Alpha Subunit (nxrA) Gene of Nitrospina in Marine Sediments. Microbial Ecology **73**: 111–122. doi:10.1007/s00248-016-0897-3

Ratnarajah, L., S. Nicol, and A. R. Bowie. 2018. Pelagic iron recycling in the Southern Ocean: Exploring the contribution of marine animals. Frontiers in Marine Science **5**: 1–9. doi:10.3389/fmars.2018.00109

Raven, J. A. 1988. The iron and molybdenum use efficiencies of plant growth with different energy, carbon and nitrogen sources. New Phytologist **109**. doi:10.1111/j.1469-8137.1988.tb04196.x

RAVEN, J. A. 1990. Predictions of Mn and Fe use efficiencies of phototrophic growth as a function of light availability for growth and of C assimilation pathway. New Phytologist **116**: 1–18. doi:10.1111/j.1469-8137.1990.tb00505.x

Raven, J. A., M. C. W. Evans, and R. E. Korb. 1999. The role of trace metals in photosynthetic electron transport in O2-evolving organisms. Photosynthesis Research **60**: 111–150. doi:10.1023/A:1006282714942

Raven, J. A., and P. G. Falkowski. 1999. Oceanic sinks for atmospheric CO2. Plant, Cell and Environment **22**: 741–755. doi:10.1046/j.1365-3040.1999.00419.x

Raven, J. A., and R. J. Geider. 1988. Temperature and algal growth. New Phytologist **110**. doi:10.1111/j.1469-8137.1988.tb00282.x

Read, J. F., R. T. Pollard, and U. Bathmann. 2002. Physical and biological patchiness of an upper ocean transect from South Africa to the ice edge near the Greenwich Meridian. Deep-Sea Research Part II: Topical Studies in Oceanography **49**: 3713–3733. doi:10.1016/S0967-0645(02)00108-X

Reay, D. S., D. B. Nedwell, J. Priddle, and J. C. Ellis-Evans. 1999. Temperature dependence of inorganic nitrogen uptake: Reduced affinity for nitrate at suboptimal temperatures in both algae and bacteria. Applied and Environmental Microbiology **65**: 2577–2584. doi:10.1128/aem.65.6.2577-2584.1999

Reay, D. S., J. Priddle, D. B. Nedwell, M. J. Whitehouse, J. C. Ellis-Evans, C. Deubert, and D. P. Connelly. 2001. Regulation by low temperature of phytoplankton growth and nutrient uptake in the Southern Ocean. Marine Ecology

Progress Series **219**. doi:10.3354/meps219051

Redfield, A. C. 1934. On the proportions of organic derivetives in sea water and their realtion to the composition of plankton, Liverpool University Press.

Rees, A. P., I. Joint, and K. M. Donald. 1999a. Early spring bloom phytoplankton-nutrient dynamics at the Celtic Sea shelf edge. Deep-Sea Research Part I: Oceanographic Research Papers. doi:10.1016/S0967-0637(98)00073-9

Rees, A. P., E. M. S. Woodward, and I. Joint. 2006. Concentrations and uptake of nitrate and ammonium in the Atlantic Ocean between 60{ring operator} N and 50{ring operator} S. Deep-Sea Research Part II: Topical Studies in Oceanography **53**: 1649–1665. doi:10.1016/j.dsr2.2006.05.008

Rees, A., M. Woodward, and I. Joint. 1999b. Measurement of nitrate and ammonium uptake at ambient concentrations in oligotrophic waters of the North-East Atlantic Ocean. Marine Ecology Progress Series **187**: 295–300. doi:10.3354/meps187295

Reuer, M. K., B. A. Barnett, M. L. Bender, P. G. Falkowski, and M. B. Hendricks. 2007. New estimates of Southern Ocean biological production rates from O2/Ar ratios and the triple isotope composition of O2. Deep-Sea Research Part I: Oceanographic Research Papers **54**: 951–974. doi:10.1016/j.dsr.2007.02.007

Richon, C., O. Aumont, and A. Tagliabue. 2020. Prey Stoichiometry Drives Iron Recycling by Zooplankton in the Global Ocean. Frontiers in Marine Science **7**: 1–12. doi:10.3389/fmars.2020.00451

Rigual-Hernández, A. S., T. W. Trull, S. G. Bray, and L. K. Armand. 2016. The fate of diatom valves in the Subantarctic and Polar Frontal Zones of the Southern Ocean: Sediment trap versus surface sediment assemblages. Palaeogeography, Palaeoclimatology, Palaeoecology **457**: 129–143. doi:10.1016/j.palaeo.2016.06.004

Riley, G. a., D. Van Hemert, and P. J. Wangersky. 1965. Organic aggregates in surface and deep waters of the Sargasso Sea. Limnology and Oceanography **10**: 354–363. doi:10.4319/lo.1965.10.3.0354

Rintoul, S. R. 2018. The global influence of localized dynamics in the Southern Ocean. Nature **558**: 209–218. doi:10.1038/s41586-018-0182-3

Ritz, C., F. Baty, J. C. Streibig, and D. Gerhard. 2015. Dose-response analysis using R. PLoS ONE **10**: 1–13. doi:10.1371/journal.pone.0146021

La Roche, J. 1983. Ammonium regeneration: its contribution to phytoplankton nitrogen requirements in a eutrophic environment. Marine Biology **75**. doi:10.1007/BF00406007

Rodrigues, R. M. N. V., and P. J. L. B. Williams. 2002. Inorganic nitrogen assimilation by picoplankton and whole plankton in a coastal ecosystem. Limnology and Oceanography **47**: 1608–1616. doi:10.4319/lo.2002.47.6.1608

Romera-Castillo, C., R. T. Letscher, and D. A. Hansell. 2016. New nutrients exert fundamental control on dissolved organic carbon accumulation in the surface Atlantic Ocean. Proceedings of the National Academy of Sciences **113**: 10497–10502. doi:10.1073/pnas.1605344113

Rose, J. M., Y. Feng, G. R. Ditullio, and others. 2009. Synergistic effects of iron and temperature on Antarctic phytoplankton and microzooplankton assemblages. Biogeosciences **6**: 3131–3147. doi:10.5194/bg-6-3131-2009

Rotthauwe, J. H., K. P. Witzel, and W. Liesack. 1997. The ammonia monooxygenase structural gene amoa as a functional marker: Molecular fine-scale analysis of natural ammonia-oxidizing populations. Applied and Environmental Microbiology. doi:10.1128/aem.63.12.4704-4712.1997

Rueter, J. G., and F. M. M. Morel. 1981. The interaction between zinc deficiency and copper toxicity as it affects the silicic acid uptake mechanisms in Thalassiosira pseudonana. Limnology and Oceanography **26**: 67–73. doi:10.4319/lo.1981.26.1.0067

Ryan-Keogh, T. J., T. N. Mtshali, N. R. van Horsten, H. J. Little, and S. J. Thomalla. 2018. Seasonal development of iron limitation in the sub-Antarctic zone. Biogeosciences **15**: 4647–4660. doi:10.5194/bg-15-4647-2018

Ryan-Keogh, T. J., S. J. Thomalla, T. N. Mtshali, and H. Little. 2017. Modelled estimates of spatial variability of iron stress in the Atlantic sector of the Southern Ocean. Biogeosciences **14**: 3883–3897. doi:10.5194/bg-14-3883-2017

Rysgaard, S., P. Thastum, T. Dalsgaard, P. B. Christensen, and N. P. Sloth. 1999. Effects of salinity on NH4+ adsorption capacity, nitrification, and denitrification in Danish estuarine sediments. Estuaries **22**: 21–30. doi:10.2307/1352923

Sabine, C. L., C. L. Sabine, R. A. Feely, and others. 2004. The Oceanic Sink for Anthropogenic CO 2. Science **367**: 2–7. doi:10.1126/science.1097403

Sahlsten, E. 1987. Nitrogenous nutrition in the euphotic zone of the central north pacific gyre. Marine Biology **96**: 433–439. doi:10.1038/164914a0

Saito, M. A., M. R. McIlvin, D. M. Moran, and others. 2020. Abundant nitrite-oxidizing metalloenzymes in the mesopelagic zone of the tropical Pacific Ocean. Nature Geoscience **13**: 355–362. doi:10.1038/s41561-020-0565-6

Sallée, J. B., K. G. Speer, and S. R. Rintoul. 2010. Zonally asymmetric response of the Southern Ocean mixed-layer depth to the Southern Annular Mode. Nature Geoscience **3**: 273–279. doi:10.1038/ngeo812

Salter, I., R. S. Lampitt, R. Sanders, A. Poulton, A. E. S. Kemp, B. Boorman, K. Saw, and R. Pearce. 2007. Estimating carbon, silica and diatom export from a naturally fertilised phytoplankton bloom in the Southern Ocean using PELAGRA: A novel drifting sediment trap. Deep-Sea Research Part II: Topical Studies in Oceanography **54**: 2233–2259. doi:10.1016/j.dsr2.2007.06.008

Sambrotto, R. N., and B. J. Mace. 2000. Coupling of biological and physical regimes across the Antarctic Polar Front as reflected by nitrogen production and recycling. Deep-Sea Research Part II: Topical Studies in Oceanography **47**: 3339–3367. doi:10.1016/S0967-0645(00)00071-0

Sanders, R., P. J. Morris, M. Stinchcombe, S. Seeyave, H. Venables, and M. Lucas. 2007. New production and the f ratio around the Crozet Plateau in austral summer 2004-2005 diagnosed from seasonal changes in inorganic nutrient levels. Deep-Sea Research Part II: Topical Studies in Oceanography **54**: 2191–2207. doi:10.1016/j.dsr2.2007.06.007

Santoro, A. E., C. Buchwald, A. N. Knapp, and others. 2020. Nitrification and nitrous oxide production in the offshore waters of the Eastern Tropical South Pacific. 1–35.

Santoro, A. E., C. Buchwald, M. R. McIlvin, and K. L. Casciotti. 2011. Isotopic Signature of N2O Produced by Marine Ammonia-Oxidizing Archaea. Science.

Santoro, A. E., and K. L. Casciotti. 2011. Enrichment and characterization of ammonia-oxidizing archaea from the open ocean: Phylogeny, physiology and stable isotope fractionation. ISME Journal **5**: 1796–1808. doi:10.1038/ismej.2011.58

Santoro, A. E., K. L. Casciotti, and C. A. Francis. 2010. Activity, abundance and diversity of nitrifying archaea and bacteria in the central California Current. Environmental Microbiology **12**. doi:10.1111/j.1462-2920.2010.02205.x

Santoro, A. E., C. L. Dupont, R. A. Richter, and others. 2015. Genomic and proteomic characterization of "Candidatus Nitrosopelagicus brevis": An ammonia-oxidizing archaeon from the open ocean. Proceedings of the National Academy of Sciences of the United States of America **112**: 1173–1178. doi:10.1073/pnas.1416223112

Santoro, A. E., M. A. Saito, T. J. Goepfert, C. H. Lamborg, C. L. Dupont, and G. R. DiTullio. 2017. Thaumarchaeal ecotype distributions across the equatorial Pacific Ocean and their potential roles in nitrification and sinking flux attenuation. Limnology and Oceanography **62**: 1984–2003. doi:10.1002/lno.10547

Santoro, A. E., C. M. Sakamoto, J. M. Smith, and others. 2013. Measurements of nitrite production in and around the primary nitrite maximum in the central California Current. Biogeosciences **10**: 7395–7410. doi:10.5194/bg-10-7395-2013

Santos, J. P., D. Mendes, M. Monteiro, H. Ribeiro, M. S. Baptista, M. T. Borges, and C. Magalhães. 2018. Salinity impact on ammonia oxidizers activity and amoA expression in estuarine sediments. Estuarine, Coastal and Shelf Science **211**: 177–187. doi:10.1016/j.ecss.2017.09.001

Santos, J. P., A. G. G. Sousa, H. Ribeiro, and C. Magalhães. 2020. The Response of Estuarine Ammonia-Oxidizing Communities to Constant and Fluctuating Salinity Regimes. Frontiers in Microbiology **11**: 1–14. doi:10.3389/fmicb.2020.574815

Sarmiento, J. L., N. Gruber, M. A. Brzezinski, and J. P. Dunne. 2004. CORRECTIONS & AMENDMENTS thermocline nutrients and low latitude biological productivity. **427**: 0–5. doi:10.1038/nature10605

Sarmiento, J. L., and J. R. Toggweiler. 1984. A new model for the role of the oceans in determining atmospheric PCO2. Nature. doi:10.1038/308621a0

Savchenko, V. G., O. A. Vladimirov, and W. J. Emery. 1978. A cyclonic eddy in the antarctic circumpolar current south of Australia: Results of !Soviet-American observations aboard the !R/V Professor Zubov. Journal of Physical Oceanography **8**. doi:10.1175/1520-0485(1978)008<0825:aceita>2.0.co;2

Savoye, N., F. Dehairs, M. Elskens, and others. 2004. Regional variation of spring N-uptake and new production in the Southern Ocean. Geophysical Research Letters **31**: 5–8. doi:10.1029/2003GL018946

Schaefer, S. C., and J. T. Hollibaugh. 2017. Temperature Decouples Ammonium and Nitrite Oxidation in Coastal Waters. Environmental Science and Technology **51**: 3157–3164. doi:10.1021/acs.est.6b03483

Schallenberg, C., S. Bestley, A. Klocker, and others. 2018. Sustained Upwelling of Subsurface Iron Supplies Seasonally Persistent Phytoplankton Blooms Around the Southern Kerguelen Plateau, Southern Ocean. Journal of Geophysical Research: Oceans **123**: 5986–6003. doi:10.1029/2018JC013932

Schlitzer, R. 2002. Carbon export fluxes in the Southern Ocean: Results from inverse modeling and comparison with satellite-based estimates. Deep-Sea Research Part II: Topical Studies in Oceanography **49**: 1623–1644. doi:10.1016/S0967-0645(02)00004-8

Schlitzer, R. 2015. Data Analysis and Visualization with Ocean Data View,.

Schlosser, C., K. Schmidt, A. Aquilina, and others. 2018. Mechanisms of dissolved and labile particulate iron supply to shelf waters and phytoplankton blooms off South Georgia, Southern Ocean. Biogeosciences **15**: 4973–4993. doi:10.5194/bg-15-4973-2018

Schneider, B., R. Schlitzer, G. Fischer, and E.-M. Nöthig. 2003. Depth-dependent elemental compositions of particulate organic matter (POM) in the ocean. Global Biogeochemical Cycles **17**: n/a-n/a. doi:10.1029/2002gb001871

Schofield, O., T. Miles, A. C. Alderkamp, and others. 2015. In situ phytoplankton distributions in the Amundsen Sea Polynya measured by autonomous gliders. Elementa. doi:10.12952/journal.elementa.000073

Schön, G. H., and H. Engel. 1962. Der Einfluß des Lichtes auf Nitrosomonas europaea Win. Archiv für Mikrobiologie. doi:10.1007/BF00409076

Schramm, A., D. DeBeer, J. van den Heuvel, S. Ottengraf, and R. Amann. 1999. Microscale Distribution of Populations and Activities of Nitrosospira and Nitrospira spp. along a Macroscale Gradient in a Nitrifying Bioreactor: Quantification by In Situ Hybridization and the Use of Microsensors. Society **65**: 3690–3696.

Sciandra, A., and R. Amara. 1994. Effects of nitrogen limitation on growth and nitrite excretion rates of the dinoflagellate Prorocentrum minimum. Marine Ecology Progress Series **105**: 301. doi:10.3354/meps105301

Sedwick, P. N., S. Blain, B. Quéguiner, F. B. Griffiths, M. Fiala, E. Bucciarelli, and M. Denis. 2002. Resource limitation of phytoplankton growth in the Crozet Basin, Subantarctic Southern Ocean. Deep-Sea Research Part II: Topical Studies in Oceanography **49**: 3327–3349. doi:10.1016/S0967-0645(02)00086-3

Sedwick, P. N., G. R. DiTullio, D. A. Hutchins, W. Boyd, B. Griffiths, A. C. Crossley, T. W. Trull, and B. Queguiner. 1999. Limitation of algal growth by iron deficiency in the Australian Subantarctic region. Geophysical Research Letters **26**: 2865–2868.

Seeyave, S., M. I. Lucas, C. M. Moore, and A. J. Poulton. 2007. Phytoplankton productivity and community structure in the vicinity of the Crozet Plateau during austral summer 2004/2005. Deep-Sea Research Part II: Topical Studies in Oceanography **54**: 2020–2044. doi:10.1016/j.dsr2.2007.06.010

Serebrennikova, Y. M., and K. A. Fanning. 2004. Nutrients in the Southern Ocean GLOBEC region: Variations, water circulation, and cycling. Deep-Sea Research Part II: Topical Studies in Oceanography **51**: 1981–2002. doi:10.1016/j.dsr2.2004.07.023

Serra, J. L., M. J. Llama, and E. Cadenas. 1978. Nitrate Utilization by the Diatom Skeletonema costatum: II. Regulation of Nitrate Uptake. Plant Physiology **62**: 991–994. doi:10.1104/pp.62.6.991

Shadwick, E. H., T. W. Trull, B. Tilbrook, A. J. Sutton, E. Schulz, and C. L. Sabine. 2015. Seasonality of biological and physical controls on surface ocean CO2 from hourly observations at the Southern Ocean Time Series site south of Australia. Global Biogeochemical Cycles **29**: 223–238. doi:10.1002/2014GB004906

Shafiee, R. T., J. T. Snow, Q. Zhang, and R. E. M. Rickaby. 2019. Iron requirements and uptake strategies of the globally abundant marine ammonia-oxidising archaeon, Nitrosopumilus maritimus SCM1. The ISME Journal. doi:10.1038/s41396-019-0434-8

Sherman, E., J. K. Moore, F. Primeau, and D. Tanouye. 2016. Temperature influence on phytoplankton community growth rates. Global Biogeochemical Cycles. doi:10.1002/2015GB005272

Shi, D., Y. Xu, B. M. Hopkinson, and F. M. M. Morel. 2010. Effect of ocean acidification on iron availability to marine phytoplankton. Science **327**: 676–679. doi:10.1126/science.1183517

Shi, T., Y. Sun, and P. G. Falkowski. 2007. Effects of iron limitation on the expression of metabolic genes in the marine cyanobacterium Trichodesmium erythraeum IMS101. Environmental Microbiology. doi:10.1111/j.1462-2920.2007.01406.x

Shiomoto, A., K. Sasaki, T. Shimoda, and S. Matsumura. 1994. Kinetics of nitrate and ammonium uptake by the natural populations of marine phytoplankton in the surface water of the Oyashio region during spring and summer. Journal of Oceanography **50**: 515–529. doi:10.1007/BF02235421

Shiozaki, T., M. Ijichi, A. Fujiwara, A. Makabe, S. Nishino, C. Yoshikawa, and N. Harada. 2019. Factors Regulating Nitrification in the Arctic Ocean: Potential Impact of Sea Ice Reduction and Ocean Acidification. Global Biogeochemical Cycles **33**: 1085–1099. doi:10.1029/2018GB006068

Shiozaki, T., M. Ijichi, K. Isobe, and others. 2016. Nitrification and its influence on biogeochemical cycles from the equatorial Pacific to the Arctic Ocean. The ISME journal 1–14. doi:10.1038/ismej.2016.18

Siegel, D. A., K. O. Buesseler, S. C. Doney, S. F. Sailley, M. J. Behrenfeld, and P. W. Boyd. 2014. Global assessment of ocean carbon export by combining satellite observations and food-web models. Global Biogeochemical Cycles **28**: 181–196. doi:10.1002/2013GB004743.Received

Siegenthaler, U., and T. Wenk. 1984. Rapid atmospheric CO2 variations and ocean circulation. Nature **308**: 624–626. doi:10.1038/308624a0

Sigman, D. M., and E. A. Boyle. 2000. Glacial/Interglacial Variations In Atmospheric Carbon Dioxide. Nature. doi:10.1038/35038000

Sigman, D. M., K. L. Casciotti, M. Andreani, C. Barford, M. Galanter, and J. K. Böhlke. 2001. A bacterial method for the nitrogen isotopic analysis of nitrate in seawater and freshwater. Analytical Chemistry **73**: 4145–4153. doi:10.1021/ac010088e

Sigman, D. M., M. P. Hain, and G. H. Haug. 2010. The polar ocean and glacial cycles in atmospheric CO2 concentration. Nature **466**: 47–55. doi:10.1038/nature09149

Sigman, D. M., A. M. a, D. C. McCorkle, R. Francois, and G. Fischer. 1999. The d15N of nitrate in the Southern Ocean: Nitrate consumption in surface waters. Global Biogeochemical Cycles **13**: 1149–1166. doi:10.1029/1999GB900038

da Silva, J. J. R., and R. J. P. Williams. 2001. The Biological Chemistry of the Elements: The Inorganic Chemistry of Life. Journal of Chemical Education 76019.

Sintes, E., K. Bergauer, D. De Corte, T. Yokokawa, and G. J. Herndl. 2013. Archaeal amoA gene diversity points to distinct biogeography of ammonia-oxidizing Crenarchaeota in the ocean. Environmental Microbiology **15**: 1647–1658. doi:10.1111/j.1462-2920.2012.02801.x

Sivasubramanian, V., and V. N. R. Rao. 1988. Uptake and assimilation of nitrogen by Navicula lucens Hustedt, a marine diatom. Acta Botanica Indica **16**: 131–142.

Slawyk, G. 1979. 13c and15n uptake by Phytoplankton in the Antarctic Upwelling Area: Results from the Antiprod I Cruise in the Indian Ocean Sector. Marine and Freshwater Research. doi:10.1071/MF9790431

Smart, S. M., S. E. Fawcett, H. Ren, and others. 2020. The Nitrogen Isotopic Composition of Tissue and Shell-Bound Organic Matter of Planktic Foraminifera in Southern Ocean Surface Waters. Geochemistry, Geophysics, Geosystems **21**: 1–29. doi:10.1029/2019GC008440

Smart, S. M., S. E. Fawcett, S. J. Thomalla, M. a Weigand, C. J. C. Reason, and D. M. Sigman. 2015. Global Biogeochemical Cycles. 1–19. doi:10.1002/2014GB005013.Received

Smetacek, V., P. Assmy, and J. Henjes. 2004. The role of grazing in structuring Southern Ocean pelagic ecosystems and biogeochemical cycles. Antarctic Science **16**. doi:10.1017/S0954102004002317

Smetacek, V., C. Klaas, V. H. Strass, and others. 2012. Deep carbon export from a Southern Ocean iron-fertilized diatom bloom. Nature **487**: 313–319. doi:10.1038/nature11229

Smith, W. O., and D. M. Nelson. 1986. Importance of Ice Edge Phytoplankton Production in the Southern Ocean. BioScience **36**: 251–257. doi:10.2307/1310215

Smith, J. M., F. P. Chavez, and C. A. Francis. 2014. Ammonium uptake by phytoplankton regulates nitrification in the sunlit ocean. PLoS ONE **9**. doi:10.1371/journal.pone.0108173

Smith, J. M., J. Damashek, F. P. Chavez, and C. A. Francis. 2016. Factors influencing nitrification rates and the abundance and transcriptional activity of ammonia-oxidizing microorganisms in the dark northeast Pacific Ocean. Limnology and Oceanography **61**: 596–609. doi:10.1002/lno.10235

Smith, W. O., R. F. Anderson, J. K. Moore, L. A. Codispoti, and J. M. Morrison. 2000. The US Southern Ocean Joint Global Ocean Flux Study : an introduction to AESOPS. **47**: 3073–3093.

Smith, W. O., and W. G. Harrison. 1991. New production in polar regions: the role of environmental controls. Deep Sea Research Part A, Oceanographic Research Papers. doi:10.1016/0198-0149(91)90085-T

Smith, W. O., and C. Lancelot. 2004. Bottom-up versus top-down control in phytoplankton of the Southern Ocean. Antarctic Science **16**: 531–539. doi:10.1017/S0954102004002305

Smythe-Wright, D., P. Chapman, C. Duncombe Rae, L. V. Shannon, and S. M. Boswell. 1998. Characteristics of the South Atlantic subtropical frontal zone between 15°W and 5°E. Deep-Sea Research Part I: Oceanographic Research Papers **45**: 167–192. doi:10.1016/S0967-0637(97)00068-X

Somville, M. 1984. Use of nitrifying activity measurements for describing the effect of salinity on nitrification in the Scheldt estuary. Applied and environmental microbiology **47**: 424–426. doi:10.1128/aem.47.2.424-426.1984

Sorokin, D. Y., S. Lücker, D. Vejmelkova, and others. 2012. Nitrification expanded: Discovery, physiology and genomics of a nitrite-oxidizing bacterium from the phylum Chloroflexi. ISME Journal **6**: 2245–2256. doi:10.1038/ismej.2012.70

Spieck, E., S. Ehrich, and J. Aamand. 1998. Isolation and immunocytochemical location of the nitrite-oxidizing system in Nitrospira moscoviensis. Arch Microbiol 225–230.

Spieck, E., S. Muller, A. Engel, E. Mandelkow, H. Patel, and E. Bock. 1996. Two-Dimensional Structure of Membrane-Bound Nitrite Oxidoreductase from Nitrobacter hamburgensis. Journal of Structural Biology **117**: 117–123.

Staal, M., F. J. R. Meysman, and L. J. Stal. 2003. Temperature excludes N2-fixing heterocystous cyanobacteria in the tropical oceans. Nature **425**: 504–507. doi:10.1038/nature01999

Starkenburg, S. R., P. S. G. Chain, L. A. Sayavedra-Soto, and others. 2006. Genome sequence of the chemolithoautotrophic nitrite-oxidizing bacterium Nitrobacter winogradskyi Nb-255. Applied and Environmental Microbiology **72**: 2050–2063. doi:10.1128/AEM.72.3.2050-2063.2006

Stawiarski, B., E. T. Buitenhuis, and C. Le Quéré. 2016. The physiological response of picophytoplankton to temperature and its model representation. Frontiers in Marine Science **3**: 1–13. doi:10.3389/fmars.2016.00164

Stehr, G., B. Böttcher, P. Dittberner, G. Rath, and H. P. Koops. 1995. The ammonia-oxidizing nitrifying population of the River Elbe estuary. FEMS Microbiology Ecology **17**: 177–186. doi:10.1016/0168-6496(95)00022-3

Stolte, W., T. McCollin, A. A. M. Noordeloos, and R. Riegman. 1994. Effect of nitrogen source on the size distribution within marine phytoplankton populations. Journal of Experimental Marine Biology and Ecology. doi:10.1016/0022-0981(94)90167-8

Strzepek, R. F., P. W. Boyd, and W. G. Sunda. 2019a. Photosynthetic adaptation to low iron, light, and temperature in Southern Ocean phytoplankton. Proceedings of the National Academy of Sciences of the United States of America **116**: 4388–4393. doi:10.1073/pnas.1810886116

Strzepek, R. F., P. W. Boyd, and W. G. Sunda. 2019b. Photosynthetic adaptation to low iron, light, and temperature in Southern Ocean phytoplankton. Proceedings of the National Academy of Sciences of the United States of America **116**: 4388–4393. doi:10.1073/pnas.1810886116

Strzepek, R. F., K. A. Hunter, R. D. Frew, P. J. Harrison, and P. W. Boyd. 2012. Iron-light interactions differ in Southern Ocean phytoplankton. Limnology and Oceanography **57**: 1182–1200. doi:10.4319/lo.2012.57.4.1182

Sun, X., C. Frey, E. Garcia-Robledo, A. Jayakumar, and B. B. Ward. 2021. Microbial niche differentiation explains nitrite oxidation in marine oxygen minimum zones. The ISME Journal 1–13. doi:10.1038/s41396-020-00852-3

Sun, X., Q. Ji, A. Jayakumar, and B. B. Ward. 2017. Dependence of nitrite oxidation on nitrite and oxygen in low-oxygen seawater. Geophysical Research Letters **44**: 7883–7891. doi:10.1002/2017GL074355

Sun, X., L. F. M. Kop, M. C. Y. Lau, J. Frank, A. Jayakumar, S. Lücker, and B. B. Ward. 2019. Uncultured Nitrospina-like species are major nitrite oxidizing bacteria in oxygen minimum zones. ISME Journal **13**: 2391–2402. doi:10.1038/s41396-019-0443-7

Sunda, W. G. 1989. Trace Metal Interactions with Marine Phytoplankton Trace Metal Interactions with Marine. **5581**: 37–41. doi:10.1080/01965581.1988.10749543

Sunda, W. G., and S. A. Huntsman. 1997. Interrelated influence of iron, light and cell size on marine phytoplankton growth. Nature. doi:10.1038/37093

Sundermeyer-Klinger, H., W. Meyer, B. Warninghoff, and E. Bock. 1984. Membrane-bound nitrite oxidoreductase of Nitrobacter: evidence for a nitrate reductase system. Archives of Microbiology **140**. doi:10.1007/BF00454918

Suzuki, I., U. Dular, and S. C. Kwok. 1974. Ammonia or ammonium ion as substrate for oxidation by Nitrosomonas europaea cells and extracts. Journal of Bacteriology **120**: 556–558. doi:10.1128/jb.120.1.556-558.1974

Suzuki, Y., and M. Takahashi. 1995. GROWTH RESPONSES OF SEVERAL DIATOM SPECIES ISOLATED FROM VARIOUS ENVIRONMENTS TO TEMPERATURE. Journal of Phycology. doi:10.1111/j.0022-3646.1995.00880.x

Sverdrup, H. U. 1953. On conditions for the vernal blooming of phytoplankton. ICES Journal of Marine Science. doi:10.1093/icesjms/18.3.287

Swart, S., S. J. Thomalla, and P. M. S. Monteiro. 2015. The seasonal cycle of mixed layer dynamics and phytoplankton biomass in the Sub-Antarctic Zone: A high-resolution glider experiment. Journal of Marine Systems **147**: 103–115. doi:10.1016/j.jmarsys.2014.06.002

Syrett, P. J. 1956. The Assimilation of Ammonia and Nitrate by Nitrogen-Starved Cells of Chlorella vulgaris: II. The Assimilation of Large Quantities of Nitrogen. Physiologia Plantarum. doi:10.1111/j.1399-3054.1956.tb08988.x

Syrett, P. J. 1981. Nitrogen metabolism of microalgae. Canadian Journal of Fisheries and Aquatic Science.

Tagliabue, A., L. Bopp, J. C. Dutay, and others. 2010. Hydrothermal contribution to the oceanic dissolved iron inventory. Nature Geoscience **3**: 252–256. doi:10.1038/ngeo818

Tagliabue, A., A. R. Bowie, J.-B. Sallée, P. W. Boyd, and S. Swart. 2014. Surface-water iron supplies in the Southern Ocean sustained by deep winter mixing. Nature Geoscience **7**: 314–320. doi:10.1038/ngeo2101

Tagliabue, A., T. Mtshali, O. Aumont, A. R. Bowie, M. B. Klunder, A. N. Roychoudhury, and S. Swart. 2012. A global compilation of dissolved iron measurements: Focus on distributions and processes in the Southern Ocean. Biogeosciences **9**: 2333–2349. doi:10.5194/bg-9-2333-2012

Takahashi, T., F. Chavez, C. Sweeney, and others. 2009. Climatological mean and decadal change in surface ocean pCO2, and net sea–air CO2 flux over the global oceans. Deep Sea Research Part II: Topical Studies in Oceanography **56**: 554–577. doi:10.1016/j.dsr2.2008.12.009

Takahashi, T., S. C. Sutherland, C. Sweeney, and others. 2002. Global sea-air CO_2 flux based on climatological surface ocean pCO_2, and seasonal biological and temperature effects. Deep-Sea Research Part II: Topical Studies in Oceanography **49**: 1601–1622. doi:10.1016/S0967-0645(02)00003-6

Takeda, S. 1998. Influence of iron availability on nutrient consumption ratio. Nature **393**: 774–777.

Talley, L. D., G. L. Pickard, W. J. Emery, and J. H. Swift. 2011. Chapter-13-Southern-Ocean_2011_Descriptive-Physical-Oceanography-Sixth-Edition-. Descriptive Physical Oceanography 437–471. doi:10.1016/b978-0-7506-4552-2.10013-7

Taylor, B. W., C. F. Keep, R. O. Hall, B. J. Koch, L. M. Tronstad, A. S. Flecker, and A. J. Ulseth. 2007. Improving the fluorometric ammonium method: matrix effects, background fluorescence, and standard additions. Journal of the North American Benthological Society **26**: 167–177. doi:10.1899/0887-3593(2007)26[167:ITFAMM]2.0.CO;2

Taylor, M. H., M. Losch, and A. Bracher. 2013. On the drivers of phytoplankton blooms in the Antarctic marginal ice zone: A modeling approach. Journal of Geophysical Research: Oceans **118**: 63–75. doi:10.1029/2012JC008418

Tedesco, L., M. Vichi, and E. Scoccimarro. 2019. Sea-ice algal phenology in a warmer Arctic. Science Advances **5**. doi:10.1126/sciadv.aav4830

Thamdrup, B., and S. Fleischer. 1998. Temperature dependence of oxygen respiration, nitrogen mineralization, and nitrification in Arctic sediments. Aquatic Microbial Ecology **15**: 191–199. doi:10.3354/ame015191

Thi Dieu Vu, H., and Y. Sohrin. 2013. Diverse stoichiometry of dissolved trace metals in the Indian Ocean. Scientific Reports **3**: 1–5. doi:10.1038/srep01745

Thomalla, S. J., N. Fauchereau, S. Swart, and P. M. S. Monteiro. 2011a. Regional scale characteristics of the seasonal cycle of chlorophyll in the Southern Ocean. Biogeosciences **8**: 2849–2866. doi:10.5194/bg-8-2849-2011

Thomalla, S. J., H. N. Waldron, M. I. Lucas, J. F. Read, I. J. Ansorge, and E. Pakhomov. 2011b. Phytoplankton distribution and nitrogen dynamics in the southwest indian subtropical gyre and Southern Ocean waters. Ocean Science **7**: 113–127. doi:10.5194/os-7-113-2011

Thomas, M. K., C. T. Kremer, C. A. Klausmeier, and E. Litchman. 2012. A global pattern of thermal adaptation in marine phytoplankton. Science **338**: 1085–1088. doi:10.1126/science.1224836

Thompson, P. A., M. -x Guo, and P. J. Harrison. 1992a. EFFECTS OF VARIATION IN TEMPERATURE. I. ON THE BIOCHEMICAL COMPOSITION OF EIGHT SPECIES OF MARINE PHYTOPLANKTON. Journal of Phycology **28**. doi:10.1111/j.0022-3646.1992.00481.x

Thompson, P. A., M. -x Guo, P. J. Harrison, and J. N. C. Whyte. 1992b. EFFECTS OF VARIATION IN TEMPERATURE. II. ON THE FATTY ACID COMPOSITION OF EIGHT SPECIES OF MARINE PHYTOPLANKTON. Journal of Phycology **28**. doi:10.1111/j.0022-3646.1992.00488.x

Thompson, P. A., M. E. Levasseur, and P. J. Harrison. 1989. Light-limited growth on ammonium vs. nitrate: What is the advantage for marine phytoplankton? Limnology and Oceanography **34**: 1014–1024. doi:10.4319/lo.1989.34.6.1014

Tilzer, M. M., and Z. Dubinsky. 1987. Effects of temperature and day length on the mass balance of Antarctic phytoplankton. Polar Biology **7**. doi:10.1007/BF00286822

Tilzer, M. M., malte Elbrächter, W. W. Gieskes, and B. Beese. 1986. Light-temperature interactions in the control of photosynthesis in Antarctic phytoplankton. Polar Biology **5**. doi:10.1007/BF00443382

Timmermans, K. R., M. A. Van Leeuwe, J. T. M. De Jong, and others. 1998. Iron stress in the Pacific region of the Southern Ocean: Evidence from enrichment bioassays. Marine Ecology Progress Series **166**: 27–41. doi:10.3354/meps166027

Timmermans, K. R., W. Stolte, H. J. W. Baar, and H. J. W. De Baar. 1994. Iron-mediated effects on nitrate reductase in marine phytoplankton. Marine Biology **121**: 389–396. doi:10.1007/BF00346749

Toggweiler, J. R., K. Dixon, and W. S. Broecker. 1991. The Peru upwelling and the ventilation of the south Pacific thermocline. Journal of Geophysical Research **96**: 20467. doi:10.1029/91jc02063

Toggweiler, J. R., A. Gnanadesikan, S. Carson, R. Murnane, and J. L. Sarmiento. 2003. Representation of the carbon cycle in box models and GCMs: 1. Solubility pump. Global Biogeochemical Cycles **17**. doi:10.1029/2001GB001401

Tolar, B. B., M. J. Ross, N. J. Wallsgrove, Q. Liu, L. I. Aluwihare, B. N. Popp, and J. T. Hollibaugh. 2016. Contribution of ammonia oxidation to chemoautotrophy in Antarctic coastal waters. The ISME Journal **10**: 2605–2619. doi:10.1038/ismej.2016.61

Toole, J. M. 1981. Sea Ice, Winter Convection, and the Temperature Minimum Layer in the Southern Ocean. Journal of Geophysical Research **86**: 8037–8047.

Tortell, P. D., C. D. Payne, Y. Li, and others. 2008. CO2 sensitivity of Southern Ocean phytoplankton. Geophysical Research Letters **35**. doi:10.1029/2007GL032583

Tovar-Sánchez, A., C. M. Duarte, J. C. Alonso, S. Lacorte, R. Tauler, and C. Galban-Malagón. 2010. Impacts of metals and nutrients released from melting multiyear Arctic sea ice. Journal of Geophysical Research C: Oceans **115**: 1–7. doi:10.1029/2009JC005685

Tozzi, S., and W. O. Smith. 2017. Contrasting Photo-physiological Responses of the Haptophyte Phaeocystis Antarctica and the Diatom Pseudonitzschia sp. in the Ross Sea (Antarctica). AIMS Geosciences **3**: 142–162. doi:10.3934/geosci.2017.2.142

Tréguer, P., C. Bowler, B. Moriceau, and others. 2018. Influence of diatom diversity on the ocean biological carbon pump. Nature Geoscience **11**: 27–37. doi:10.1038/s41561-017-0028-x

Tréguer, P., and G. Jacques. 1992. Dynamics of nutrients and phytoplankton, and fluxes of carbon, nitrogen and silicon in the Antarctic Ocean. Polar Biology **12**: 149–162. doi:10.1007/BF00238255

Tréguer, P., D. M. Nelson, A. J. Van Bennekom, D. J. Demaster, A. Leynaert, and B. Quéguiner. 1995. The silica balance in the world ocean: A reestimate. Science **268**: 375–379. doi:10.1126/science.268.5209.375

Tréguer, P., and P. Pondaven. 2000. Global change: Silica control of carbon dioxide. Nature **406**.

Tremblay, J. E., M. I. Lucas, G. Kattner, R. Pollard, V. H. Strass, U. Bathmann, and A. Bracher. 2002. Significance of the Polar Frontal Zone for large-sized diatoms and new production during summer in the Atlantic sector of the Southern Ocean. Deep-Sea Research Part II: Topical Studies in Oceanography **49**: 3793–3811. doi:10.1016/S0967-0645(02)00111-X

Treusch, A. H., S. Leininger, A. Kietzin, S. C. Schuster, H. P. Klenk, and C. Schleper. 2005. Novel genes for nitrite reductase and Amo-related proteins indicate a role of uncultivated mesophilic crenarchaeota in nitrogen cycling. Environmental Microbiology **7**. doi:10.1111/j.1462-2920.2005.00906.x

Trimborn, S., S. Thoms, K. Bischof, and S. Beszteri. 2019. Susceptibility of two southern ocean phytoplankton key species to iron limitation and high light. Frontiers in Marine Science **6**. doi:10.3389/fmars.2019.00167

Tripathy, S. C., S. Patra, K. Vishnu Vardhan, A. Sarkar, R. K. Mishra, and N. Anilkumar. 2017. Nitrogen uptake by phytoplankton in surface waters of the Indian sector of Southern Ocean during austral summer. Frontiers of Earth Science 1–11. doi:10.1007/s11707-017-0649-9

Trull, T. W., and L. Armand. 2001. Insights into Southern Ocean carbon export from the δ13c of particles and dissolved inorganic carbon during the SOIREE iron release experiment. Deep-Sea Research Part II: Topical Studies in Oceanography **48**: 2655–2680. doi:10.1016/S0967-0645(01)00013-3

Trull, T. W., D. Davies, and K. Casciotti. 2008. Insights into nutrient assimilation and export in naturally iron-fertilized waters of the Southern Ocean from nitrogen, carbon and oxygen isotopes. Deep-Sea Research Part II: Topical Studies in Oceanography **55**: 820–840. doi:10.1016/j.dsr2.2007.12.035

Tsoularis, A., and J. Wallace. 2002. Analysis of logistic growth models. Mathematical Biosciences **179**: 21–55.

Tupas, L., and I. Koike. 1990. Amino acid and ammonium utilization by heterotrophic marine bacteria grown in enriched seawater. Limnol. Oceanogr **35**: 1145–155. doi:10.4319/lo.1990.35.5.1145

Tupas, L., and I. Koike. 1991. Simultaneous uptake and regeneration of ammonium by mixed assemblages of heterotrophic marine bacteria. Marine Ecology Progress Series **70**: 273–382. doi:10.3354/meps070273

Turner, J., T. Phillips, G. J. Marshall, J. S. Hosking, J. O. Pope, T. J. Bracegirdle, and P. Deb. 2017. Unprecedented springtime retreat of Antarctic sea ice in 2016. Geophysical Research Letters **44**: 6868–6875. doi:10.1002/2017GL073656

Twining, B. S., and S. B. Baines. 2013. The trace metal composition of marine phytoplankton. Annual Review of Marine Science **5**: 191–215. doi:10.1146/annurev-marine-121211-172322

Ushiki, N., M. Jinno, H. Fujitani, T. Suenaga, A. Terada, and S. Tsuneda. 2017. Nitrite oxidation kinetics of two Nitrospira strains : The quest for competition and ecological niche differentiation. Journal of Bioscience and Bioengineering **123**: 581–589. doi:10.1016/j.jbiosc.2016.12.016

Vaccaro, R. F., and J. H. Ryther. 1960. Marine Phytoplankton and the Distribution of Nitrite in the Sea*. ICES Journal of Marine Science **25**: 260–271. doi:10.1093/icesjms/25.3.260

Vajrala, N., W. Martens-Habbena, L. A. Sayavedra-Soto, A. Schauer, P. J. Bottomley, D. A. Stahl, and D. J. Arp. 2013. Hydroxylamine as an intermediate in ammonia oxidation by globally abundant marine archaea. Proceedings of the National Academy of Sciences of the United States of America **110**: 1006–1011. doi:10.1073/pnas.1214272110

Vanzella, A., M. Guerrero, and R. Jones. 1989. Effect of CO and light on ammonium and nitrite oxidation by chemolithotrophic bacteria. Marine Ecology Progress Series **57**: 69–76. doi:10.3354/meps057069

Varela, D. E., and P. J. Harrison. 1999. Seasonal variability in nitrogenous nutrition of phytoplankton assemblages in the northeastern subarctic Pacific Ocean. Deep-Sea Research Part II: Topical Studies in Oceanography **46**. doi:10.1016/S0967-0645(99)00074-0

Vekeman, B., S. Hoefman, P. De Vos, E. Spieck, and K. Heylen. 2013. A generally applicable cryopreservation method for nitrite-oxidizing bacteria. Systematic and Applied Microbiology **36**: 579–584. doi:10.1016/j.syapm.2013.07.002

Vernet, M., K. Sines, D. Chakos, A. O. Cefarelli, and L. Ekern. 2011. Impacts on phytoplankton dynamics by free-drifting icebergs in the NW Weddell Sea. Deep-Sea Research Part II: Topical Studies in Oceanography **58**: 1422–1435. doi:10.1016/j.dsr2.2010.11.022

VERSTREATE, D. R., T. A. STORCH, and V. L. DUNHAM. 1980. A comparison of the influence of iron on the growth and nitrate metabolism of Anabaena and Scenedesmus. Physiologia Plantarum **50**. doi:10.1111/j.1399-3054.1980.tb02682.x

Vichi, M., N. Pinardi, and S. Masina. 2007. A generalized model of pelagic biogeochemistry for the global ocean ecosystem. Part I: Theory. Journal of Marine Systems **64**: 89–109. doi:10.1016/j.jmarsys.2006.03.006

Viljoen, J. J., R. Philibert, N. Van Horsten, T. Mtshali, A. N. Roychoudhury, S. Thomalla, and S. Fietz. 2018. Phytoplankton response in growth, photophysiology and community structure to iron and light in the Polar Frontal Zone and Antarctic waters. Deep-Sea Research Part I: Oceanographic Research Papers **141**: 118–129. doi:10.1016/j.dsr.2018.09.006

Viljoen, J. J., I. Weir, S. Fietz, R. Cloete, J. Loock, R. Philibert, and A. N. Roychoudhury. 2019. Links between the phytoplankton community composition and trace metal distribution in summer surface waters of the Atlantic southern ocean. Frontiers in Marine Science **6**: 1–17. doi:10.3389/fmars.2019.00295

Volk, T., and M. I. Hoffert. 1985. Ocean carbon pumps: analysis of relative strengths and efficiencies in ocean-driven atmospheric CO2 changes. The carbon cycle and atmospheric CO.

Waldron, H. N., C. G. Attwood, T. A. Probyn, and M. I. Lucas. 1995. Nitrogen dynamics in the Bellingshausen Sea during the Austral spring of 1992. Deep-Sea Research Part II **42**: 1253–1276. doi:10.1016/0967-0645(95)00063-V

Walker, C. B., J. R. De La Torre, M. G. Klotz, and others. 2010. Nitrosopumilus maritimus genome reveals unique mechanisms for nitrification and autotrophy in globally distributed marine crenarchaea. Proceedings of the National Academy of Sciences of the United States of America **107**: 8818–8823. doi:10.1073/pnas.0913533107

Wan, X. S., H. X. Sheng, M. Dai, and others. 2018. Ambient nitrate switches the ammonium consumption pathway in the euphotic ocean. Nature Communications **9**: 1–9. doi:10.1038/s41467-018-03363-0

Wang, S., D. Bailey, K. Lindsay, J. K. Moore, and M. Holland. 2014. Impact of sea ice on the marine iron cycle and phytoplankton productivity. Biogeosciences **11**: 4713–4731. doi:10.5194/bg-11-4713-2014

Wang, Y. F., and J. D. Gu. 2014. Effects of allylthiourea, salinity, and pH on ammonia/ammonium-oxidizing prokaryotes in mangrove sediment incubated in laboratory microcosms. Applied Microbiology and Biotechnology **98**: 3257–3274. doi:10.1007/s00253-013-5399-3

Wankel, S. D., C. Kendall, J. T. Pennington, F. P. Chavez, and A. Paytan. 2007. Nitrification in the euphotic zone as evidenced by nitrate dual isotopic composition: Observations from Monterey Bay, California. Global Biogeochemical Cycles **21**: 1–13. doi:10.1029/2006GB002723

Ward, B. B. 1985. Light and substrate concentration relationships with marine ammonium assimilation and oxidation rates. Marine Chemistry. doi:10.1016/0304-4203(85)90052-0

Ward, B. B. 1987. Kinetic studies on ammonia and methane oxidation by. Archives of Microbiology **147**: 126–133.

Ward, B. B. 2005a. Temporal variability in nitrification rates and related biogeochemical factors in Monterey Bay, California, USA. Marine Ecology Progress Series **292**: 97–109. doi:10.3354/meps292097

Ward, B. B. 2005b. Molecular Approaches To Marine Microbial Ecology and the Marine Nitrogen Cycle. Annual Review of Earth and Planetary Sciences **33**: 301–333. doi:10.1146/annurev.earth.33.092203.122514

Ward, B. B. 2008. Chapter 5 - Nitrification in Marine Systems, p. 199–261. *In* Nitrogen in the Marine Environment (2nd Edition).

Ward, B. B. 2011. Measurement and distribution of nitrification rates in the oceans, 1st ed. Elsevier Inc.

Ward, B. B., D. Eveillard, J. D. Kirshtein, J. D. Nelson, M. A. Voytek, and G. A. Jackson. 2007. Ammonia-oxidizing bacterial community composition in estuarine and oceanic environments assessed using a functional gene microarray. Environmental Microbiology **9**: 2522–2538. doi:10.1111/j.1462-2920.2007.01371.x

Ward, B. B., and K. A. Kilpatrick. 1990. Relationship between substrate concentration and oxidation of ammonium and methane in a stratified water column. Continental Shelf Research **10**: 1193–1208. doi:10.1016/0278-4343(90)90016-F

Ward, B. B., and K. A. Kilpatrick. 1991. Nitrogen Transformations in the Oxic Layer of Permanent Anoxic Basins: The Black Sea and the Cariaco Trench, *In* Black Sea Oceanography.

Ward, B. B., K. A. Kilpatrick, E. H. Renger, and R. W. Eppley. 1989. Biological nitrogen cycling in the nitracline. Limnology and Oceanography **34**: 493–513.

Ward, B. B., M. C. Talbot, and M. J. Perry. 1984. Contributions of phytoplankton and nitrifying bacteria to ammonium and nitrite dynamics in coastal waters. Continental Shelf Research **3**: 383–398. doi:10.1016/0278-4343(84)90018-9

Ward, B. B., and O. C. Zafiriou. 1988. Nitrification and nitric oxide in the oxygen minimum of the eastern tropical North Pacific. Deep Sea Research Part A, Oceanographic Research Papers **35**: 1127–1142. doi:10.1016/0198-0149(88)90005-2

Watson, A. J., U. Schuster, J. D. Shutler, T. Holding, I. G. C. Ashton, P. Landschützer, D. K. Woolf, and L. Goddijn-Murphy. 2020. Revised estimates of ocean-atmosphere CO2 flux are consistent with ocean carbon inventory. Nature Communications **11**: 1–6. doi:10.1038/s41467-020-18203-3

Watson, S. W., E. Bock, F. W. Valois, J. B. Waterbury, and U. Schlosser. 1986. Nitrospira marina gen. nov. sp. nov.: a chemolithotrophic nitrite-oxidizing bacterium. Archives of Microbiology. doi:10.1007/BF00454947

Watson, S. W., and J. B. Waterbury. 1971. Characteristics of Two Marine Nitrite Oxidizing Bacteria,. Microscopy **77**: 203–230.

Weber, L. H., and S. Z. El-sayed. 1987. Contributions of the net, nano- and picoplankton to the phytoplankton standing crop and primary productivity in the Southern Ocean. Journal of Plankton Research **9**. doi:10.1093/plankt/9.5.973

Weber, T. S., and C. Deutsch. 2010. Ocean nutrient ratios governed by plankton biogeography. Nature **467**: 550–554. doi:10.1038/nature09403

Wei, X., N. Vajrala, L. Hauser, L. A. Sayavedra-Soto, and D. J. Arp. 2006. Iron nutrition and physiological responses to iron stress in Nitrosomonas europaea. Archives of Microbiology **186**: 107–118. doi:10.1007/s00203-006-0126-4

Weigand, M. A., J. Foriel, B. Barnett, S. Oleynik, and D. M. Sigman. 2016. Updates to instrumentation and protocols for isotopic analysis of nitrate by the denitrifier method. Rapid Communications in Mass Spectrometry **30**: 1365–1383. doi:10.1002/rcm.7570

Weir, I., S. Fawcett, S. Smith, D. Walker, T. Bornman, and S. Fietz. 2020. Winter biogenic silica and diatom distribution in the Indian Sector of the Southern Ocean. Deep Sea Research Part I: Oceanographic Research Papers 103421. doi:10.1016/j.dsr.2020.103421

Westwood, K. J., P. G. Thomson, R. L. van den Enden, L. E. Maher, S. W. Wright, and A. T. Davidson. 2018. Ocean acidification impacts primary and bacterial production in Antarctic coastal waters during austral summer. Journal of Experimental Marine Biology and Ecology **498**: 46–60. doi:10.1016/j.jembe.2017.11.003

Wheeler, P. A., and S. A. Kokkinakis. 1990. Ammonium recycling limits nitrate use in the oceanic subarctic Pacific. Limnology and Oceanography **35**: 1267–1278. doi:10.4319/lo.1990.35.6.1267

Whitworth, T. 1980. Zonation and geostrophic flow of the Antarctic circumpolar current at Drake Passage. Deep Sea Research Part A, Oceanographic Research Papers **27**. doi:10.1016/0198-0149(80)90036-9

Whitworth, T., and W. D. Nowlin. 1987. Water Masses and Currents of the Southern Ocean at the Greenwich Meridian. geophysical Research **92**: 6462–6476.

Widner, B., C. A. Fuchsman, B. X. Chang, G. Rocap, and M. R. Mulholland. 2018. Utilization of urea and cyanate in waters overlying and within the eastern tropical north Pacific oxygen deficient zone. FEMS Microbiology Ecology **94**: 1–15. doi:10.1093/femsec/fiy138

Widner, B., and M. R. Mulholland. 2017. Cyanate distribution and uptake in North Atlantic coastal waters. Limnology and Oceanography **62**: 2538–2549. doi:10.1002/lno.10588

Widner, B., M. R. Mulholland, and K. Mopper. 2016. Distribution, Sources, and Sinks of Cyanate in the Coastal North Atlantic Ocean. Environmental Science and Technology Letters **3**: 297–302. doi:10.1021/acs.estlett.6b00165

Wojtasiewicz, B., T. W. Trull, L. Clementson, D. M. Davies, N. L. Patten, C. Schallenberg, and N. J. Hardman-Mountford. 2019. Factors Controlling the Lack of Phytoplankton Biomass in Naturally Iron Fertilized Waters Near Heard and McDonald Islands in the Southern Ocean. Frontiers in Marine Science **6**. doi:10.3389/fmars.2019.00531

Wright, S. W., R. L. van den Enden, I. Pearce, A. T. Davidson, F. J. Scott, and K. J. Westwood. 2010. Phytoplankton community structure and stocks in the Southern Ocean (30-80°E) determined by CHEMTAX analysis of HPLC pigment signatures. Deep-Sea Research Part II: Topical Studies in Oceanography **57**: 758–778. doi:10.1016/j.dsr2.2009.06.015

Wu, M., J. S. P. McCain, E. Rowland, R. Middag, M. Sandgren, A. E. Allen, and E. M. Bertrand. 2019. Manganese and iron deficiency in Southern Ocean Phaeocystis antarctica populations revealed through taxon-specific protein indicators. Nature Communications **10**: 1–10. doi:10.1038/s41467-019-11426-z

Wuchter, C., B. Abbas, M. J. L. Coolen, and others. 2006. Archaeal nitrification in the ocean. Proceedings of the National Academy of Sciences of the United States of America **103**: 12317–12322. doi:10.1073/pnas.0600756103

Xia, F., J. G. Wang, T. Zhu, B. Zou, S. K. Rhee, and Z. X. Quan. 2018. Ubiquity and diversity of complete ammonia oxidizers (comammox). Applied and Environmental Microbiology **84**: 1–14. doi:10.1128/AEM.01390-18

Xu, M. N., X. Li, D. Shi, Y. Zhang, M. Dai, T. Huang, P. M. Glibert, and S. J. Kao. 2019. Coupled effect of substrate and light on assimilation and oxidation of regenerated nitrogen in the euphotic ocean. Limnology and Oceanography **64**: 1270–1283. doi:10.1002/lno.11114

Yager, P. L., and J. W. Deming. 1999. Pelagic microbial activity in an arctic polynya: Testing for temperature and substrate interactions using a kinetic approach. Limnology and Oceanography **44**: 1882–1893. doi:10.4319/lo.1999.44.8.1882

Yin, K., P. J. Harrison, and Q. Dortch. 1998. Lack of ammonium inhibition of nitrate uptake for a diatom grown under low light conditions. Journal of Experimental Marine Biology and Ecology **228**. doi:10.1016/S0022-0981(98)00025-2

Yool, A., A. P. Martin, C. Fernández, and D. R. Clark. 2007. The significance of nitrification for oceanic new production. Nature **447**: 999–1002. doi:10.1038/nature05885

Zakem, E. J., A. Al-Haj, M. J. Church, and others. 2018. Ecological control of nitrite in the upper ocean. Nature Communications **9**. doi:10.1038/s41467-018-03553-w

Zehr, J. P. 2009. Minimum Zones. **106**: 4575–4576.

Zhang, L., M. A. Altabet, T. Wu, and O. Hadas. 2007. Sensitive measurement of NH4+15N/ 14N (δ15NH4+) at natural abundance levels in fresh and saltwaters. Analytical Chemistry **79**: 5297–5303. doi:10.1021/ac070106d

Zhang, R., Y. Li, W. Yan, and others. 2020a. Viral control of biomass and diversity of bacterioplankton in the deep sea. Communications Biology **3**: 1–10. doi:10.1038/s42003-020-0974-5

Zhang, Y., L. Chen, T. Dai, J. Tian, and D. Wen. 2015. The influence of salinity on the abundance, transcriptional activity, and diversity of AOA and AOB in an estuarine sediment: a microcosm study. Applied Microbiology and Biotechnology **99**: 9825–9833. doi:10.1007/s00253-015-6804-x

Zhang, Y., F. Lacan, and C. Jeandel. 2008. Dissolved rare earth elements tracing lithogenic inputs over the Kerguelen Plateau (Southern Ocean). Deep-Sea Research Part II: Topical Studies in Oceanography **55**: 638–652. doi:10.1016/j.dsr2.2007.12.029

Zhang, Y., W. Qin, L. Hou, and others. 2020b. Nitrifier adaptation to low energy flux controls inventory of reduced nitrogen in the dark ocean. Proceedings of the National Academy of Sciences of the United States of America **117**: 4823–4830. doi:10.1073/pnas.1912367117

Zheng, L., T. Minami, S. Takano, H. Minami, and Y. Sohrin. 2017. Distribution and stoichiometry of Al, Mn, Fe, Co, Ni, Cu, Zn, Cd, and Pb in seawater around the Juan de Fuca Ridge. Journal of Oceanography **73**: 669–685. doi:10.1007/s10872-017-0424-2

Zhu, Z., K. Xu, F. Fu, J. L. Spackeen, D. A. Bronk, and D. A. Hutchins. 2016. A comparative study of iron and temperature interactive effects on diatoms and Phaeocystis antarctica from the Ross Sea, Antarctica. Marine Ecology Progress Series **550**: 39–51. doi:10.3354/meps11732

Appendices

Appendix A

The seasonal cycle of nitrogen uptake and nitrification in the Atlantic sector of the Southern Ocean

Text A2.1: Potential for ^{15}N-ammonium isotope dilution due to ammonium regeneration

Ammonium (NH_4^+) regeneration is ubiquitous in marine systems. During $^{15}NH_4^+$ uptake experiments, failure to account for isotope dilution due to NH_4^+ regeneration (i.e., the dilution of the $^{15}NH_4^+$ pool by the ammonification of unlabeled particulate organic N) can result in underestimates of ρNH_4^+ (Glibert et al., 1982) and by extension, overestimates of the f-ratio. I did not measure NH_4^+ regeneration in this study, such that the reported values of ρNH_4^+ may be lower than the rates actually occurring in the environment, with implications for estimates of carbon export potential. However, it is unlikely that accounting for NH_4^+ regeneration would have changed the major findings. My reasoning is as follows.

First, unlike in much of the (sub)tropical and temperate ocean (the focus of the original Glibert et al. (1982) study on NH_4^+ isotope dilution), the NH_4^+ concentrations that I measured across the Southern Ocean were fairly high (>0.5 µM on average (range of 0-1.6 µM) in winter and 0.13 µM on average (range of 0-0.84 µM) in summer). This acts to "buffer" the computed NH_4^+ uptake rates against isotope dilution to some extent.

Second, while very few estimates of NH_4^+ regeneration exist for the open Southern Ocean (with the only available estimate suggesting 50-60 nM d^{-1} in the open Polar Antarctic Zone in summer; Goeyens et al., 1991), a range of regeneration rates can be used to evaluate the sensitivity of my conclusions to NH_4^+ regeneration. I use the equations outlined in Glibert et al. (1982) and Harrison and Harris (1986), along with the measured NH_4^+ and PON concentrations, ^{15}N-PON, ^{15}N-atom% of the NH_4^+ tracer, and the calculated uptake rates, to "correct" ρNH_4^+ for potential isotope dilution associated with NH_4^+ regeneration. For an NH_4^+ regeneration rate of 50 nM d^{-1}, the NH_4^+ uptake rates are underestimated by a factor of 1.19 on average (range of 1.09-1.24). For an NH_4^+ regeneration rate of 100 nM d^{-1}, this increases to a

factor of 1.39 on average (range of 1.17-1.48). While the potential underestimation of ρNH_4^+ implied by these calculations is not trivial, it also does not change the general trend of my observations. Indeed, with the exception of one depth at one station (20 m at station 1) – and in this case, only if I assume NH_4^+ regeneration is ≥100 nM d^{-1} – the ratio of NO_3^- to NH_4^+ uptake remains >1 (i.e., ρNO_3^- dominates) in all cases where it was >1 when NH_4^+ regeneration was assumed to be zero.

Third, plotting V_C against V_{N_total} (i.e., the specific carbon uptake rate against the specific rate of total N uptake) yields an average close to 1:1 for all but stations 3 and 4 (albeit with a fair amount of variability) (Figure 2.10a). If NH_4^+ uptake had been significantly underestimated, the data should fall above the 1:1 line. This is because the regeneration of DIC that occurred coincident with any NH_4^+ regeneration would have no effect on the isotopic composition of the DIC pool in the incubation bottles, and so would not yield an underestimate of the carbon fixation rates – for example, an NH_4^+ regeneration rate of 50 nM d^{-1} (100 nM d^{-1}) would yield a DIC regeneration rate of 331 nM d^{-1} (662 nM d^{-1}) assuming Redfield stoichiometry. The background DIC concentration of ≥2000 μM, along with the fact that the DIC pool was only 5% ^{13}C-labeled at the start of the experiments, means that ~55 μM (i.e., equivalent to >8 μmol NH_4^+ L^{-1} d^{-1}) would have to be remineralized just to decrease the ^{13}C-enrichment of the ambient DIC pool by 0.1%. Thus, the fact that the carbon and total N uptake rates are well-coupled at most of the stations suggests that I have not greatly underestimated the NH_4^+ uptake rates.

As an aside, I note that there will be no effect of isotope dilution associated with nitrate regeneration (nitrification) because 1) the ambient NO_3^- concentrations are so high and 2) the NO_3^- regeneration rates are relatively low. For instance, using the highest nitrification rates measured in winter (0.2 μmol N L^{-1} d^{-1}) and an ambient NO_3^- concentration of 15 μM (which is on the low end of the surface NO_3^- concentrations encountered in the Southern Ocean), NO_3^- isotope dilution would cause the ^{15}N-atom% of the initial NO_3^- pool to decrease by ~0.1% and the computed NO_3^- uptake rate to rise by <2%, which is well within the error of the rate measurements. For lower nitrification rates and/or higher ambient NO_3^- concentrations, the effect would be less significant.

Text A2.2: Carbon and nitrogen cycling in potentially naturally iron-fertilized regions

As is typical of high-latitude HNLC regions, primary production in the Southern Ocean is not limited by N but by a combination of iron (Martin 1990; Smetacek et al., 2012) and light

availability (Nelson and Smith, 1991), with silicate playing a role in SAZ waters (Hutchins et al., 2001). However, there are naturally iron-fertilized regions of the Southern Ocean that have been shown to support high rates of NPP and NO_3^- uptake (yielding high estimates of carbon export potential). For example, the waters surrounding the South Georgia plateau (Korb et al., 2005), Crozet Island (Seeyave et al., 2007), and the Kerguelen Plateau (Blain et al., 2007; Cavagna et al., 2015), where bathymetrically-driven upward mixing of iron (and silicate) enhance phytoplankton growth. Indeed, rates of NPP near South Georgia and Crozet Island have been reported to be as high as 172 mmol C m^{-2} d^{-1} and 89 mmol C m^{-2} d^{-1}, respectively, with a phytoplankton community dominated by large diatoms (constituting up to 87% and 72% of the autotrophs; Korb et al., 2005; Seeyave et al., 2007). NPP over the Kerguelen Plateau has been shown to be even higher (>250 mmol C m^{-2} d^{-1}), and significantly higher (~8-fold) than NPP measured in the adjacent HNLC waters east of the plateau (13 mmol C m^{-2} d^{-1}; Cavagna et al., 2015). The dominance of large diatoms in this region has been explained as a consequence of the alleviation of iron and silicate co-limitation (Boyd et al., 1999; Hutchins et al., 2001; Sedwick et al., 2002), with the availability of the former controlling the use of the latter (i.e., the extent of silicification and ratio of silicate to N uptake; Franck et al., 2000; Martin-Jézéquel et al., 2000; Ragueneau et al., 2000; Mosseri et al., 2008).

Large phytoplankton blooms are frequently observed in association with melting sea ice and ice shelves (Wang et al., 2014; St Laurent et al., 2019; Twelves et al., 2020). A major reason for this is that sea ice accumulates high concentrations of iron from dust deposition and the entrainment of seawater nutrients during freezing (Lancelot et al., 2009; Lannuzel et al., 2011; Wang et al., 2014). Indeed, measured iron concentrations in sea ice can be up to two orders of magnitude higher than in the underlying seawater (Aguilar-Islas et al., 2008; Lannuzel et al., 2007, 2008; van der Merwe et al., 2011). The ice-associated iron is released into surface waters when ice melts (Aguilar-Islas et al., 2008; Tovar-Sánchez et al., 2010), which also stratifies the water column, shoaling the mixed layer and alleviating light limitation of phytoplankton (Taylor et al., 2013). Combined, these conditions can stimulate high rates of phytoplankton growth. Phytoplankton biomass accumulates to extraordinarily high concentrations in the marginal ice zone during spring and summer sea-ice retreat (Smith and Nelson, 1986) and phytoplankton blooms have also been documented in the vicinity of Antarctic ice shelves such as Abbot (Gerringa et al., 2012) and Amery (Herraiz-Borrenguero et al., 2016).

Iron concentrations were not measured in this study so iron limitation of phytoplankton (or the extent of its alleviation) cannot be directly evaluated. However, two of the summer stations are positioned in regions that might be expected to experience iron-replete (or at least, less iron-limited) conditions – near the island of South Georgia (55˚S; 33˚W) and at the Fimbul Ice Shelf (70˚S; 07˚E) (SG and IS, respectively; Figure 1). The SG station is characterized by a higher ρNO_3^- and f-ratio than all the other stations, and a higher rate of NPP than all but station 3 (Table 1), suggesting the alleviation of iron-limited conditions. Moreover, the NO_3^- concentration gradient between the surface layer and the T_{min} is much steeper at SG (8.6 µM) than at the other AZ station located at the same latitude (station 4; 1.5 µM) as well as at the more northern PFZ station (station 3; 1.1 µM) (Figure 3b), indicating a much higher degree of seasonal NO_3^- drawdown at SG. In addition, the T_{min}-to-surface gradient in silicate concentration is 17.9 µM at SG and only 4.2 µM at station 4 (data not shown, although Figure 9b shows that the surface layer-integrated silicate concentration is significantly higher at station 4 than at SG). Thus, the silicate distribution also suggests higher seasonal productivity at SG, and further implies that production is driven largely by diatoms, which are considered disproportionately important for the biological carbon pump (Buesseler 1998b). These observations can be explained by the alleviation of phytoplankton iron limitation, which enhances NO_3^- reductase activity (Timmermans et al., 1994) and may increase the affinity of diatoms for silicate (through a change in their maximum uptake rate (V_{max}) and/or half saturation constant (K_m); Brzezinski et al., 2005; Mosseri et al., 2008). Dissolved iron concentrations have been shown to be elevated in the upper 200 m of the water column around South Georgia in summer (ranging from 0.1-7.70 nM, versus <0.4 nM in the open Atlantic sector; Nielsdóttir et al., 2012; Tagliabue et al., 2012; Schlosser et al., 2018; Mtshali et al., 2019). The high concentrations are thought to derive mainly from the volcanic sediments overlying the island's broad and shallow shelf, augmented by excretion from krill (Nielsdóttir et al., 2012; Schlosser et al., 2018). These iron supply mechanisms, combined with an average (although highly variable) shelf depth of 200 m that allows vertical mixing to fairly easily resuspend seafloor sediments, suggest that the iron flux to South Georgia surface waters could actually be higher than the ambient concentrations imply. In any case, it should not come as a surprise that SG was more productive than the HNLC stations (stations 1-4) given that areally-extensive and long-lasting phytoplankton blooms are regularly observed downstream of South Georgia (Atkinson et al. 2001; Korb et al., 2004; Borrione and Schlizer, 2013), fueling the largest drawdown of CO_2 observed in the Antarctic Circumpolar Current (Jones et al., 2012; 2015).

Despite the evidence for the alleviation of iron limitation near South Georgia, the ratio of silicate to NO_3^- drawdown was higher than expected for iron-replete diatoms (2.1:1 vs. 1:1; Hutchins and Bruland 1998; Takeda 1998; Mosseri et al., 2008). This implies that the consumption of as much as 9.3 µM silicate occurred without NO_3^- (i.e., 17.9 µM – 8.6 µM = 9.3 µM of "missing" NO_3^-, assuming a Si:N uptake ratio of 1:1; Ragueneau et al., 2000). One possibility is that diatoms relied heavily on NH_4^+ to support their growth. Indeed, Mosseri et al. (2008) found that while the ratio of the instantaneous rates of silicate and NO_3^- uptake for diatoms growing in the iron-replete waters of the Kerguelen Plateau was 1:1, the seasonal consumption of silicate and NO_3^- occurred in a ratio closer to 3:1, with diatoms relying on NH_4^+ for 39-77% of their N. At the time of sampling, NH_4^+ accounted for 13% of total N uptake at SG (Table 1). This equates to only 1.3 µM N if the rate-derived proportion of NH_4^+ to NO_3^- uptake (i.e., 13% to 87%) is applied seasonally, leaving 8.0 µM of N still unaccounted for. Another possibility is that diatoms consumed regenerated NO_3^- nitrified in surface waters from recycled NH_4^+. $NO_2^-{}_{ox}$ in the SG euphotic zone was fairly high compared to the other summer stations, accounting for as much as 10% of the assimilated NO_3^- (Table 1); assuming this is representative of the seasonal contribution of nitrification to the surface NO_3^- pool (at least up until the time of sampling), regenerated NO_3^- could yield ~0.8 µM N to support silicate consumption. Accounting for regenerated NH_4^+ and NO_3^- uptake lowers the apparent ratio of silicate to N consumption to 1.7:1, which is still considerably higher than 1:1. Of course, my rate data yield only a temporal snapshot of the SG N cycle while the T_{min}-to-surface gradient in silicate and NO_3^- concentrations represents net seasonal removal. It is thus possible that enhanced NH_4^+ uptake by diatoms occurred earlier in the growing season when light levels were too low for NO_3^- assimilation to be favourable. Another possibility is that while the SG diatoms experienced higher iron concentrations than phytoplankton at the HNLC stations, these were not high enough to completely alleviate iron limitation, such that the ratio of Si:N uptake by the SG diatoms was >1:1 (Franck et al., 2000; Brzezinski et al., 2003). Indeed, a recent study of dissolved iron and macronutrient cycling in the vicinity of the Kerguelen Plateau, which is considered iron-rich compared to the surrounding Southern Ocean (Blain et al., 2007; Cavagna et al., 2015), found that almost all stations, regardless of their proximity to the islands, experienced some degree of iron limitation (Holmes et al., 2019). It seems likely that this was also the case for the SG station, particularly given that attempts to-date to balance the apparent iron demand of phytoplankton off South Georgia with the available iron sources have been unsuccessful (Schlosser et al., 2018).

In contrast to SG, there appears to be no stimulation of productivity at the IS station where I measured the lowest summertime rates of NPP and NH_4^+ uptake, and NO_3^- uptake rates that were higher only than those measured at stations 1 and 2 (Table 1). Interestingly, the f-ratio at this station was higher than at all the other summer stations except SG. There is considerable evidence in the literature for elevated biological activity in the vicinity of ice shelves, which is typically attributed to the alleviation of iron limitation due to local iron inputs associated with melting sea ice (Aguilar-Islas et al., 2008; Tovar-Sánchez et al., 2010; Gerringa et al., 2012; 2015; Herraiz-Borrenguero et al., 2016). That this was not the case at the time of my study is probably because sampling occurred too late in the season to capture the period of intense sea-ice melt. In other words, by the time of sampling in late January, any iron supplied to the waters near the ice shelf from melting sea ice had already been consumed by an earlier phytoplankton bloom. This is consistent with the observation that summer POC (i.e., biomass) concentrations were highest at IS while NPP was lowest (Figure 3h and 7d). The high f-ratio at IS can be attributed to the fact that the MLD was significantly shallower than the euphotic zone, allowing enough light into the mixed layer to favor NO_3^- reduction. The implication of this is that iron (rather than light) exerted the dominant control on productivity at the Fimbul Ice Shelf at the time of sampling, but by limiting rather than stimulating phytoplankton growth.

Text A2.3: Nitrite concentrations in the upper layer of the Southern Ocean

It is curious that the NO_2^- concentration over the upper ~200 m of the Southern Ocean remains fairly constant at ~0.1-0.2 µM, regardless of season, zone, or sector (Figure 3e and f; Key et al., 2015; Olsen et al., 2016; Zakem et al., 2018; Fripiat et al., 2019). This implies that the fluxes of NO_2^- supply (via mixing, NH_4^+ oxidation, and/or incomplete NO_3^- reduction by phytoplankton) and removal (via mixing, oxidation to NO_3^-, and/or consumption by phytoplankton) are roughly balanced, but that in net, more NO_2^- is supplied than removed. One possibility is that a physiological limitation prevents the drawdown of the surface NO_2^- pool below a threshold concentration of ~0.1-0.2 µM.

The limited available data on Southern Ocean phytoplankton NO_2^- uptake kinetics suggest that the affinity of diatoms for NO_2^- is low (i.e., the K_m is high, >10 µM) (Sivasubramanian and Rao, 1988). In addition, the perennially-high NO_3^-+NO_2^- concentrations that characterize Southern Ocean surface waters should not favor phytoplankton with a high affinity for NO_3^- or

NO_2^- (MacIsaac and Dugdale, 1969), and it is even possible that high NO_3^- concentrations impede the ability of phytoplankton to consume NO_2^- (Cordoba et al., 1986). With regard to nitrifiers, recent work has suggested that NO_2^- oxidizing bacteria (NOB) are on average larger than ammonia oxidizing archaea and bacteria (AOA and AOB) (Pachiadaki et al. 2017), which implies that their affinity for NO_2^- is lower than the affinity of AOA/AOB for NH_4^+, restricting the degree to which they can deplete the available NO_2^- (Zakem et al., 2018). Indeed, the K_m for NO_2^- oxidation has been estimated from pure cultures of NOB to be high (6-544 µM) (Blackburne et al., 2007; Nowka et al., 2015; Ushiki et al., 2017) and from the environment to be on the order of 0.25 µM (Sun et al., 2017). In addition, the available data suggest that NOB are more sensitive to light than AOA and AOB (Bock, 1965; Olson, 1981b; Qin et al., 2014), which may limit the rate of NO_2^- oxidation more than NH_4^+ oxidation in upper Southern Ocean waters.

Ambient NH_4^+ concentrations appear to be elevated throughout the upper 200 m of the Southern Ocean in winter (and significantly higher than the co-occurring NO_2^- concentrations; Figure 3d and e) and possibly also in autumn due to intense remineralization following the phytoplankton growing season (El-Sayed, 1987; Smart et al. 2015; Kemeny et al. 2018). This likely renders AOA and AOB substrate-replete, even considering the possibility of competition with heterotrophic bacteria for NH_4^+ (see the latter paragraphs of section 4.1 of the main text), thus giving NH_4^+ oxidizers a further advantage over NOB. Conditions that generally favor NH_4^+ oxidizers, combined with the fact that surface NO_3^-+NO_2^- is never completely consumed by Southern Ocean phytoplankton and that light-limited phytoplankton may at times efflux NO_2^- following incomplete NO_3^- reduction (Serra et al., 1978; Collos 1998; Campbell 1999), may account for the limited extent to which NO_2^- can be drawn down, leading to an approximately constant and non-zero mean surface NO_2^- concentration.

Appendix B

The kinetics of ammonium uptake and oxidation across the African sector of the Southern Ocean

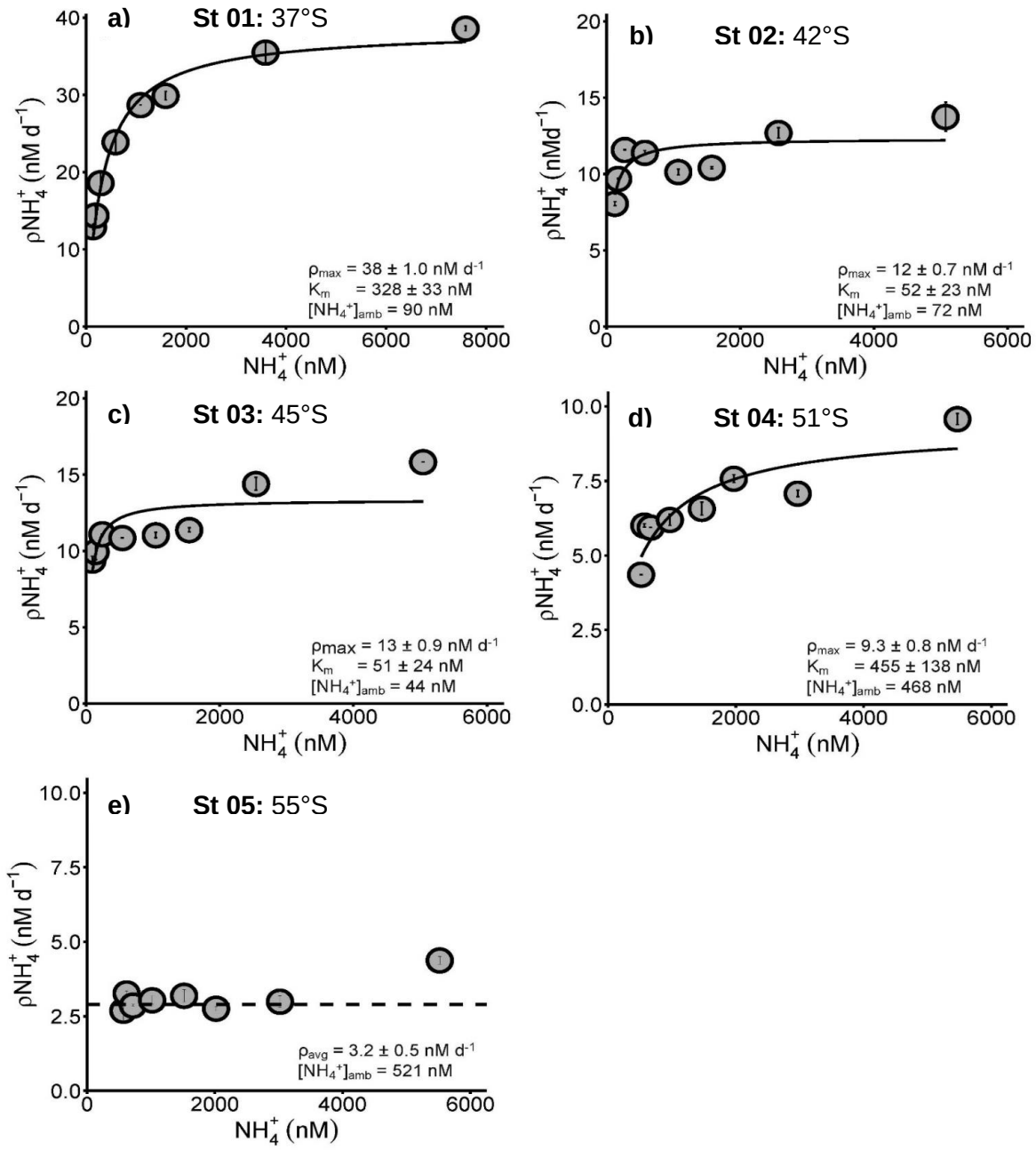

Figure B3.1: The dependence of NH_4^+ uptake rates (i.e., transport rates; nM d^{-1}) on $[NH_4^+]$ at the surface (~7 m) in winter at a) St 01: 37°S (STZ), b) St 02: 42°S (STF), c) St 03: 45°S (SAZ), d) St 04: 51°S (PFZ), and e) St 05: 55°S (AZ). The solid line shows the Michaelis-Menten fit, with the derived values of ρ_{max} and K_m, as well as the ambient ammonium concentration ($[NH_4^+]_{amb}$), indicated on each panel. At station 5, a Michaelis-Menten relationship was not observed; here, the dashed horizontal line indicates the average NH_4^+ uptake rate (ρ_{avg}). Error bars indicate the standard error of replicate experiments, each measured at least twice. Where errors bars are not visible, they are smaller than the data markers

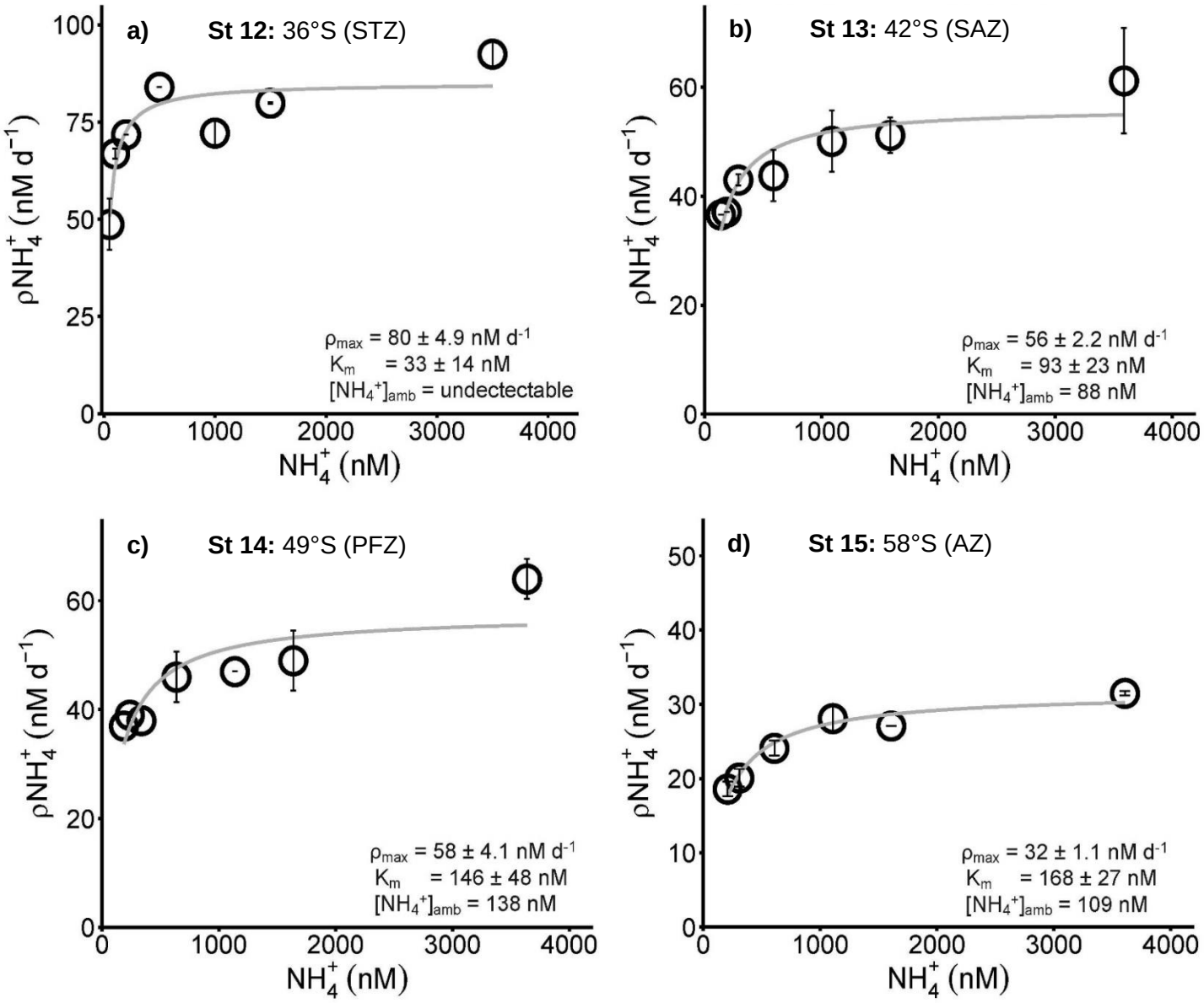

Figure B3.2: The dependence of ammonium uptake rates (i.e., transport rates; nM d^{-1}) on $[NH_4^+]$ at the surface (~7 m) in summer at a) St 12: 36°S (STZ), b) St 13: 43°S (SAZ), c) St 14: 49°S (PFZ), and d) St 15: 58°S (AZ). The solid line shows the Michaelis-Menten fit, with the derived values of ρ_{max} and K_m, as well as the ambient ammonium concentration ($[NH_4^+]_{amb}$), indicated on each panel. Error bars indicate the standard error of replicate experiments, each measured at least twice. Where errors bars are not visible, they are smaller than the data markers.

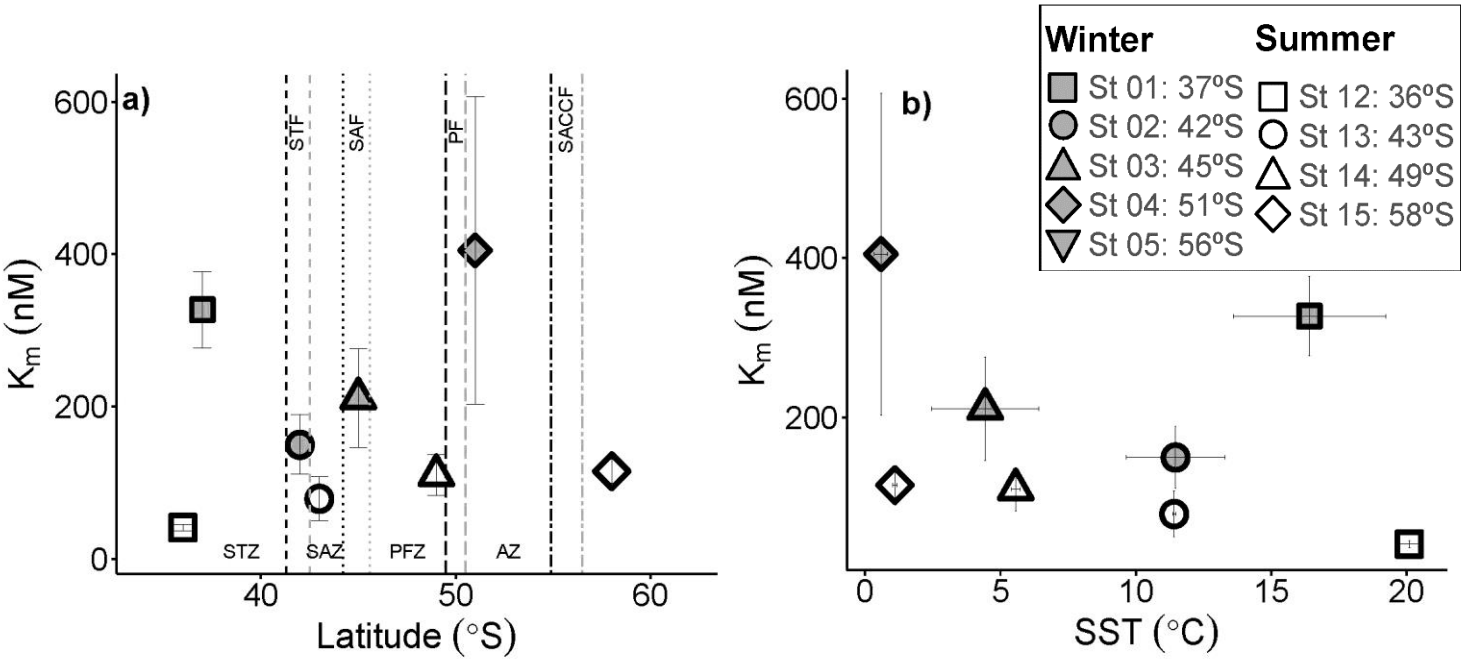

Figure B3.3: Potential controls on the kinetic parameters associated with NH_4^+ uptake. K_m is shown as a function of a) latitude and b) SST. Open symbols represent summer and filled symbols represent winter. Vertical error bars show the propagated error associated with K_m as computed using the drc package in R (Ritz et al. 2015), while the symbols and horizontal error bars on panel b indicate the average (± standard deviation) SST experienced by the samples during the 3- to 6-hour incubations. In panel a, the vertical lines show the frontal positions in winter (grey) and summer (black), with the fronts and zones of the Southern Ocean labelled on the plot: STZ, Subtropical Zone; STF, Subtropical Front; SAZ, Subantarctic Zone; SAF, Subantarctic Front; PFZ, Polar Frontal Zone; PF, Polar Front; AZ, Antarctic Zone; SACCF, Southern Antarctic Circumpolar Front.

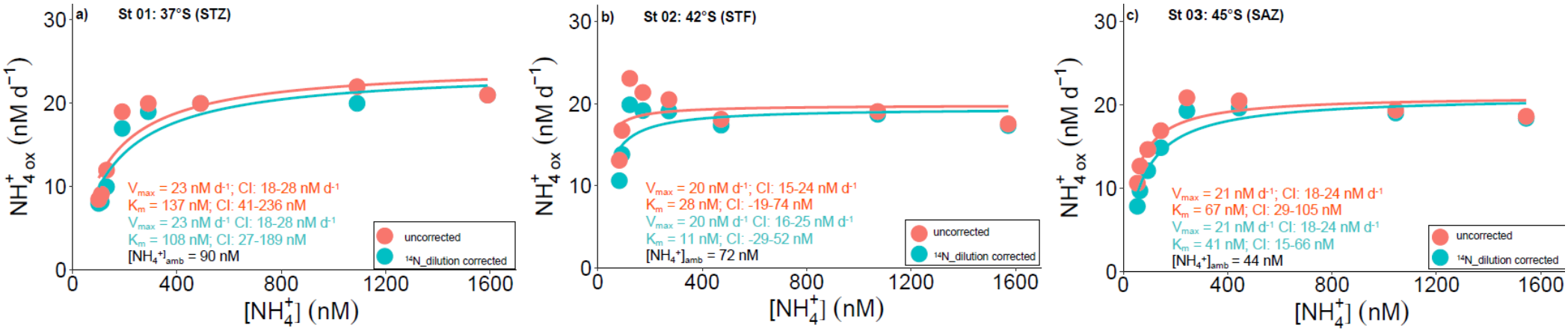

Figure B3.4: NH_4^+ oxidation rates for the kinetics experiments where a Michaelis-Menten relationship with NH_4^+ concentration was observed, before and after correcting for ^{14}N isotope dilution due to coincident NH_4^+ regeneration (see text for details; *Potential implications of isotopic dilution of $^{15}NH_4^+$ by co-occurring $^{14}NH_4^+$ regeneration*). The orange-red colour shows the original data (as presented in Figure 3.5a-c) and the blue colour shows the rates after correction for ^{14}N dilution, assuming a hypothetical NH_4^+ regeneration rate of 20 nM d^{-1} (Goeyens et al. 1991). The derived kinetic parameters are labelled on the panels in the corresponding colour, with "CI" indicating the 95% confidence interval. This exercise reveals that while isotope dilution hardly changes V_{max}, it can change K_m considerably.

Table B3.1: Kinetic experiment stations displaying kinetics parameters with confidence intervals

Experiment	Season	Station name	Vmax	CI: 95%	Km	CI: 95%
Uptake	Winter	St 01	7.9	7.1-8.6	327	205-448
Uptake	Winter	St 02	3.4	2.9-3.8	150	54-247
Uptake	Winter	St 03	3.9	3.2-4.6	211	51-371
Uptake	Winter	St 04	3.23	2.4-4.0	486	48-924
Uptake	Winter	St 05	1.2	0.9-1.6		
Uptake	Summer	St 12	8.0	7.6-8.3	41	30-52
Uptake	Summer	St 13	4.1	3.5-4.8	79	4.3-154
Uptake	Summer	St 14	3.5	3.1-3.9	110	41-179
Uptake	Summer	St 15	1.6	1.4-1.7	115	74-157
Oxidation	Winter	St 01	23	18-28	137	39-235
Oxidation	Winter	St 02	19	15-24	28	-19-80
Oxidation	Winter	St 03	21	18-24	67	29-105

Appendix C

Controls on nitrite oxidation in the upper Southern Ocean: insights from winter kinetics experiments across the Indian sector

Text C4.1: Method

NO_3^- uptake kinetics experiments: To assess the response of phytoplankton to increasing NO_3^- availability, NO_3^- uptake kinetics experiments were conducted at two stations on Leg 1 where the ambient NO_3^- concentrations were low enough to potentially be limiting – the most northern stations, St 01 (37ºS) and St 02 (42ºS). Seawater was collected from the underway system (~7 m) in a 25 L carboy, thoroughly mixed, sieved through a 200 µm nylon mesh to remove large zooplankton, and dispensed into eight pairs of 1 L clear polycarbonate bottles. The $^{15}NO_3^-$ tracer additions, added to duplicate bottles, were different at the two stations, ranging from 0.05 to 20 µM at St 01 and from 0.5 to 30 µM at St 02. Following tracer addition, the bottles were then transferred to custom-built deck-board incubators equipped with neutral density screens allowing only the penetration of 55% of surface photosynthetically active radiation (PAR). The bottles were kept at *in situ* temperature by a supply of continuously-running seawater from the underway system. Samples were incubated for 3-6 hours, and incubations were terminated by filtering the bottle contents through a pre-combusted (450°C for 8 hours) 0.3 µm glass fibre filter (GF-75; Sterlitech) that was enclosed in a foil envelop (pre-combusted at 500°C for 5 hours) and stored in a -80°C freezer until analysis.

Equation 4.3 below, was used to calculate the kinetic parameters for NO_3^- uptake, for details of the equation please see main text.

$$V = \frac{V_{max} \times (S-c)}{K_{m*} + (S-c)} \qquad (4.3)$$

Text C4.2: Results

NO_3^- uptake kinetics experiments: V_{max} ranged from 0.3 0.0 ± to 1.3 ± 0.1 x10^{-3} h^{-1} (with an average of 0.8 ± 0.5 x10^{-3} h^{-1}), K_m ranged between 2.8 ± 0.8 and 5.7 ± 1.0 µM (with an average of 4.3 ± 1.5 µM), C value was ranging from 1.9 ± 0.5 to 3.9 ± 0.5 µM (with an average of 2.5 ± 0.6 µM). V_{max} at St 02 was 4.3 higher than at St 01, while K_m and C values at St 02 were double the values at St 01. K_m values were slightly lower than $[NO_3^-]_{amb}$ at both stations.

C4: Figures

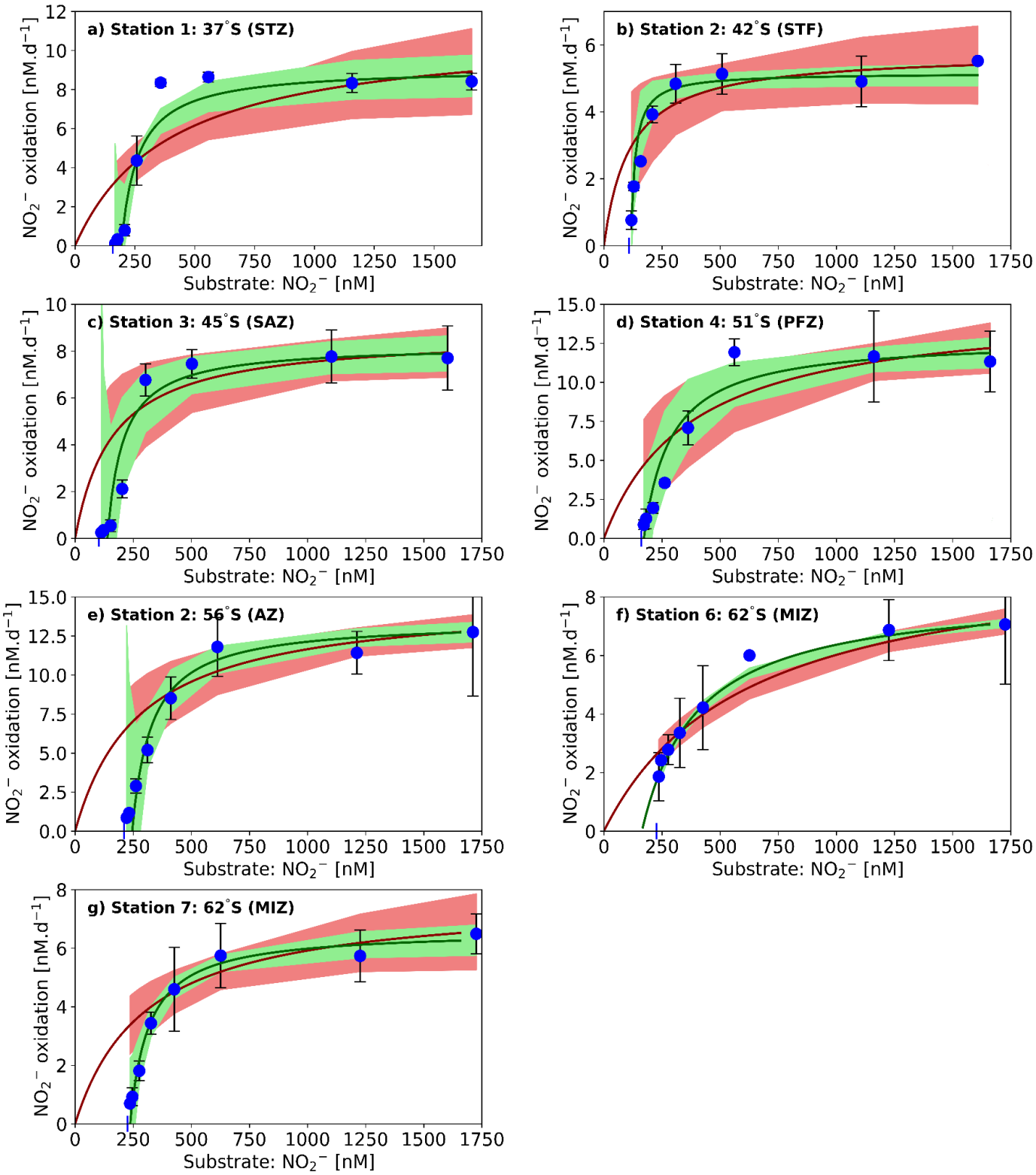

Figure C4.1: Kinetic experiment stations displaying two kinetics curves fitted using two different methods. Panels: a) St 01: 37°S (STZ), b) St 02: 42°S (STF), c) St 03: 45°S (SAZ), d) St 04: 51°S (PFZ), e) St 05: 55°S (AZ), f) St 06: 62°S (MIZ), and g) St 07: 62°S (MIZ). The solid lines show the Michaelis-Menten (MM) fit: the red line is the MM curve fitted using traditional method (equation 4.2), blue line is the modified MM curve fitted using equation 4.3. Error bars indicate the standard

error of replicate experiments, each measured at least twice. Where errors bars are not visible, they are smaller than the data markers., Red shaded area is the 95% confidence interval derived using equation 4.2, Blue shaded area is the 95% confidence interval derived using equation 4.3.

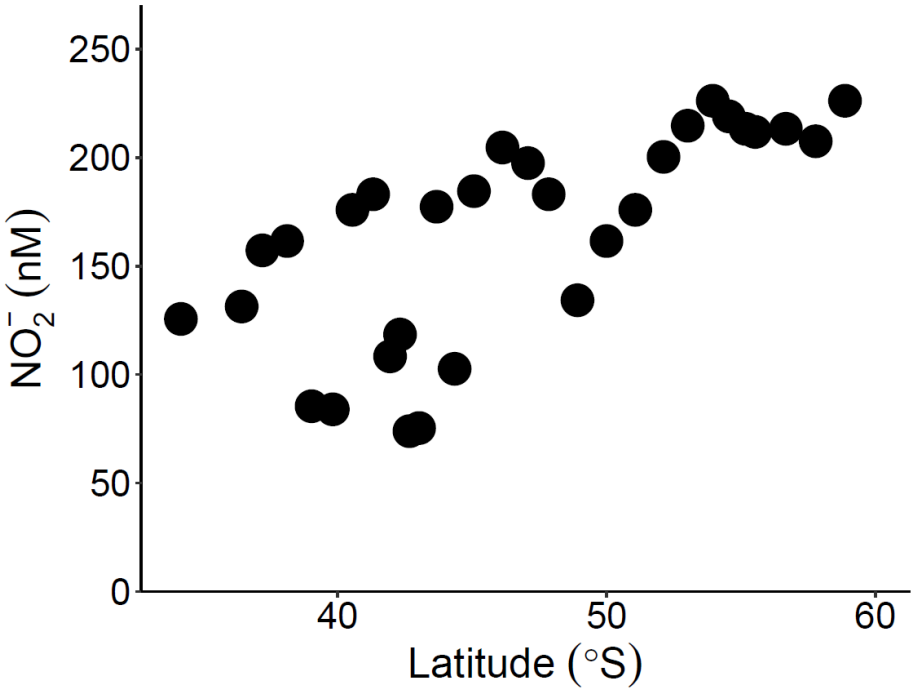

Figure C4.2: Surface nitrite concentrations ($[NO_2^-]_{amb}$) measured every four hours across the transect (Leg 1) between 34°S and 59°S

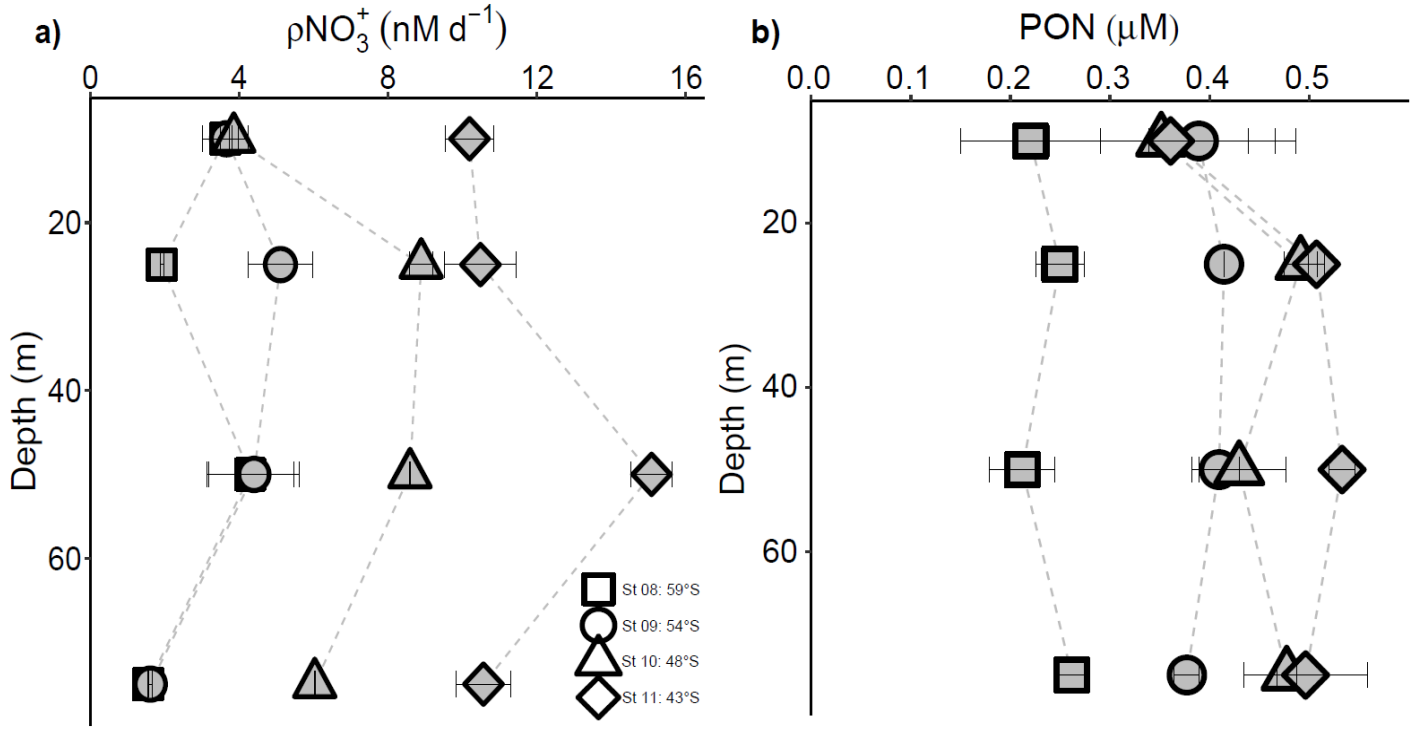

Figure C4.3: Upper 75 m- a) rates of NO_3^- uptake (ρNO_3^-) and b) concentrations of particulate organic nitrogen (PON) for samples collected at the depth profile stations (St 08 to St 11; Leg 2). Error bars indicate the standard error of replicate experiments/collections, each measured at least twice. Where errors bars are not visible, they are smaller than the data markers.

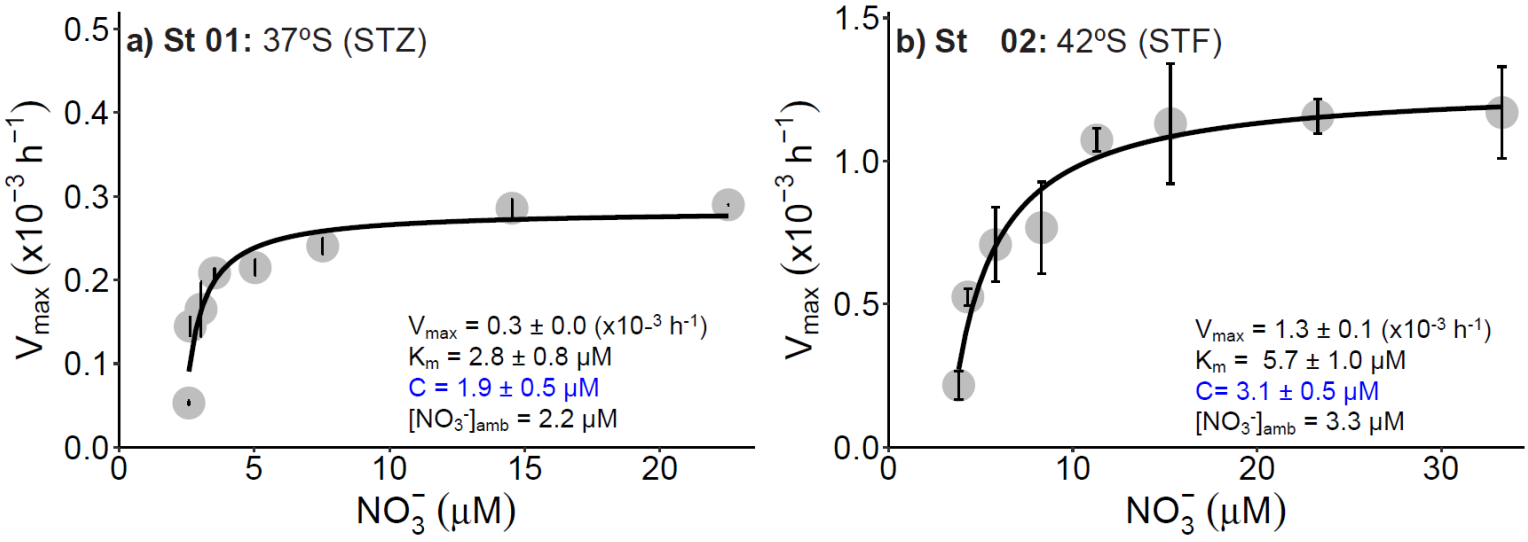

Figure C4.4: The dependence of NO_3^- uptake rates on $[NO_3^-]$ at the surface (~7 m) at a) station 1: 37°S (STZ) and b) station 2: 42°S (STF). The solid line shows the Michaelis-Menten fit, with the derived values of V_{max}, K_m, and C, as well as the ambient nitrate concentrations ($[NO_3^-]_{amb}$), indicated on each panel. Error bars show the standard error of replicate experiments, each measured at least twice. Where errors bars are not visible, they are smaller than the data markers.

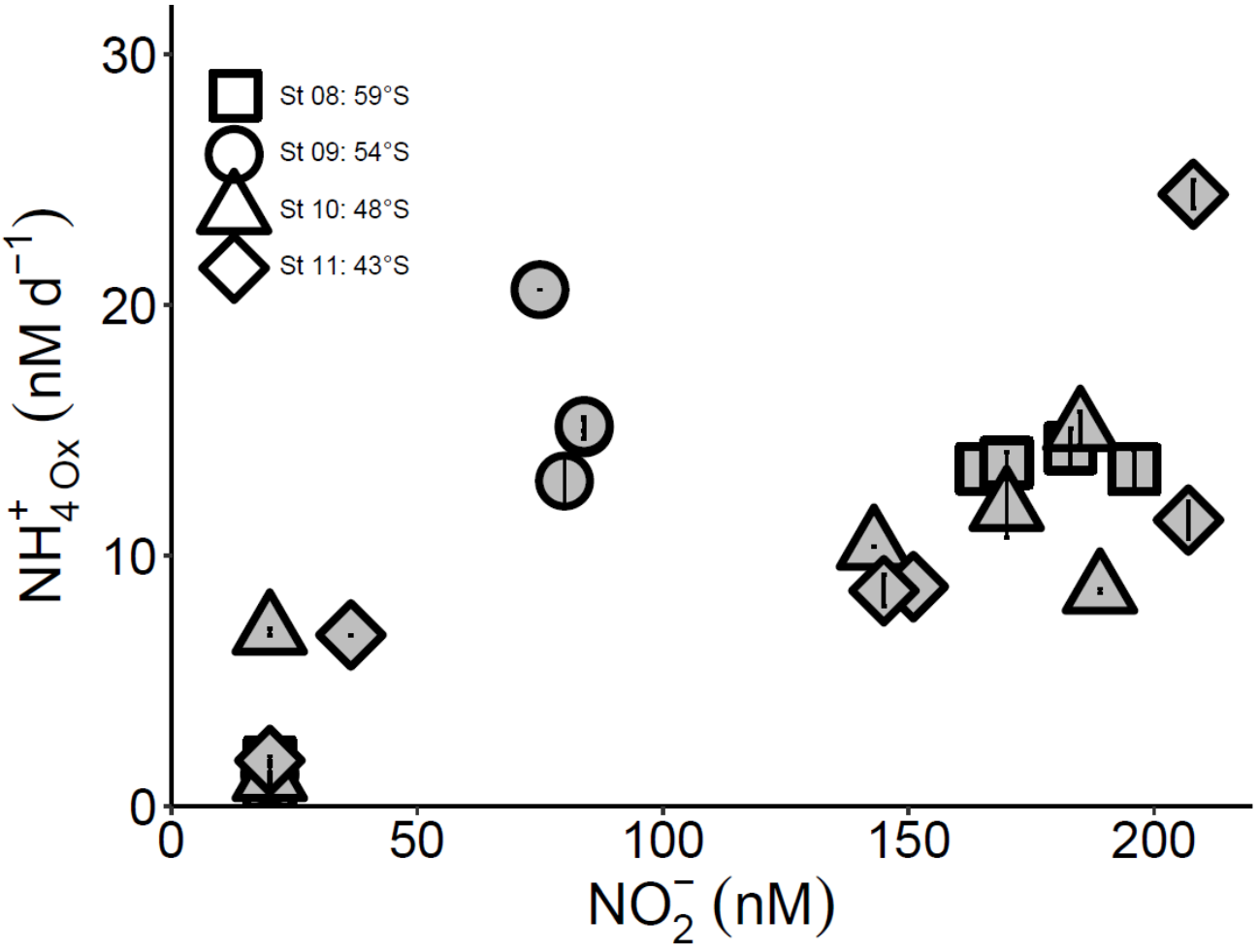

Figure C4. 5: Depth profile (0-75 m) rates (St 08 to St 11) of NH_4^+ oxidation (nM d^{-1}) plotted against coincident measurements of NO_2^- concentration (nM). Error bars show the standard error of replicate experiments or collections, each measured at least twice.

Table C4.1: Kinetic parameters calculated for each NO_2^- oxidation kinetics experiment using two different models. The values shaded in grey were computed using the traditional Michaelis-Menten (MM) model (equation 4.2 in the main text), while the on a white background were derived using a modified form of the MM model (equation 4.3 in the main text). The numbers in red are the values used throughout the main text.

			Confidence interval						
Station	**Equation**	**Kinetic parameter**	**99,73%**	**95,45%**	**68,27%**	**Best fit**	**68,27%**	**95,45%**	**99,73%**
1	4.2	Vmax	5.0	7.6	9.4	11.1	13.1	16.5	28.6
1	4.2	Km	11	156	277	400	564	890	2335
1	4.3	Vmax	6.7	***7.9***	8.6	**9.1**	9.6	***10.4***	infinity
1	4.3	c	-829	***144***	182	**193**	199	***206***	214
1	4.3	derived Km	31	48	59	70	88	145	infinity
1	4.3	Km	-798	***192***	241	**263**	287	***350***	infinity
2	4.2	Vmax	3.5	4.5	5.2	5.8	6.5	7.8	12.1
2	4.2	Km	-43	6	56	112	191	353	1052
2	4.3	Vmax	4.5	***4.8***	5.0	**5.2**	5.3	***5.5***	6.0
2	4.3	c	72	***105***	112	**115**	117	***119***	124
2	4.3	derived Km	0	4	11	18	28	43	87
2	4.3	Km	72	***109***	123	**134**	145	***163***	212
3	4.2	Vmax	6.0	7.2	8.0	8.7	9.6	11.2	18.3
3	4.2	Km	-47	21	88	162	269	500	1706
3	4.3	Vmax	6.5	***7.4***	7.9	***8.3***	8.7	***9.3***	infinity
3	4.3	c	neg infinity	***-11***	117	***139***	152	***169***	180
3	4.3	derived Km	neg infinity	26	47	67	96	204	infinity
3	4.3	Km	0	***15***	164	**206**	248	***373***	infinity
4	4.2	Vmax	9.7	11.7	13.3	14.9	17.4	23.3	100.9
4	4.2	Km	-15	99	223	374	619	1263	10118
4	4.3	Vmax	10.2	***11.4***	12.2	**12.8**	13.6	***15.2***	infinity
4	4.3	c	-1646	***68***	148	**172**	186	***204***	243
4	4.3	derived Km	6	36	75	117	176	335	infinity
4	4.3	Km	-1640	***104***	223	**288**	363	***538***	infinity
5	4.2	Vmax	11.1	12.7	13.9	14.9	16.1	18.2	25.0
5	4.2	Km	-15	93	185	279	401	631	1441
5	4.3	Vmax	11.8	***12.6***	13.1	**13.5**	13.9	***14.6***	infinity
5	4.3	c	neg infinity	***138***	221	**245**	259	***272***	292
5	4.3	derived Km	20	45	64	84	112	186	infinity
5	4.3	Km	20	***183***	285	**329**	371	***458***	infinity
6	4.2	Vmax	7.7	8.5	9.2	9.7	10.3	11.3	13.5
6	4.2	Km	294	421	519	609	718	897	1359
6	4.3	Vmax	7.6	***7.9***	8.1	**8.2**	8.3	***8.6***	9.2
6	4.3	c	70	***129***	151	**163**	174	***187***	204
6	4.3	derived Km	154	191	217	239	266	312	448
6	4.3	Km	224	***320***	368	**403**	440	***499***	652
7	4.2	Vmax	4.3	5.7	6.8	7.7	8.9	10.9	16.8
7	4.2	Km	-50	79	191	304	450	722	1636
7	4.3	Vmax	5.4	***6.0***	6.3	**6.6**	6.9	***7.4***	8.6
7	4.3	c	-47	***190***	223	**237**	246	***255***	269
7	4.3	derived Km	19	45	64	80	101	140	396
7	4.3	Km	-28	***234***	287	**317**	346	***395***	664

Note: the equation number corresponds to the numbering in the methods text

Table C4.2 Upper 75 m- average specific rates of NO_3^- uptake (numbers in parentheses () are propagated standard error of replicate experiments, each measured at least twice), and integrated transport rates of NO_3^- uptake, NO_2^- oxidation, and the ratio of NO_2^- oxidation to NO_3^- uptake.

Station name	Avg PON (µM)	NO_3^- specific uptake ($x10^{-3}$ h^{-1})	$NO_2^-{}_{Ox}$ (mmol m^{-2} d^{-1})	ρNO_3^- (mmol m^{-2} d^{-1})	$NO_2^-{}_{Ox}/\rho NO_3^-$
St 08: 59°S	0.27 (0.08)	1.48 (0.99)	0.61	0.26	2.37
St 09: 54°S	0.38 (0.04)	1.03 (0.63)	0.19	0.30	0.63
St 10: 48°S	0.47 (0.09)	1.52 (0.82)	0.52	0.71	0.73
St 11: 43°S	0.44 (0.09)	2.09 (1.09)	1.65	1.44	1.15